EXAMPLES OF TECTONIC MECHANISMS FOR LOCAL CONTRACTION AND EXHUMATION OF THE LEADING EDGE OF INDIA. SOUTHERN TIBET (28-29 °N; 89-91 °E) AND NANGA PARBAT, PAKISTAN

by

Michael A. Edwards

A Dissertation

Submitted to the University at Albany, State University of New York

in Partial Fulfillment of

the Requirements for the Degree of

Doctor of Philosophy

College of Arts & Sciences

Department of Earth & Atmospheric Sciences

1998

ABSTRACT

In Gonto La valley, southern Tibet, a continuous, planar, ~10°N dipping detachment horizon juxtaposes Tethyan slates over a footwall of leucogranite that intrudes a S-dipping injection complex layer that I regard as a rotated Southern Tibet Detachment System (STDS) horizon. This is deformed & partially cut by the leucogranite which forms a pluton extending throughout Khula Kangri massif. In collaboration, ^{208}Pb-^{232}Th measurements on 12 monazite grains of the leucogranite gave a crystallization age of 12.5±0.4 Ma. Integrated estimates of magnitude, and rate, of detachment displacement suggest that STDS displacement continued after granite crystallisation for 1-3 m.y. Therefore N-S extension in southern Tibet continued into the Late Miocene. A new geologic map of the Khula Kangri and Kanga Punzum-Monlakarchung High Himalayan ranges is presented using field, satellite & topographic data. These define a fork in the High Himalaya that results in a repetition of the main geological section. The STDS can be traced around both ranges and is a continuous surface. A simple model of post detachment, scissor faulting and block rotation is proposed. In SE Nanga Parbat Haramosh Massif (NPHM), Pakistan, field and microstructural analysis of strain and sense of shear trends indicate that several km of metasedimentary schists and gneisses are Himalayan Main Mantle Thrust (MMT) footwall rocks rotated to vertical due to NW-SE directed shortening. Near the NPHM summit region, several km of non-coaxially sheared granitic orthogneiss show W over E displacement structures. Although deformation mechanisms appear lower temperature than in the MMT footwall rocks, a major "uplift" structure (the Rupal Chichi shear zone - RCSZ) is proposed. To the SW, an E-over W shear zone (the Diamir Shear Zone - DSZ) that coincides with a syn-kinematically intruded granite (the Jalhari Granite) is recognised. In collaboration, ^{208}Pb-^{232}Th measurements on monazite grains of the Jalhari indicate displacement has continued from ~9 to <3 Ma. The DSZ is regarded as the mechanical continuation of the Raikot Fault. The Raikot-DSZ, together with the RCSZ define a conjugate pair that is interpreted to mark a pop-up structure, allowing the skywards displacement of NPHM.

DEDICATION

For Anna,

who remained in Albany

until shortly after I left

ACKNOWLEDGEMENTS

Committe Members: Harper, Kidd & Means, Nelson.

Discussion & ideas: Asif Khan, Burchfiel, Burg, Coulton, Delano, Dannenmann, Davidson, Gilotti, Grujic, Guillot, Hanson, Harris, Harrison, Hayman, Heilbronner, Hollister, Koons, Kosanke, Law, Le Fort, Meltzer, S. Park, Y-D. Park, Parrish, Pêcher, Ratschbacher, Ross, Royden, Rutter, Samson, Scaillet, Schneider, Seeber, Shroder, Spencer, Teyssier, Treagus, Vannay, Zeitler.

Facilities & general help: Alsdorf, Akhtar Karim, Aslam Mohammed, Bickford, Cogan, Clark, Fernandes, Fielding, Jerram, Hauck, Herrmann, Linsley, Maguires, Makovsky, Paton, Plesch, Seimon, Short, Wemple, Zahler.

[Names on this this list are in alphabetical order. Names do not appear twice. This list is only of professional acknowledgements and does not include those who are solely friends, even if they specifically asked to be named here (e.g., Susi Herrmann)]

TABLE OF CONTENTS

LIST OF FIGURES

Page

CHAPTER TWO

LIST OF TABLES

Page

CHAPTER ONE

INTRODUCTION

1.1 PURPOSE OF THE STUDY

The "leading edge" (northern margin) of the Indian continent is presently underthrusting (Schelling and Arita, 1991; Zhao et al., 1993) the accreted terranes (Chang et al., 1986; Kidd et al., 1988) that made up the southern margin of Asia before the India-Asia collision began (Argand, 1924). The accumulation of strain arising from the convergence of these plates since collision began, about ~50 Ma (Patriat and Achache, 1984; Rowley, 1996, 1998) or 65 Ma (Searle, 1986; Beck et al., 1996) has resulted in the >2000 km long Himalayan mountain chain, and the Tibet plateau (~3500 x 1500 km), respectively the highest range and largest plateau on the planet, and comprising >25% of Earth's elevated regions (Fielding, 1996). This area is the Earth's best example of continental collision, however, in part from difficulty of access, it is relatively little studied. Knowing the timing and nature of deformation within this region can increase understanding of the mechanisms that possibly contribute(d) to the growth of the Himalaya and the Tibet plateau, and their geological consequences (e.g., Dewey and Burke, 1973; Tapponnier et al., 1986; Zhao and Morgan, 1985, Harrison et al., 1992). Additionally, this understanding can significantly refine models of (1) crustal rheology (e.g., England and Housemann, 1986) and (2) Cenozoic global climate change that may result from plateau uplift (e.g., Harrison et al., 1992; Molnar et al., 1993). My studies of the tectonic mechanisms for local contraction and exhumation in southern Tibet (28-29°N; 89-91°E) and at the Nanga Parbat-Haramosh Massif (NPHM), Pakistan Himalaya, provide constraints on the mechanisms and timing of principal processes in the

development of the High Himalaya. In addition, they provide an illustration of some of the different deformation styles of the upper Himalaya in southern Tibet and at Nanga Parbat.

The junction between India and the northern margin of Asia is defined by the Indus-Yarlung-Tsangpo suture in southern Tibet (Gansser, 1964; Burg, 1983), and by the Main Mantle thrust (MMT - Tahirkheli, 1979; Tahirkheli et al. 1979), also termed "Southern suture" (Gansser, 1980), in the NW Himalaya, where the Kohistan-Ladakh fossil island arc is locally included in the collision (Tahirkheli, 1979; Bard et al., 1980). The area between the suture and the presently exposed high grade metamorphic rocks in the "midland" areas of the mountain belt is comprised of the deformed, low (southern Tibet) to high (Nanga Parbat) metamorphic grade (meta-) sedimentary rocks (the Tethyan sequences) that were deposited on the passive margin of India (Gansser, 1964; Burg, 1983). The high grade rocks of Nanga Parbat are largely exposed by the results of tectonic processes that have exhumed this massif since ~5 Ma (Zeitler, 1985; Zeitler et al., 1993; Winslow et al., 1995), whereas the high grade rocks exposed in the upper part of the main Himalaya were largely exhumed by (1) erosion, and (2) extensional displacement of the southern Tibet detachment system (STDS Burg, 1983; Burg et al., 1984; Herren, 1987; Burchfiel et al., 1992; Edwards et al., 1996) mostly in the early to middle Miocene (Coleman and Parrish, 1995; Hodges et al., 1995; Harrison et al., 1995b; Noble and Searle, 1995; Searle et al., 1997; Edwards & Harrison 1997; Harrison et al., 1997). In both these areas, there is a close association between metamorphism, plutonism, and exhumation, extremity of slope and large displacement structures (Zeitler, 1985; Zeitler et al., 1993; Winslow et al., 1995; Coleman and Parrish, 1995; Hodges et al., 1995; Harrison et al., 1995b; Noble and Searle, 1995; Searle et al., 1997; Edwards & Harrison 1997; Harrison et al., 1997). Studies at Nanga Parbat Haramosh Massif (NPHM) and in southern Tibet (28-29°N; 89-91°E), investigating the nature and

history of deformation and exhumation of the high grade rocks, the interrelationship with adjacent lower grade rocks, and the association of plutonism, are the primary focus of this thesis.

1.2 SCOPE OF STUDY

Investigations in southern Tibet, over the course of two field seasons, involved general mapping, local structural mapping of areas not previously visited by geologists, and sampling for structural analyses and geochronology. Data from these investigations have been used to make maps, and cross-sections, and samples were used for further structural investigation under the microscope. In addition, data are compiled from earlier preliminary studies together with interpretation of new satellite imagery and topography both for local areas and for Bhutan (which I did not visit). Collaboration for structure and tectonics studies in southern Tibet has involved W.S.F. Kidd, Jixiang Li, K.D. Nelson, A. Pêcher, and B.C. Burchfiel. Collaboration for geochronologic studies in Southern Tibet is with T.M. Harrison using ion-microprobe Th-Pb techniques on monazite. My studies were conducted as part of research (Project INDEPTH) funded by the US National Science Foundation.

In Nanga Parbat in the Pakistan Himalaya, investigations over three field seasons involved structural mapping, and sampling for microstructural analyses and geochronology. Because of clear evidence for polymetamorphism in the area, both field and microstructural investigations attempt to recognise, and attribute specific tectonic event(s) to, the sense of displacement trends, and deformation mechanisms. Collaboration for structure and tectonics studies in Nanga Parbat has involved W.S.F. Kidd, M. Asif Khan, A. Pêcher, P. Le Fort and L. Seeber. Collaboration for geochronologic studies in Nanga Parbat is with D.A. Schneider using ion-microprobe

Th-Pb techniques on monazite and U-Pb techniques on Zircon. My studies were conducted as part of research (Nanga Parbat Continental Dynamics Project) funded by the US National Science Foundation.

1.3 FORMAT OF STUDY

Results from southern Tibet (28-29 °N; 89-91 °E) are presented in chapters two, three and four. Results from Nanga Parbat (in the NW Himalaya in Pakistan) are presented in chapter five. Plate 1 is a geological map of the ~N-S section that forms a part of, and was made in conjunction with, the project INDEPTH seismic traverse across southern Tibet. Plate 2 is a geological map of valleys visited in southern NPHM. An appendix with general information about rock types and structures is provided for the INDEPTH plate, which otherwise stands alone.

Chapter Two is an article published in 1996, in *Tectonophysics*, volume 260, pages 1 to 20, with co-authors William S. F. Kidd, Jixiang Li, Yongjun Yue, and Marin Clark. Observations of the STDS in the Gonto La valley in southern Tibet and along the high Himalaya to the east of Gonto La valley are presented. Based upon cross-cutting relationships, an order of events is established for the emplacement of the leucogranite that forms a large part of the Khula Kangri massif and periods of displacement along the STDS. Evidence is presented for discrete early and late periods of north-south extension (STDS displacement) separated by plutonism and apparent local shortening.

Chapter Three is an article published in 1997, in *Geology*, volume 25, pages 543 to 546, with co-author T. Mark. Harrison. A crystallisation age is presented for the Khula Kangri granite based upon Pb-Th ion microprobe dating of separated monazites performed by T. M. Harrison in collaboration. Because the Khula Kangri

granite is cut by the STDS, a new, (very young) minimum age for STDS displacement (and hence north-south extension) in this part of southern Tibet is established. The very young age indicates that a marked temporal change accompanies the left offset of the STDS (and the whole Himalayan chain) that occurs between the Khula Kangri area and Nepal/Sikkim. Possible reasons for this marked temporal change are discussed.

Chapter Four is an article submitted to *Journal of Geology* in 1998, with co-authors A. Pêcher, W.S.F. Kidd, B.C. Burchfiel and L.H. Royden. It compiles my field observations with unpublished data from other workers in the Khula Kangri area, and uses satellite imagery and topographic data to present a new map and cross-sections of the geology of the Khula Kangri massif and a second, less well-documented massif to the south, in Bhutan. There is a large regional Z-bend in the surface trace of the SDTS in this area. Although the regional structure indicated from the completed map and cross sections could suggest a repetition in the upper part of the Himalayan sequence, this is not required; a scissor fault and folding is proposed as tectonic solution.

Chapter Five is the Nanga Parbat chapter. It presents results from structural mapping around western, southern, and eastern Nanga Parbat. The principal rock types and structures are initially established in the SE, focusing in Lower Rupal Valley. These rock types and structures are then correlated through into other valleys in the east and SE, including north into the Astor Gorge area. Results are subsequently presented from Central and Upper Rupal, including the Chhichi valley. Local plutons and structures are reported, and a major NW-dipping shear zone is described. The southwestern part of Nanga Parbat is then described. Principal rock types and structures are reported and a new major E-dipping shear zone involving a partly synkinematic granite is described. This shear zone is correlated with the other major structures at NPHM. Finally, in conjunction with collaborators' geochronology,

the timing of principal structures is discussed, the two sides of Nanga Parbat are considered together and an overall tectonic model for NPHM is proposed.

CHAPTER TWO

MULTI STAGE DEVELOPMENT OF THE SOUTHERN TIBET DETACHMENT SYSTEM NEAR KHULA KANGRI. NEW DATA FROM GONTO LA.

Multi stage development of the southern Tibet detachment system near Khula Kangri. New data from Gonto La.

Michael. A. Edwards[1], William S. F. Kidd[1],
Jixiang Li[2†], Yongjun Yue[2], and Marin Clark[3††]

Tectonophysics volume, 260, pages 1 to 20

1. Department of Geological Sciences, State University of New York at Albany, 1400 Washington Avenue, Albany, NY 12222, USA

2. Chinese Academy of Geological Sciences, Baiwanzuang Rd, Beijing 100037, China

3. Institute for the Study of Continents, Snee Hall, Cornell University, Ithaca, NY, 14853, USA

† Now at: Dept. of Earth Sciences, Syracuse University, Syracuse, NY 13244

†† Now at: Dept. of Earth, Atmospheric and Planetary Sciences, MIT, Cambridge, MA 02130

2.1 INTRODUCTION

The Southern Tibet Detachment System (STDS) is a series of north-dipping, low-angle detachments, found along the north flank of the high Himalaya. It was first identified (and termed the north Himalayan normal fault) by Burg (1981), and was described in detail by Burchfiel et al. (1992). The detachment system juxtaposes Tethyan sedimentary rocks against crystalline rock of the footwall; the high Himalayan Crystalline series (HHC). Typically, the detachment system has a footwall containing several hundred metres of mylonitic rock with injections of leucogranite (Burg, 1983; Burchfiel et al., 1992). In the Everest area, significant movement on the principal detachment probably occurred between approximately 22 Ma and 19 Ma (Hodges et al., 1992). These data, taken together with an age of movement on the Main Central Thrust (MCT) constrained to ~20.9 Ma at one locality (Hubbard and Harrison, 1989), reflect a local simultaneity of N-S extension in the upper Himalaya with shortening at structurally deeper levels, (e.g. Burg et al., 1984; Burchfiel & Royden, 1985). Evidence from the western Himalaya (Herren, 1987; Searle et al., 1988) suggests that this extension developed along much of the orogen (Burchfiel et al., 1992). The term STDS is used here to mean the system which has allowed upper level extension of the Himalaya, including both the brittle detachment fault(s) (detachment *sensu stricto*; Davis et al., 1980) and any earlier related mylonitic horizons which accommodated ductile extensional deformation.

The Khula Kangri massif is part of the high Himalaya, situated north of the Bhutan frontier (fig. 2.1). It is ~100km south of the Yarlung-Zangpo suture and ~100km east of the major (~70km) plan view offset of the high peaks of the Himalayan chain termed the "Yadong cross structure" (Burchfiel et al., 1992). The Yadong cross structure is marked by the Chomolhari-Masang Kang range, which

Figure 2.1

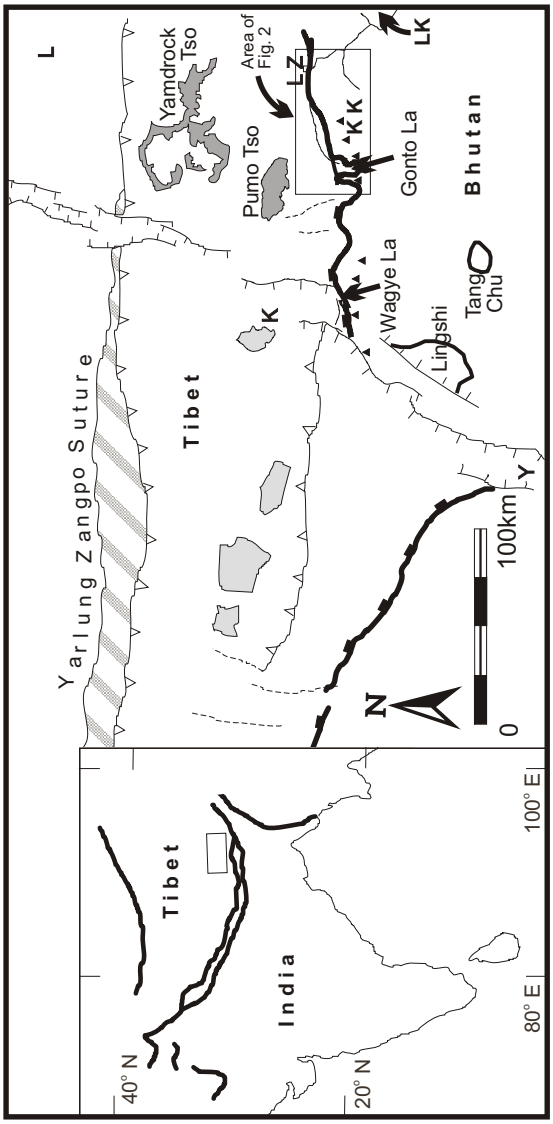

Figure 2.1 Map showing main geological features of Southern Tibet. Stripes: Zangpo suture ophiolites and sediments of Xigaze Group; light grey: leucogranites of Lhagoi-Kangri belt; dark grey: lakes; lines with single barbs: Quaternary normal faults; lines with triangular barbs: thrusts; heavy lines with boxes: approximate trace of STDS; KK, Khula Kangri massif; LZ, Lhozag; LK, La Kang. Inset shows regional location of map area (box) in which thick black lines are major tectonic discontinuities. Modified after Burg et al. (1984). [L - Lhasa; K - Kangmar; Y - Yadong]

bounds part of the N-S trending Yadong-Gulu rift system developed in response to late-Miocene to Recent E-W extension of southern Tibet (Armijo et al., 1986). The Khula Kangri massif is thought to consist mostly of the Khula Kangri leucogranite pluton (chapter appendix 2.8.1) and gneisses of the HHC (Pêcher et al., 1994), as is typical of the high Himalaya (Gansser, 1964; Le Fort, 1973). Less typical is the belt of Mesozoic Tethyan sedimentary rocks (structurally above the HHC and leucogranite) which dip south on the southern side of the massif (Bureau of Geology and Mineral Resources of Xizang (Tibet) Autonomous Region, 1993; Dietrich and Gansser, 1981; Burchfiel et al., 1992; Pêcher et al., 1994). Based upon the observations of the previous workers, the overall structure of the massif is that of a regional antiform (fig. 2.2). On the eastern side of the massif, between the town of Lhozag, to the north, and La Kang, in the south (fig. 2.2), the relationship between Tethyan Sedimentary rocks and the HHC is complex and the sequence has been intruded out in several places by the Khula Kangri pluton (Burg et al., 1984; Burchfiel et al., 1992; Pêcher et al., 1994). Here, both our observations and those of Burchfiel et al. (1992) revealed no obvious major detachment structure. Between Lhozag-La Kang and Wagye La, 80km to the west (fig. 2.1), where the STDS is last recognised (Burchfiel et al., 1992; Edwards et al., 1994), the valley of Gonto La cuts deep into the high Himalaya (fig. 2.2). We visited the Gonto La valley to address the problem presented by this change in nature of the STDS from west to east along the Tibet-Bhutan Himalaya. We were able to recognise the STDS in the Gonto La valley but unlike localities to the west (e.g. Burchfiel et al., 1992), we see evidence here for complex, multi-stage development of the STDS. Coupled with further investigation of the STDS between Lhozag and La Kang and a re-evaluation of other sparse data pertaining to the area, we present the general hypothesis that there were two distinct periods of broadly N-S extension involving the STDS in the Khula Kangri area (both Gonto La and Lhozag-

Figure 2.2

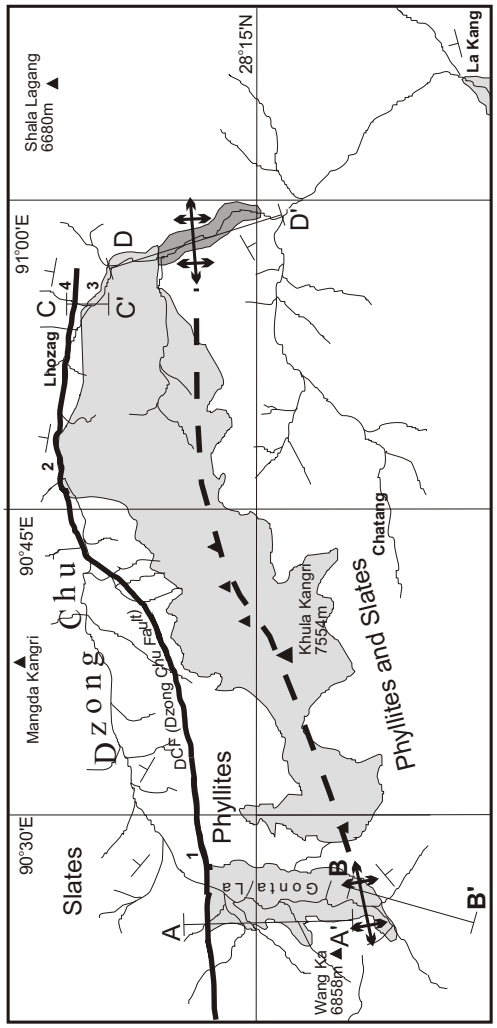

Figure 2.2 Geologic summary map of Khula Kangri area (box in fig. 2.1). Light grey: Khula Kangri leucogranite pluton; dark grey: High Himalayan Crystallines structural window to High Himalayan crystalline series; black triangles: peaks over 6500m; dashed black line: approximate trace of regional antiform; numbers: locations referred to in text. Tethyan sequences named in their approximate location. Cross section locations are shown. Some high peaks are capped by slate and phyllite (not shown).

La Kang) separated by a period of folding, major plutonism and sufficient relative uplift to renew local N-S extension, at least near Gonto La.

2.2 GONTO LA

2.2.1 Geological observations

Gonto La is a 5450m high pass through the high Himalaya between Tibet and Bhutan, located SW of Khula Kangri and north of Kanga Punzum (7500m). The main glacial valley leading north from Gonto La crosses the ENE trending line of the high Himalayan chain, where it cuts a ~13km long N-S trough deep (>2km) into the local topography. This valley we term the Gonto La valley.

The Gonto La detachment outcrops all along the central and northern parts of the Gonto La valley on both the west and east valley walls. It is a planar, low-angle, gently north-dipping (~10^{o}) normal fault. The hanging wall contains a unit of marbles and an overlying unit of phyllites. The footwall comprises leucogranite in the north and a gneissic sequence below a mylonitic leucogranite injection complex in the south (figs. 2.3 & 2.4). The detachment was visited at locations 1 and 2 (fig. 2.3). The Gonto La detachment is seen to extend from the points visited to the central portions of the Gonto La valley (fig. 2.5), rising gradually in outcrop height to the south. From south of where last seen, the detachment projects to the upper levels of Kanga Punzum (7550m, fig 4); the Bhutan frontier. From the Dzong Chu valley, the Gonto La detachment rises up to the main Khula Kangri peaks east of the Gonto La valley and, to the west, up to the three peaks of Wang Ka. Interpolation of Thematic Mapper (TM) and topographic satellite imagery with the field observations shows the low-angle, north-dipping Gonto La detachment continuing for some distance to both the east and west of Gonto La valley. In addition, west of Wang Ka, we have

Figure 2.3

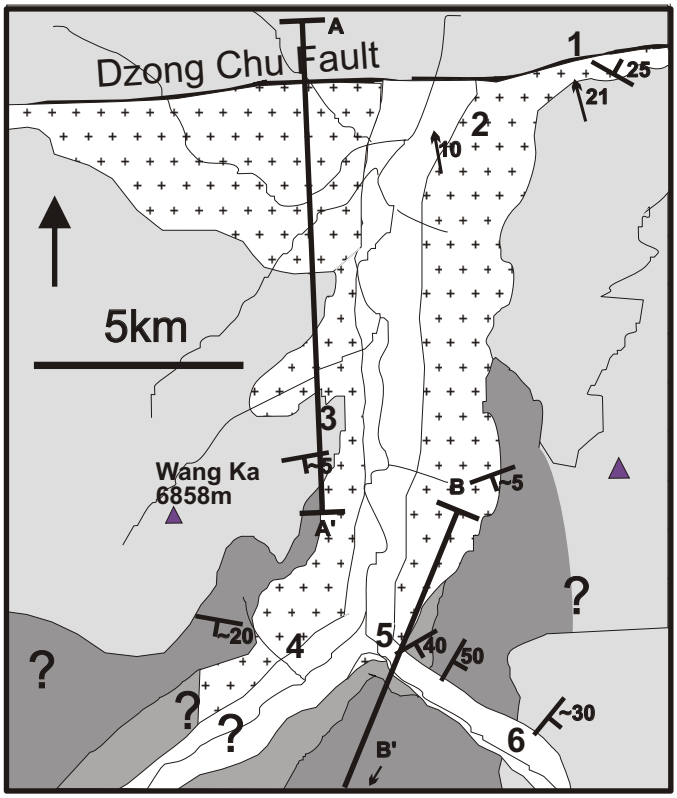

Figure 2.3 Geologic map of Gonto La valley (box in fig. 2.2). Crosses: leucogranite; light grey: Tethyan Mesozoic marble and phyllite; dark grey: injection complex; medium grey: gneiss; white: Quaternary cover and slates north of Dzong Chu fault. Numbers are locations referred to in text. Strike and dip symbols refer to foliation, arrows are lineation measurements (remote measurements are given as approximate dips). Question marks indicate specific uncertainty. A-A' and B-B' are cross section lines.

Figure 2.4

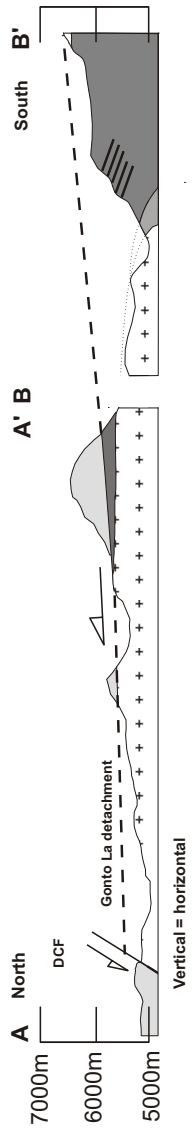

Figure 2.4 Cross Section A-A' and B-B' along Gonto La valley (located on fig. 2.3). Section A-A' is along western side of Gonto La valley, projected on to east facing line. Gap in section indicates join of two sections. Lines on south wall represent foliation within injection complex .Small unshaded area in south is snow line on north shoulder of Kanga Punzum. Shading as for fig. 2.3.

Figure 2.5a

Figure 2.5a see caption on next page

Figure 2.5b

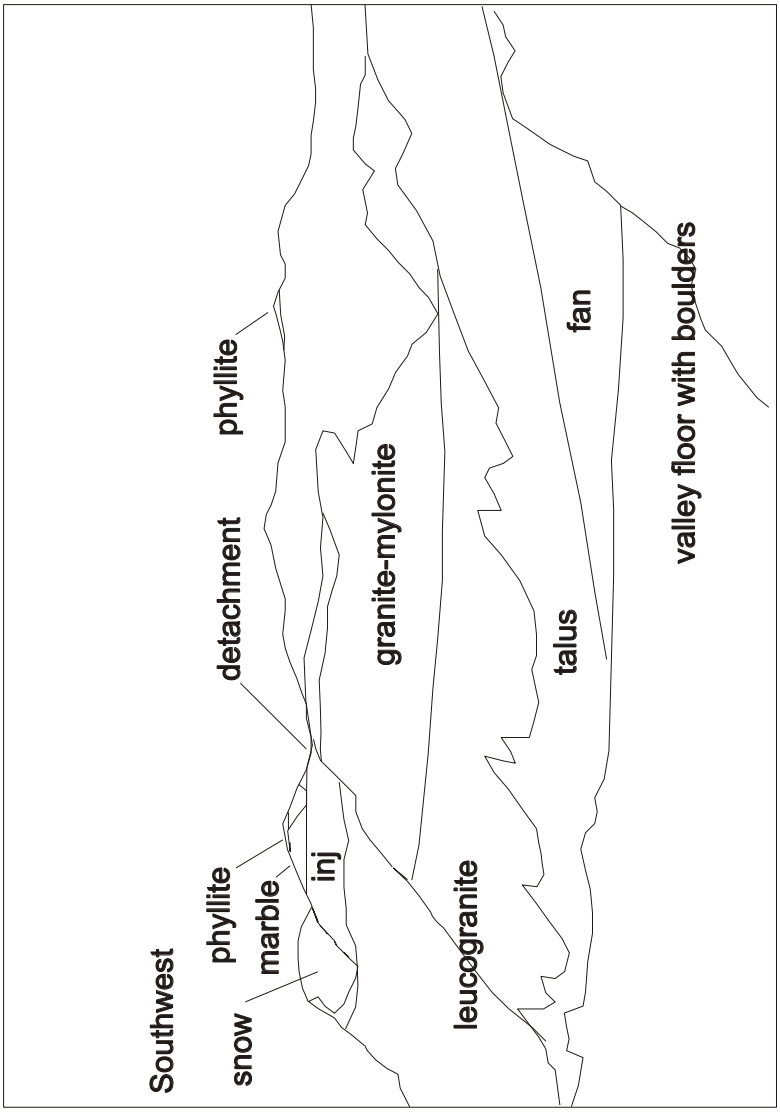

Figure 2.5b [a (previous page) & b] Photo and line drawing looking WSW from location 1 (fig. 2.3) at N end of Gonto La valley. Gonta La detachment is continuous line running across hillside, dipping approximately 10°N. Upper 300m up to detachment is granite-mylonite. Jagged cliffs in foreground are leucogranite of Khula Kangri pluton. Light and dark horizontal bands on peaks above detachment are gently north-dipping sequences of marble and phyllite respectively (described in text). Note thin outcrop of gently south dipping injection complex (inj) at location 3 (fig. 2.3), which illustrates gradual excision by both Gonto La detachment above, and pluton below. Towards south, injection complex layer systematically increases in both thickness and angle of dip (see description in text). DCF outcrops to right, outside field of view.

identified gently-dipping planar surfaces that are interpreted to be the westward continuation of the Gonto La detachment by remote observation from the SE part of Nieru Valley, east of Wagye La.

The hanging wall of the Gonto La detachment is made up of a series of gently north-dipping marbles and overlying phyllites (fig. 2.4). The phyllites may be Triassic or Jurassic in age based upon correlation along the Dzong Chu valley to the Lhozag area (fig. 2.2) where *Danubites sp*. have been found in local slates (Bureau of Geology and Mineral Resources of Xizang (Tibet) Autonomous Region, 1993). The marbles are light to dark grey and, close to the granite, contain a number of inclusions of leucogranite a few to tens of centimetres in diameter. The marble shows intense, colour-laminated structural foliation, and shows inhomogeneous deformation, with seemingly chaotic folding of the main foliation around the inclusions. The overall foliation is broadly parallel with foliation in the leucogranite in the footwall. The marble horizon tapers northward from >100m thickness at location 3 (fig. 2.3) to entire removal at location 1 (fig. 2.3). The phyllites are mostly black, reach upper greenschist facies near their contact with the marble horizon. Some contain prominent porphyroblasts of andalusite, cordierite and/or chloritoid. The phyllite extends to above present erosion level and therefore must have >400m of structural thickness. The foliation broadly parallels the detachment below.

The footwall of the Gonto La detachment contains both a main intrusive leucogranite body (part of the Khula Kangri pluton), and a gneissic sequence overlain by a leucogranite injection-bearing high strain horizon (which we term the injection complex). The detachment footwall consists mostly of leucogranite in the central portions, and exclusively of leucogranite in the northern portions. (figs. 2.2 & 2.3). In the southern portion, the gneissic sequence and the injection complex lie structurally above, and are in intrusive contact with the leucogranite (fig. 2.6). Here, the margin of the pluton cuts, at a low angle, both the foliation of the gneissic sequence and the

Figure 2.6a

Figure 2.6a see caption on next page

Figure 2.6b

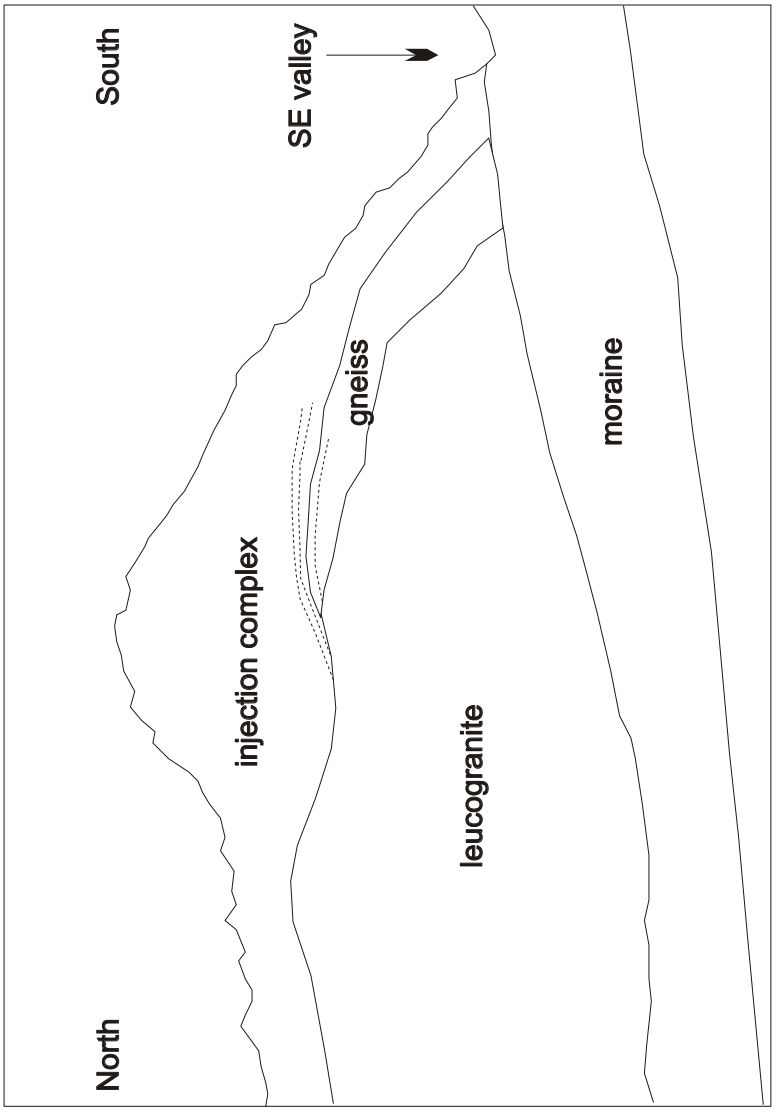

Figure 2.6b [a (previous page) & b] Photo and line drawing from location 4 (fig. 2.3) ~200m above valley floor on SW corner of main Gonto La valley looking across to entrance to SE valley (location 5, fig. 2.3). View shows intrusive southern contact of leucogranite of Khula Kangri pluton truncating the gneiss and, to left, cutting leucogranite sills which define macroscopic foliation. The leucogranite is unfoliated at this contact. This cross-cutting relationship requires that the granite post-dates development of the mylonite of the injection complex (see text). Mesozoic (?) phyllites, structurally above the injection complex, outcrop up the SE valley, out of view. The Gonto La detachment projects from where it last outcrops to the north (left) to above present erosion level. Apparent antiformal shape of foliation (dashed lines on line drawing) is distortion due to perspective.

leucogranite sills that define the macroscopic foliation of the injection complex. The profile of the foliation of both the gneiss and the injection complex, like that of the pluton margin, forms a gentle curve. It dips ~40° to the south in the southern portions of the Gonto La valley and systematically becomes more shallowly-dipping towards the central part of the valley, where the mylonitic injection complex is nearly flat-lying (fig. 2.3). This approximates the southern part of an antiformal structure, which, in the N-S section of the Gonto La valley, may be thought of as half of an open fold. Any northern section of the antiformal structure would have been truncated by the ~10^{o}N-dipping Gonto La detachment.

The leucogranite is predominantly medium-grained and contains quartz, feldspar, biotite, muscovite and tourmaline. In the northern parts of the valley (locations 1 & 2, fig. 2.2) the uppermost part of the leucogranite pluton has a strong subsolidus foliation. The foliation dips ~10^{o}N and contains a well-defined down-dip stretching lineation which is oriented 350° ±5°. This is consistent with a stretching lineation of ~25° towards 350º measured near Summit 6301 between Gonto La and Khula Kangri by Pêcher et al. (1994). The foliation displays shear bands and a mesoscopic and microscopic S-C fabric (fig. 2.7) which demonstrate top-to-north sense of shear (e.g. Berthé et al., 1979; Simpson and Schmid, 1983; Passchier and Simpson, 1986). This defines a horizon of granite-mylonite which extends down for ~300m from where the pluton is cut by the planar detachment contact with the marble and phyllite above. Shear strain increases vertically upwards towards the detachment. The remaining parts of the leucogranite pluton within Gonto La are unfoliated although mineralogically the same as the foliated portions.

The rocks of the gneissic sequence consist of both schists and gneisses of quartzofeldspathic and mafic composition. There is a continuous macroscopic foliation throughout the sequence, which changes from gently- to more steeply-dipping towards the south. Near the pluton margin, the gneisses show hornfels effect.

Figure 2.7

Figure 2.7 Photomicrograph of mylonitic horizon of leucogranite (appendix B) from location 2 (fig. 2.3) in northern Gonto La valley illustrating typical sense of shear indicators observed. Cut perpendicular to foliation, parallel to lineation (350°); crossed polars. Side of image is ~4.0mm. North is to base, south to top. Polycrystalline quartz and feldspar ribbon aggregates define S-surfaces. In lower centre, asymmetry of inclusion tails of feldspar grain and mica fish show sinistral sense of shear (top-to-north).

This includes (1) sillimanite overgrowing biotite and (2) recovery of quartz grains in areas of high strain where garnet foliation is at a high angle to the main foliation (fig. 2.8 and chapter appendix 2.8.2). Within the gneiss there are a number of cm-m wide quartz and quartz-muscovite-tourmaline veins filling steeply south- to southeast-dipping tension gash zones. The gneissic foliation is observed to bend into the tension gashes before being truncated on vein margins. The shear sense of fracture opening is top-to-south (normal sense) and is indicated by the bending of the foliation and en-echelon veins. The amount of extensional strain accumulated is minor (<1%). The fractures may be either (1) antithetic Riedel shears or (2) the result of pluton emplacement and/or antiformal folding. If they are antithetic Riedel shears, they require top-to-north displacement on the host shear zone, which is most likely the injection complex, or the Gonto La detachment, above.

Above the gneissic sequence is a high-strain horizon infested with leucogranite injection sills and dykes; the injection complex (fig. 2.6). The foliation of the injection complex (high strain horizon) has a shallower foliation dip than, and cuts, the foliation of the gneissic sequence below. Where the contact projects across the SE valley onto the back wall at the head of the main valley (fig. 2.3), the gneissic sequence attains its maximum thickness of ~200m. From here, the injection complex continues for >700m to the limit of exposure (the snow line). Approximately 4km up the SE valley from the gneiss contact, the injection complex passes to a structurally overlying phyllite sequence and, based upon the dip where last measured, we estimate the injection complex to be ~1000m thick. If the gneiss forms a xenolithic lens within the injection complex, the original injection complex thickness may be greater. Typical STDS injection complex thicknesses are <1000m (Burchfiel et al., 1992). Within the injection complex, leucogranite sills injected parallel with the foliation range in width from a few centimetres to several tens of metres and are foliated. Thinner sills are observed to be both isoclinally folded and show boudin structures. Some of the sills

Figure 2.8

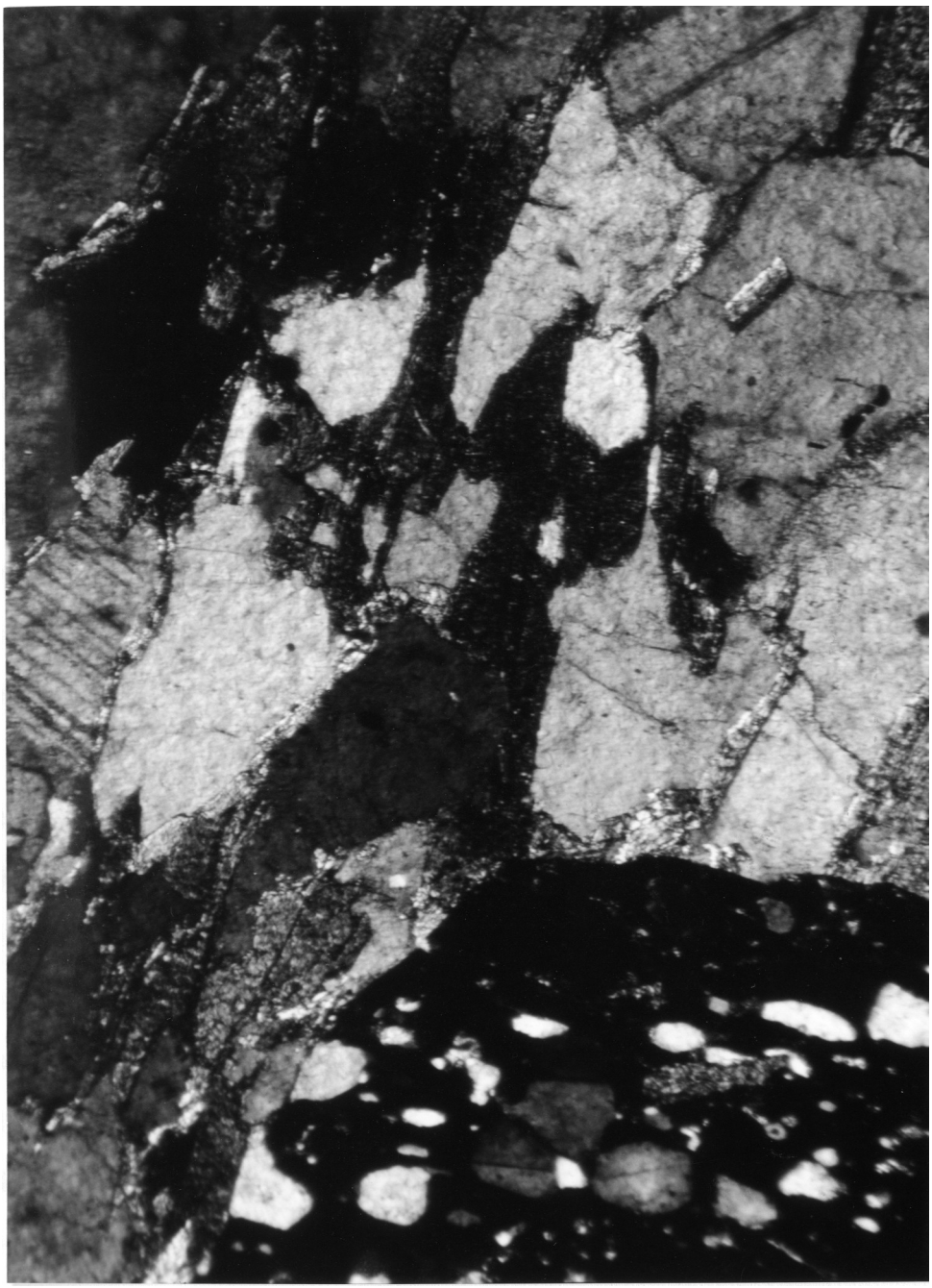

Figure 2.8 Photomicrograph of biotite-sillimanite gneiss (appendix B) near intrusive contact in southern Gonto La valley (location 5, fig. 2.3). Side of image is ~4.0mm. S_1 (in garnet grain) shows a foliation at a high angle to S_2, the gneissic foliation. Crossed polars.

are asymmetrically folded and the apparent vergence suggests a top-to-north (in present orientation, thrust) sense of shear. The high-strain horizon in which the leucogranite sills occur is a mylonite augen gneiss with a well-defined S-C fabric. The mylonite contains ubiquitous augen and boudins of feldspar and quartz (1-5 mm in diameter) forming pale, mm horizons within thicker, intensely black, biotite-rich layers. The appearance is notably different from both the gneisses and the granite-mylonite. Within the mylonitic augen gneiss, the presence of abundant cm-m thick lensoidal leucogranite layers, results in conspicuous light and dark bands which characterise the injection complex. Within the injection complex, directly below the detachment at location 3 (fig. 2.3), multiple, steep, north-dipping normal faults of a few metres offset are prominent. These are thought to be the macroscopic equivalent of narrow extensional shear-bands, developed in response to the relative northward motion of the hanging wall of the Gonto La detachment.

At the northern end of the Gonto La valley (location 1, fig. 2.2), the leucogranite and, consequently, the Gonto La detachment, are truncated by an E-W striking normal fault, dipping 22°N. This fault downthrows Mesozoic dark slates in the hanging wall against the leucogranite footwall. Here, a siliceous cataclasite about 2m thick has developed above the unfoliated granite. Within the slate, there are numerous minor extensional structures (low- and high-angle, N-dipping faults, kink and shear bands). The unfoliated nature of the leucogranite footwall discriminates this fault from a bend in the Gonto La detachment. Additionally, there is evidence a few hundred metres north of this location for a steeper DCF splay in the form of groundbreak features and float colour changes. Movement on the DCF is later than final movement on the Gonto La detachment.

At location 6 (fig. 2.3), remote observations show the injection complex overlain by a phyllite whose foliation is ~SE dipping and parallel with the foliation of the injection complex below. Based upon phyllite samples in float, some contain

cordierite porphyroblasts. From previous reports (Bureau of Geology and Mineral Resources of Xizang (Tibet) Autonomous Region, 1993; Gansser, 1981; Pêcher et al., 1994) this is part of the large belt of Mesozoic Tethyan sedimentary rocks which lie south of Khula Kangri, defining part of the broad antiformal culmination (here the southern limb) which mantles the Khula Kangri massif. TM imagery is consistent with this and shows the phyllite contact as a sharp colour contrast in the valley wall which continues along the south side of the massif to the south-dipping slates and phyllites at La Kang (Burchfiel et al., 1992). If the north-dipping, planar Gonto La detachment does continue up to Kanga Punzum (composed predominantly of HHC [Gansser, 1983]) then these phyllites must be part of the present footwall. It is possible, however, that the Gonto La detachment suddenly bends and dips south, hence forming the phyllite / injection complex contact.

2.2.2 Interpretation.

The presence of a detachment footwall containing an injection complex made up of a thick sequence of boudined, isoclinally folded, mylonitic augen gneiss with asymmetrically folded leucogranite sills fits the summary STDS appearance given by Burchfiel et al. (1992). What is different here is that the foliation of the injection complex is south-dipping. We suggest that the thick sequence of the injection complex is the horizon, originally north-dipping, on which strain was localised during earlier ductile N-S extension in this area. Rotated to north-dipping, the apparent thrust sense structural indicators give a normal sense of shear. This would then be consistent with the overall N-S extensional mechanism which led to the north-dipping Gonto La detachment. Accordingly, we propose the following series of events: 1. The thick mylonite augen gneiss of the injection complex layer was formed before the final intrusion of the leucogranite (fig. 2.9A), from N-S extension on a N-dipping horizon. This would have excised any Palaeozoic of the Tethyan sequence at Gonto

Figure 2.9

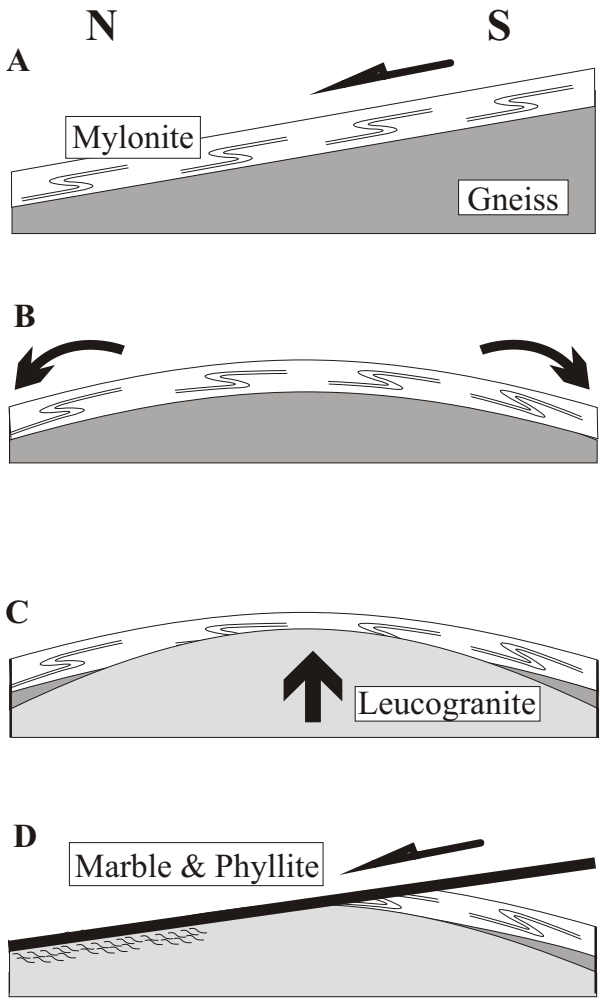

Figure 2.9 Schematic illustration of interpreted history of Gonto La area. A: early N-S extension develops thick mylonitic injection complex horizon; a ductile, normal sense shear zone above gneiss (asymmetric fold symbols are general represention of sense of shear indicators found). B: folding or other mechanism causes rotation of southern part of mylonitic horizon to S-dipping (possibly associated with leucogranite intrusion, see discussion in text). C: Emplacement of Khula Kangri pluton truncates foliation of gneiss and injection complex. D: later N-S extension causes further normal faulting (the observed Gonto La detachment) juxtaposing Mesozoic slate over leucogranite, gneisses, and injection complex. The implied hiatus in N-S extension is not required; displacement may have transferred to a structurally higher level before pluton emplacement.

La. 2. The observed south-dipping foliation has been rotated to its present position by antiformal folding (fig. 2.9B), which could be related to the emplacement of the leucogranite (fig. 2.9C). During or after emplacement, the Gonto La detachment formed (fig. 2.9D) and was active at least while the pluton cooled through solidus temperatures causing the granite-mylonite, the non-coaxially deformed marble horizon, the shear bands, and the steep normal faults.

2.3 THE DZONG CHU FAULT

The Dzong Chu Fault (DCF, Burchfiel et al., 1992) is named for the Dzong Chu (or Kuru Chu) valley, along which it outcrops (fig. 2.2). It is a north side down normal fault which dips moderately to steeply to the north. It was first recognised by Burg (1983) who regarded it as part of the STDS (Burg's "Faille Normale Nord Himalayenne"). Although for much of its length along the Dzong Chu valley, the DCF forms the contact between the Mesozoic sedimentary rocks and the Khula Kangri pluton, Tethyan sequences also make up part of the footwall, and thus it is not a detachment of the STDS *sensu classico*. The DCF is observed in outcrop at, amongst others, locations 1, 2 & 4 (fig. 2.2). Location 1 is the 22°N-dipping normal fault which truncates the Gonto La detachment. It is interpreted to be a shallowly-dipping splay. At location 2, leucogranite injected into gneiss, outcropping on the N-side of the Dzong Chu, forms the footwall of an approximately 40-50^{o}N-dipping fault plane which has brown Mesozoic slates as the hanging wall. At location 4, about 600m north of where an intrusive contact of the Khula Kangri leucogranite outcrops at location 3 (fig. 2.2 and chapter appendix 2.8.1), the DCF juxtaposes light Mesozoic slate upon dark Mesozoic slate. The fault plane dips 50-70^{o}N and the fault forms a steep gully, or notch, on each side of the main, N-trending local valley. We find it of

interest that at location 2, the hanging wall slates show no evidence of metamorphism from, or intrusion by offshoots of, the leucogranite, while the leucogranite intrusive contact at location 3 has a planar surface similar to location 2 yet is clearly not a fault plane; there is no evidence of any surface (brittle or ductile deformation horizon) within granite, or near it, within the metasedimentary aureole, which could have accommodated significant offset. The planar and steeply-dipping leucogranite intrusive contact at location 3 (fig. 2.2), may be the result of a pre-existing planar fault surface delimiting the local emplacement horizon of the pluton. A splay of the Dzong Chu fault, which outcrops ~600m to the north, would provide such a surface. This may be required based upon geobarometric data obtained by Guillot et al. (1995a) from unspecified localities in this general area ranging between 290 ±40MPa and 440±60MPa, which may imply several kilometres of throw. Additionally, this may mean there is some extensional strain not yet recognised within the aureole.

The fault contacts at locations 4 and 2 are obvious on the TM image of this region, and truncation of the black slate is also visible on the image on the east side of the foot of the Gonto La valley, immediately opposite location 1. The fault is identifiable all along the Dzong Chu valley forming a belt in places up to 10km wide that consists of both a main, continuous structure, and a number of apparently less-continuous splays. The fault can also be traced to near Wagye La, at the SE end of Nieru Valley, where a similar fault has been recognised, including conspicuous ground-break features indicative of an active fault (Edwards et al., 1994), and traced to SE Nieru, where it is observed to be cut by a N-S trending, graben-bounding normal fault (fig. 2.1). Offset on the DCF is not known but, from correlation of the two slates juxtaposed by the DCF at location 4 to where they outcrop in more-continuous sequence, net throw is estimated to be a minimum of several hundreds of metres, and previous field mapping (Burg, 1993) and the geobarometric data of Guillot et al. (1995a) suggest several kilometres.

Because the DCF cuts all other sets of structures in the area, it is interpreted to be very late, after latest movement on the Gonto La detachment and possibly coeval with minor steep E-W trending normal faults which are observed from Lhozag to La Kang.

2.4 LHOZAG - LA KANG

2.4.1 Geology

In an attempt to unravel the structurally complex nature of the STDS reported by Burchfiel et al. (1992) from their traverse between Lhozag and La Kang, and to try and correlate with the STDS seen at Gonto La, we revisited this section (fig. 2.2).

In the northern part of the section (fig.10, C-C') the Khula Kangri pluton is found in intrusive contact with N-dipping Mesozoic black shale, 600m south of the DCF. The intrusive contact outcrops discontinuously over 5-7km south from where the contact is first observed south of the DCF. The discontinuous nature of the outcrop is largely due to a series of steep (40-70^{o}) normal faults dipping both north and south. These offset the contact from a few to several tens of metres. Beyond ~10 km south from where our traverse begins (fig. 2.10), leucogranite abruptly gives way to high grade metamorphic rocks. These consist of a series of quartzofeldspathic, notably mica-poor schists and gneisses of upper amphibolite facies, with mafic-rich horizons, containing very pale quartz and feldspar augen structures. Following Burchfiel et al. (1992), we regard these as part of the HHC, and regard their exposure in the core of the broad antiform of Mesozoic Tethyan sequences as a structural window (fig 2.10, D-D').

The southern contact between the main leucogranite pluton and the HHC was not reached due to the severity of topography. Burchfiel et al. (1992) show the

Figure 2.10

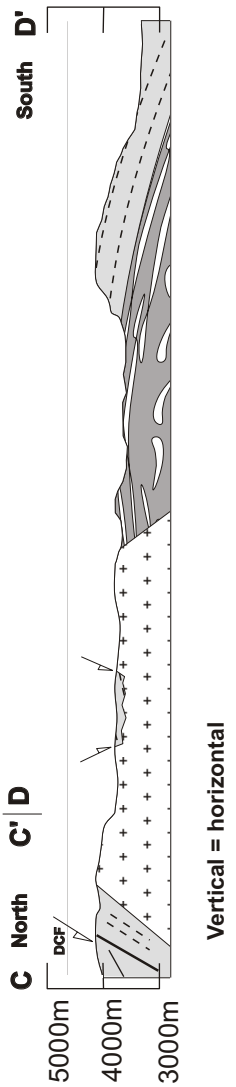

Figure 2.10 Cross section C-C' and D-D' from Lhozag to the Chatang valley confluence point, ~15km north of La Kang (located on fig. 2.2). Shows antiformal culmination with HHC exposed in central portions Light grey: Mesozoic slate (ornament indicates foliation); crosses: leucogranite; dark grey: general HHC (ornament showing shematic augen represents quartzofeldspathic augen gneiss and marbles; lens-shaped ornament is injection complex above); Injection complex is thought to be the location for the extensional horizon on which the Palaeozoic is excised.

contact to be a down-to-S normal fault. While there may have been down-to-south fault displacement here, the abruptness of the change, we hypothesise, is more likely due to a steep, southerly-dipping planar margin of the leucogranite, similar to the northern margin at location 3 (fig. 2.2). The outcrop of gneissic rock represents the crest of a large antiform which spans the section from Lhozag to ~10 km north of La Kang. (fig. 2.10). To the North, the schistosity of the Mesozoic slates and phyllites (and observed portions of the leucogranite contact) changes from gently to steeply north-dipping. To the south, the gneissic layering and overlying sedimentary sequences change dip from gently to steeply south-dipping.

To the south, lying structurally above the gneissic layer, is a series of leucogranite injections within a lower-grade amphibolite facies, mica-bearing schist sequence whose foliation is south-dipping. Structurally above this is a thick sequence of south dipping Mesozoic slates. Within the slates are multiple, steep (40° to 70°N) normal faults, similar to those found to the north. We were unable to determine if the contact between the slate and the leucogranite injection complex that is structurally above the HHC window is an old, now south-dipping detachment surface (*sensu lato*), due to inaccessibility of critical outcrops. Burchfiel et al. (1992) infer that the leucogranite injections below the phyllite and slate sequence have intruded out a major extensional horizon which pre-dates the development of the present antiform.

Our detailed field investigation was terminated here but Burchfiel et al. (1992, fig. 40) report synformal folding of the Mesozoic slate further to the south and, presumably, folding of the underlying, pre-existing detachment (as suggested on the cross-section), which causes the sequence to become N-dipping in the area of La Kang. In this area, the north dipping Mesozoic slates lie upon the broad planar top of an injection complex above leucogranite. From detailed study in the area of La Kang, Burchfiel et al. (1992) suggest this to be a further outcrop of the extensional horizon inferred at the HHC structural window.

2.4.2 Interpretation

The present juxtaposition of Mesozoic sedimentary rocks on the HHC requires excision of the entire Palaeozoic section of the Tethyan sequence through some process and therefore we, as do Burchfiel et al. (1992), interpret the schist sequences to represent a horizon that is a part of the STDS that has enjoyed enough N-S extension to remove the Palaeozoic. The antiformal folding must, therefore, also fold the inferred earlier detachment. A south-dipping sequence of Mesozoic rock upon a gently folded detachment is very similar to what is observed in southern Gonto La and we consequently infer the early sequence of events seen at Gonto La to have occurred at Lhozag-La Kang; namely (1) early N-S extension which generated a high strain horizon and excised the Palaeozoic sequences, (2) folding of the horizon, and (3) later intrusion of the Khula Kangri leucogranite pluton which, as for Gonto La, intrudes out parts of the older detachment horizon. The plutonism may or may not be related to the folding.

2.5 THE STDS IN BHUTAN

The ~70km plan view offset in the high Himalayan crest between Nepal and Bhutan (fig. 2.1), represented by the Yadong-Dogen rift, includes an associated offset of the STDS but not of the MCT/MBT (Nelson et al., 1995). Surface exposure of HHC per unit length of orogen is accordingly greater in Bhutan. There are, however, two outliers of Palaeozoic Tethyan sedimentary rock in Bhutan (fig 2.1), the Lingshi and Tang Chu areas (Gansser, 1983). These contain fossiliferous limestones, slates and quartz conglomerates which characterise passive margin sequences deposited in shallower water than the extensive Mesozoic black slates of the Khula Kangri area. At Tang Chu, trilobite- and brachiopod-bearing Devonian limestones lie <500m above

sillimanite gneisses intruded by leucogranite (Gansser, 1983, his fig. 54). We infer that the low grade Palaeozoic sedimentary rocks are juxtaposed upon higher grade HHC by a normal fault, and we offer the hypothesis that they represent klippen of Palaeozoic Tethyan sequences overlying an early horizon of the STDS. This is consistent with well-documented outcrop of the STDS along strike to the west (e.g. Everest, Dingye, Pali), where Palaeozoic Tethyan sedimentary sequences are also found in normal fault contact with the underlying HHC (Burg, 1983; Pêcher, 1991; Burchfiel et al., 1992; Guillot et al., 1993; Lombardo et al., 1993; Wu et al., 1995).

2.6 DISCUSSION

2.6.1 Gonto La

The close relationship between leucogranite emplacement and extensional shear zones is well-displayed in the high Himalaya (e.g. Burg, 1984; Pêcher, 1991; Gapais et al., 1992), and complexities of shape due to syn-extensional laccolith injection (e.g. at Manaslu, Guillot et al., 1993) have been demonstrated in analogue modeling (Roman-Berdiel et al., 1995). We are unable, however, to constrain the specific mechanism that has operated at Gonto La. The rotation of the older extensional horizon at Gonto La may be due to isostatic rebound of the footwall of a low angle fault (e.g. Davis, 1983; Wernicke and Axen, 1988; Block and Royden, 1990) as has been shown to occur in core complexes both with syn-extensional plutonism (e.g. Crittenden et al., 1980; Brun and Van Den Driessche, 1994; Lister and Baldwin, 1994) and without (e.g. Lister and Davis, 1989; Davis, 1994). Timing of any early plutonism is not constrained, and a core complex model can describe the history before final pluton emplacement insofar as a south dipping early horizon is predicted to accompany a northward directed hanging wall (e.g. Lister and Davis, 1989, fig.

20d, or Brun et al., 1994, fig. 2.4). The later stages of plutonism at Khula Kangri are well-constrained, however: The present southern margin cooled through solidus temperatures after motion on the early high strain horizon at Gonto La had ceased. This is reflected by the absence of foliation in the pluton at the intrusive contact at location 5 (fig. 2.3) and by the absence of evidence for non-coaxial flow in the adjacent gneiss. These field relationships therefore eliminate the following scenarios for Gonto La: 1. a core complex model for the overall history; 2. the possibility that the pluton acted as an obstacle around which the deformation horizon had to bend; 3. any concept of "ballooning" by the rising pluton, previously suggested by Edwards et al. (1995). This key field relationship does not, however, exclude syn-kinematic plutonism and folding in a contractional scenario (e.g. Hutton and Ingram, 1994). A contractional setting has been proposed for plutonism synchronous with thrusting and thickening due to the MCT hanging wall in Bhutan (Davidson et al, 1995; Hollister et al, 1995). The Khula Kangri pluton may therefore be emplaced in a large ramp anticline in the hanging wall of a south directed thrust. Any such period of shortening might suggest a hiatus in N-S extension in the area, but this is not required; extension may have been localised upon structurally higher levels (i.e. the Gonto La detachment) before or during pluton emplacement.

2.6.2 Lhozag-La Kang

N-S extension which post-dates the emplacement of the Khula Kangri pluton (and accompanied minor folding and relative uplift in the area) has been accommodated at Lhozag-La Kang, at least in part, by minor offset on a series of steeply-dipping normal faults. We did not recognise, however, a major low angle normal fault equivalent to the Gonto La detachment. Burchfiel et al. (1992) proposed that the Khula Kangri pluton had a final period of emplacement in the area of Lhozag after the last movement on the local STDS horizon. Our observations at Gonto La

support this hypothesis, insofar as the pluton intrudes the early, now-folded part of the inferred extensional horizon of the STDS both at Gonto La, and at Lhozag-La Kang. The question of whether there is a late detachment at Lhozag-La Kang remains. We identify three possibilities: (1) No late detachment developed at Lhozag-La Kang, perhaps due to an insufficient local topographic gradient (the HHC outcrops at a lower elevation than in Gonto La valley, and surrounding present day topography is generally lower). Post-plutonism, N-S extension (less than at Gonto La) was accommodated mostly by offset on the steep normal faults. (2 & 3) A late detachment developed but was restricted to the slate sequences and is now above present erosion level. It is not seen where it projects to the north as either (2) downthrow on the DCF has dropped it to below present erosion level, or (3) it has been cut out by later plutonism in the north part of the Lhozag - La Kang section (near the DCF), The last possibility requires a diachroneity in the late history of either general pluton emplacement or movement on the detachment.

We tend to favour the first suggestion (no late detachment at Lhozag-La Kang) as the hypothesis is consistent with the idea that the development of the STDS may be diachronous and show punctuated activity. It is also consistent with preliminary observations from the high country of Khula Kangri (Pêcher et al., 1994), where lineation trends seen within the leucogranite are identical to that observed at Gonto La and yet, singularly, no detachment was observed.

2.6.3 Regional Relationships

Figure 2.11 shows a cartoon which illustrates the main features we have discussed regarding the relationship of the STDS between Tibet and Bhutan. The Tethyan outliers in Bhutan are shown as klippen (see above), underlain by segments

Figure 2.11

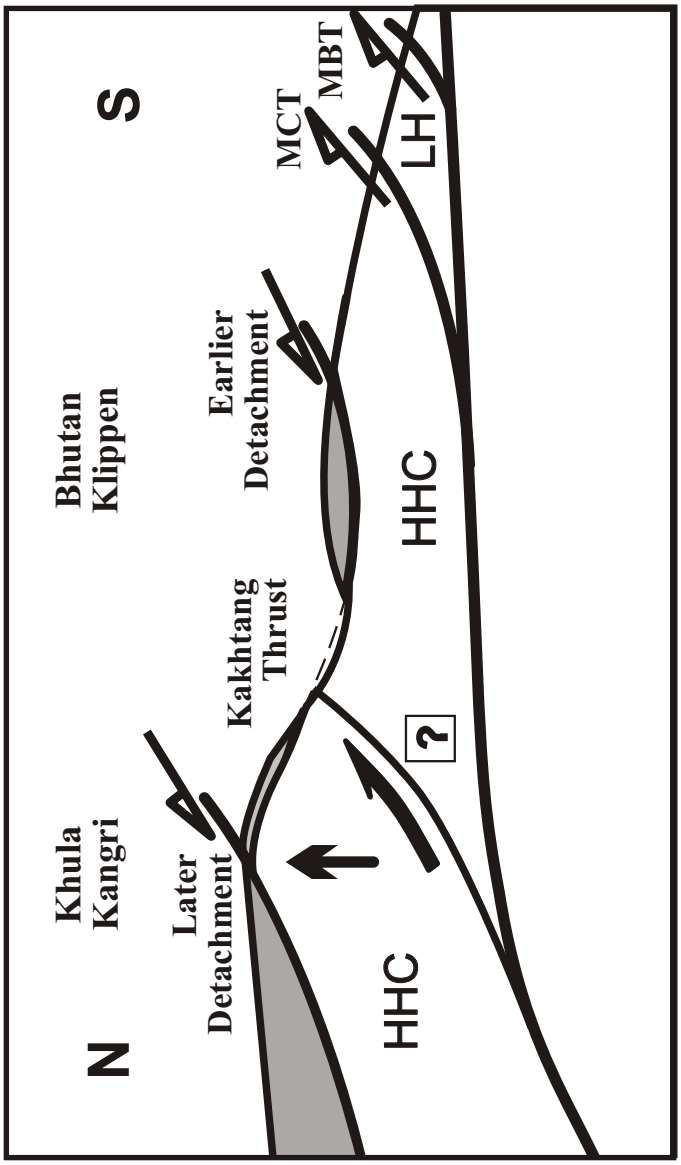

Figure 2.11 Cartoon crustal section to show hypothesis of large scale relationship between early and late detachments in southern Tibet and Bhutan. Grey shade: Tethyan sedimentary sequences; HHC, High Himalayan crystalline series; LH, Lesser Himalayan sequences; heavy lines: faults. Half-arrows show direction of relative offset of hanging wall. Large half arrow and full arrow represent general mechanism of rise of magma and uplift relative to lower Bhutan. Kakhtang thrust is suggestively added as one of the possibilities for a general magma pathway, relative uplift and folding of earlier STDS horizon(s) (see discussion in text). Footwall and hanging wall thicknesses are not intended to be accurate representations.

of an early detachment, and are broadly equated with the folded early STDS horizons of Gonto La and Lhozag-La Kang. For simplicity, this is shown as one structure, although the relationship could well be more complex. A later detachment (the Gonto La detachment) is shown truncating the folded, earlier detachment.

Assuming the development of a new topographic high to initiate movement on the younger detachment (Burchfiel and Royden, 1985), and assuming close association between plutonism and uplift (see England and Molnar, 1993, for a partial review) we suggest that, if the Khula Kangri pluton is a notably younger structure (chapter appendix 2.8.1), the Bhutan Himalaya represents a later topographic front. It is likely some structure exists beneath Khula Kangri (and Kanga Punzum) area to account for the plutonism and any relative uplift. Additionally, the folding of the earlier detachment in the Khula Kangri area may be similarly related to the relative uplift. The Kakhtang thrust in Bhutan, documented by Gansser (1983), is a major crustal feature which outcrops <20km south of Kanga Punzum. This may be a structure on which late shortening has allowed relative uplift of the Khula Kangri - Kanga Punzum area, and which has provided a source for local leucogranite generation (e.g. Le Fort, 1981) and/or a pathway to bring the leucogranite up to emplacement levels (likely only if all magmatism is part of the same event, e.g. Deniel et al., 1987). Melt-present thrusting has been reported from central Bhutan (Hollister et al., 1995), and substantial migration of melt into the Khula Kangri area may have occurred by this mechanism. We note the Kakhtang thrust would then be out-of-sequence with, and cut, the older STDS horizon. Alternatively, but we think less likely, is a horse or steep frontal ramp at depth on the MCT/MBT sole, of enough magnitude to give a crustal-scale ramp anticline that provides local uplift (e.g. Nelson et al., 1995).

2.6.4 Estimates of strain

In Gonto La valley, based upon the absence of any part of the injection complex or leucogranite in the hanging wall, relative displacement on the Gonto La detachment fault is >15km (assuming a net slip direction of 350°); the distance from the DCF to where phyllite is first seen in the footwall. If the Gonto La detachment occurs in the Kanga Punzum massif, and there represents the HHC / Tethyan sequence junction, fault displacement is >20km. We cannot estimate horizontal extensional strain accommodated by the 300m thick granite-mylonite horizon below the detachment (before development of brittle strain features), as cooling history for the Khula Kangri pluton is unconstrained. 20km is less than the 35km minimum relative displacement for the Chomolungma detachment at Mt Everest determined by Burchfiel et al. (1992), however, the Gonto La detachment appears to be restricted to Mesozoic rocks. Very speculatively, assuming a Gonto La detachment angle of 10° and 20km fault offset and a constant displacement vector, a vertical displacement of ~3.5km is indicated. Added to an estimate of the excised Palaeozoic, based upon the section near Nyalam and Everest, of ~4km (Burchfiel et al., 1992), or perhaps more (Lombardo et al., 1993), net throw is consistent with the Burchfiel et al. (1992) estimate of >5km for the Chomolangma detachment. When added to the (unmeasured) amount of displacement represented by the exhumed HHC, net throw may approach the ~18km calculated from Herren (1987) for the Zanskar Shear Zone,

At Lhozag-La Kang we estimate the net throw of the series of post-plutonism steep faults is <1km. This is small relative to the estimates of strain at Gonto La. Assuming no late detachment or diachroneity in final plutonism, the difference in net throw could indicate (1) a strain gradient, decreasing to the east, or/and (2) differential slip on the DCF.

2.6.5 Timing

Middle to late Miocene cooling ages have been determined for the Khula Kangri pluton (Debon et al., 1985; Maluski et al., 1988; Guillot et al., submitted; chapter appendix 2.8.1). These are substantially younger than cooling ages typically obtained for leucogranites in the central high Himalaya (see Burchfiel et al., 1992, for a review). The Gonto La detachment cuts the Khula Kangri pluton and we therefore infer that the Gonto La detachment was probably active during middle to late Miocene times. If so, this is the youngest age yet recognised for movement along a main detachment of the STDS.

A minimum age for cessation of extension along earlier detachment horizons south of the Khula Kangri antiformal trace is represented by the age of relative uplift of the Khula Kangri massif which accompanies folding of such horizons (this is assuming a given STDS horizon remains N-dipping whilst active). A probable middle to late Miocene age is indicated by the field relationships. We have suggested that the early STDS horizons may be more closely related to the STDS west of the Yadong cross structure than to the Gonto La detachment. This is also supported by plutonism at ~22Ma cutting main detachments at Rongbuk (Hodges et al., 1992) and Manaslu (Harrison et al., 1995). We emphasise however that this is not required by our field observations, and that the hiatus in N-S extension observed at Gonto La may be minimal.

Field relationships near Annapurna in Nepal have been interpreted to suggest that approximately N-S extension on the local detachment gave way to E-W extension between ~17 and 14 Ma (Coleman and Hodges, 1995). It has consequently been suggested that this time period represents the onset of E-W extension for all of southern Tibet and the cessation of STDS activity in the form of N-S extension related to Himalayan topographic collapse (Searle, 1995, Coleman and Hodges, 1995). It is not clear to us if the onset of E-W extension is indeed coupled to the end

of STDS activity, but the observation that the Gonto La detachment cuts the apparently middle to late Miocene Khula Kangri pluton is not consistent with the suggestion that all STDS movement ended between 17 and 14 Ma. More importantly, we have shown the complexity of STDS extension in this area, involving multi stage detachment development interrupted by folding. Additionally, previous workers have shown that the STDS may (1) involve substantial wrench motion, (2) locally consist of more than one structure, and (3) be laterally discontinuous (Pêcher, 1991; Burchfiel et al., 1992; Lombardo et al., 1993; Guillot et al., 1993; Hodges et al., 1994). We therefore stress that the southern Tibet detachment system is a complex system of detachment faults of varying periods of activity which cannot be regarded as one continuous, simple planar structure. Moreover, it is unlikely that a single portion of the STDS can give an unequivocal measure of such things as the change of the horizontal stress field in southern Tibet, in spite of suggestions to the contrary (Searle, 1995).

2.7 CONCLUSION

The valley of Gonto La provides the best observation to date of the STDS east of the Yadong cross structure offset of the high Himalaya. The Gonto La detachment is a planar, low-angle north-dipping, normal fault which juxtaposes Tethyan sequences over the middle to late Miocene Khula Kangri leucogranite pluton. The Khula Kangri leucogranite pluton has one of the youngest ages in the main belt of the HHC. Because the Gonto La detachment cuts the pluton, it represents very late N-S extension in this area. The N-S extension shows a strain history from leucogranite sub-magmatic fabric development in the main detachment footwall to truncation of the detachment by the steeper, brittle Dzong Chu fault. The Khula Kangri

leucogranite cuts the S-dipping high-strain horizon in southern Gonto La valley after cessation of extension on this horizon. The overlying, also south-dipping Tethyan sequences are inferred be included in the footwall of the Gonto La detachment. The amount of HHC exhumed by the present Gonto La detachment pivots on whether our hypothesis that there are Tethyan sedimentary rocks in the footwall is correct (minor exhumation), or whether the detachment is tightly folded in southern Gonto La and the Tethyan rocks are in the hanging wall (major exhumation). The question of whether there can be a significant hiatus in N-S extension in this area is also central to this hypothesis. The S-dipping, high-strain horizon and Tethyan sequences at Gonto La are correlated to Lhozag-La Kang where rocks of the HHC are exposed below Mesozoic rocks, and the Palaeozoic is excised. Our observations indicate the STDS is a complex system of detachment horizons, and not a simple horizon with a restricted age of activity.

2.8 CHAPTER APPENDICES

2.8.1 The Khula Kangri pluton

The Khula Kangri pluton is a phaneritic leucogranite, . It outcrops in the Gonto La valley and at various localities around the Khula Kangri massif (fig. 2.2). We interpret the massif to be underlain by a large leucogranite pluton with a minimum areal extent of ~50km x 15km. The pluton has been determined to have a depth of emplacement of about 12km (Guillot et al., 1995a) similar to Himalayan leucogranites in Nepal (Guillot et al., 1995b).

The intrusive contact of the leucogranite at location 3 (fig. 2.2) has an extremely steep metamorphic gradient; <70m away from the contact, black slate shows no obvious effects of the intrusion. The metasediment at the intrusive contact is

in (or near) amphibolite facies; a biotite-muscovite-garnet fine-grained schist with 50%-60% injection material is seen within 5m of the contact. The relatively thin aureole of this intrusive contact, compared with the regional size of the pluton, may be the result of either (1) a later, local phase of leucogranite emplacement or (2) unrecognised extensional shear across the margin.

K-Ar analyses: Debon et al. (1985) determined an isotopic cooling age for the Khula Kangri leucogranite of 13.3 Ma ±1.0 based upon two muscovite samples. $^{40}Ar/^{39}Ar$ analyses: Maluski et al. (1988) obtained ages of 10.9 and 10.8Ma (muscovite) and 10.7 Ma and 11.4 Ma (biotite) from two samples near Lhozag. Guillot et al. (submitted) report muscovite ages of 10.7-11.1 Ma and biotite ages of 11.6-13.0 Ma. The large contrast in $^{40}Ar/^{39}Ar$ cooling ages may be due to techniques of analytical and statistical error calculations (e.g. Harrison and Mahon, 1995). The range of ages probably is close to the crystallisation age. This is because sample locations (for those that are known) are near the intrusive pluton margin where the effects of rapid cooling are expected to cause prompt closure of micas to argon diffusion (McDougal and Harrison, 1988). Significant rapid cooling of the leucogranite may additionally have been through extensional unroofing along the Gonto La detachment (e.g. Pan and Kidd, 1990).

2.8.2 Lithological and structural descriptions

2.8.2.1 Granite mylonite

Mesoscopic fabric: Down dip stretching lineation is 5° towards 350°±5°. Shear bands dip 30°N ±5° overprinting S-C fabric. Microscopic fabric: sections normal to foliation and parallel to lineation show S-C fabric. Top-to-north sense of shear is reflected by S/C fabric, by asymmetry of clasts defined by dynamically recrystallised tails, and by pressure shadows. Such is characteristic of a granite-mylonite (Berthé et al., 1979; Simpson and Schmid, 1983; Passchier and Simpson,

1986). Later shear bands are also apparent, and also demonstrate top to north sense of shear. Towards the top of the deformation horizon (metres from the marble layer) microstructures are composed of quartz laminae anastomosing around lesser-deformed augen of feldspar which suggests strain here is greater (e.g. Behrmann and Mainprice, 1987).

2.8.2.2 Gneiss

Mesoscopic fabric: The foliation is defined by biotite- and/or hornblende-rich layers. Foliation dips range from 40° towards 150° at the pluton margin (location 5, fig. 2.3) to 50° towards 120°, ~200m up the SE Gonto La valley. There is an intermittently-developed biotite stretching lineation, plunging towards 170°±30°. The structurally lowermost portions of the sequence are in intrusive contact with the pluton. Microscopic fabric: Many examples of sillimanite replacing biotite. This is interpreted to be a hornfels effect from the intrusion. Closer to the pluton margin are equant, low-strain grains of quartz. Grains observed are only modestly elliptical and display a small size range. The quartz grains occur amongst common (<2mm) garnets displaying bands of inclusions, typically non-parallel to the gneissic foliation (see fig. 2.8), perhaps due to rotation from prolonged strain.

CHAPTER THREE

WHEN DID THE ROOF COLLAPSE? LATE MIOCENE NORTH - SOUTH EXTENSION IN THE HIGH HIMALAYA REVEALED BY TH-PB MONAZITE DATING OF THE KHULA KANGRI GRANITE

When did the roof collapse? Late Miocene north - south extension in the high Himalaya revealed by Th-Pb monazite dating of the Khula Kangri granite

Michael. A. Edwards[1], T. Mark. Harrison[2]

Geology volume 25, pages 543 to 546

1. Department of Geological Sciences, State University of New York at Albany, 1400 Washington Avenue, Albany, NY 12222, USA

2. Department of Earth and Space Sciences and Institute for Geophysics and Planetary Physics, University of California, Los Angeles, California 90024

3.1 INTRODUCTION

The Himalayan mountains and Tibet are the prototypical products of continental collision and have been termed the "roof of the world" (Le Fort, 1975). Surprisingly, perhaps, two distinctive features of this textbook example of collisional tectonics are extensional and represent collapse of this "roof"; the Southern Tibet detachment system (Burg et al., 1984; Burchfiel et al., 1992) accommodated north directed Himalayan extension whereas the north - south trending rifts of southern Tibet accommodated east - west extension (Armijo et al., 1986; Harrison et al., 1995a). Knowing the timing of both these features improves our understanding of the India-Asia collision and the evolution of both the Himalaya and the Tibet plateau.

Arguably the two major Himalayan structures are the Main Central thrust and the Southern Tibet detachment, continuous for >2000 km along the orogen (Gansser, 1981; Burchfiel et al., 1992). The former probably accommodated between 150 and ~500 km of north - south India and Asia convergence (e.g., Schelling and Arita, 1991), whereas the latter allowed north directed upper Himalayan extension (Burg et al., 1984; Herren, 1987; Searle et al., 1988; Burchfiel et al., 1992; Edwards et al., 1996). Burg et al. (1984) first suggested synchronous detachment extension and Main Central thrust contraction. This is consistent with more recent chronometric data for both structures: the Main Central thrust Between Zanskar and eastern Nepal (Fig. 3.1A), probably moved significantly during the early Miocene, ~24 - 19 Ma (Schärer, 1984; Hubbard and Harrison, 1988; Coleman and Parrish, 1995; Noble and Searle, 1995; Harrison et al., 1995b). In this same area, dating of plutons and pods of leucogranite that are prekinematic, synkinematic, and postkinematic to the basal Southern Tibet detachment indicate it was active ~25 - 18 Ma (Burg et al., 1984; Le Fort et al., 1987; Coleman and Parrish, 1995; Hodges et al., 1995; Harrison et al.,

Figure 3.1A

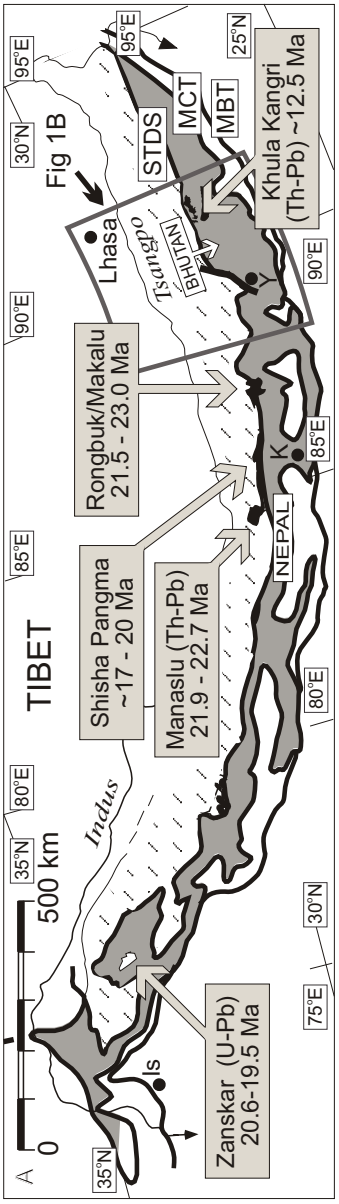

Figure 3.1A Tectonic map of Himalaya (after Gansser, 1983; Pêcher, 1991). White: Lesser Himalayan sequences. Grey: Greater Himalayan crystalline sequence. White with dashed hatch: Tethyan sedimentary sequence. Black areas adjacent to arrows: high Himalayan granite plutons. Boxes with arrows locate specific crystallization ages of granites (from west to east, sources are: Noble and Searle, 1995; Harrison et al., 1995b; Searle et al., 1997; Harrison et al., 1995b; this study). STDS is southern Tibet detachment system; MCT is main central thrust; MBT is main boundary thrust.

1995b; Noble and Searle, 1995; Searle et al., 1997). The crustal anatexis (partial melting) responsible for these leucogranites may well be due to Main Central thrust motion (Le Fort et al., 1987), north directed extension is likely a result of orogen collapse (Burg et al., 1984), and there is a marked association between plutonism, high topography, extremity of slope, and the detachment system (Burg, 1983; Molnar et al., 1993; Edwards et al., 1996; Fielding, 1996). It is now generally recognized, therefore, that the main high Himalayan events involved (1) a major period of Main Central thrust movement, (2) leucogranite generation and emplacement, (3) attainment of critical topography and/or stress in the orogenic wedge, and (4) unroofing via significant north directed extension that, between Zanskar and eastern Nepal (Fig. 3.1A) occurred prior to ca. 20 Ma.

Between Nepal and Bhutan (Fig. 3.1, A and B), both the crest of the high Himalaya and the Southern Tibet detachment are left laterally offset >70 km (Burg, 1983; Burchfiel et al., 1992; Wu et al., 1995; Fielding, 1996) by a feature termed the Yadong cross structure (Burchfiel et al., 1992). The Main Central thrust is not offset however, giving a greater surface exposure of high grade detachment footwall rocks in Bhutan relative to Nepal (Gansser, 1981, 1983; Schelling and Arita, 1991). This change across the Yadong cross structure, and others (e.g. differing generations of kinematic structures), have been noted before (Burchfiel et al., 1992; Edwards et al., 1996), however, no clear constraints hitherto existed for any significant geochronologic difference. Existing data for Bhutan leucogranites include a broad suite of cooling ages from ~11 - 18 Ma (Dietrich and Gansser, 1981; Debon et al., 1985; Villa and Lombardo, 1986; Maluski et al., 1988; Ferrara et al., 1991), but no crystallization ages. We report here the first crystallization age for a leucogranite found in the Tibet-Bhutan high Himalaya, the Khula Kangri granite, and show that there is an abrupt younging across the Yadong cross structure.

Figure 3.1B

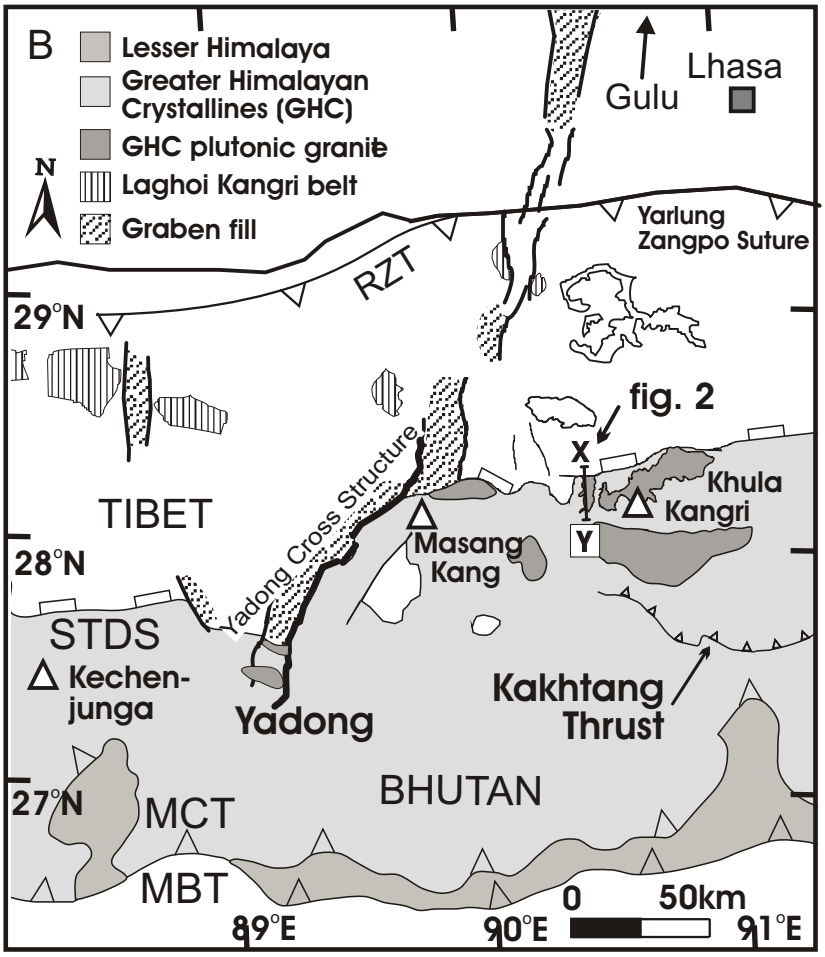

Figure 3.1B Tectonic map of area around southern Yadong-Gulu rift system (after Gansser, 1983; Burg, 1983; Burchfiel et al., 1992; Edwards et al., 1996). White (between STDS and suture): Tethyan sedimentary sequence. Heavy north - south trending lines: normal faults due to east - west extension. White triangles: major peaks. Yadong Cross structure is represented by ~70 km offset of high peaks and trace of STDS. Gulu, (at north end of Yadong - Gulu rift) is ~100 km north - northeast of arrow.

3.2 LOCAL GEOLOGY

The Khula Kangri granite is a high Himalayan pluton >750 km², located near the Bhutan frontier. It is a typical high Himalayan two-mica (± tourmaline) leucogranite, truncated by the Gonto La detachment (Fig. 3.2) that, in classic fashion (Burchfiel et al., 1992), places Tethyan metasedimentary rocks over rocks of the Greater Himalayan crystallines (Edwards et al., 1996). An ~300-m-thick horizon of granite mylonite lies directly below the detachment; strain magnitude decreases downward (Edwards et al., 1996). Based upon hanging wall - footwall correlations, the Gonto La detachment accommodated a minimum of 15 km of displacement after emplacement of the Khula Kangri granite, and probably much more (Edwards et al., 1996). For want of a better constraint, we take the Himalayan convergence rate of 10-15 mm/yr (Lyon-Caen and Molnar, 1985) as a displacement rate, for the detachment, requiring it to remain active for 1-2 m.y. following granite emplacement, given the mapped minimum displacement of 15 km (Edwards et al., 1996). Detailed mapping shows that the Southern Tibet detachment continues west to where it is cut by, and hence is older than, one of the north trending rifts that represent east - west extension of the plateau: the Yadong-Gulu rift (Edwards et al., 1996).

3.3 ANALYTICAL TECHNIQUES

We separated monazite from a sample (IE-26) obtained from the lowermost part of the granite mylonite underlying the detachment (Fig. 3.2) and measured 208Pb/232Th ages using the CAMECA ims 1270 ion microprobe at UCLA. Details

Figure 3.2

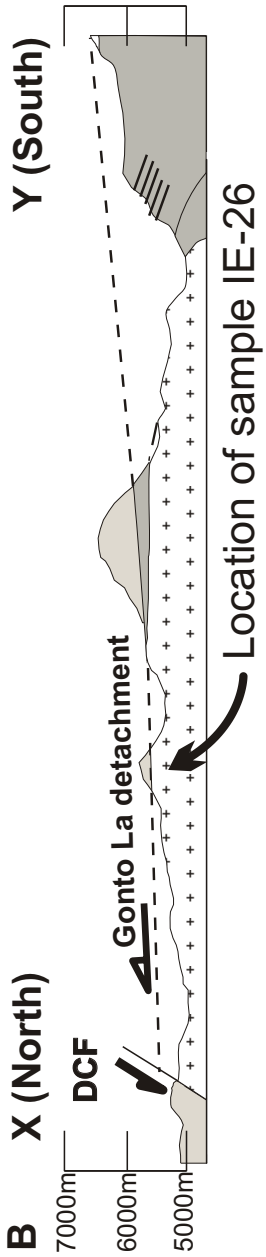

Figure 3.2 Generalized cross section (x-y) through Gonto La valley. Plus pattern is Khula Kangri granite. Darker shading is general Greater Himalayan crystalline sequence. Lighter shading above detachment is Tethyan sedimentary sequence. DCF is Dzong Chu normal fault. Location of sample IE-26 is immediately below ~300 m - thick granite-mylonite horizon which is below Gonto La detachment. Half - arrows show relative movement direction of fault hanging walls. After Edwards et al. (1996).

of our analytical methods are summarized elsewhere (Harrison et al., 1995b). A mass resolving power of about 4500 is adequate to separate all molecular interferences (mostly light rare earth element (PO2)+) in the 204 to 208 mass range, and instrumental mass discrimination of Pb isotopes is not detectable. Ages are determined relative to monazite standard 554, which yields a 208Pb/232Th age of 45 ± 1 Ma. The precision of the method is not limited by counting statistics but by the reproducibility of the standard calibration curve which is typically ± 1% - 2%. Advantages of this approach over conventional U-Pb dating of Tertiary monazites include (1) the absence of unsupported 208Pb, (2) typical radiogenic yields >85%, and (3) the ability to directly image, and thus avoid, restitic cores (Harrison et al., 1995b). The diffusion of Pb in monazite is sufficiently sluggish (Smith and Giletti, 1994) at the peak melting temperatures of Himalayan leucogranites (680-730 °C; Montel, 1993), to ensure that crystallization ages are recorded in the cores of ~100 μm sized grains.

3.4 RESULTS

We initially measured 35 208Pb/232Th ages on 12 monazite grains from sample IE-26. 26 ages obtained from all but one of these grains yield a weighted mean of 12.5 ± 0.15 Ma (2 s) with a mean squared weighted deviates (MSWD; $\chi^2/[n-1]$) of 6. For this number of ages, an MSWD of 6 indicates that analytical uncertainty alone cannot explain the distribution of ages and accordingly we have increased the error by √MSWD to account for the excess scatter, yielding 12.5 ± 0.4 Ma. However, most of the excess χ^2 is derived from three measurements (esp1, fsp1, ksp1) and removing those data reduces the MSWD by half (table 3.1). One crystal (grain c, Fig. 3.3) yields a bimodal distribution of ages with a cluster at ~12

Figure 3.3

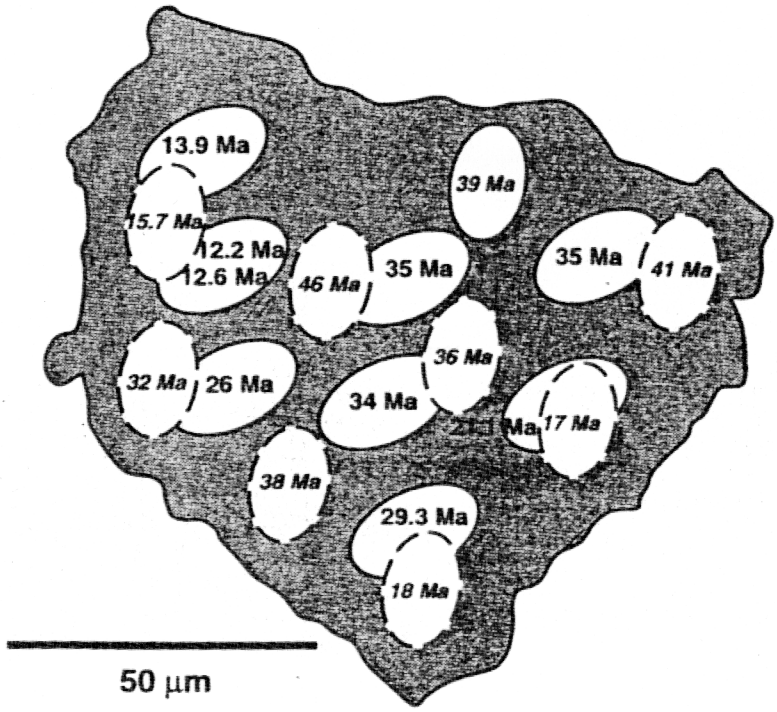

Figure 3.3 Map of monazite grain c, sample IE-26, showing locations and ages of individual ion microprobe analysis spots. Results from first and second analysis set are respectively shown as solid and dashed ellipses. Note proximity between oldest (46 Ma) and youngest (12 Ma) results (see text). Because old core likely represents Eo-Himalayan metamorphism and youngest age represents time of anatexis, lack of equilibration over ~10 μm distance restricts time at peak temperature to no more than ~1 m.y.

Table 3.1

analysis	$^{204}Pb/^{206}Pb$	σ	$^{208}Pb/^{232}Th$	σ	$^{232}ThO_2/Th$	σ	$frac_{com\ Pb}$	σ	Age (Ma)	± (Ma)
asp1	0.00166	0.00001	0.0309	0.00004	5.88	0.0025	0.066	0.0005	13.2	0.4
asp2	0.00169	0.00001	0.0309	0.00002	5.90	0.0035	0.067	0.0004	13.1	0.4
bsp1	0.00222	0.00003	0.0286	0.00003	5.79	0.0017	0.088	0.0011	12.3	0.4
csp1	0.00113	0.00001	0.0737	0.00004	5.62	0.0021	0.045	0.0005	34.1	0.7
dsp1	0.00344	0.00013	0.0212	0.00004	4.70	0.0102	0.137	0.0051	11.0	0.7
csp2	0.00343	0.00006	0.0299	0.00017	5.66	0.0060	0.136	0.0025	12.6	0.6
csp3	0.00109	0.00003	0.0699	0.00010	5.29	0.0043	0.044	0.0013	34.9	0.6
csp4	0.00206	0.00008	0.0566	0.00083	5.00	0.0928	0.082	0.0032	29.3	1.0
csp5	0.00131	0.00005	0.0333	0.00013	3.70	0.0067	0.052	0.0020	25.9	0.6
csp6	0.00128	0.00003	0.0432	0.00011	3.60	0.0055	0.051	0.0010	35.2	0.6
csp7	0.00690	0.00010	0.0229	0.00024	3.65	0.0089	0.275	0.0041	13.9	2.1
csp8	0.00179	0.00008	0.0372	0.00008	4.62	0.0059	0.071	0.0033	21.1	0.6
csp2@1	0.00193	0.00015	0.0089	0.00006	2.40	0.0058	0.077	0.0061	12.2	0.3
esp1	0.00418	0.00016	0.0211	0.00006	4.85	0.0033	0.166	0.0064	10.1	0.6
esp2	0.00441	0.00008	0.0256	0.00005	5.33	0.0058	0.175	0.0032	10.9	0.7
fsp1	0.00517	0.00041	0.0251	0.00004	5.07	0.0122	0.206	0.0163	10.5	0.3
gsp1	0.00713	0.00023	0.0359	0.00030	6.70	0.0238	0.284	0.0080	10.1	0.9
gsp2	0.00828	0.00062	0.0364	0.00029	6.69	0.0036	0.330	0.0245	10.0	0.7
asp3	0.00538	0.00018	0.0369	0.00010	6.41	0.0068	0.214	0.0062	12.4	1.0
fsp2	0.00339	0.00009	0.0203	0.00003	4.11	0.0023	0.135	0.0034	12.8	0.4
gsp3	0.00131	0.00003	0.0255	0.00006	5.36	0.0073	0.052	0.0011	12.7	0.3
hsp1	0.00506	0.00043	0.0347	0.00178	5.97	0.0040	0.201	0.0172	12.5	0.6
hsp2	0.00278	0.00015	0.0367	0.00008	6.53	0.0081	0.111	0.0061	13.2	0.4
isp1	0.00235	0.00015	0.0273	0.00008	5.54	0.0042	0.093	0.0060	11.9	0.3
isp2	0.00436	0.00023	0.0284	0.00010	5.66	0.0080	0.173	0.0092	11.3	0.5
jsp1	0.00183	0.00017	0.0233	0.00005	4.77	0.0029	0.073	0.0068	12.7	0.2
lsp3	0.00248	0.00044	0.0259	0.00005	5.45	0.0042	0.099	0.0175	11.7	0.5
ksp1	0.00228	0.00014	0.0382	0.00008	6.75	0.0084	0.091	0.0056	13.6	0.2
ksp2	0.00239	0.00009	0.0348	0.00009	6.48	0.0034	0.095	0.0036	13.0	0.3
lsp1	0.00255	0.00012	0.0322	0.00007	6.03	0.0012	0.102	0.0381	12.9	0.5
lsp2	0.00156	0.00006	0.0212	0.00002	4.44	0.0043	0.062	0.0024	12.7	0.3
jsp2	0.00184	0.00004	0.0277	0.00002	5.73	0.0050	0.073	0.0015	12.3	0.3
jsp3	0.00156	0.00006	0.0264	0.00005	5.49	0.0023	0.062	0.0025	12.3	0.3
jsp3@1	0.00200	0.00005	0.0220	0.00011	4.65	0.0132	0.080	0.0022	12.4	0.4
lsp3	0.00154	0.00128	0.0160	0.00004	3.76	0.0033	0.061	0.0511	12.0	0.3

Table 3.1 Th-Pb monazite results for sample IE-26 (12 monazite grains "a" to "l").

Ma and another cluster between 35 and 21 Ma which we interpret to reflect a restitic core encompassed by a magmatic overgrowth (Fig. 3.3). The three youngest ages, all from one edge of the crystal (csp2, csp2@1, csp7), yield a weighted mean of 12.4 ± 0.4 Ma (MSWD = 0.5), which is indistinguishable from the average of that obtained from the other 11 grains. The other six ages, which vary from 21 to 35 Ma, are consistent with this being a restitic monazite grain that formed in the Indian basement during Eo-Himalayan metamorphism (i.e., Le Fort, 1996) of the granite protolith. To gain further insight into this age distribution, we repolished the sample and measured eight additional spots which yielded ages between 15 and 46 Ma (Fig. 3.3). The pattern of ages is consistent with the first run (Fig. 3.3) and we interpret the oldest age of 46 Ma as a minimum age of the protolith. The preservation of inherited Pb* in this grain indicates that the thermal history during anatexis was insufficient to cause diffusive equilibration of Pb over length scales of 10-50 mm. We can thus infer that the age of 12.5 ± 0.4 Ma dates the episode of magmatism that resulted in the emplacement of the Khula Kangri granite, and that individual monazite grains did not allow significant Pb* loss while at high temperature. Based upon the high Thorium content of grain c and the consistency in age from the other 11 grains, we do not think that the determined age is a metamorphic age.

3.5 IMPLICATIONS

Khula Kangri's 12.5 ± 0.4 Ma crystallization age is the youngest reported from the high Himalaya. It is ~10 m.y. younger than that of high Himalayan leucogranites west of the Yadong cross structure but it is similar in age to the Laghoi Kangri Belt (also north Himalayan Granite Belt - Le Fort et al., 1987). Taking the previously proposed detachment displacement rate of ~10 mm/yr, our result suggests that north

directed extension accommodated by the Southern Tibet detachment system in the eastern Himalaya continued until ca. 10 Ma. This is 8 - 10 m. y. younger than has been previously suggested for main detachment activity (Hodges et al., 1992; Coleman and Hodges, 1995; Searle, 1995; Noble and Searle, 1995).

Two alternative interpretations are possible. 1. There is an abrupt ~10 m.y. younging of main Himalayan events across the Yadong cross structure. The Main Central thrust did not accommodate significant displacement during the ca. 12 Ma Bhutan Himalaya events as it is not offset across the Yadong cross structure. The additional south directed shortening required in Bhutan, and the anatexis, migration and emplacement of the Khula Kangri granite, may therefore be related to motion on a later thrust fault structurally above, and thus out of sequence with, the Main Central thrust. The Kakhtang thrust (Fig. 3.1B), located midway between the Main Central thrust and the crest of the Himalaya, and documented only in Bhutan (Gansser, 1983), is a possible proxy for the Main Central thrust. This hypothesis requires that the detachment along the Bhutan Himalaya is wholly separate from, although mechanically equivalent to, the detachment west of the Yadong cross structure. This is consistent with interpreted deep seismic reflection profiles on either side of the Yadong cross structure that show that the detachment on the Nepal side continues to ~27 km depth (Hauck and Edwards, 1997), whereas on the Bhutan side, the detachment continues for >100 km at <10 km depth (Nelson et al., 1996). A west to east detachment system discontinuity is consistent with changes across the projection north from the Yadong cross structure that include (1) a predominance of deeper water facies, (2) possible left-lateral offset of the Laghoi Kangri belt (Fig. 3.1B), and (3) excision of the Gangdese thrust, Xigaze Group and ophiolitic remnants (Burg, 1983; Yin et al., 1994). If there is a separate mechanism for accommodating the detachment hanging wall on the east side of the Yadong cross structure, the north-vergent Renbu Zedong thrust (Fig. 3.1B) may be involved. This thrust defines the

Yarlung Zangpo suture along much of its eastern portion (Yin et al., 1994) and has locally accommodated >20 km of slip ca. 18 - 11 Ma (Ratschbacher et al., 1994; Quidelleur et al., 1997). This may indicate that there was some synchronous movement on the two structures and/or movement on the Renbu Zedong thrust that allowed sufficient change in the local stress tensor east of the Yadong cross structure to trigger north directed extension at Khula Kangri. Interpreted deep seismic reflection profiles are consistent with the two faults connecting at depth (Nelson et al., 1996).

The second interpretation precludes the first, and assumes that the Southern Tibet detachment is a single northward propagating fault whose surface is continuous across the Yadong cross structure. In this case, 70 km of offset accompanies the Yadong cross structure because the exposed portion of the Southern Tibet detachment on the Tibet - Bhutan frontier is 70 km closer to the propagating tip of the detachment surface (relative to Nepal). Detachment footwall anatexis is therefore younger in the north, as evidenced by the 12.5 ± 0.4 Ma Khula Kangri granite. This would imply a continuous portion, or strip, of the Southern Tibet detachment footwall along which plutonism is ~10 m.y. younger than, and ~70 km north of, the portion of the detachment exposed along the Nepal high Himalaya. We note that the Khula Kangri granite is similar in age, and outcrops near, the Laghoi Kangri belt that extends along the arc west of the Yadong cross structure, 50 - 100 km north of the Nepal high Himalaya (Schärer at al, 1986). We can therefore propose that the two are tectonically equivalent, although the Khula Kangri granite has the morphology of a high Himalayan pluton whereas the Laghoi Kangri belt comprises diapirically emplaced domes. The morphological contrasts can be explained by the relative depths of crustal exposure across the Yadong cross structure; the basal portions of the Khula Kangri granite are exposed, whereas only the diapirically intruding tips of the north Himalayan Granite belt are presently visible.

Because the Southern Tibet detachment is cut by the north - south trending Yadong-Gulu rift, north directed extension probably (although not necessarily) ceased before the initiation of east - west extension. Our data constrain detachment system extension to 12.5 ± 0.4 Ma, and indicate that it continued until ca. 10 Ma (and possibly younger), implying that the Yadong Gulu Rift is younger than ca. 10 Ma. This is consistent with initial opening of the Yadong-Gulu rift at 8 ± 1 Ma (Harrison et al., 1995a). Several models suggest that the current east - west extension in southern Tibet reflects a change in the stress regime within the plateau caused by attainment of a critical elevation (Tapponnier et al., 1986; Dewey, 1988; England and Houseman, 1989; Molnar et al., 1993). Harrison et al. (1995a), proposed that this change in the stress regime occurred ca. 8 Ma, as opposed to between 17 and 14 Ma (Coleman and Hodges, 1995). Based on our results, we concur. Other effects possibly related to plateau uplift include intensification of the Asian monsoon (Kroon et al., 1991) and a major climatological shift in the Himalayan foreland (Quade et al., 1989), documented to have initiated ca. 8 Ma.

3.6 CONCLUSION

1. A 12.5 ± 0.4 Ma Th-Pb monazite date is interpreted as the crystallization age for the Khula Kangri pluton. North directed extension of the high Himalaya is clearly later than plutonism, and probably continued until ca. 10 Ma (and possibly younger), significantly younger than previously recognized.
2. The Yadong cross structure appears to mark an abrupt younging in the age of granites in the Southern Tibet detachment footwall, allowing two alternative hypotheses: 1. Main Himalayan orogenic events in Bhutan are ~10 m.y. younger than to the west in Nepal and Zanskar. 2. Khula Kangri is part of a belt of plutonism in the

detachment footwall that is ~10 m.y. younger than, and ~70 km north of, detachment exposed along the Nepal / Zanskar Himalaya.

3. Because the Southern Tibet detachment is cut by the Yadong-Gulu rift, the onset of east - west extension of the plateau must be much younger than ca. 12 Ma, and probably younger than ca. 10 Ma. This is consistent with previous geologic and tectonic data that indicate that the Yadong Gulu rift began to open ca. 8 Ma.

CHAPTER FOUR

SOUTHERN TIBET DETACHMENT SYSTEM (STDS) AT KHULA KANGRI, EASTERN HIMALAYA: A LARGE AREA, SHALLOW DETACHMENT STRETCHING INTO BHUTAN?

Southern Tibet Detachment System (STDS) at Khula Kangri, Eastern Himalaya: A large area, shallow detachment stretching into Bhutan?

M. A. Edwards[1], A. Pêcher[2], W.S.F. Kidd[1] B.C. Burchfiel[3], L.H. Royden[3]

Journal of Geology, submitted

1. Department of Geological Sciences, State University of New York at Albany, 1400 Washington Avenue, Albany, NY 12222, USA
2. CNRS, UPRES-A 5025, Institut Dolomieu, 38031 Grenoble Cedex, France
3. Dept. of Earth, Atmospheric and Planetary Sciences, MIT, Cambridge, MA 02130, USA

4.1 INTRODUCTION

The southern Tibet Detachment System (STDS, also North Himalayan Normal Fault, Burg, 1983) marks the structural contact in the Himalayan orogen between the High Himalayan Crystalline rocks (HHC - containing typically sillimanite gneisses and leucogranite) and overlying Tethyan sedimentary rocks (Burg, 1983; Burg et al., 1984; Herren, 1987; Pecher, 1991; Burchfiel et al., 1992; Edwards et al., 1996). The STDS is a pan-Himalayan feature (fig. 4.1) which represents several kilometres of net normal fault throw. The data and hypotheses we present here arise from the coming together of recent geological investigations in the area of the Khula Kangri massif in an attempt to further constrain the STDS in this eastern part of the Himalaya, across the Tibet/Bhutan frontier (fig. 4.2). Because of the political and logistical difficulties for access to the area, we have attempted a definitive compilation of published and unpublished data, and have compiled an archival geologic map of the area (fig. 4.3, and chapter appendix 4.8.1). This is built around material from Burchfiel et al. (1992), Pêcher et al. (1994), and Edwards et al. (1996), combined with detailed interpolation using previously unavailable satellite imagery (Thematic Mapper - TM), topographic data, and observations by Gansser (1983) from Bhutan.

The Khula Kangri massif is part of the High Himalaya situated north of Bhutan, wholly within Tibet (figs. 4.1 & 4.2). The geology appears to be very similar to other High Himalaya massifs: it is comprised of gneisses locally capped by Tethyan sedimentary rocks, and intrusive Miocene leucogranite. In the Gonto La valley (fig. 4.2), the contact between the Tethyan rocks and the Higher Himalaya Crystallines (HHC - including the leucogranite) appears to be a low-angle STDS detachment

Figure 4.1

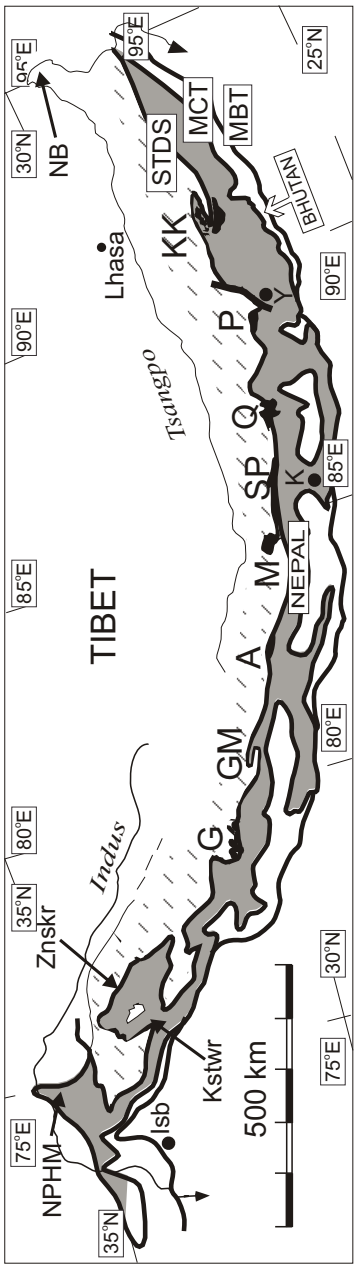

Figure 4.1 General geologic map of Himalayan chain. Light grey: Higher Himalaya Crystalline sequence (HHC). White with broken hatch pattern: Tethyan sedimentary sequence. White: Lesser Himalayan sequences (where part of MCT footwall). Black blobs: High Himalayan granite plutons; letters are associated high peaks [Ga; Gangotri, GM; Ghurla Mandhata, A; Annapurna, M; Manaslu, SP; Shisha Pangma, Q; Mt. Everest, P; Pauhunri, KK; Khula Kangri]. NPHM: Nanga Parbat Haramosh Massif, Isb: Islamabad, Kstwr: Kishtwar window, Znskr: Zanskar, K: Kathmandu, Y: Yadong, NB: Namche Barwah. STDS: Southern Tibet Detachment System. MCT: Main Central Thrust. MBT: Main Boundary Thrust

Figure 4.2

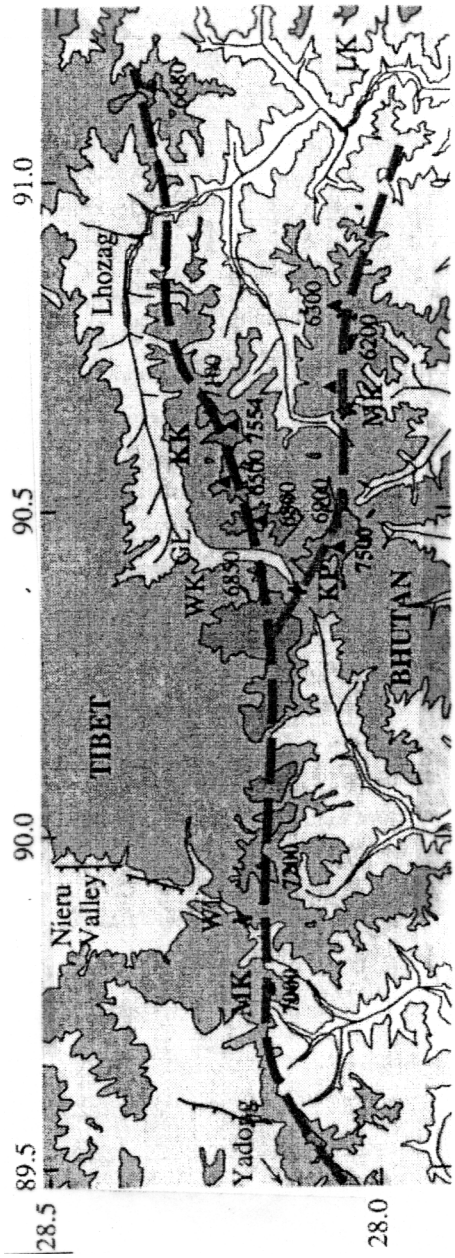

Figure 4.2 Regional topographic map of Tibet-Bhutan frontier area Himalaya immediately east of Yadong-Gulu rift system. Numbers are degrees east (89.5, etc), or north (28.0, etc.). Contour interval: 1000m; darkest shading is >6000 m (>7000m not discriminated). Fine dashed lines are approximate trace of main rivers. Thick line is approximate line of high peaks. Selective peaks and passes are shown: WL; Wagye La, MgK; Masang Kang, WK; Wang Ka, GL; Gonto La, KK; Khula Kangri, KP; Kanga Punzum, MK Monlakarchung La, LK; La Kang. Note bifurcation in line of high topography (High Himalaya) is co-incident with repetition of main High Himalaya geologic sequence. Khula Kangri range is north fork, Kanga Punzum-Monlakarchung range is south fork.

Figure 4.3

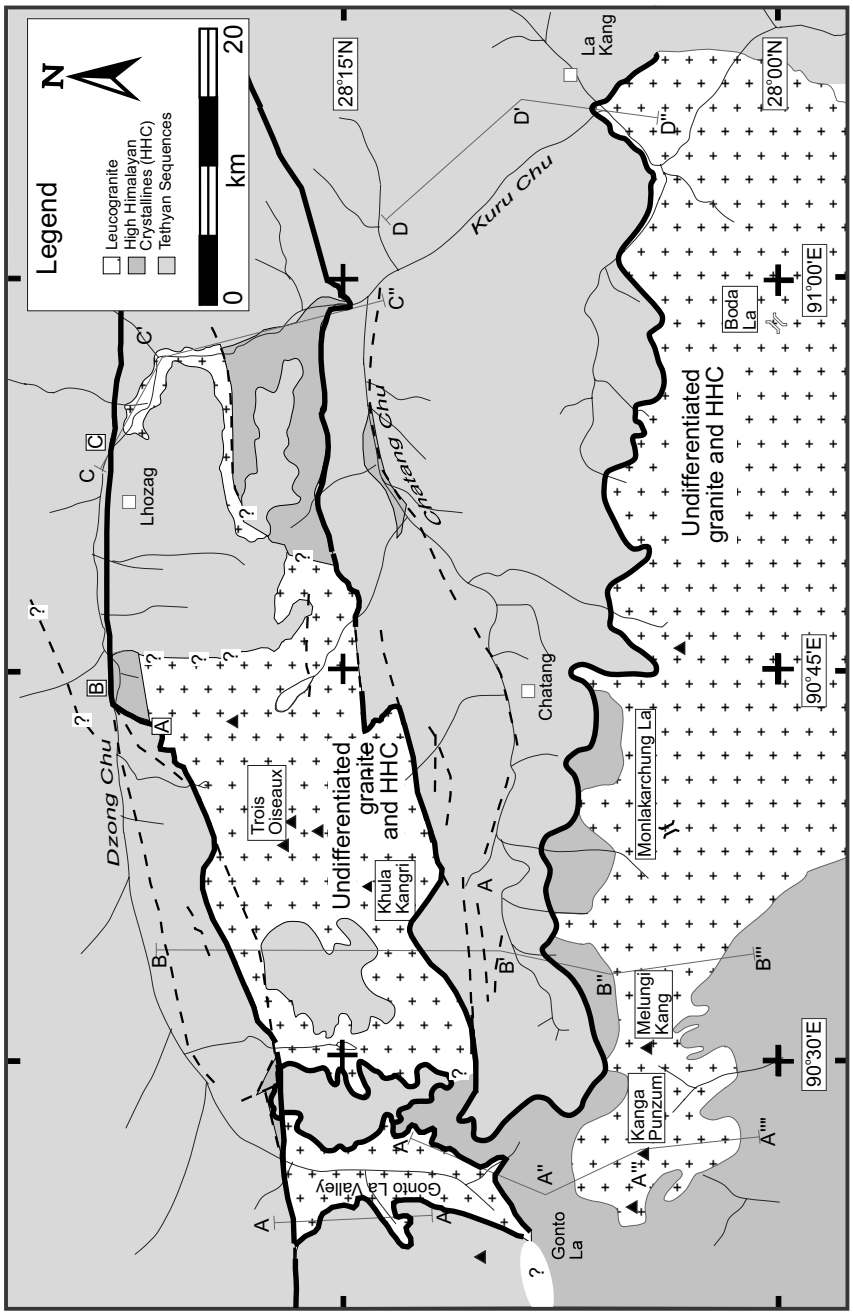

Figure 4.3 Summary of archival geologic map of Khula Kangri and Kanga Punzum-Monlakarchung massifs (see appendix A). Plus pattern: leucogranite; light grey fill: Tethyan (Mesozoic) sedimentary rocks; dark grey fill: High Himalayan crystalline rock (HHC); A-A' etc., are cross section locations. Letters in square boxes are locations referred to in text. Thick black line marks STDS. Dashed black lines are other faults. Question marks indicate specific uncertainty. For map sources, see appendix A.

fault (the Gonto La detachment, Edwards et al., 1996). This is consistent with descriptions of other High Himalaya areas (e.g. Gansser 1964, 1983; Burg, 1983; Burchfiel et al., 1992). Dissimilar in this case is the occurrence of a second mountain range, the Kanga Punzum-Monlakarchung (KPMK) range, to the south, apparently structurally below the HHC belt of the Khula Kangri massif. Within this second mountain range, large amounts of Tethyan rocks overlie the HHC/leucogranite. This morphological and geological duplication of the crest of the High Himalaya, briefly noted by Dietrich and Gansser (1981), suggests that the STDS is also duplicated. In the following we examine this geomorphologic and geological repetition and attempt to constrain the nature of the STDS in this apparently atypical part of the Himalaya.

4.2 MORPHOLOGY

In this part of Himalaya, a morphological discrimination using topography described in Fielding et al. (1994) into five groups is clearly apparent. From north to south:

(1) The Tibet plateau. In this area it averages >5000 m, and consists of Tethyan sedimentary rocks. Locally, it is interrupted by the valleys of the Yadong-Gulu rift system (Armijo et al., 1986), e.g. the Nieru valley half graben (Cogan et al., 1998).

(2) The southern edge of the Tibet Plateau. This is marked by the abrupt topographic change to the High Himalayan Masang Kang-Khula Kangri range ("Tibet-Bhutan frontier Himalaya" of Edwards et al., 1996), where main summits, mostly consisting of granite, are over 7000m. It coincides with the northern surface trace of the STDS.

(3) The Southern flank of the Khula Kangri massif. This drops steeply to the Chatang valley, a broad syncline of sedimentary rocks. Topographic data suggests that this steep surface coincides with several steep south dipping faults (fig. 4.3 and fig. 4.4).

(4) To the south, the Chatang valley. Its southern side rises abruptly to become the Kanga Punzum-Monlakarchung range, another granite-dominated high range. Taken together, the Khula Kangri and the Kanga Punzum-Monlakarchung ranges define a bifurcation in the crest of the High Himalaya, changing at about 90.4°E, with their separation increasing towards the east.

(5) South of the Kanga Punzum-Monlakarchung range, the surface falls away abruptly to where the crystalline rocks are exposed in central Bhutan (e.g. Gansser, 1983; Grujic et al., 1996).

4.3 GEOLOGY

We divide the geology into three main units that coincide with the three main morphological portions relevant to this study. From north to south they are the Khula Kangri range, the Chatang valley, and the Kanga Punzum-Monlakarchung range.

4.3.1 Khula Kangri range

The Khula Kangri range forms the northern portion of the High Himalaya. In the western Khula Kangri massif (fig. 4.3), the Gonto La valley provides a N-S cross section >15 km long, and in places >2 km deep, (fig. 4.4a) that exposes the 2-mica tourmaline Khula Kangri leucogranite along most of the valley (Edwards et al., 1996). In the southern part of the section, the granite terminates at an intrusive contact with the HHC. From the central part of this section,

Figure 4.4

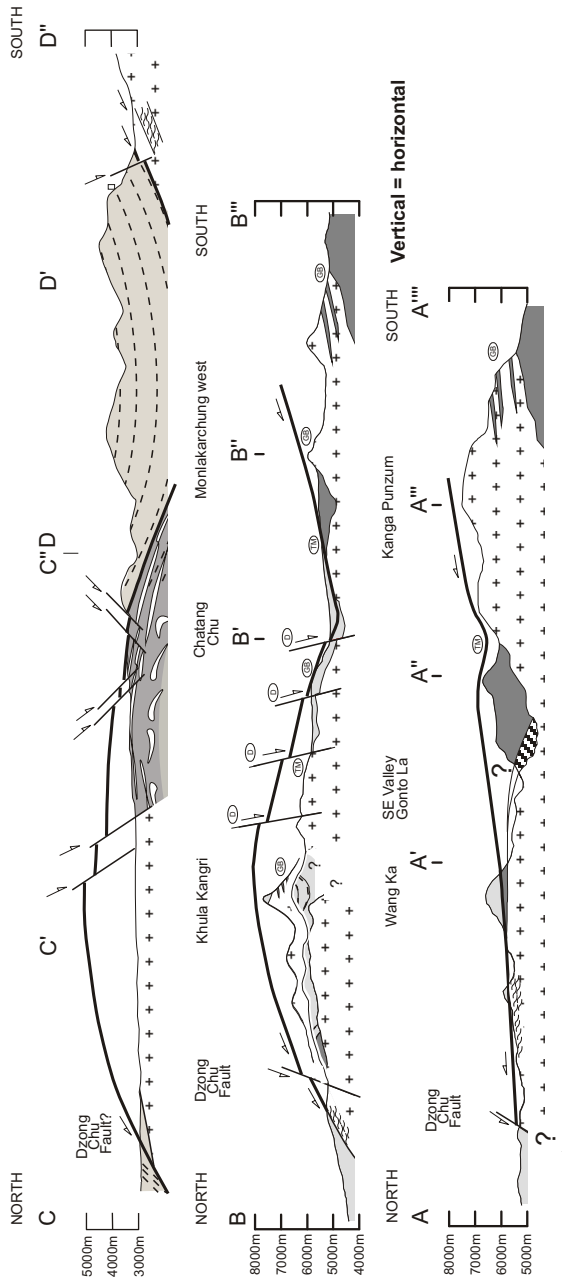

Figure 4.4 A, B, and C. Geologic cross sections continuous across both massif areas. Interpreted geology is either from Gansser (1983) in Bhutan ("GB") or interpolation from Thematic Mapper image ("TM"); see appendix A. Faults marked with "D" are approximate locations based upon topographic data. DCF is Dzong Chu Fault. A: cross section A-A"" is from DCF, through Gonto La valley to south of Kanga Punzum (A-A" is after Edwards et al., 1996). B: cross section B-B' is from DCF, across 7554 m summit of Khula Kangri to SW of Molakarchung La. C: cross section C-C'-D-D' is from Lozhag to La Kang, after Burchfiel et al. (1992).

Edwards and Harrison (1997) obtained a crystallisation age for the granite of 12.5 +/- 0.15 Ma (Th-Pb on eleven monazite grains).

To the east of the Gonto La valley, at higher altitudes within the Khula Kangri massif, our compilation map draws upon previously unpublished data (from A.P.) from mapping in selected areas, that help to further constrain the geology and structure of the Khula Kangri massif. Within this area, in what we term the Khula Kangri summit section, most of the area exposes leucogranite. The granite has the same appearance as the granite exposed in Gonto La, and has an observed thickness of more than 2.5 km (fig. 4.4b). In the northernmost part of the section, the Khula-Kangri granite locally intrudes the High Himalayan migmatitic gneisses which are capped by dark Tethyan calcareous schists. More commonly, the granite directly intrudes the Tethyan sediments. The irregularly shaped intrusive contact can be clearly followed in the landscape, from 4500m to the northern part of the section, to approximately 7400m close to the summit of Khula Kangri, where a small layer of dark rock caps the top of the Western summit ridge. In this Khula Kangri summit section, a very obvious metamorphic aureole can be observed in the Tethyan sedimentary rocks. Within black schists, growths of biotite + garnet + staurolite + sillimanite are developed very close to the contact. These pass to large chiastolitic andalusite over a layer of several hundred meters thickness. Also common are granitic sills and lenses, metres to tens of metres in thickness, that are close to, and parallel with, main granite intrusive contact.

The easternmost part of the Khula Kangri range is exposed immediately east of Lhozag, along the Lhozag-La Kang traverse conducted by Burchfiel et al. (1992), where a greater than 6 km section of the Khula Kangri granite is found (Fig. 4.4c). At its northern margin, the granite intrudes into, and locally metamorphoses, dark Tethyan slates. Approximately 600 metres north of this contact (location C, fig 3), is an intra-Tethyan ~40° north dipping normal fault

(Burg, 1983; Burchfiel et al., 1992, Edwards et al., 1996), which has been regarded (Burchfiel et al., 1992, Edwards et al., 1996) as a part of the Dzong Chu Fault (DCF - see below). Guillot et al. (1995), investigating metamorphic equilibrium geobarometry of footwall and hanging wall rocks at location C, obtained respective values of 440+/- 60 and 290+/- 40 MPa. This geobarometric contrast allows us to estimate a throw of 4 to 5 km.

Interpretation of TM imagery and topography allows interpolation of the outline and distribution of the Khula Kangri granite between these outcrop constraints. This has notably been of most use to trace the southern margin of the Khula Kangri granite. The only existing published field data for the wall forming southern side of Khula Kangri are remote observations by Gansser (1983) from Monlakarchung La, and Gwen La (outside map area). Gansser (1983) described leucogranite sheets of tens to hundreds of metres thickness within the HHC of the southern wall of the Khula Kangri massif, and reported this as the total extent of granite at Khula Kangri. , TM interpretation building on our field observations, shows that the actual exposure of the granite is orders of magnitude greater (>750 km²), and that the Khula Kangri massif is dominated by the granite of the Khula Kangri pluton.

4.3.2 Chatang valley

From Gwen La and from Monlakarchung La in the Kanga Punzum-Monlakarchung range (fig. 4.2 & fig. 4.3), Gansser (1983) identified a belt of extensive black slates and phyllites in the Chatang valley. These dark rocks are clearly identifiable on the TM, and are easily traced to the confluence of the Chatang Chu with the Kuru Chu. This confluence area forms a portion within the detailed N-S geologic section of Burchfiel et al. (1992) that crosses both ranges. The section defines a broad synform of Mesozoic age shales and slates a few km

thick (fig. 4.4c). Chinese mapping (Bureau of Geology and Mineral Resources of Xizang (Tibet) Autonomous Region, 1993), shows a re-entrant of Mesozoic sedimentary rock that coincides with the Chatang valley, consistent with the TM interpretation.

In the Gonto La valley section (fig. 4.4a), black phyllites are found everywhere above the granite, and to the south of the granite in the southeast tributary valley, in a synformal flexure (Edwards et al., 1996). These dark rocks are again clearly visible on the TM, and form part of the continuous belt across to the Chatang valley

The Chatang valley belt of sedimentary rocks are therefore part of the Tethyan sedimentary series, and on a large scale are indistinguishable from the Tethyan rocks found along the north flank of the Khula Kangri massif (Burchfiel, et al., 1992; Pecher et al., 1994; Edwards et al., 1996).

4.3.3 The Kanga Punzum-Monlakarchung range

This range forms the southern branch of the High Himalaya (fig. 4.2 and fig. 4.3). Gansser (1983) described the southern boundary (structural base) of the Monlakarchung-Passalum leucogranite pluton that makes up much of this range, and described the intrusive margins with the HHC (fig. 4.3 and chapter appendix 4.8.2). It is a two-mica granite, locally tourmaline rich, typical of the High Himalaya (Gansser, 1964, Debon et al., 1986; Le Fort 1996). The intrusive margin on the eastern shoulder of Kanga Punzum at Melunghi Kang (6900m) is typical for the Monlakarchung-Passalum pluton. Here, an outcrop area of several square km exposes sills and dykes injected into marbles, gneisses and migmatites (HHC). These continue to the west and make up much of the south wall of Kanga Punzum (Gansser, 1983).

In the eastern Kanga Punzum-Monlakarchung range, near the village of La Kang, Burchfiel et al. (1992) have described an extensive two-mica - tourmaline granite structurally below Tethyan sedimentary rocks of the Chatang valley. It is identical to the Khula Kangri leucogranite and Gansser's (1983) description of the Monlakarchung-Passalum granite. The granite is observed to continue for many kilometres to the west and to the south into Bhutan. Although Burchfiel et al. (1992) loosely grouped this with the Khula Kangri pluton, our mapping and TM interpretation show that it is a separate body at the surface. Moreover, TM interpretation shows this granite as a conspicuous pale body that is continuous between La Kang and the numerous localities where the Monlakarchung-Passalum pluton was observed by Gansser (1983). We have consequently modified Gansser's (1983) delimitation of the northern margins of the Monlakarchung-Passalum pluton (fig 3). This has been re-drawn from projection of Gansser's (1983) sketches and photos onto topographic surfaces to constrain map traces, in conjunction with TM interpolation and the field observations at La Kang (Burchfiel et al., 1992).

Extensive HHC rocks were observed (Edwards et al., 1996) on southern wall of Gonto La. In this wall, which forms the northern side of Kanga Punzum, granite intrudes the HHC gneisses. This is consistent with similar relationships documented by Gansser (1983) on the immediate south side of Kanga Punzum. Additionally, the HHC can be recognized on the TM as a pale band that continues to the south east, towards Monlakarchung where the granite is recognised (chapter appendix 4.8.2).

We conclude that the crystalline rocks that form the Kanga Punzum-Monlakarchung range are continuous from the point of the morphological bifurcation of the range (near Gonto La) to tens of km southeast of La Kang. For the most part, the crystallines are dominated by the Monlakarchung-Passalum leucogranite, whose surface outcrop area is now seen to be greater than 1500 sq.

km. Both the petrography and the tectonic setting (i.e., intrusive into the HHC gneisses of the uppermost Himalaya) of this granite are typical of High Himalayan Miocene leucogranites. For this body, however, there exists no published age. The nearest age for a HHC/granitic rock, apart from the 12.5 Ma Khula Kangri granite (Edwards & Harrison, 1997), is a pegmatite crosscutting a Cambrian augen-gneiss at Doli La, about 20 km south of the southern margin of the Monlakarchung-Passalum pluton. Here, a zircon within the pegmatite gives a U/Pb age of 25-26 Ma (Parrish et al., 1997; c.f. Gansser et al., fig. 91).

4.4 STRUCTURE

4.4.1. The crystalline-sedimentary rock contact

Our mapping indicates that the HHC-Tethyan sedimentary rock contact can be followed as a continuous feature across the two branches of both Himalayan ranges. The contact has the form of an originally continuous surface that is now gently folded (~10 km wavelength), and is cut locally by various minor E-W trending, steep faults. The apparent duplication of the High Himalaya is not a product of tectonic imbrication and the two discrete Himalayan branches do not correspond to a structural repetition and superposition of the upper part of the Himalayan sequence within a single tectono-stratigraphic column. We interpret the contact as an STDS detachment extending across both ranges (fig. 4.4).

4.4.1.1. Gonto La valley and Khula Kangri summit section.

In Gonto La valley, the contact is a top-to-north, low angle detachment fault of more than 15 km displacement; the Gonto La detachment (fig. 4.4a). Isolated outcrops of the Gonto La detachment occur in adjacent minor valleys

further east (fig. 4.3). In this area, the granite and Tethyan rocks are cut by small, down-to-north normal faults that strike ~60°E to 130°E. We regard these minor faults as splays of the DCF (see below), and we group them with previously described examples (Burchfiel et al., 1992; Edwards et al., 1996).

East of Gonto La, in the Khula Kangri summit section (fig. 4.4b), the Tethyan-HHC contact is mostly an intrusive contact (see above). In the northern part of this section, however, the Tethyan-HHC contact is clearly seen to be a detachment in that it is marked by a granitic footwall with a strong post-magmatic S-C fabric. The mylonitic C surface dips 10° to 30° to the north or northwest, with stretching lineations oriented towards 350°. Kinematic structures record a clear top-to-north sense of shear. Structurally below are discrete S-C mylonitic shear-bands of tens of metres thickness. These shear bands are less steep than the main contact, but also display a north-south stretching lineation and a top to the north sense of shear.

The kinematics of the structures here on both the main contact and the underlying shear zones is consistent with the Gonto La detachment footwall, where top-to-north shear sense granite mylonite fabric dips ~10° to the north, and stretching lineations plunge ~10° towards 350° (Edwards et al., 1996). We note, however, that our new data from the Khula Kangri summit section (from A.P.) allows us to constrain a gradual west to east steepening of the northward dip of the detachment.

In the southern part of the Khula Kangri summit section, where granite intrudes Tethyan rocks, the detachment position is above the granite and "intra-Tethyan". This re-opens the "Palaeozoic problem" (c.f. Burchfiel et al., 1992, Edwards et al., 1996), i.e. the apparent absence of several kilometres of the Palaeozoic part of the Tethyan column, but is an issue not further discussed here.

Interpolation of the detachment contact between our outcrop observations using TM allows the detachment to be traced east of the Khula Kangri summit section, where topography indicates that the west to east steepening of detachment surface progressively continues to location A (fig. 4.3) where it dips ~35°N. At this location, it is truncated by, or merges with, the Dzong Chu fault, which locally dips ~40° to the north (loc. B, fig. 4.3).

4.4.1.2. Lhozag - La Kang section.

The easternmost parts of the two ranges are exposed along the Burchfiel et al. (1992) Lhozag-La Kang section (fig. 4.4c). In this section, the Tethyan sedimentary rocks of the Chatang Valley are seen to form a broad synform (syncline) between the two crystalline belts. The southern contact of the dark phyllites with the Monlakarchung-Passalum leucogranite is clear. A planar, north-dipping surface of granite appears intrusive into the Tethyan rocks, insofar as a continuous garnet isograd surface can be mapped in the overlying phyllites (Burchfiel et al., 1992). However, tens of metres thick horizons of mylonite, notably parallel to the planar upper contact of the granite body, are found in the upper part of the granite. As in Khula Kangri summit section, shear related lineation is directed NNW. Burchfiel et al. (1992) report 5-25° plunge towards 315-340°), and shear sense is top-to-north.. The regional contact between the granite and the Tethyan rocks is regarded by(Burchfiel et al. (1992) as a major detachment, and we note that the structure of the upper contact of the Monlakarchung-Passalum pluton is highly similar to that of the Khula Kangri pluton.

In the northern half of this eastern section, the Tethyan-crystalline contact across the Khula Kangri range is more complex.

(1) On the southern flank of the Khula Kangri range, where the Chatang Valley Tethyan rocks structurally overlie HHC, a detachment (sensu-stricto) has

not been described. However, based upon the observed large metamorphic contrast, previous workers (Burchfiel et al., 1992, Edwards et al., 1996) inferred a detachment to be located here. This contact is clearly recognisable on the TM image, and it can be traced around the western end of the dark rocks of the Chatang synform (Fig. 4.3). Where the Lhozag-La Kang section of Burchfiel et al. (1992) crosses the southern flank of the Khula Kangri range, sequences of extensional E-W trending steep faults are present. The faults can be recognized on the TM, by color contrast, and on topographic imagery by hypsometry variation. Integration of these criteria allows us to recognize steep south-dipping faults, all along the southern flank of the Khula Kangri range. We interpret these as extensional faults that are similar to, and part of, a suite that includes the south-dipping faults of the Lhozag-La Kang section (Burchfiel et al., 1992).

(2) On the northern flank of the Khula Kangri range in this Lhozag - La Kang section, the detachment is apparently not seen, and the granite-Tethyan contact is intrusive. Near Lhozag, ~600m north of the granite intrusive contact, the fault at location C (fig. 4.3) either is the detachment, or cuts the detachment (see below), depending on the significance attributed to the fault.

4.4.2 THE DZONG CHU FAULT

The Dzong Chu Fault (DCF) has been described in detail elsewhere (Burg, 1983; Burchfiel et al., 1992; Edwards et al., 1996). Our new field observations show several minor splays of the DCF, in and around the Dzong Chu valley (larger faults are shown on fig. 4.3, others are additionally detailed on the 1:100 000 map). TM spectra and DEM form analyses allow clear recognition of the main

fault branches, and confident interpolation of the DCF across the north flank of the Khula Kangri range is now possible.

In previous articles (Burchfiel et al., 1992; Edwards et al., 1996), the DCF has been regarded as younger than the regional STDS (i.e. Gonto La) detachment, including those localities where the DCF is not observed to cut the detachment. Our new data clearly indicate that the Gonto La detachment gradually steepens from west to east across the Khula Kangri range. It appears that at a certain point, the dip of the Gonto La detachment approaches that of the DCF. At location B (fig. 4.3) for example, the difference in angle between the two fault dips appears to be less then 10°. At this point, the distinction between DCF and Gonto La detachment becomes uncertain. Substantially east of this point, at location C (fig. 4.3) is the fault that was previously interpreted by Burchfiel et al. (1992) and Edwards et al. (1996), to be part of the DCF, and to post-date and cut the Gonto La detachment (fig. 4.5, option A). With our constraint of the Gonto La detachment steepening from west to east, it is now equally plausible that the fault at location C is actually the detachment (fig. 4.5, option B), and not an eastern continuation of the DCF that cuts the detachment. As can be seen from the cross sections (fig. 4.4), a gentle buckling of the detachment will give a concordance with the fault at location C. A throw of several km across the fault at location C is indicated by the geobarometric data (Guillot et al., 1995) and we think that this contrast is at least partly a product of the juxtaposition of, and relative exhumation associated with, the footwall and hanging wall of the Gonto La detachment. We cannot, however, determine if the Gonto La detachment footwall / hanging wall contrast has been increased, and hence modified by, the fault at location C (fig. 4.5, option A). Elsewhere along the Dzong Chu valley, the intersection between the two tectonic contacts is largely above erosion level, hence the general question of the DCF versus the Gonto La detachment is not resolvable. We can, however,

Figure 4.5

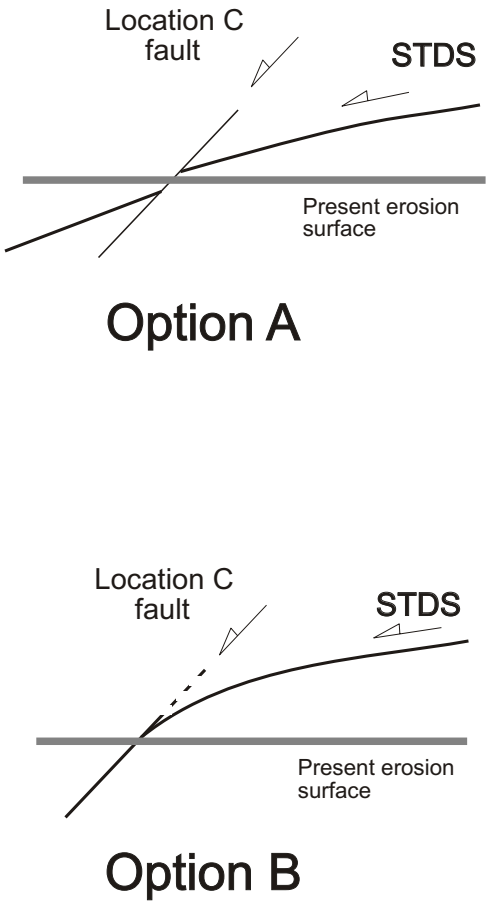

Figure 4.5 Cartoon illustrating the two options for the interpretation of the fault at location C, near Lhozag. In option A, the DCF is the fault, and cuts the detachment, displacing it , and slightly modifying the Gonto La detachment footwall / hanging wall contrast. In option B, the location C fault is the actual detachment.

eliminate DCF hypothesis #1 (no STDS detachment in eastern Khula Kangri range) of Edwards et al. (1996).

4.5 INTERPRETATION OF MECHANISMS

We interpret the two Himalayan ranges as being originally joined as one, and whose present separation has been accommodated by a scissor fault, wherein each range has rotated about an axis plunging ~W (with a pinning point at the point of bifurcation). This has caused (1) kilometric wavelength, low-amplitude buckling of the detachment surface, and (2) offset on steep normal faults, whose respective (1) amplitude and (2) net displacement increase from west to east. We note that the surface separation both of the range crests, and of the detachment trace, increases from west to east commensurate with the west-east increase in (1) the dip of the detachment and (2) the net displacement in the steep faults. This is consistent with a scissor fault mechanism, where net fault displacement increases along the fault plane. A conceptual "backrotation" (clockwise as viewed in fig. 4.4) of the two ranges restores them to a single, more typical Himalayan range where HHC gneisses are intruded by various leucogranite bodies and cut by a single, continuous gently N-dipping STDS detachment surface. In our scissor fault model, the apparently buckled STDS is therefore not a product of significant north-south shortening that post dates the ubiquitous (Burchfiel et al., 1992) upper Himalayan north-south STDS extension, but a product of local vertical displacements, accompanied by local flexure. Although the surface area of the two plutons is apparently very large, the mean thickness of each body is but a few kilometres. The two plutons are therefore not regarded as anomalous insofar as Himalayan batholiths are often described as sub-horizontal lenses of a few km thickness, formed by coalesced leucogranite dykes (e.g. Scaillet et al., 1995).

It is noteworthy that the surface trace of the STDS (and Tethyan/HHC contact) forms a major "Z-bend" in the area of the two ranges. This is unusual when viewed in context with the overall orogen, where the STDS trace along the high Himalaya rarely departs from a generally planar surface (discounting N-S normal fault offsets; e.g. Dingye, or Yadong Cross Structure - Burchfiel et al., 1992). Interestingly, the STDS Z-bend at this location in the eastern Himalaya is similar to another (slightly larger) major meander in the trace of the Tethyan/HHC contact in the western Himalaya, near Ghurla Mandhata/Api, (Gansser, 1964; Murphy et al., 1997). In this case however, the meander forms an "S-bend", the reverse sense to the Z-bend in the eastern Himalaya.

4.6 GEOCHRONOLOGY

Edwards & Harrison (1997) determined a Th-Pb monazite age of 12.5+/-0.4 Ma for the Khula Kangri granite. Our structural model allows that the two plutons are part of the same, originally continuous body. In this case, a crystallisation age of ~12.5 Ma is predicted for the Monlakarchung-Passalum pluton. Alternatively, if the two plutons are discrete, and are simply close neighbours, we predict an age for the Monlakarchung-Passalum pluton that is (1) not younger than ~12 Ma, based upon the Gonto La detachment deforming the Khula Kangri pluton during post emplacement cooling (Edwards et al., 1996), and (2) probably not older than ~25 Ma - the age of granite plutonism further south indicated by the pegmatite at Doli La (Parrish et al., 1997), and a common upper age limit for (neo) Himalayan plutonism (c.f. Harrison et al., 1997).

4.7 Conclusion

Our integrated mapping , interpretation of topographic and TM data, and re-examination of Gansser (1983) data, allows us to identify and interpret the following hitherto unrecognised features:

1 - There is an eastward bifurcation in the crest of high peaks that results in a geomorphological and co-incident geological repetition in this part of the High Himalaya.

2 - The lithology, metamorphic contrasts, nature of plutonism and structural evolution of both ranges are similar.

3 - We propose that this is a result of kilometric scale scissor faulting of a single "parent" range that is younger than the regional N-S extension that formed the STDS detachment. The scissor fault model allows a simple restoration of the familiar High Himalayan sequence.

4 - The repetition is not due to post-STDS regional N-S shortening that imbricates the upper Himalayan section; a continuous STDS surface exists across both ranges, the map trace of which forms a large Z-bend.

4.8. chapter Appendices

4.8.1 Map and satellite imagery information

An archival, colour, 1:100 000 digitised version of fig. 4.3 (main geological map) is kept within the collection of geological maps produced by members of Project INDEPTH (**In**ternational **D**eep **P**rofiling of **T**ibet and the **H**imalaya) and is available for inspection on request. Contact M.A. Edwards, W.S .F. Kidd or Project INDEPTH at Cornell University, Ithaca, NY

(http://www.geo.cornell.edu/geology/INDEPTH for further information. Thematic Mapper (TM) image was projected using ER Mapper©.

4.8.2 Margins of the Pasalum-Monlakarchung leucogranite (after Gansser, 1983)

At SW pluton margin, near Melunghi Kang (Gansser fig. 94, photo 41 and 66), the volume of leucogranite gradually decreases west from within the pluton proper at Kanga Punzum. Decametric xenolithic lenses of biotite gneiss in the pluton increase in number and grade into biotite - sillimanite gneiss containing leucogranite lenses ("a chaotic net-like dyke system"). HHC is largely sillimanite bearing gneiss and marble with cross-cutting, high strain migmatitic bodies. At the pluton southern margin in upper Chamkar Chu, near Tsamba, (Gansser, fig. 93), an intrusive contact is marked by series of leucogranite dykes and sills that intrude and grade into marble and calc-silicates. These overlie biotite-sillimanite psammite gneiss. At the SE margin, near Dermalung, several 100m overall, containing decametric tourmaline leucogranite apophysae within layered NNW-dipping psammite gneisses lie structurally below a local non-planar, discordant pluton intrusive contact. Above, within the contact zone, are rotated xenoliths of gneiss (Gansser, fig. 96). At the northern margin, mapping and remote observations from Monlakarchung La indicate north dipping HHC and dark slates/phyllites passing into Chatang valley (Gansser, 1983, fig. 119, and p.167, photos 64, 72).

CHAPTER FIVE

STRUCTURAL GEOLOGY AND TECTONICS OF NANGA PARBAT-HARAMOSH MASSIF, PAKISTAN HIMALAYA

5.1 INTRODUCTION

5.1.1 Regional background

The contact between collider India & the overthrust fossil island arc Kohistan-Ladakh series (KLS), which is preserved only in the NW Himalaya, is regionally termed the Main Mantle Thrust (MMT; Tahirkheli et al., 1979; Tahirkheli 1979; Bard et al., 1980; Bard 1983) or the southern suture (Gansser, 1964). The western Himalayan syntaxis (Wadia, 1931, 1932), coincides with the main bend in the orogen (the limit of the Himalayan belt sensu stricto), and includes the Indian-plate Nanga Parbat Haramosh Massif (NPHM; fig. ***5.1***). The NPHM/KLS contact forms a plan-view, "oxbow" shape around NPHM (Coward et al., 1986; Butler et al., 1992; Lemennicier et al., 1996; Pecher and Le Fort, 1998), and it is locally removed on NPHM's western side by subsequent predominantly E-side up faulting (Lawrence and Shroder, 1984; Madin 1986; Butler and Prior, 1988a; Butler et al., 1989; Madin et al., 1989; Owen, 1989). NPHM is not, however, a relict promontory of India that has acted as a horizontal indenter and "bowed out" the visible MMT. This is recognised by the absence of appropriate deformation of the northern margin of the KLS (Butler et al., 1992; Lemennicier et al., 1996; Pecher and Le Fort, 1998), and by the absence of significant "post-Himalayan" (see section 5.1.3 Exhumational versus extensional structures) wrench motion kinematic indicators on the western and eastern margins (Verplanck, 1986; Butler et al., 1989; Madin et al., 1989; Treloar et al., 1991; Butler et al., 1992; Pognante et al., 1993; Wheeler et al., 1995). The oxbow shape is due to

Figure 5.1A

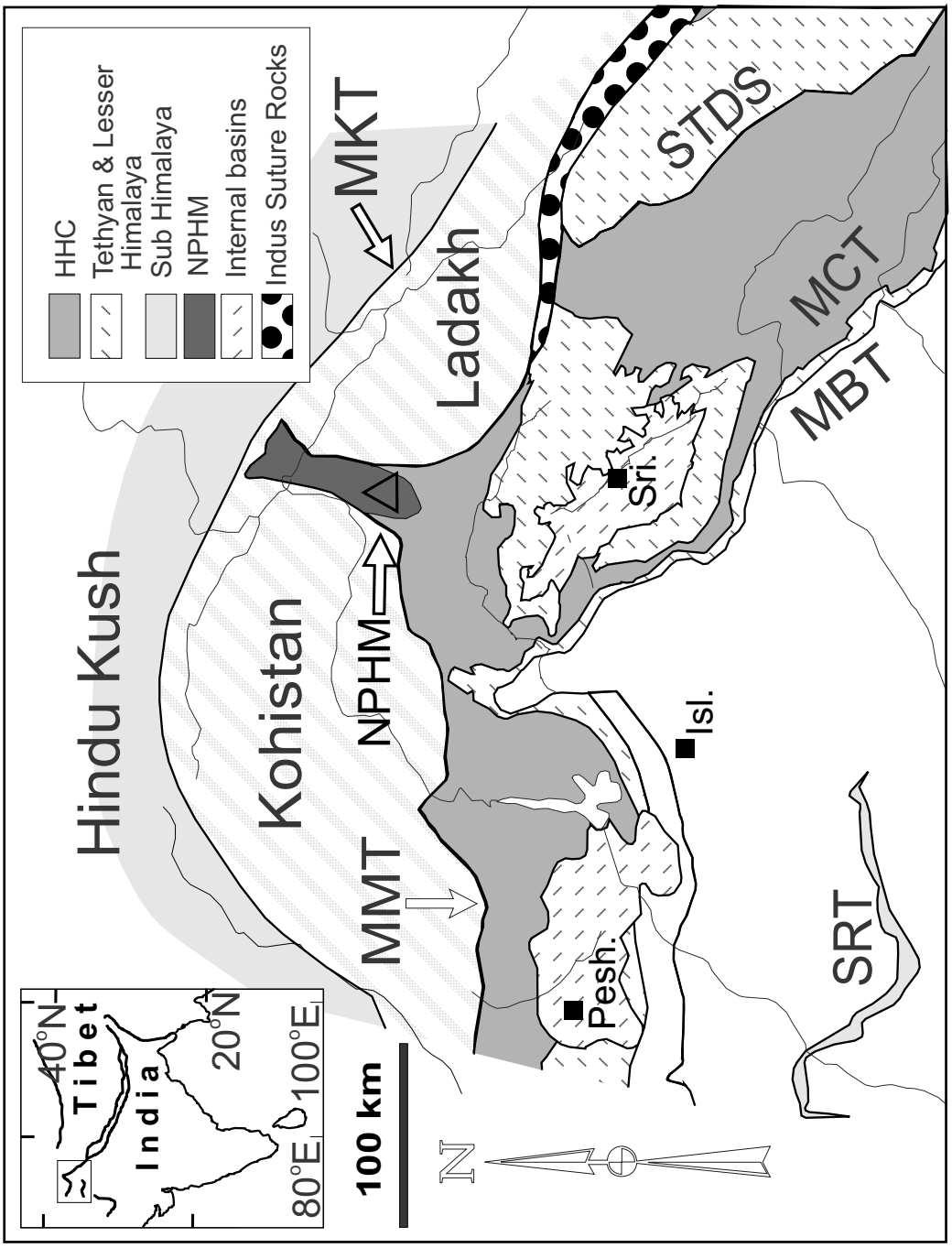

Figure 5.1A Regional Map of northwest Himalaya. MKT - Main Karakoram Thrust; MMT - Main Mantle Thrust; SRT - Salt Range Thrust, STDS - Southern Tibet Detachment System (section shown is Zanskar Shear Zone); MCT - Main Central Thrust; MBT - Main Boundary Thrust. Compiled by W.S.F. Kidd from Gansser, 1964; Coward et al., 1988; Searle et al., 1988; Greco and Spencer, 1993.

Figure 5.1B

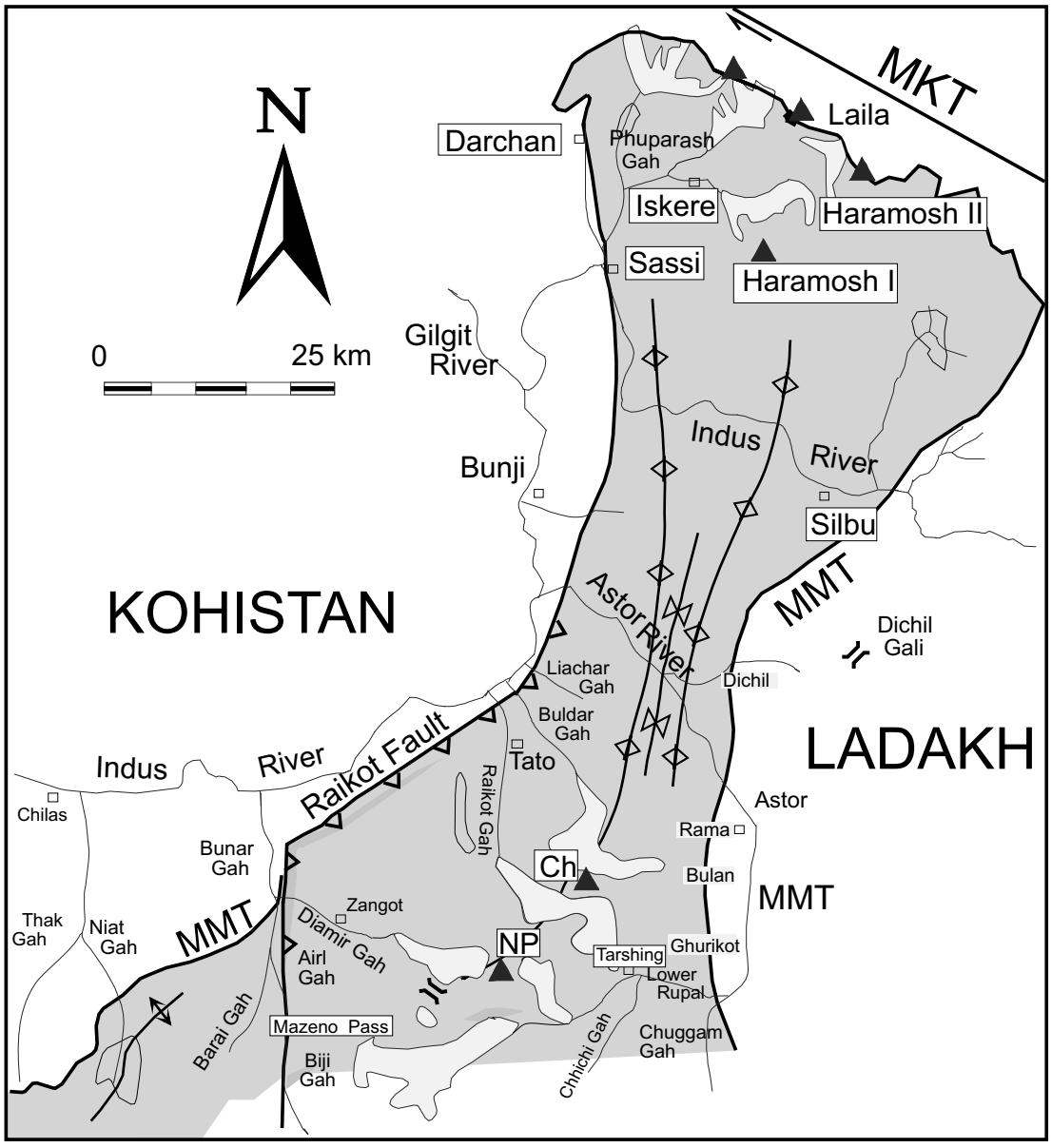

Figure 5.1B Overview map of NPHM. Selected valleys and towns shown. Grey - undifferentiated Indian rocks; white - undifferentiated KLS rocks or (north of MKT) undifferentiated Karakoram Terrane . NP - Nanga Parbat; Ch - Chongra Northern Peak; MKT - Main Karakoram Thrust. Heavy lines with barbs - reverse faults; paired barbs represent (W-E) Burdish Ridge Antiform, Dashkin synform, and Dichil Antiform, respectively (c.f., fig. 3). Black triangles - major peaks. Open squares - villages. Map sources: this study and Madin, 1986; Madin et al., 1989; Treloar et al., 1991; Lemmenicier et al., 1996; Pêcher et Le Fort, 1998.

general crustal scale antiformal folding (Gansser, 1964; Coward et al., 1985) with NNE-trending axes of folding recognised within NPHM (Madin 1986; Madin et al., 1989; Treloar et al., 1991; Butler et al., 1992). Northward deflection of the MMT trace around NPHM has resulted in historically diverse nomenclature for the NPHM-KLS regional margin to the east, including "Southern Suture" (Gansser, 1980), "Indus-Tsangpo Suture" (Coward et al., 1986), and "Stak Fault" (Burbank et al., 1996, fig 1; Brozovic et al., 1997, fig. 1). Where the NPHM-KLS contact can be recognised as MMT, I preserve that use of the term.

NPHM has drawn attention for several reasons: (1) It represents the NW terminus of the >2500 km Himalayan arc (e.g. Fielding et al., 1994) - the western "syntaxis" of Wadia (1931, 1932). (2) It forms an anomalous spur of Himalayan rock that has resulted from high grade Indian plate gneisses being exhumed from beneath the structurally overlying rocks of the upper Indian plate and overthrust KLS (Coward, 1985). (3) It is composed of Indian plate crystalline rock that seems to be reworked ~1.8 Ga crust (Zeitler et al., 1989; Chamberlain et al., 1989; Smith et al., 1992; Zeitler et al., 1993; Winslow et al., 1996; Schneider et al., 1997), a feature presently unreported from (e.g. ion microprobe) studies of the Himalayan crystalline slab outside of the NW main High Himalaya. (4) It represents an area of exceedingly young (~0.9 to >9.0 Ma) plutonism, metamorphism and cooling (Chamberlain et al., 1989; George and Bartlett, 1996; George et al., 1993, 1995; Schneider et al., 1997; Smith et al., 1992; Treloar et al., 1989; Whittington, 1996; Winslow et al., 1994, 1995, 1996; Villa et al., 1996; Zeitler, 1985; Zeitler and Chamberlain, 1991; Zeitler et al., 1982, 1989, 1993.) within an area of the Himalaya where anatectic and orogenic events are otherwise much older (~47-50 Ma - Zeitler and Chamberlain, 1989; Tonarini et al., 1993; Smith et al., 1994) than principal orogenic events in the main High Himalaya (~23 to 12.5 Ma - Edwards & Harrison, 1997). (5) These young

events require exhumation of up to 5-10 mm/yr (Craw et al., 1994). (6) This requires 10's km of rock to have been denuded in the last few m.y. from this rapidly uplifting[1] youthful area at the edge of the Himalaya.

Because of the reasons outlined in the preceding paragraph, at least thirty-one published refereed journal articles exist that expressly investigate the tectonic history of the Nanga Parbat - Haramosh Massif (Brozovic et al., 1997; Burbank et al., 1996; Butler and Prior 1988a, 1988b; Butler et al., 1989, 1992, 1997; Chamberlain et al., 1995; Coward, 1985; Craw et al., 1994; Cronin et al., 1993; George and Bartlett, 1996; George et al., 1993, 1995; Hubbard et al., 1995; Madin et al., 1989; Owen, 1989; Pognante et al., 1993; Smith et al., 1992; Treloar et al., 1991; Wadia, 1932; Wheeler et al., 1995; Whittington, 1996; Winlsow et al., 1994, 1995, 1996; Zeitler, 1985; Zeitler and Chamberlain, 1991; Zeitler et al., 1982, 1989, 1993) yet, at the time of writing, no structural mapping or structural sampling has been reported for the southern side of Nanga Parbat, and only preliminary and very sparse foliation measurements are published for the eastern side of Nanga Parbat (Winslow et al., 1995). Some local sparse structural mapping and structural sampling is published for the southwest side (Hubbard et al., 1995), although the nature of this is contentious (Burg et al., 1986; Asif Khan, personal comm.). The areas lacking in attention (south west and east) represent over 70% of the Nanga Parbat area. In an attempt to redress this lack of attention, and to further elucidate the tectonic history of this exciting part of the Himalayan Belt, I have conducted structural mapping across the western, southern and eastern portions, in conjunction with collaborators listed in section 1.2. The results of this mapping are presented in this thesis chapter. In addition to structural mapping, my objectives were to (1) look for exhumational structures, and/or deformation generally related to exhumation, (2) discriminate older (i.e.,

1. Uplift: Nanga Parbat has gone up relative to Kohistan (Chamberlain et al., 1989)

Himalayan) strain from strain related to exhumation of NPHM, and (3), propose a general tectonic model based upon both the new and previous observations. Items 1 and 2 are respectively introduced in the following two sections.

5.1.2 Exhumational versus extensional structures.

The apparent absence of large sediment storage areas within NPHM, requires the tens of kilometres of crustal section that are inferred to have been unroofed from NPHM in the Neogene to have been completely removed from the Middle Indus River drainage area. In the absence of reliable published sediment load values for the Middle-Upper Indus River system, philosophical thought experiment numerical calculations were developed (P. O. Koons, personal comm.). These indicated that, assuming a steady state of exhumational erosion since ~4 Ma, the present Middle-Upper Indus River system could have carried only few percent of the calculated volume of removed material. With the exception of extreme reconsideration (e.g., a re-assessment of the principles governing interpretation of (1) Ar/Ar, (2) U-Th-Pb, and (3) fission track ages), it seemed (at the start of the Nanga Parbat Continental Dynamics Project) that some component of the ~10 m.y. of very fast exhumation at NPHM required normal faulting of sufficient displacement (several kilometres), and sufficient ratio of fault dip to relative height (i.e. low-angle), to detach and displace large volumes of the upper massif out of the Middle-Upper Indus River system. One of the main goals upon undertaking of fieldwork around NPHM was, therefore, to search for such a structure. Although an STDS type structure (Burg et al., 1984; Burchfiel et al., 1992) would have displacement of probably several kilometres, and have a sufficient ratio of fault dip to relative height, an STDS structure that is continuous along strike was ruled out because no such structure is indicated from mapping at the North and West margins (e.g., Madin et al., 1989; Burg et al., 1996). The only possible scenario, therefore, for any exhumational faulting involved a south-

directed (and thus out of the Upper-Middle Indus drainage basin) normal sense detachment-type structure that would be highly localised to NPHM. Modelling of any such normal sense structure remains tricky in view of the fact that the theoretical structure is not long and narrow, and thus STDS-type plane strain models (e.g., Burg et al., 1984; Burchfiel and Royden, 1985; Yin, 1993; Grujic et al., 1996) are difficult to apply. As is shown, a large detachment-type structure highly localised to NPHM is not recognised, and although sediment load values for the actual Indus River system are still not available, glacier debris volume calculations have been recently been made (Shroder at al., submitted to Science), that do not require a tectonic denudation of the massif.

In consideration of the possibility of a low angle detachment structure at Nanga Parbat, it is worth noting that a confusion between (1) a regime of general extension and (2) syn-convergence (low-angle or detachment) normal faulting may exist. Lower level convergence contemporaneous with upper orogen extension (orogenic collapse, also called "gravitational collapse") is well documented from the Himalaya involving fault surfaces that are dipping both gently (Burg, 1981; Burg, 1983; Caby et al., 1983; Burg et al., 1984; Pêcher, 1991; Burchfiel et al., 1992; Gapais et al., 1992; Edwards et al., 1996; Hodges et al., 1997; Searle et al., 1997; Wu et al., 1998) and more-steeply (Searle, 1986; Herren, 1987), although in the enduring image (Burchfiel et al., 1992, fig. 43), the STDS dips <20°N. Hitherto, there was no data for the absence or presence of low angle normal faulting at NHPM. Numerous authors have entirely attributed the circumstances at NPHM to erosion, reporting "an absence of any extension at NPHM" (e.g., Burbank et al., 1996; Whittington, 1996; Brozovic et al., 1997; Butler et al., 1997; Whittington et al., in press), despite the existence hitherto of large unmapped portions of the massif. Such statements claiming an absence of extension are incorrect; in this thesis I show (sections 5.6 & 5.7) that there is (1) evidence for locally-restricted extension at NPHM, and (2)

separate evidence for low angle structures that could be (or have been) truly exhumational in character. The distinction outlined above (specific to NPHM) between a purely extensional structure and an overall exhumational structure is therefore important to bear in mind.

5.1.3 Himalayan and NPHM related strain

5.1.3.1 Principal Himalayan Fabric

The principal Himalayan fabric arises from the principal Himalayan collision, and includes the common trends of foliation, lineation and sense of displacement that are seen throughout the NW High Himalaya. In this thesis chapter, the term "principal Himalayan collision" is used to mean the high grade metamorphism, anatexis, and relative uplift that accompanied large thrust (±normal sense) displacement on both the MMT[2] and in the MMT footwall in general. Because NPHM is, in a first order sense, a N-S trending crustal scale antiform that locally folds and modifies the Himalayan fabric (e.g., Gansser, 1964; Coward et al., 1985), it is worthwhile to consider the age and appearance of the regional fabrics that were developed during the principal Himalayan collision, before investigating how they might appear upon subsequent modification by the exhumation of NPHM.

In the NW Himalaya, away from NPHM, it appears that the principal High Himalayan events occurred between 47-50 Ma (Treloar & Rex, 1990; Chamberlain et al., 1991; Tonarini et al., 1993; Smith et al., 1994), although N-directed

2. For the purposes of this discussion of rotation of fabric, I use "MMT" to mean an idealised package of rocks that have been homogeneously, and non-coaxially sheared. The MMT is defined as the contact of NW India with the KLS (op. cit.) and is not defined by any strict consideration of strain gradient. Although thrust (±normal) sense strain continues for several kilometres depth in the Himalayan rocks directly below the KLS contact (*sensu stricto*), for the purposes of lithological discussion I follow others (e.g. Treloar et al., 1989; Burg et al., 1996) and include all Himalayan rock as part of the general "MMT footwall". A distinctions such as "MMT", "non-MMT", and "MMT zone" are not practical. The term "MMT footwall" therefore carries no inferences about strain. (c.f., "MCT zone" - Davidson et al., 1995; Le Fort, 1996; Harrison et al. 1997).

underthrusting below Kohistan of the Indian plate that is now exposed at NPHM may have continued until late Oligocene times (George et al., 1993) based upon dating of muscovitic leucocratic dykes within the Kohistan batholith, that are preserved on the NPHM western margin, and that show thrust sense involvement with the MMT (George et al., 1993). Principal lineation fabrics that resulted from the principal High Himalayan events are regionally NW- to NE-plunging, and associated displacement sense is recognised to be predominantly thrust sense, top-to-south (Chaudhry and Ghazanfar, 1987, 1989; Greco et al., 1989; Treloar et al., 1989; Burg 1996; Anczkiewitz et al., 1997).

5.1.3.2 Rotation of Himalayan thrust fabric

Figure 5.2A to C illustrates the anticipated appearance of MMT fabrics as they become rotated towards or into vertical limbs in a simple case of crustal scale antiformal folding, assuming that there has been a largely "passive" rotation (i.e., no significant reworking of fabric). Although observed principal lineation trends in the NW Himalaya depart from north plunging by ±45° (references above), in the case of the upright antiformal folding represented in figure 5.2C, once the limbs are steepened to vertical, and assuming no large inhomogeneous strain, lineation will be rotated by the folding to plunge moderately in the approximate direction of the fold axial surface strike. As shown in figure 5.2C, apparent right-lateral displacement sense is anticipated on the east margin and apparent left-lateral displacement sense is anticipated on the west margin. In the case of NPHM, studies along the Indus Gorge indicate upright to steep tight folds whose axial traces trend ~NNE (Madin, 1986; Madin et al., 1989; Treloar et al., 1991), and consequently, where lineation trends approximately NNE, it is regarded as rotated Himalayan fabric. I have recognised similar trends of folding in SE NPHM (described in this thesis chapter). Although, as

Figure 5.2

Figure 5.2 A & B (next page)

A: (upper figure - next page) shows N-S cross sectional view of initial situation after S-directed thrusting along the MMT. A thick ductile, thrust sense, high strain horizon has developed (asymmetric fold symbols are general representation of sense of shear indicators found).

B: (lower figure - next page) shows equivalent W-E cross sectional view of A. Note use of "head and tail of arrow" (this convention is used throughout this thesis) indicating that the hanging wall ("Kohistan-Ladakh Series") has moved outward (with respect to the plane of view) while the footwall ("Indian rocks") has moved inward.

Figure 5.2

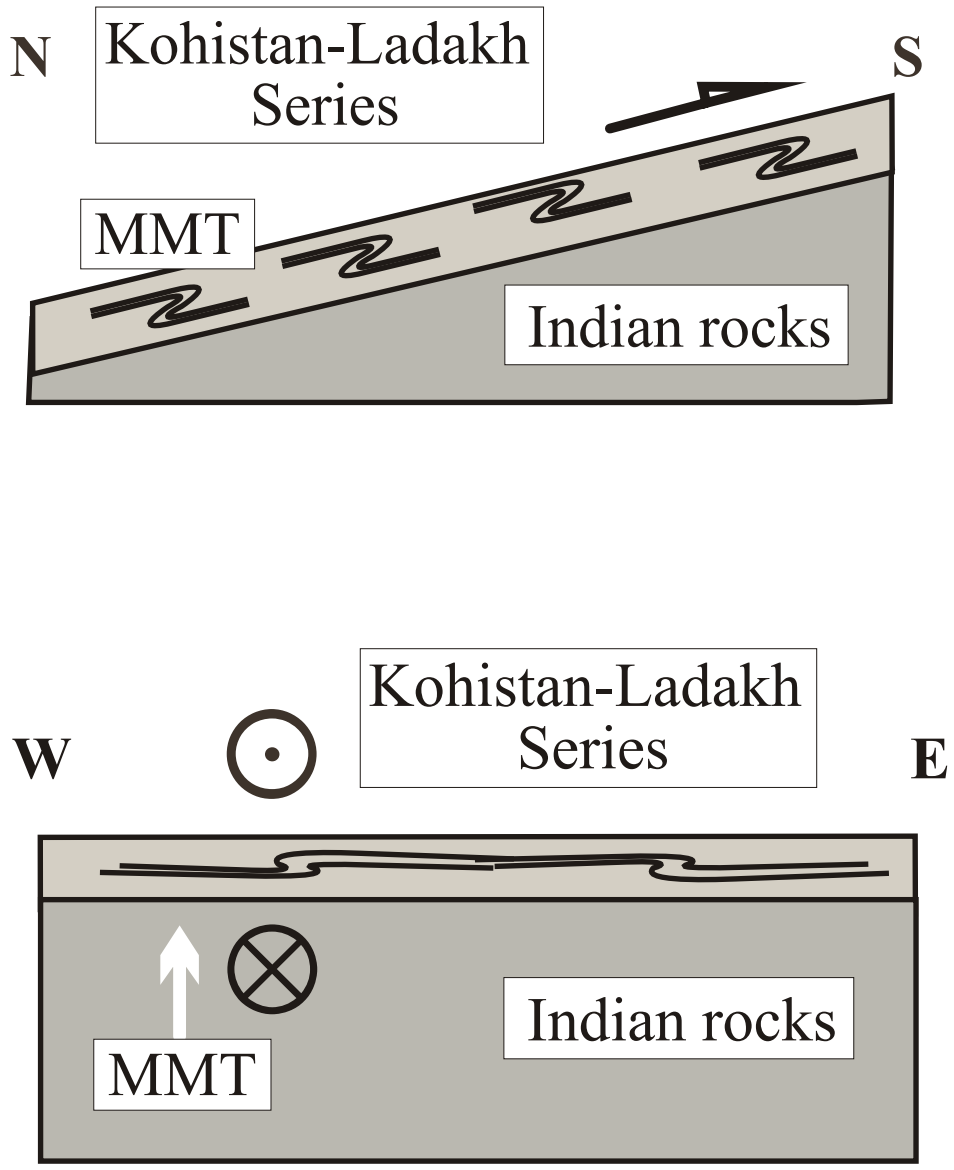

Figure 5.2A & B see previous page for caption

Figure 5.2C

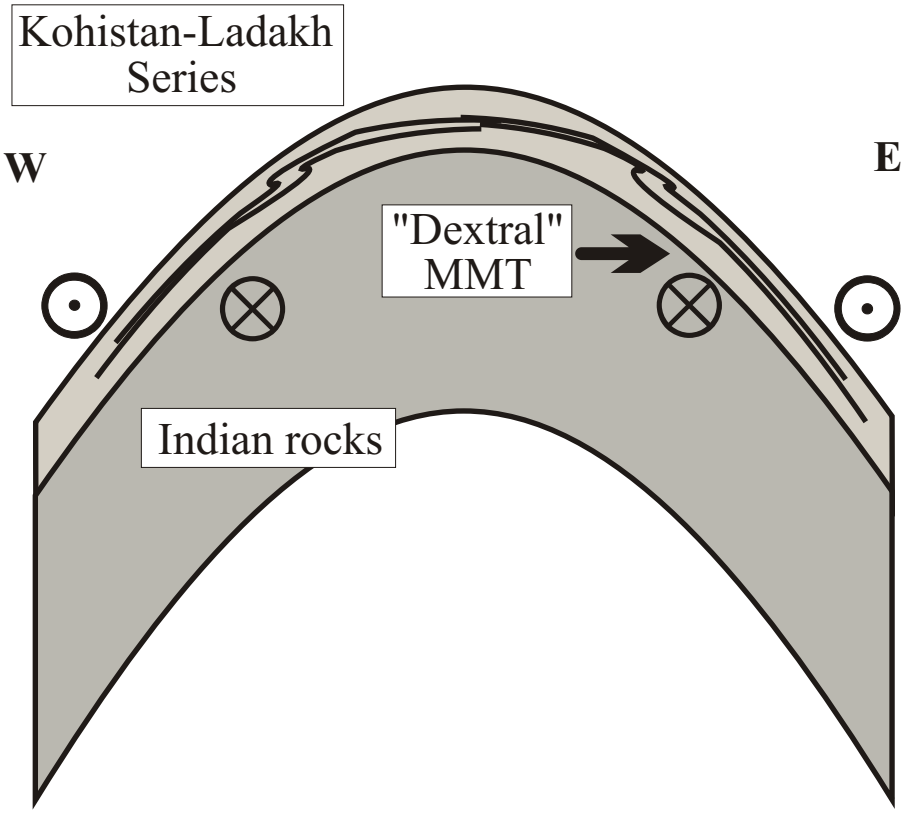

Figure 5.2C W-E cross sectional view of MMT after crustal scale antiformal folding. With continued tightening of the fold, steepening of limbs will bring the MMT high strain zone developed in 5.2A to near vertical. Apparent sense of shear will be left lateral on left (west) side, right lateral on right (east).

will be shown, NPHM is more complex than a simple crustal-scale antiform, the first order concept of right-lateral shear on the east margin and left-lateral on the west margin should be remembered.

5.1.3.3 Himalayan normal sense fabric

Large amounts of normal motion, syn-convergence extension that results in top-to-north, high grade ("mylonitic") deformation accompanied by approximately parallel lineation fabric, but opposing displacement sense to the general thrust fabric, have not been widely reported from the NW Himalaya (in either MMT footwall or hanging wall). In this way, the NW Himalaya are unlike the main Himalaya where this type of (STDS) normal fabric is ubiquitous in the uppermost part of the Himalayan crystalline slab (references above). Some extensional "collapse" in the MMT footwall is recognised from (1) kilometric-scale folding (Burg et al., 1996) and (2) discrete lower temperature shears of a few metres width that are directly below the MMT (Vince and Treloar, 1996) or a few kilometres below the MMT (Treloar et al., 1991). At the time of writing, however, a thorough reversal of top-to-south, thrust sense fabric through overprinting by normal sense, top-to-north motion has not been reported from the MMT footwall. Because syn-convergence extension is a major issue in the Himalaya, and in orogenic belts in general, evidence for MMT normal motion of both low and high grade deformation mechanisms is investigated and discussed in this thesis.

Concerning an STDS-type normal sense overprinting, let us consider the situation at NPHM if normal sense deformation did overprint a portion of the MMT that was subsequently rotated to the present steep, ~NNE trending attitude at NPHM. In such a case, we would anticipate apparent left-lateral on the east margin and apparent right-lateral on the west margin; the reverse of the case described above for original MMT thrust fabric, folded by a simple crustal scale antiform. Again, this

assumes a passive rotation and no substantial ductile reworking of the upper MMT footwall.

5.1.3.4 NPHM exhumation-related fabric

In addition to MMT normal motion that may have overprinted MMT thrust fabric(s), younger fabrics resulting from major structures related to exhumation of NPHM must post-date, and hence can locally overprint, both the thrust and normal motion fabrics. The Raikot Fault is a noteworthy example that cuts away the MMT at the large bend in the Indus River near Raikot Bridge (plate 2). In the hanging wall of the Raikot Fault (NPHM rocks), a strong SE-plunging lineation is developed (Madin, 1986; Butler & Prior, 1988; Madin et al., 1989; Butler et al., 1990). These authors report that displacement sense is consistent with NPHM moving upwards with respect to Kohistan, and conclude that NPHM-related strain overprints, and fully obliterates, the earlier Himalayan fabric (i.e. NNE-trending lineation).

I attempt to differentiate between possible overprinting of deformation signatures associated with MMT thrust-, MMT normal-, and NPHM exhumation-related tectonics. In cases where overprinting is associated with conspicuous re-orientation of lineation, such as in the Raikot example above, displacement sense will be considered using sense of shear criteria[3] applied at the hand-specimen scale and at the microscopic scale. Differentiation between phases of deformation is more tricky in cases where contrasts in fabrics are not as dramatic as in the Raikot Fault. For example, microstructure indicating deformation mechanisms related to Himalayan deformation may be either enhanced or "annealed" (caused to recover) by NPHM tectonic processe (e.g., heat). The phenomena of recovery and enhancement will be addressed where appropriate. In the case of each rock type or sample considered,

3. Chapter appendix ***5.X.1*** details procedures and assumptions underlying observed phenomena that have been used in sense of shear analyses. In this way, detailed description within the main body of the chapter is not broken up by discussions and references.

principal (micro)fabric including sense of displacement and possible deformation mechanism[4] will be described with a view to recognising the main tectonic event as being associated with pre-, thrust-, normal-, or post-Himalayan (i.e., NPHM) events.

5.2 LITHOLOGIC BACKGROUND

The KLS rocks are all from the fossil volcanic arc and are mostly mafic (Tahirkheli et al, 1979; Tahirkheli and Jan, 1979; Bard et al., 1980; Tahirkheli, 1982; Bard, 1983; Coward et al., 1988; Williams, 1989; Lemmenicier et al., 1996 Anczkiewicz et al., 1997), and have therefore been distinguished on a first order basis from the metasedimentary schists and gneisses that are regionally recognised to comprise the Himalayan Rocks at Nanga Parbat (Coward, 1985; Madin, 1986; Madin et al., 1989; Treloar et al., 1991; George et al., 1993; Chamberlain and Zeitler, 1996; Lemmenicier et al., 1996; Pêcher and Le Fort, in press). Even when viewed from several kilometres away, the green rocks of the KLS mark a striking colour contrast with the orange and brown layering of the Himalayan metasedimentary schists and gneisses of NPHM. Along the eastern Indus, KLS rocks (rocks in the MMT hanging wall) are marked by thick sequences of amphibolite, (grano)diorite, metabasite, and undifferentiated greenstone (Tahirkheli and Jan, 1979; Verplanck, 1986; Treloar et al., 1991; Pognante et al., 1993; Lemmenicier et al., 1996). The NPHM rocks include Indian "cover" sequence schists and gneisses (garnet-staurolite grade) and "basement" gneiss (sillimanite grade along the Indus; granulite facies ±cordierite-bearing anatectic segregations closer to the Nanga Parbat summit area (Madin, 1986; Madin et al.,

4. Chapter appendix ***5.X.2*** details procedures and assumptions underlying observed phenomena that have been used in attempting to infer deformation mechanisms from microstructure.

1989; Treloar et al., 1991; Pognante et al., 1993; Smith et al., Treloar et al., 1995; Winslow 1996; Butler et al., 1997; Whittington et al., in press).

Within this thesis chapter, I occasionally substitute the term "MMT" for "NPHM/KLS contact" where it is necessary to make the jump to regional considerations. Various workers (e.g., Madin, 1986; Madin et al., 1989; Treloar et al., 1991; Butler et al., 1992; Wheeler et al., 1995; Pecher and Le Fort, in press) have shown that the assumption that the MMT is equivalent to the NPHM/KLS contact is valid when there is no significant local overprinting due to NPHM exhumation. As can be seen in the Astor Gorge descriptions (section 5.4), this assumption holds for the simple antiform that is seen in southeastern NPHM.

5.2.1 Indian basement and cover at NPHM

In this thesis chapter, a rigid discrimination of cover and basement is not sought because the distinction between cover and basement at NPHM is not well defined, and different workers often base the distinction upon different grounds. Accordingly, some space for discussion is made here.

5.2.1.1 Basement

The pre-Himalayan tectonism (metamorphism & deformation) recognised at NPHM is thought to be Precambrian (e.g. Treloar et al. 1991; Wheeler et al., 1995). This is because (1) numerous amphibolite dykes that are probably Permian-age[5] "Panjal Traps" (Wadia, 1931; Papritz and Rey, 1989; Greco et al., 1989) cross-cut the fabric of, and hence post-date, a major (pre-Himalayan) phase of metamorphism and deformation within the high grade gneisses of Nanga Parbat, and (2) preserved Tethyan passive margin rocks of India show a fairly continuous stratigraphy from

5. Note that basaltic volcanism from the early Cretaceous has also been reported in this part of the Himalaya (Sutre, 1991).

Cambrian to the onset of collision (e.g., Lombardo et al., 1993). This proposal of Precambrian metamorphism is consistent with upper intercept ages of ~1.8 Ga for zircons from NPHM high grade gneisses (e.g. Zeitler et al., 1979; Smith et al., 1992; Schneider et al., 1997) and ~1.8 Ga upper intercept ages for zircons from young NPHM granites (Smith et al., 1992; Zeitler et al., 1993; Winlsow et al., 1996; Schneider et al., 1997). It has therefore been widely assumed that gneisses that are cross-cut by amphibolite dykes and/or those that contain 1.8 Ga zircons are part of the high grade rock that formed the continental crystalline basement to the Cambrian and younger rocks of the Indian passive margin. I use the term basement with some reservation in this thesis chapter, however, based upon observations from central Rupal, from Chichi #1 glacier, and from Diamir valley (fig 5.3) that may offer a note a caution regarding (1) the assumed Permian age for the NPHM cross-cutting amphibolites, and (2) the possibility of the 1.8 Ga zircons in the high grade gneisses being detrital (see 5.X discussion).

5.2.1.2 Cover

The same probably Permian basic igneous rocks that cross-cut much of the high grade NPHM gneiss were repeatedly intruded as sills or extruded as flows during the development of a carbonate platform on the NW passive margin of India resulting in a widespread sequence of interlayered marbles and amphibolites and pelites that define part of the recognised cover rocks in the NW Himalaya (Wadia, 1931; Honegger et al., 1982; Papritz & Rey, 1989; Greco et al., 1989; DiPietro et al., 1993; Anczkiewicz et al., 1997). Presumably equivalent, contrasting black and white interlayered marble and amphibolite are commonly found in parts of the NPHM margins and are regarded as part of the cover sequence (e.g., Wheeler et al., 1995). Characteristic garnetiferous metapelites and other recognisable metasedimentary rocks are often associated with the interlayered marbles and amphibolites around NPHM.

An equivalent package of metasedimentary rocks and interlayered marbles and amphibolites has also been recognised in various forms along the footwall of the MMT, away from NPHM, both by me and other workers (Greco et al., 1989; DiPietro et al., 1993; Burg et al., 1996; Anczkiewicz et al., 1997; Asif Khan, personal comm.). Where I recognise this package at NPHM near the MMT, I interpret it as part of the original Indian plate cover sequences.

5.3 GEOLOGICAL OBSERVATIONS IN SE NPHM

5.3.1 General procedures

Geological observations of valleys investigated in SE NPHM are reported consecutively, beginning with Lower Rupal where I mapped the first fairly complete section (plate 2). The central to upper portion of Rupal valley nominally begins west of Chongra Glacier, and so this is addressed later in the chapter. In Lower Rupal, outcrop and/or thin section description are followed by local interpretation. Afterwards, a general interpretation and conclusion is presented for SE NPHM, along with a discussion.

Initial investigations were in the Lower Rupal valley because outcrop of NPHM rocks is fairly continuous and the Rupal valley forms a good section through the eastern portions of SE NPHM (plate 2). Initial investigations were to (1) establish a basis for the both the structural and lithologic character of rocks in southeast NPHM (this was successful - a large consistency in both rock types and deformation styles is found), and (2) the building of a tectonostratigraphic sequence (this was partly successful - a true tectonostratigraphic sequence that is continuous from valley to valley was not recognised everywhere). Because most of the main rock types and structural trends of SE NPHM are typified by those seen in the Lower Rupal valley,

greater detail is given to rock descriptions and to structural trends in this part of the section than elsewhere. This detail serves as an introduction, whereby large amounts of repetition are avoided by referring back to the Lower Rupal Valley descriptions.

5.3.2 Lower Rupal Valley

5.3.2.1 NPHM/KLS contact

Although outcrop is largely continuous along the Lower Rupal Valley, the actual NPHM/KLS contact is not exposed, although it is visible as a contrast between green, to the east, and orange and brown, to the west, up in the hills around Rampur Eck (fig. 5.3 and plate 2). Note that layering is all east-dipping in the lower portions of Rampur Ridge. This trend continues along most of the left bank[6] of Lower Rupal Valley. The sudden overturning of layering to east dipping that is just visible at the top of the ridge is significant; in all other valleys that I include as part of SE NPHM (Rattu, Ghurikot, Bulan, and Rama valleys), the MMT sequence is everywhere overturned and dips west.

West of where the KLS/NPHM contact projects down from the ridge top at Rampur Eck, a few 100's metres of outcrop are exposed in cliff into which the jeep track is cut. Here (outcrop #13) there is a continuous sequence of mm-cm-10's cm layered garnetiferous metapelites interlayered with cm to 10's cm amphibolite and biotite schists, gneisses and marble layers. Clear compositional changes between layers are recognised by (1) brown staining due to Fe-weathering, (2) size of garnets <1 - >10 mm, (3) continuity and intensity of stretching fabric, and (4) ratio of micas or amphiboles to feldspars and quartz grains, (figs. 5.4 and 5.5). The layered

6. To specify locations within valleys, I employ the convention of left and right (the observer faces downstream or "downglacier"). This eliminates compass ambiguity when valleys are not straight.

Figure 5.3

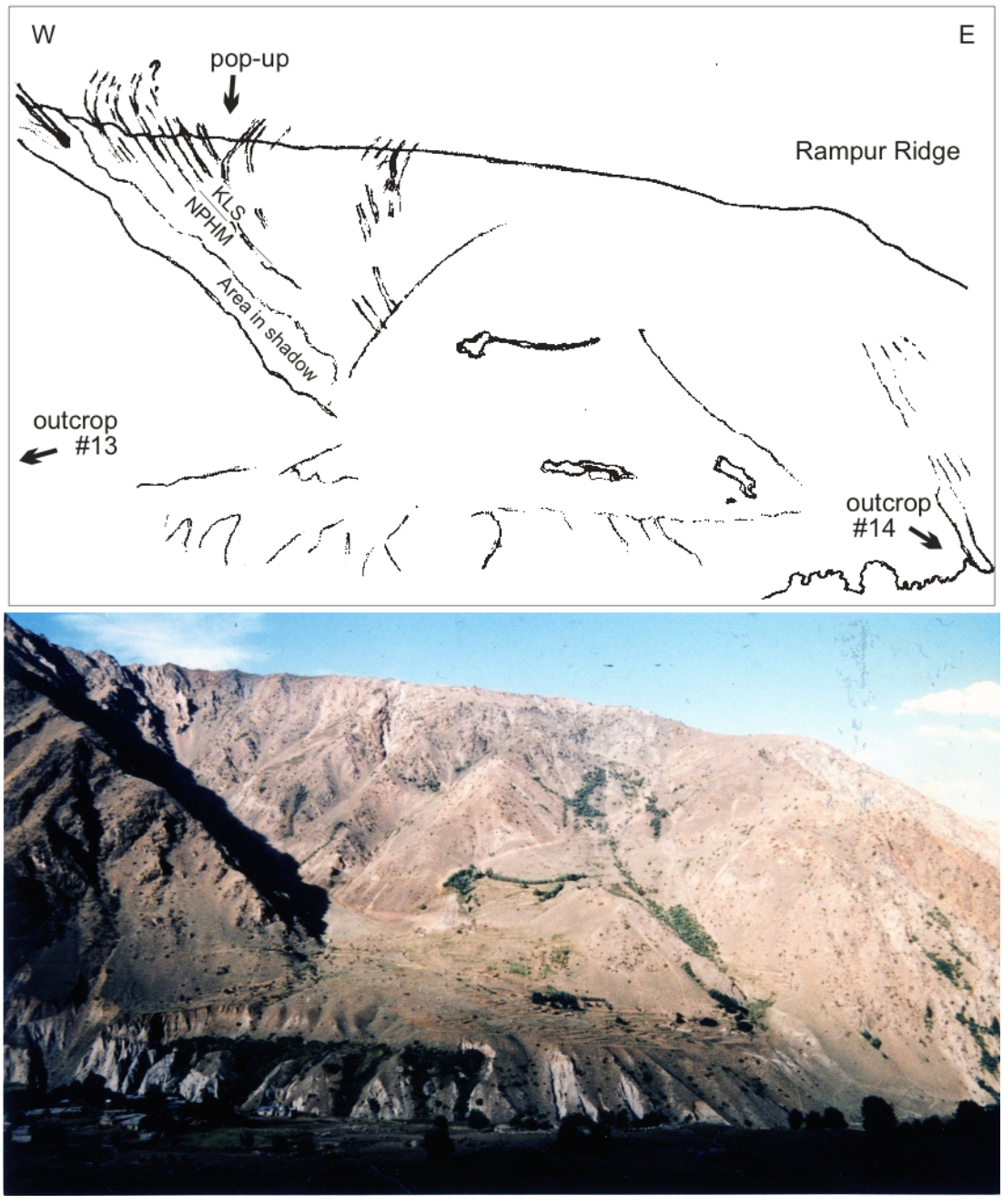

Figure 5.3 (field photo and line drawing). View to north of Rampur Ridge that forms easternmost portion of left bank of Lower Rupal Valley. Scattered fields and trees on level in foreground are ~2600 m in elevation. Central portion of Rampur Ridge is ~3700 m. Outcrop #14 is visible. Outcrop #13 is ~200 m beyond left edge of field of view. Contact between Kohistan Ladakh Series (KLS) and NPHM is present in hillside below Rampur Ridge and identified by pale brown east-dipping layers (labelled NPHM on line drawing) structurally below dark green layers (labelled KLS on line drawing). Note (1) local ~100 m wide pop-up structure and overturning of KLS layers east of pop-up. Photo 21/9/96 no.5.

Figure 5.4

Figure 5.4 Looking N. to left bank of Lower Rupal Valley. Cascade folding of mm-cm-10's cm layered garnetiferous metapelites interlayered with cm to 10's cm amphibolite and biotite schist. Trend is ~005° to 025° and axial planes dip ~65-75° W. Note overall monoclinal flexure is steep to left (west). Layers further steepen to left of field of view, and are overturned and truncated by a series of 40-80° west-dipping, brittle fault sets of west-side up minor (centimetre to metre) displacement. Jeep track is cut into hillside directly below field of view. Thickest dark band in lower centre is ~0.75m. Photo 21/9/96, no.3. View from right bank of Lower Rupal Valley.

Figure 5.5

Figure 5.5 Compositional layering within garnetiferous metapelites at outcrop #13, left bank of Lower Rupal Valley (c.f. fig 5.4). Note well-laminated quartzofeldspathic portions possibly suggesting high strain (c.f. fig. 5.8). Hammer for scale. Photo 6/7/95, no.5a

metapelites are very steeply dipping and generally strike[7] 005° to 025° (Fig 5.6) and are locally buckled on a 10's cm wavelength (fig. 5.7). The fold axial planes are steeply (~65-75°) west-dipping and the overall buckling morphology defines a suite of asymmetric folds and monoclinal flexures that cascade to the east. Fold hinges trend ~15-25° towards 355-025°. There is a lineation approximately parallel to the fold hinges defined by (1) a biotite mineral lineation, and (2) crenulation intersection (seen clearly in fig. 5.7). These metasedimentary rocks are a good illustration of layering preserved from the sedimentary protolith that is assumed to be "Tethyan"; the cover rock of the pre-collision Indian passive margin. Compositional layering on the outcrop scale is illustrated in figure 5.4, whereas figure 5.8 illustrates compositional layering at the mm - cm scale shown by thin section[8] 5/29F - a garnet-biotite amphibole schist, one of the finer-grained metapelites. In 5/29F, the compositional layering is picked out within the field of view by the hornblende rich and poor portions (relative to the quartz and feldspar). The garnets visible in 5/29F (fig. 5.8) are small (~500 mm) compared to other layers within this sequence of metapelites (garnets >10 mm). Figure 5.8 additionally provides a good opportunity for discussion of histories of garnet growth and strain. The garnets in 5/29F show little evidence of growth that is syn-kinematic to a non-coaxial strain; the garnets lack, for example, (1) asymmetry of pressure shadows or (2) the classic garnet spirals that result from host rock fabric that is progressively incorporated into the garnet while the garnet grows and rotates with respect to the host fabric. One garnet grain seems to have a partial ribbon of quartz partly squashed around it, indicating some shortening after garnet

7. In this thesis, orientations use standard compass conventions. Numbers increase clockwise from 001° to 360°. Lines are said to "plunge" (downhill direction) 01° to 89° "towards" (or "@") 001° to 360°, or pitch is given; 01-89°N. Planes are said to "strike" or "trend" from 001° to 180°, and dip from 01° to 89°, followed by N,S,W or E to eliminate ambiguity.
8. 5/29F refers to a thin section cut from lithological field sample NE95/29-VI. Thin sections and samples are detailed in table form in Chapter Appendix 5.XX.3 and are referred to in this manner throughout the chapter. A clarification of nomenclature accompanies the tables.

Figure 5.6

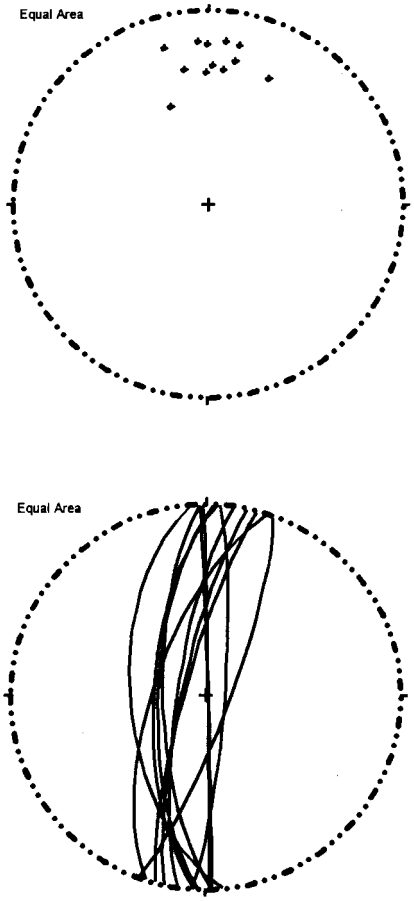

Figure 5.6 Lower hemisphere equal area projection of foliation poles and lineation of main fabric of all rocks in Lower Rupal Valley east of Tarshing.

Figure 5.7

Figure 5.7 Looking S and upwards, on right bank of Lower Rupal Valley (few 10's m W of outcrop #50). Mitch Wemple standing on cascade folds within layered garnetiferous metapelites. Trend is ~178° - 015° and axial planes dip ~68° W. Hinge lines plunge ~38°@005°. Note (1) prominent fold hinges in centre, and (2) crenulation intersection lineation developed below Mitch's left foot. Photo 21/9/96, no.4.

Figure 5.8

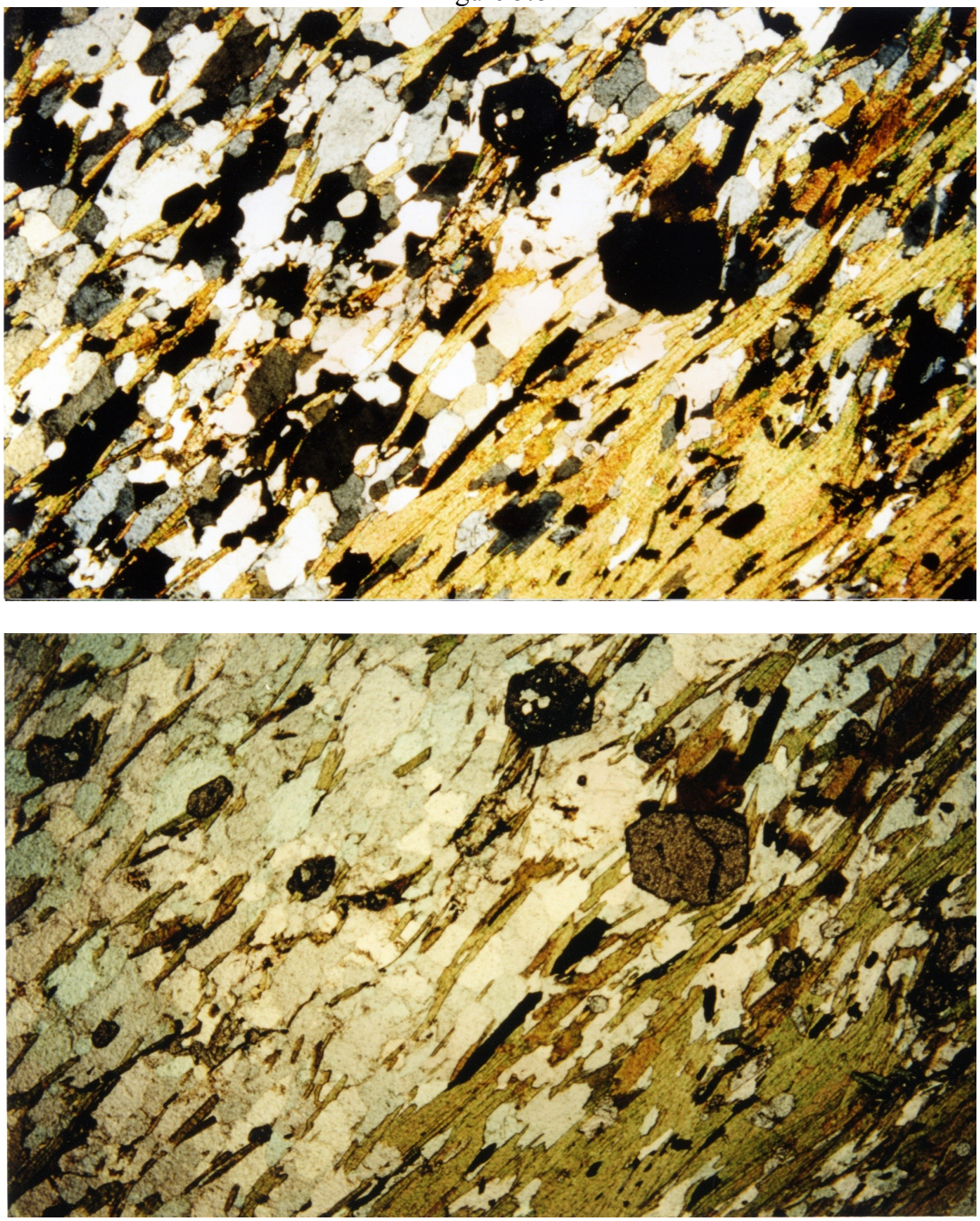

Figure 5.8 Optical photomicrographs (upper - crossed polars, lower - plane polarised light) of thin section 5/29F (cut from NE95/29-VI), garnet-biotite-amphibole schist from outcrop #13. Photo is taken with foliation oblique to horizontal to emphasise (1) proto-sedimentary layering (hornblende rich & poor portions) and (2) lattice preferred orientation in hornblende. See text for sense of shear discussion. South is to bottom left, north is to top right. Cut parallel with lineation (20°@005°), perpendicular to foliation (010°/85°E). Image base is 5.5 mm.

growth. Part of the grain, however, has the appearance of having partly grown into the ribbon and into a hornblende needle (slightly clearer in plane-polarised light [PPL] view). This may be evidence that garnet growth is syn-, to post-kinematic to a coaxial deformation[9]. Although the garnets show no real asymmetry, there is some asymmetry in the quartz ribbons. Elsewhere in the thin section, sigmoidal tails of quartz clasts and mica fish are present, and both show sinistral[10] sense of shear. Although high strain is suggested by well-defined quartz ribbons that form part of the microfabric, there do not appear to be any signs of patchy or undulose extinction within the quartz grains, and many grain to grain boundaries appear quite sharp; i.e., individual grain morphologies do not show evidence for significant intragranular deformation mechanisms having operated. Occasionally, there is perhaps some suggestion of grain boundary migration based upon small lobate fingers of quartz poking out from otherwise non-undulatory grain boundaries. I suggest that (1) this rock has been deformed at 400-600°C (see discussion in section 5.9.2) to generate the ribbons, and (2) there has been subsequent (static) recovery, possibly overlapping in time with the garnet growth. This recovery has restored the sharpness of grain to grain contacts and removed dislocation pile ups that can cause patchy or undulose extinction (section 5.3.2.6).

The absence of obvious non-coaxial syn-kinematic garnet growth in thin section 5/29F is also seen in some of the other small garnets within the schists and metapelites. Larger garnets however, frequently show "S" or "Z" shapes defined by tails or asymmetric pressure shadows, and contain spiral inclusion trails. Figure 5.9

9. Passchier and Trouw (1996) would probably use the term "syn-tectonic" rather than "syn-kinematic". These authors propose a more refined scheme involving a fourth category "intertectonic" in addition to "pre-, syn-, and post-tectonic". Such a scheme has not been employed here in spite of the clear polyphase nature of deformation at Nanga Parbat, as I have not attempted to assign D_1, D_2, D_3, etc., to observed strain features.

10. Throughout this chapter, sinistral and dextral are used with respect to present orientation to describe strike slip component of shear.

Figure 5.9

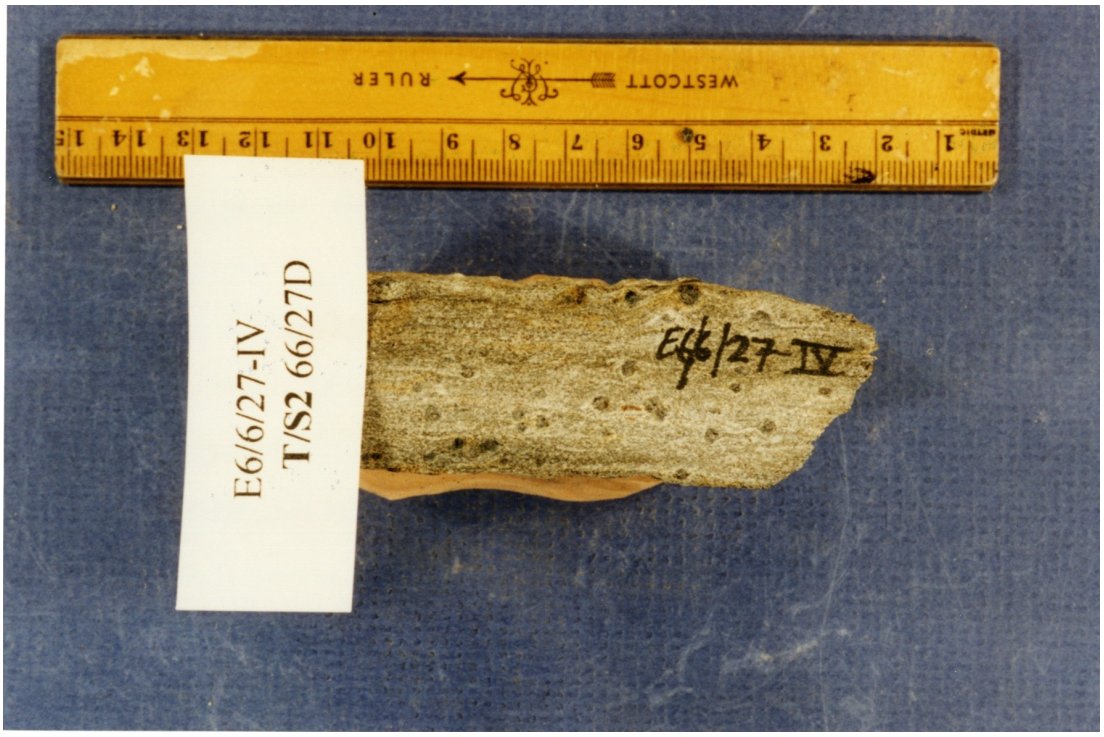

Figure 5.9 Sample E6/6/27-IV from near KLS/NPHM contact on left bank of E Astor Gorge. 170°/89°E, 15°@170°. Illustrates pressure shadow asymmetry in a garnetiferous metapelite. Sense of shear is dextral, consistent with fig. 5.10 (thin section 66/27D). This is typical for sense of shear observed in metasedimentary rocks along E. Astor Gorge.

(sample E6/6/27-IV) illustrates pressure shadow asymmetry in a garnetiferous metapelite. In thin section (figure 5.10, thin section 66/27D, cut from E6/6/27-IV) the ~3 mm garnet shows good inclusion trails which suggest a rotation of the garnet relative to the principal fabric defined by the micas (the photomicrograph oriented with the image base approximately parallel to the principal fabric). On all sides, the micas seem to bend around the garnet and there appears to be no post-kinematic growth. Other garnet porphyroblasts in this thin section (66/27D) are consistent. Sense of shear is not discussed here because 66/27D is actually from an equivalent section of metasedimentary rock near the NPHM/KLS contact on E. Astor Gorge (see 5.4.4). The rock is typical, however, of much of the garnetiferous metapelite found at outcrop #13, in the Lower Rupal Valley section of NPHM, and so is included in this general introduction to lithologies that is part of the Lower Rupal Valley description.

A clear sinistral shear sense is seen in thin section 5/29F and in parent sample NE95/29-VI. This is the consistent with outcrop evidence from (1) garnets in which matrix inclusions can actually be observed to be incorporated in a rotational pattern, and (2) sigmoidal trails from 1-4 mm feldspar augen in the more gneissic portions of the metapelite that are between the coarse garnet layers. Other field samples and observations from this portion of the Lower Rupal Valley (outcrop #13) are less conclusive with respect to sense of shear as there is frequently outcrop evidence for both sinistral and dextral sense, or quite often there is no clear sense of shear (e.g., E6/7/5-III). The amphibolite layers frequently show no internal sense of shear (e.g.,. E6/7/5-II and NE95/29-VII).

The sinistral sense of shear observed in this area is inconsistent with a simple steepening of MMT (Himalayan) thrust fabric as discussed above (e.g., fig. 5.8 5/29F). The observed sinistral sense can be explained by two scenarios: 1. This section of cascading folds is the western limb of a local, large (>300 m?) intrafolial

Figure 5.10

Figure 5.10 (next page) Optical photomicrographs (upper - crossed polars. lower - plane polarised light) of thin section 66/27D, (cut from sample E6/6/27-IV). Illustrates pressure shadow asymmetry in a garnetiferous metapelite. Garnet shows good inclusion trails that suggest a rotation (in this case, clockwise i.e., dextral sense) of the garnet relative to the principal fabric defined by the micas (photomicrograph oriented with base of image approximately parallel to principal fabric). On all sides, the micas seem to bend around the garnet and there appears to be no post-kinematic growth. Other garnet porphyroblasts in this thin section are consistent. Sense of shear is dextral , consistent with other metasedimentary rocks along this part of E. Astor Gorge. Cut parallel with lineation (15°@170°), perpendicular to foliation (170°/89°E). South is on left. Base of image is 5.5 mm.

Figure 5.10

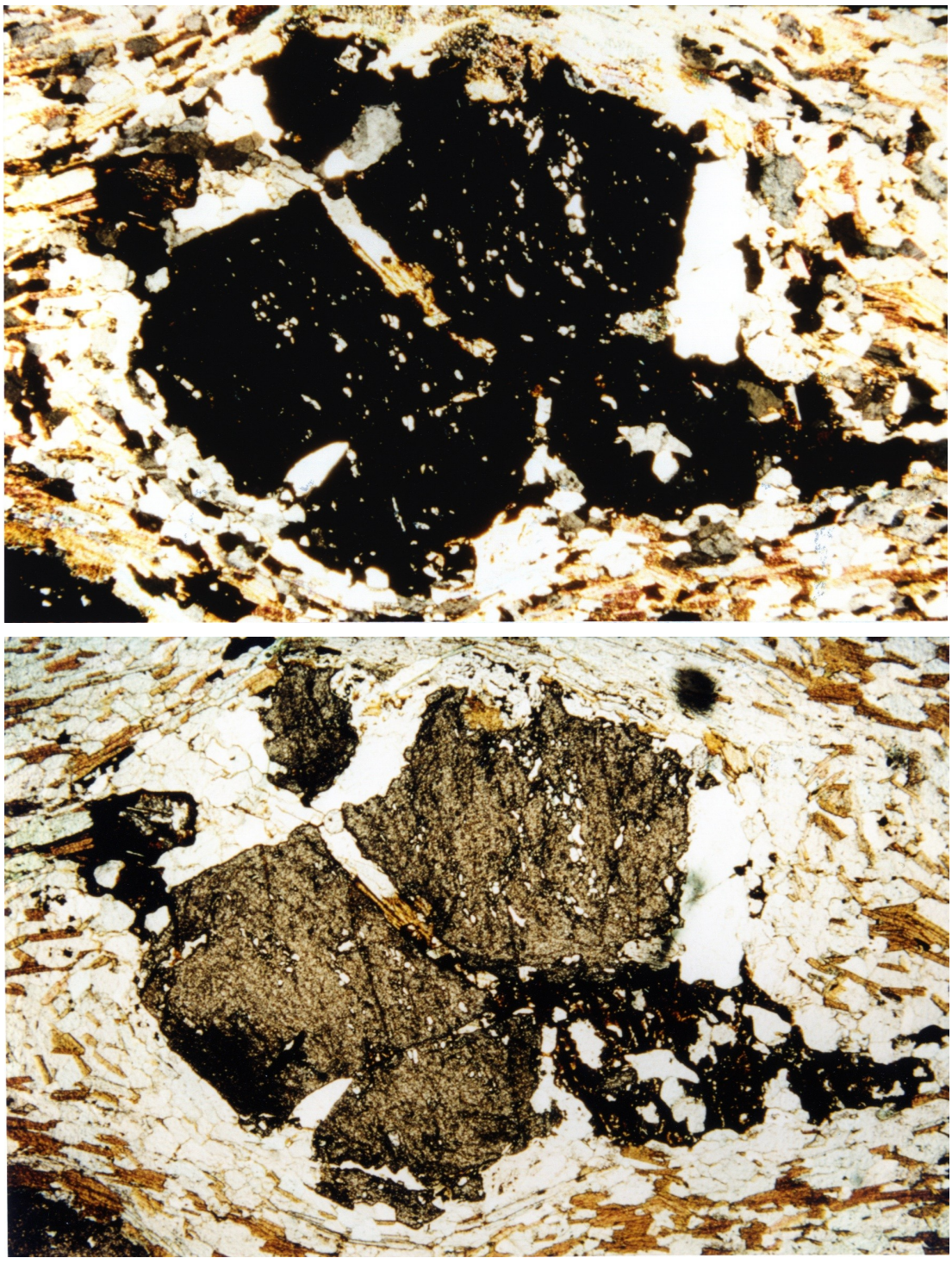

Figure 5.10 See previous page for figure caption.

antiformal fold that re-rotates the layers by 180°. 2. This section of cascading folds is a local horizon of originally normal motion on the MMT, in the upper 1 km of the MMT footwall (as discussed in section *5.1.3.3 Himalayan normal sense fabric*). There is no local field evidence to suggest that there is any reversal of the section through a major fold (although see section *5.3.2.3 Churit Fault Zone* and fig. 5.11), and I infer that the sinistral shear sense in 5/29F reflects a local horizon of normal motion on the MMT in the upper MMT footwall. This is consistent with other discrete horizons displaying sinistral sense of shear that are present elsewhere (detailed below).

Hand samples and outcrop observations show that in places there is a somewhat cryptic sub-horizontal spaced foliation suite that fractures cleanly when hit, weathers preferentially, and is picked out by reflections from schools of biotite flecks that are preferentially grown on the sub-horizontal surface. The sub-horizontal spaced foliation suite is sometimes well developed (i.e. clearly visible), and sometimes not. The extent of fracture development does not appear to be associated with any particular lithology. This phenomenon of mica growth that marks a cryptic sub-horizontal spaced foliation suite is found throughout the metasedimentary sequences of SE NPHM, most notably in Dichil Gah where the possible significance of the biotite orientation was bought to my attention by A. Pêcher (personal comm.). I infer that the fabric is a late feature related to general WNW-directed shortening across NPHM. Biotite geochronologic studies at NPHM that have given anomalous results (e.g., "future 87Sr/86Sr biotite ages" of Gazis et al., 1996) have not considered separate generations/suites of biotite discriminated and separated prior to analyses (although c.f. George and Bartlett, 1996). Cooling age differences are not thought likely to be discernible, however (D. Schneider, personal comm.).

A few hundred metres west along the jeep track that is cut into the cliff near outcrop #13 (to the left [west] of field of view of fig. 5.4; to right [east] of field of

Figure 5.11

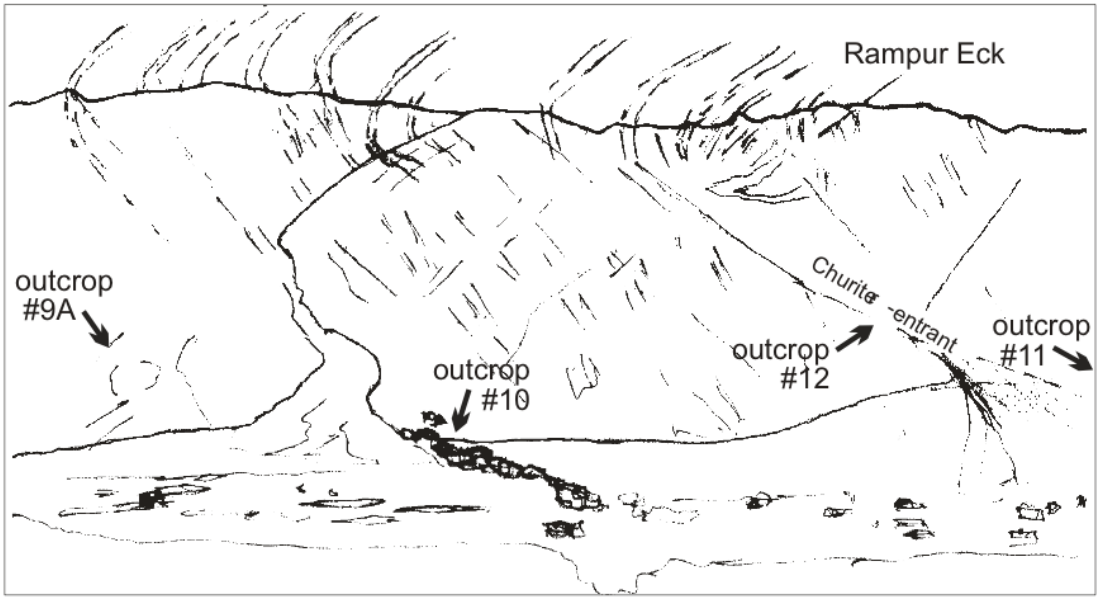

Figure 5.11 (field photo and line drawing). View to north of Churit Ridge that forms central portion of left bank of Lower Rupal Valley. Scattered low buildings and trees on level in foreground are Churit Village (2685m). Rampur Eck (west of Rampur Ridge) is 3884m. Outcrops #9A, #10, and #12 are visible. Churit re-entrant is marked byapparent closure of orange band and by fan descending to bottom right of field of view. Churit faults are distributed throughout re-entrant (see text). Travertine deposits of outcrop #10 coincide with freshwater spring and top of line of trees. Main layering above Churit is 70-89°E but appears less steep due to perspective. For discussion of steep/overturned layers, see text. Photo 21/9/96 no.8.

view of fig. 5.11), the cascade folds within the metasediments terminate in a series of 40-80° west-dipping, brittle fault sets of west-side up minor (centimetre to metre) displacement. This is the beginning of a several 100 m wide zone of spaced fractures and local folding that show W over E sense - the Churit fault zone. The morphology and sense of vergence of the cascade folds at outcrop #13 is consistent with a general footwall folding and overturning that is due to accommodation of the steep W over E brittle faults.

5.3.2.2 Churit to Tarshing

About 1 km west of outcrop #13, directly west of Churit school for Boys (plate 2), is a several 100 m wide fan-filled gully that is immediately east of the village of Churit (fig. 5.11). This fan flows out of a prominent contour re-entrant, the Churit re-entrant, that is within the Churit Fault Zone. Outcrop #11, directly above Churit School for Boys, is on the east side of the re-entrant, immediately out of the field of view of figure 5.11. The rock types at this outcrop are metasediments that are similar to #13, although there is slightly less amphibolite interlayered in the garnetiferous metapelite. In addition, there is a greater amount of well-foliated quartzofeldspathic gneiss than at #13. Mineral lineation in the gneiss is locally more visible than foliation (i.e., L>S[11]). Layering is ~N-S and very steep (e.g. 170°/85°W) and lineation plunges 15-20°(N). Samples NE95/28-IX and NE95/28-X are metapelites with very coarse (up to 10 mm) garnets, and are taken from the general area of outcrop #11. Both samples show some evidence for Macro-scale sinistral sense of shear based upon (1) 2-5 cm long C' surfaces that are clearly visible upon approximately foliation normal surfaces in finer-grained layers of the metapelite, and (2) asymmetric tails of 0.3-0.8

11. Throughout this chapter, "L" and "S" refer to lineation and foliation, respectively, and (following Wheeler et al., 1995) I use the convention (e.g.) L>S to describe a lineation more apparant than foliation. No implications of "prolate" and "oblate" fields on the Flinn diagram (Flinn, 1962) are intended. Nowhere in this thesis has strain analysis been conducted or is the Flinn diagram used.

cm garnet grains that are apparently rotating into and growing with the garnet porphyroblasts. The sinistral sense of shear recognised in the field is also recognised in thin section. In thin section 5/28J (not shown - cut from NE95/28-X), some (~80%) garnet porphyroclasts (0.5-4 mm) show inclusion fabric spirals with an anticlockwise rotation (sinistral sense of shear), some (~20%) show a clockwise rotation. Additionally, 200-500 μm mica fish, 1-2 mm clumps of mica or garnets bounded by C'-surfaces, sigmoidal 300-600 μm quartz ribbons, and 300-500 μm feldspar porphyroclasts with thin tails all show sinistral sense of shear.

East of outcrop #11 (the edge of the fan in the Churit re-entrant), spectacular float from pelitic-amphibolitic gneiss is found in alluvial float within the main fan (fig. 5.12). This seems to be part of a finely layered, highly-strained sequence of amphibolites, marbles and quartzofeldspathic gneiss. Figure 5.13 provides a good example of this sequence (from Bulan Gah, in an equivalent position in the section). Sense of shear in figure 5.12 is not possible as the sample is float.

Within the main fan that flows out from the Churit re-entrant, a mixture of rocks are found. The ubiquitous garnetiferous metapelite is present in the float alongside jet back amphibolite schists (always <3-4 cm foliation width), spectacular L>S quartzofeldspathic gneisses and schists, and rarer garnet-migmatite gneisses. A highly-identifiable gneiss characterised by mm-scale rods (L>>S) of quartz and feldspar that resemble very thin spaghetti ("angel hair"). I term this rock the "angel hair" unit (fig. 5.14). It was first recognised here in the float of the Churit re-entrant fan. This rock has mm-scale augen, typically has a greyish purple to greyish pink groundmass and often contains small garnets. It represents very high strain based upon the appearance, and this is consistent with microstructure (fig. 5.15). In one part of the fan in particular, large amounts of the angel hair unit were found concentrated in a drainage rut. The angel hair unit was not seen anywhere in outcrop on the left bank of Lower Rupal, however.

Figure 5.12

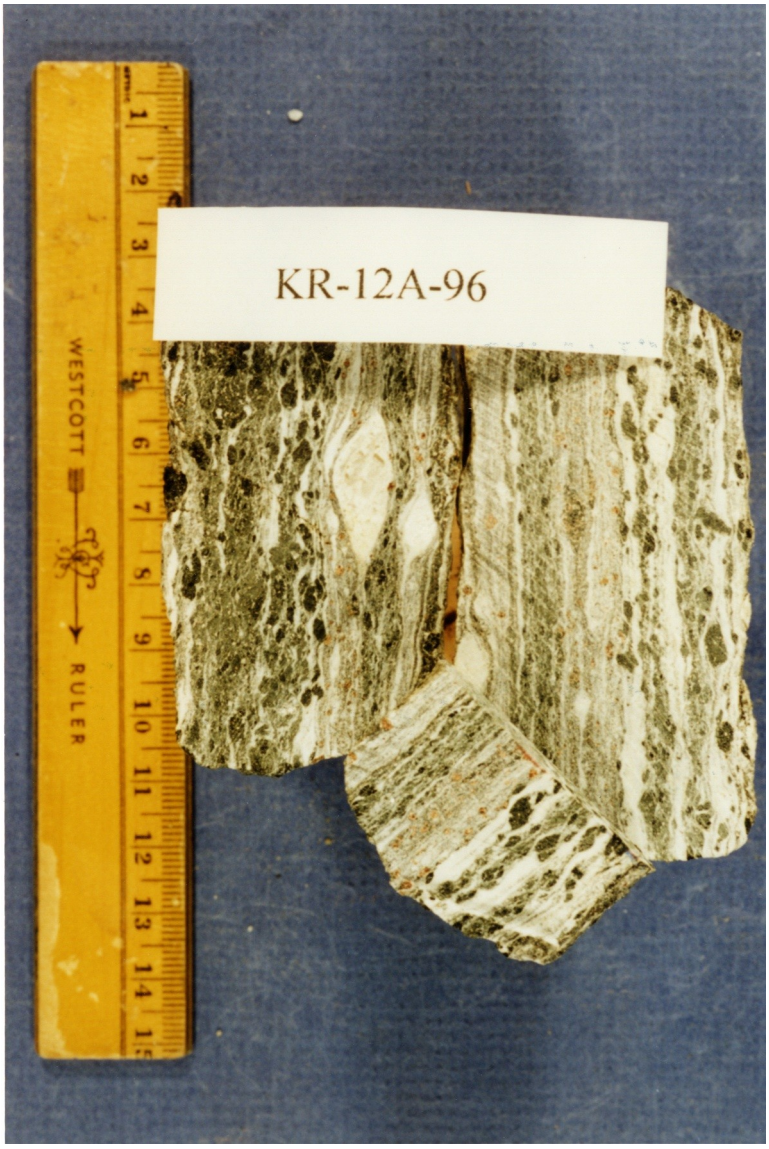

Figure 5.12 Photo of quartzofeldspathic-biotite-amphibolite gneiss found as float from scree on eastern edge of fan flowing out of Churit re-entrant. Very high strain is more clearly seen in fig. 5.13 (below).

Figure 5.13

Figure 5.13 High strain zone near outcrop #70A, within a ~60° west-dipping sequence of amphibolites, marbles and quartzofeldspathic gneiss on right bank of Bulan Gah. East is to left of picture, west is to right (note that layering of NPHM rocks throughout Bulan Gah dip gently to steeply west). Metre-scale boudins of amphibolite gneiss suggest sinistral sense of shear based upon boudin asymmetry and pinch and swell morphology. Also note asymmetric pinching fold adjacent to left hand side of flat top of main boulder in foreground suggesting sinistral sense of shear (flat top of boulder is approximately 3m wide). Photo 9/10/96 no.2, ~ 1.5 km upstream (W) from #70.

Figure 5.14

Figure 5.14 Angel hair unit at outcrop #62 on Rama left bank. Foliation: 159°/33°W, lineation: 7°@332°. Very stretched mm-scale rods of quartz and feldspar (where L>>S) define high strain zone. Note cm-scale compositional banding, mm-scale augen and rusty garnets. "Matrix" typically is greyish pink. Lens cap for scale. Photo 7/10/96 no.1.

Figure 5.15

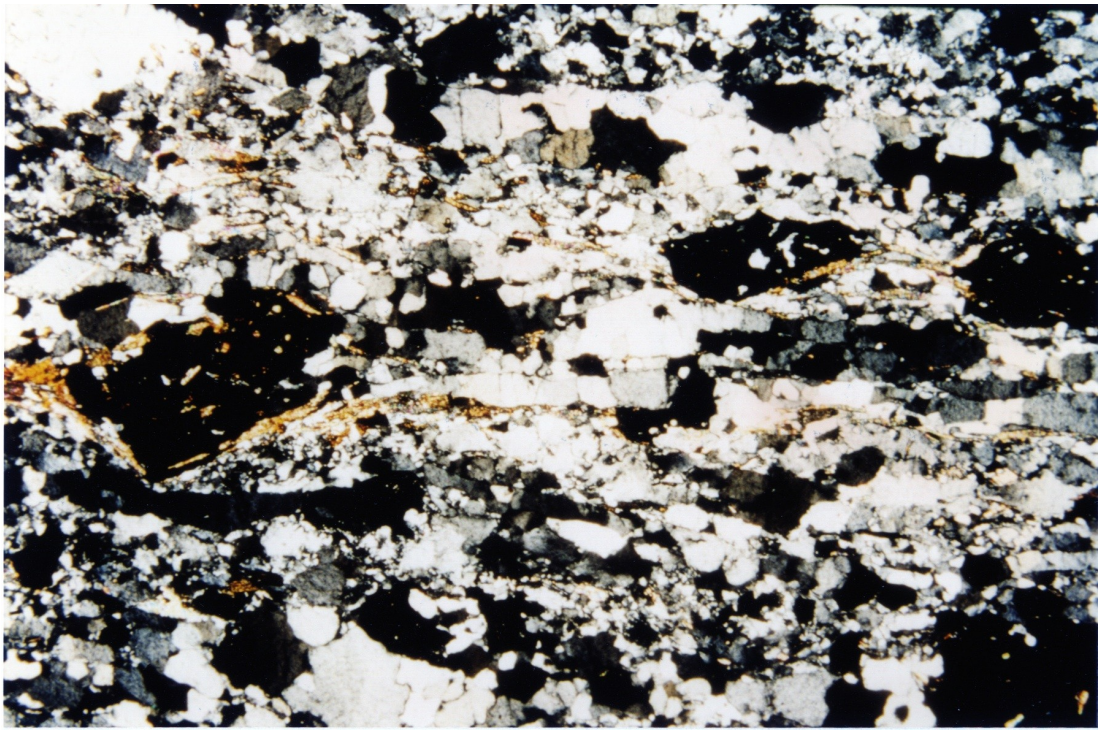

Figure 5.15 Optical photomicrograph of thin section 610/10A, (cut from sample E6/10/10-I, angel hair unit, ~750 m east of outcrop #73 on Dichil Gah left bank. 016°/53°W, 32°N-pitch). Illustrates likely tectonic grain size reduction based upon bimodal grain size distribution into ~300µm thick monomineralic quartz ribbons, and ribbons of very fine-grained (50-200µm) quartz and feldspar. Larger feldspar grains show suturing of margins to give partial core and mantle texture (not visible in figure). Sense of shear indicators are poorly developed both in figure and elsewhere in thin section. Left lateral is suggested by asymmetry of strain shadows and stepping of ribbons and trails associated with garnets, and slight development of oblique grains in lower part of picture. Cut parallel with lineation, perpendicular to foliation. South is on left. Base of image is 5.5 mm. Crossed polars.

The garnetiferous metapelite is found again in outcrop higher up within the centre of the fan. Foliation and lineation are consistent with the previously described outcrop (e.g. 010°/85°, 32°@010°), but sense of shear is not wholly clear in thin sectioned field samples from here. In thin section 5/29E (not shown - cut from NE95/29-V), garnet porphyroclasts show no clear patterns of inclusions. 0.5-3.0 cm C'-surfaces are well developed around 1-4 mm garnet grains, displaying dextral sense of shear. Additionally consistent are 100-400 μm possibly sigmoidal quartz ribbons and 400-1000 μm feldspar porphyroclasts, suggesting a dextral sense of shear. Mica fish and sigmoidally shaped clusters of mica suggest sinistral sense of shear, however.

Immediately on the west side of the fan, ~200 m higher in elevation than Churit village (fig 5.11), a highly-strained garnet-biotite-quartzofeldspathic gneiss outcrops over several 10's metres, approximately 100 m east of outcrop #12 (NE95/29-II - fig. 5.16). Layering continues to trend N-NNE but locally is buckled and dips gently to steeply west (e.g. 020°/40-60°W, 20° to N) before returning to dip steeply to vertical ~100 m further to the west. These locally buckled parts of the section are present throughout the area around the Churit re-entrant (see discussion of buckling under *5.3.2.3 Churit fault zone, below*). The high strain within the garnet-biotite-quartzofeldspathic gneiss that is seen in outcrop is also clearly seen in thin section (5/29C - not shown). Dextral shear sense is clear based upon (1) oblique foliation of fine-grained (50-100μm) "matrix", (2) tail asymmetry and strain shadows of 0.5-1.5 mm quartz and feldspar porphyroclasts that form good augen, (3) S-shapes in 100-300 μm quartz ribbons that are locally bent & thinned at stress contacts ("corners") of porphyroclast and/or porphyroblast margins, and (4) mica fish. Figure 5.15 shows that fine lamination in this rock is less continuous and evenly distributed, and the composition is less well defined, than in the angel hair unit. I note that this is the first unequivocal observation of dextral shear sense within the section, moving

Figure 5.16

Figure 5.16 Sample NE95/29-III, highly-strained garnet-biotite-quartzofeldspathic gneiss, immediately east of outcrop #12 (020°/40°W, 20° to N). Thin section (T/S2 5/29C - not shown) illustrates clear dextral shear sense based upon (1) oblique foliation of fine-grained component (~50-100µm), (2) tail asymmetry and strain shadows in quartz and feldspar augen (0.5-1.5 µm). (3) S-shapes in 100-300 µm quartz ribbons, locally bent & thinned at stress contacts ("corners") of clast margins, and (4) mica fish.

westward from the NPHM/KLS contact (i.e., structurally downwards into the MMT footwall). The observed dextral shear sense is consistent with thrust sense on the MMT, in the model involving crustal scale folding where SE NPHM is the eastern limb of the fold (see fig. 5.2).

A few tens of metres west of the fan in the Churit re-entrant, a notably granitic orthogneiss of 50 to 75 km width is present within the section of outcrop. Foliation is typically N-S and steep to vertical (e.g., 180°/70°W). Lineation plunges 5-15° towards the north. The granitic orthogneiss is finely laminated with L>S. Elongated, lamination-parallel 0.5-2.0 mm sigmoidal quartz and feldspar augen mark S-surfaces and flat biotites define C-surfaces both displaying a dextral shear sense. Rare, 1-3 mm garnets are present. Figure 5.17 shows the granitic orthogneiss in thin section (5/29D). Most evident in the photomicrograph are (1) long ribbons of quartz with even thickness (200-300 μm) that are parallel to the C-surface, (2) an ~300 μm thick biotite grain, also parallel to the C-surface, and (3) generally homogeneous flattening of the finer grained (<100 μm) quartz groundmass (below the biotite). Although not well illustrated in figure 5.17, dextral sense of shear is demonstrated elsewhere in the thin section by (1) sigmoidal ribbon shapes and tails from clasts (forming the augen), (2) oblique foliation of flattened quartz grains, and (3) mica fish. Garnets are inferred to be syn-kinematic during their early growth history insofar as they overgrow part of the main fabric, but part of the main fabric is bent around them. Within the garnets, inclusion spirals are absent, and appearance is generally cleaner than in the garnets found in the metapelites. Based upon the homogeneously flattened grains of quartz, the core and mantle texture, and the development of ribbons, I infer that this rock was deformed between 400 and 600°C.

At outcrop #12, a very-fine-grained garnet biotite quartzofeldspathic gneiss is present in which thick (mm-cm) blebs of quartz and feldspar are stretched out into striking mm thick rods (slightly thicker than in the angel hair unit), typically resulting

Figure 5.17

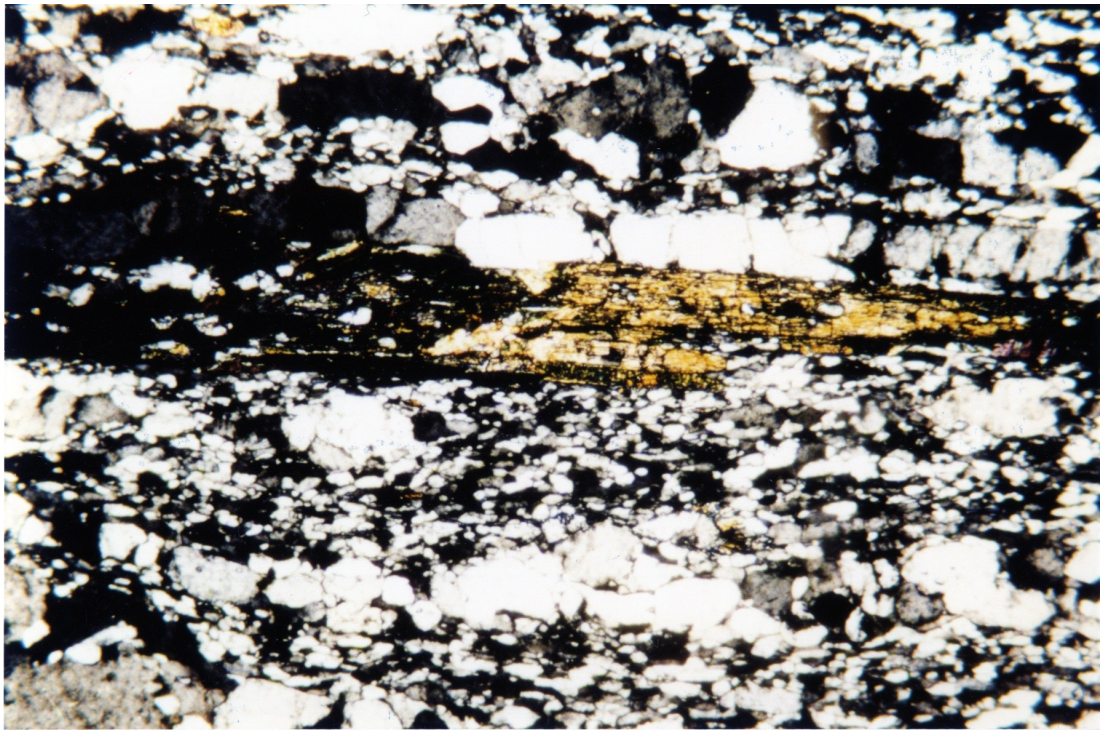

Figure 5.17 Optical photomicrograph of thin section 5/29D (cut from sample NE95/29-IV), fine-grained (50-100μm) L>>S granitic orthogneiss from west side of Churit re-entrant, ~50 m east of outcrop #12. Conditions of deformation are indicated by (1) C-surface parallel ribbons of quartz with even thickness (200-200 μm), (2) ~300 μm thick biotite grain that defines C-surface, (3) core and mantle appearance of certain feldspars (clearly seen in top left of photo) and (4) generally homogeneous flattening of <100 μm quartz groundmass (below biotite grain). Dextral sense of shear. Cut parallel with lineation (10°@359), perpendicular to foliation (180°/70°W). South is on left. Base of image is 5.5 mm and parallel with main fabric. Crossed polars.

in lineation that is stronger than foliation. The gneiss trends 005°/89°E with a mineral lineation plunging 10° towards 005°. Sample NE95/29-II (fig. 5.18) clearly illustrates the both white, mm-cm thick quartz and feldspar blebs, and ~1-3 mm thick quartz and feldspar rods that are stretched through this rock. Garnets (~2-5 mm) and quartz and feldspar augen show sigmoidal and deltoidal trails. Figure 5.19 provides an example of this rock in thin section (5/29B - cut from sample NE95/29-II). The sutured grain margins of the large (1-3 mm) augen and the fine (50-100 μm) groundmass indicate extensive grain boundary migration. Monomineralic quartz ribbons 0.5-1.0 mm thick suggest advanced states of dynamic recrystallisation (involving quartz subgrain rotation). Elsewhere in the sample, ribbon to ribbon contacts are very sharp and continuous (not shown in fig. 5.19), and their undulatory nature would seem to require grain (i.e., ribbon) boundary sliding with accommodation involving some form of diffusive mass transfer. Note that with respect to the groundmass, evidence is not present for wholesale diffusive mass transfer (i.e., grain size sensitive flow has not occurred). In particular, the relative roughness of grain boundaries (due to sutured grain margins) and the relative coarseness of the grains (>50 μm) are inconsistent with grain size sensitive flow processes. Based upon the spectacular development of monomineralic quartz ribbons, and the widespread grain size reduction, I would interpret the preserved microstructure to be a result of deformation at ~600°C (chapter appendix 5.9.2). A Dextral sense of shear is suggested by (1) oblique foliation the groundmass, (2) Sigmoidal shape of the quartz ribbon, (3) mica fish (not shown), (4) strain shadows on garnet and hornblende grains (not shown) and (5) tails from feldspar augen (not shown). The quartz and feldspar blebs may have an originally granitoid/migmatitic source but their present state of strain precludes a statement regarding their origin. There is evidence of migmatisation nearby, however, between here (outcrop #12) and outcrop #10.

Figure 5.18

Figure 5.18 Sample NE95/29-II, fine-grained L>>S garnet biotite quartzofeldspathic gneiss from outcrop #12 on west side of Churit re-entrant. Note blebs of quartz and feldspar stretched out into striking 1-3 mm thick rods indicating very high strain. Garnets (~2-5 mm) and quartz and feldspar augen show sigmoidal and deltoidal trails.

Figure 5.19

Figure 5.19 Optical photomicrograph of thin section 5/29B (cut from sample NE95/29-II), fine-grained (50-100µm) L>>S garnet biotite quartzofeldspathic gneiss from outcrop #12, west of Churit re-entrant. Prominent 0.25-0.75 mm monomineralic quartz ribbon suggests dextral sense of shear, as does oblique foliation (more conspicuous below ribbon). Dextral shear sense is also shown by mica fish, strain shadows on garnet and hornblende grains and tails from feldspar augen, elsewhere in thin section (not shown). Very finely sutured grain margins of large (1-3 mm) augen and fine (50-100 µm) groundmass indicate extensive grain boundary migration. Cut parallel with lineation (10°@005°), perpendicular to foliation (005°/89°W). South is on left. Base of image is 5.5 mm and parallel with main fabric. Crossed polars.

West of outcrop #12, approximately 300m from outcrop #10, another very granitic orthogneiss is present (NE95/29-I). Where the rock was sampled, foliation trends 020°/80°E, and a mineral lineation plunges 29°@022°. In this rock, foliation is stronger than lineation, and there seems to be a strong migmatite component to the layering within the gneiss. Small 1-5 mm clean brown garnets are present. The migmatitic component of this rock is most clearly visible where it cuts across the main foliation. It does not entirely post-date the foliation, however, and it is still affected by the general flattening. Additionally, the migmatite is not accompanied by any melanosome. Elsewhere, a migmatitic component is less demonstrable; leucocratic layers that make up part of the overall gneissic foliation have a similar appearance to the cross cutting migmatite portions. Their possible migmatitic origin is further suggested by their microstructure. In thin section (Fig. 5.20) this rock shows a remarkably "unstrained" appearance in view of the intense foliation and lineation displayed by this rock in outcrop. The feldspars are quite "clean" in appearance - little to no significant build up of dislocation tangles is indicated by the absence of noteworthy patchy/undulose extinction. Similarly, there is little core and mantle texture developed. There is some suturing of grain boundaries, and a limited operation of grain boundary migration can be inferred. The feldspars do have something of a "pitted" appearance and seem to have large cracks. Cracked grains , commonly show a lattice continuity across the cracks (i.e., extinction angles do not change across cracks) and thus they are inferred to be growth features and not (e.g.) feldspar microcracks of Tullis and Yund (1987). Portions of the rock enriched in biotite laths (<100 μm) define part of the compositional foliation. The laths are widely spaced, however (300-500 μm) and interestingly, they are not oriented parallel to the fabric. It is likely that there has been a large amount of recovery in this rock in view of the fact that high strain (similar to strain in the surrounding gneisses) is suggested by the macroscopic fabric whereas accommodation of but a modest strain is suggested

Figure 5.20

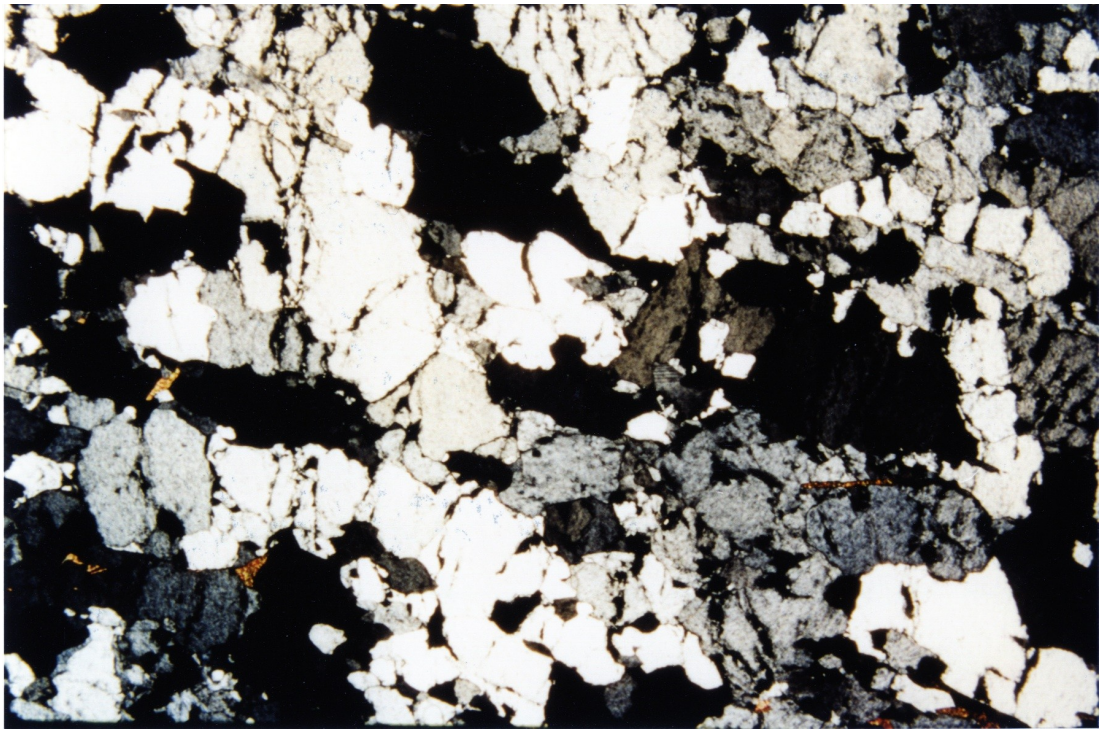

Figure 5.20 Optical photomicrograph of thin section 5/29A (cut from sample NE95/29-I, 020°/80°E; 20°N). Note generally "unstrained" appearance. Feldspars are clean; little to no significant patchy/undulose extinction. Some suturing of grain boundaries indicating limited operation of grain boundary migration. Note feldspars have "pitted" appearance. Large cracks in feldspars are not associated with extinction angle variation, suggesting lattice continuity. Cracks are inferred to be growth features (see text for discussion). Cut parallel with lineation, perpendicular to foliation. South is on left. Base of image is 5.5 mm and parallel with main fabric. Crossed polars.

by the microstructure (dissimilar to the surrounding gneisses). I would propose that the migmatite that is mobilised in this rock post dates much of the observed (inferred) strain. A combination of (1) recovery ("annealing" due to the heat of migmatite mobilisation) and (2) wholesale grain renewal (by the addition of granitic melt) is responsible for the youthful appearance of microstructure. The fabric throughout the outcrop is consistent with that of the surrounding rock, and hence is interpreted to be Himalayan. The intense fabric, including much of the migmatite portion, is therefore probably older than the exhumation of NPHM. I conclude that there was some migmatite generation late in the history of main Himalayan events.

West of where the migmatitic granitic orthogneiss is present, the sequence continues with interlayered granitic and metapelitic schists and gneisses. The volume of migmatite present varies throughout the section. In some rocks, there is no evidence for migmatite mobility while in others the migmatite component is quite striking. Figure 5.21 shows the field appearance of a migmatite rich portion of the typical garnet-pelitic gneiss. This photo is actually taken from the equivalent position in Ghurikot main valley (outcrop #69) but it is included here as part of the overall introduction. About 50 m east of outcrop #10, there is a several 100 m thick section where migmatite is absent and metapelites with large garnets are present (e.g., NE95/28-XI). These are very similar in appearance to the garnet metapelites at outcrop #13. Foliation is generally N-S, dipping 50-70°W, with lineation plunging gently north. In hand specimen, garnet pressure shadow asymmetry and spirals, where seen, indicate sinistral shear sense. Observations of thin section 5/28K (not shown - sectioned from NE95/28-XI) are consistent, showing good sinistral sense of shear. This is based upon (1) sigmoidal 100-300 μm quartz ribbons show sutured margins of grains that are not part of the ribbon boundary, indicating good grain boundary migration in the direction of the ribbon, (2) 50-200 μm thick, <2 mm long mica packages between C'-surfaces, and (3) small (~200 μm) feldspar porphyroclasts

Figure 5.21

Figure 5.21 Migmatite-rich portion of garnet-pelitic gneiss within general cover sequences (outcrop #69 - west of Churit Fault Zone in Ghurikot main valley). South is on left, view is from above. Foliation: 160°/65°W; lineation: 2°N. Based upon stepping directions of augen and leucosome tails, sense of shear is dextral, however, 1-2 cm long C'-surfaces (below arrow to top left of compass) trending NNE-SSW suggest sinistral sense of shear. Compass for scale. Photo 8/10/96, no.4.

with tails sitting nicely between C and S surfaces. Garnet grains (1-5 mm) show no useful inclusion patterns. This several 100 m thick section of garnetiferous metapelite shows sinistral shear sense that is opposite to the dextral sense of shear that is almost universally displayed by the various gneisses and schists between here (50 m east of outcrop #10) and the west side of the Churit re-entrant. I note that there is no evidence in this section for a major fold that could cause this observed reversal, and regard the sinistral sense of shear as evidence for a discrete (>200 m) horizon in the original MMT footwall upon which some normal motion has occurred, relative to the surrounding footwall rocks.

In the general vicinity of outcrop #10, numerous coarse (5-15 mm) crystalline carbonate rocks are found. At outcrop #10, a freshwater spring occurs below a thick (several metres), well-indurated sequence of travertine accumulations. These are all probably related to hydrothermal activity that accompanies the exhumation of NPHM (e.g., Craw et al., 1994).

West of outcrop #10, there is a decrease in metapelitic rocks and a dominance of granitic orthogneiss (±migmatite). NE95/28-IV is typical of the granitic orthogneisses that are seen; <1 cm migmatite layers, well foliated and lineated. Layering continues to trend 010-020° dipping steeply west to vertical (c.f. fig 5.11 where foliation appears east-dipping). A mineral lineation plunging gently north, for the most part.

At outcrop 9A, a garnet bearing amphibolite is present (NE95/28-III - 010°/89°W). Because surrounding rock is largely granitic orthogneiss, it is not clear if this amphibolite was part of the cover or not (i.e., was it (1) originally a volcanic flow or sill on/in the passive margin, or (2) a cross-cutting dyke?). No obvious cross-cutting relationships are seen here. However, my observations of basic dykes elsewhere have shown that cross-cutting relationships in the amphibolite dykes are frequently cryptic (because of high strain).

From outcrop 9A to Tarshing, rocks become almost exclusively granitic orthogneiss and pass into the Rupal-Chichi shear zone (RCSZ; see 5.X.X.X). Layering is still ~NNE dipping steeply west to vertical. The margin of the RCSZ is somewhat arbitrary (because of its gradational nature) and roughly coincides with a switch in mineral lineation from N- to S-plunging. The rocks in the area of Tarshing are discussed in the section on the Rupal-Chichi shear zone.

5.3.2.3 Churit Fault Zone

In the general area of the Churit re-entrant, a series of distributed fractures and faults defines the Churit Fault Zone. The Churit faults typically have metres to tens of metres of W-side up, east-vergent displacement. Some displacement however, is locally west-vergent, where complimentary, antithetic fractures have formed. Faults are frequently are associated with buckling and folding that is locally very tight. Figures 5.22 and 5.23A show good examples of this local folding. Figure 5.22 additionally illustrates how jointing that is related to W-vergent displacement can become folded and occasionally can mimic gneissic layering from a distance. Figure 5.23B is a cut-away 3D perspective view of the area of the apparent synformal closure that coincides with the Churit Fault Zone, on the east side of the Churit re-entrant. The 3D block is used to illustrate the view of a surface observed in the field that is approximately perpendicular to the N-S oriented face on which the apparent synformal closure is seen (also shown in fig. 5.11). The cut away block illustrates that the closure is due to pinching out of a several metres thick boudin whose neck line plunges steeply E. The ptygmatically folded lower surface of the boudin is consistent with a general W-E shortening (i.e. normal to the neck line) where L>S, (L is ~N-S). It is therefore apparent that there is no large scale fold associated with the Churit fault.

Figure 5.22

Figure 5.22 Field photo looking north to left bank of main valley in Ghurikot Gah (near outcrop #68). Illustrates local buckling and fracturing associated with a zone of E-vergent displacement within Churit Fault zone. Note moderate west dip of overall gneissic layering and area in foreground where jointing is antiformally folded. Tree in top right of photo is about 8 m high. Photo 8/10/96, no.3.

Figure 5.23

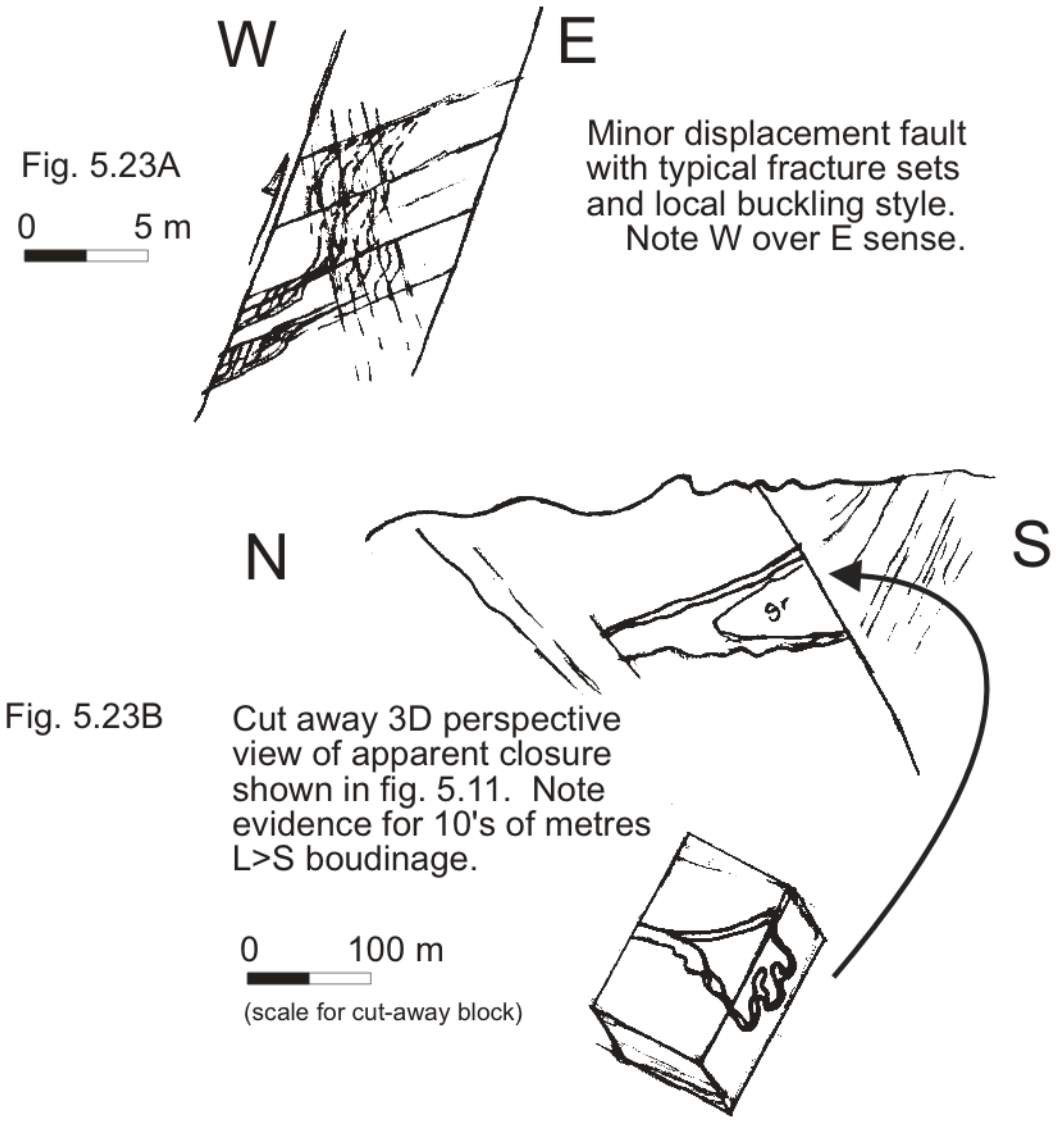

Figure 5.23 (A & B) Line drawings of field sketches around Churit re-entrant.
A. Illustrates typical E-vergent structure within Churit Fault zone. Layering is represented by monoclinally folded double lines. Low angle (~30°W) fracture planes are well-developed. Steeply, E-dipping fractures are less-developed.
B. Illustrates apparent closure is due to limited perspective of pinched out boudin (see text for discussion). Note ptygmatically folded base of boudin.

The true width of the Churit Fault Zone is not clear. The eastern margin is well-defined where the cascading folds at outcrop #13 pass abruptly to a set of 40-80°W dipping faults (see section 5.3.2.1 above). The western margin is less-clear however; fractures with little significant displacement are present for several 100 m west of outcrop #10. The recent carbonate and travertine deposits that are found in the area are presumably a result of fluid networks maintained until recently by the fractures. I nominally regard the Churit Fault Zone as being ~2 km wide, the distance from outcrop #12 to outcrop #10.

5.3.2.4 Ladakh Rocks

Although rocks of the KLS are not really part of the study, I briefly describe the Ladakh rocks that are found east of the contact (i.e., in the MMT hanging wall) to (1) provide a more complete picture of the SE NPHM geology, and (2) compare deformation styles of the KLS rocks in the immediate MMT hanging wall with Himalayan rocks in the MMT footwall.

Approximately 1.5 km east of the trace of the KLS/NPHM contact, at outcrop #14, a several 10's metre thick section of pale green, very fine grained tremolite/actinolite schist with continuous, mm-cm compositional layering and spectacular mm-cm deep green, post-kinematically grown hornblende needles is present (fig 5.24, samples NE95/29-VIII and E6/7/5-I). This unit trends ~N and dips steeply W (e.g., 010°/85°W). Asif Khan (personal comm.), based upon MMT hanging wall lithologies seen elsewhere, away from NPHM, has suggested that the fine-grained nature of this layer implies it may be a retrograded and statically recovered mylonite. My mapping on the south side of Rama valley, in Bulan Gah, and in the three Ghurikot valleys reveals that the fine-grained layer of actinolite schist continues with a similar width for >15 km to the north. In all cases, the schist shows the same fine lamination and spectacular compositional layering and post-kinematic

Figure 5.24

Figure 5.24 Field photo at outcrop #14 showing hornblende needles post-kinematically grown on foliation plane of very fine grained actinolite/tremolite schist (revealed by W.S.F. Kidd). Very continuous, even, m-cm compositional layering (not seen) suggests original metamorphism associated with high strain (see text for discussion). Rock is part of Kohistan Ladakh series (KLS). Photo 5/7/96, no.4.

hornblende growth, and has the appearance of a mylonitic rock. Post-kinematically grown hornblende needles are also present away from the actinolite schist, elsewhere in the section. Their degree of development varies along the section, often accompanied by changes in size and nature of garnets that may be present, presumably as a result of compositional changes within the general amphibolite schists.

A few 100's metres east of where the fine tremolite/actinolite schist outcrops, the section passes to darker green metadiorites. The metadiorites are mostly massive and notably punctuated by cm -10's cm continuous shear zones, sometimes of classic appearance (i.e., Ramsay and Graham, 1970). A dextral sense of shear can frequently be determined from dragging of fabric at shear zone margins. Locally present within the western part of this section are a series of 5-20 m wide felsic (granitic to granodioritic) layers (e.g., NE95/29-IX). These felsic layers strike NNE and dip moderately west (e.g.. 015°/60°W) and a mineral lineation (picked out by biotite and amphibole grains) plunges (e.g.) 41° towards 355°. Fabric at the outcrop scale is very cryptic in this rock as the quartzofeldspathic component has a very clean appearance. In thin section, however, a clear microstructure is apparent, even at low magnification. Biotite laths, 100-300 μm in width are parallel with C-planes and parallel with 50-300 μm quartz ribbons. Additionally, a very pleochroic (blue to green) amphibole is present. Postkinematic euhedral garnets (200-500 μm) are also present. There is a good bimodal distribution amongst the quartzofeldspathic portion. Between the ribbons and thin rare augen are <100 μm, often notably flattened, quartz grains. Where the flattened grains are oblique to the C-surface, they indicate dextral sense of shear. This is consistent with dextral sense of shear indicated by (1) the S-shapes in some of the ribbons, and (2) trails from the rare augen. The conditions of deformation (>400°C ?) and dextral sense of shear are highly consistent with many of the more highly strained rocks west of the NPHM/KLS contact (i.e. in the MMT footwall). I therefore regard the granodioritic orthogneiss as evidence that main

Himalayan thrusting deformation styles are preserved in at least part of the Ladakh sequence that is in the lower portion of the MMT hanging wall.

5.3.2.5 Right bank of Lower Rupal Valley

The KLS/NPHM contact is not exposed on the right bank of the Lower Rupal Valley. Outcrop is somewhat more sparse than on the left bank, and rocks of the KLS are not exposed at all. Cascading folds similar to those seen at outcrop #13 are well-exposed near outcrop #50 (fig. 5.7, above). Layering is remarkably consistent with the left bank, striking ~NNE and steeply west dipping. Fold hinges and (parallel) crenulation intersection lineation are also consistent with measurements on the left bank, plunging 25-40° towards north. Sense of shear from augen and garnet spirals near outcrop #50 was not clear.

West of the cascading folds, along a steep scree slope, the angel hair unit and granitic orthogneiss units similar to those present on the west side of the Churit re-entrant are found in the float. Further west, amphibolites are interlayered with mm-rodded pelitic gneisses, consistent with the sequence near outcrop #10 on the opposite bank. Again layering is consistent, trending NNE and dipping steeply east. The presence of the pelitic component increases and decreases over a few 100 m in this part of the section. Some layers are noteworthy for their migmatitic appearance, generally similar to NE95/29-I (fig. 5.20, above). West of the pelitic portion, the sequence consists of dominantly granitic orthogneiss that passes into the Rupal Chichi Shear Zone.

5.3.2.6 Discussion and conclusion for Lower Rupal Valley

The NPHM/KLS contact is not exposed in the Lower Rupal Valley. Its location is inferred, however, based upon remote observations of the Rampur Ridge that are consistent with my own observations of the NPHM/KLS contact in localities

previously reported by others elsewhere in the massif (e.g., western Indus Gorge, eastern Indus Gorge, Bunar Gah, Niat Gah - Treloar et al., 1991; Pognante et al., 1993; Wheeler et al., 1995; Hubbard et al., 1995; Lemmenicier et al., 1996; Asif Khan, personal comm.). East of where the contact is inferred, the extensive amphibolites, metabasites and granodiorites that are present are consistent with my own observations, and other workers' descriptions, of the KLS from elsewhere (Tahirkheli et al, 1979; Tahirkheli and Jan, 1979; Bard et al., 1980; Tahirkheli, 1982; Bard, 1983; Coward et al., 1988; Williams, 1989; Hubbard et al., 1995; Wheeler et al., 1995; Lemmenicier et al., 1996; Asif Khan, personal comm.). I therefore regard the sequence that is present east of where the contact is inferred, to be part of the KLS.

West of where the contact is inferred, the extensive sequence of garnetiferous metapelitic and quartzofeldspathic schists and gneisses are consistent with both my own observations, and other workers' descriptions, of Indian cover sequences from the MMT footwall that are found elsewhere in both the Nanga Parbat massif (Hubbard et al., 1995; Wheeler et al., 1995; Lemmenicier et al., 1996; Pêcher and Le Fort, in press; Asif Khan, personal comm.), and in the Pakistan Himalaya in general (Tahirkheli et al, 1979; Tahirkheli, 1982; Greco et al., 1989; Papritz and Rey, 1989; Chaudhry and Ghazanfar, 1990; Burg et al., 1996; Anczkiewicz et al., 1997). Furthermore, extensive amphibolite is not present west of the inferred KLS/NPHM contact; amphibolite occurs only as rather uncommon <1 m horizons that are everywhere interlayered with the other gneisses and schists. I therefore interpret the sequence that is present west of the inferred KLS/NPHM contact to be part of the Indian plate cover sequences in the original MMT footwall.

The section of schists and gneisses around outcrop #13 nearby have been subjected to deformation at temperatures of several hundred degrees Celsius, some of which has demonstrably sinistral sense of shear. Sinistral sense of shear at similar

temperatures is apparent in the metapelites ~1 km to the west at outcrop #11, above the Churit School for Boys. Taken together, it is possible that the two outcrops mark a 1 km section of sinistral sense of shear. There is no evidence for a reversal across a major fold of the original MMT footwall between the Churit re-entrant and the cascade folding at outcrop #13; the apparent synformal closure on the east wall of the Churit re-entrant is seen to be part of a large boudin. I therefore interpret the sinistral motion seen within this part of the section to be a product of normal motion on the MMT that has been subsequently rotated to steep/vertical as part of the eastern limb of the NPHM crustal-scale antiform. Based upon descriptions from elsewhere of MMT horizons that display normal motion (e.g. Vince & Treloar, 1996), it is more likely that two discrete MMT normal motion horizons of several 10's to a few hundred metres thickness are present, than a single horizon of >1 km. Preliminary metamorphic petrogenic grid studies have not found any evidence for a W-E metamorphic break anywhere in the Lower Rupal Valley section.

West of the Churit re-entrant, microstructures reveal that rocks have experienced similar amounts of strain, and been subjected to similar temperatures of deformation as the rocks east of the Churit re-entrant. This is based upon the development of (e.g.) monomineralic ribbons and layers, and upon grain size differentiation. This consistency in deformation conditions is perhaps counter-intuitive to the contrast in the general appearance of high strain fabric seen in outcrop across the Churit re-entrant. The rocks to the west, for example, are more gneissic and have more spectacular quartzofeldspathic rodding than those to the east.

Sense of shear in the schists and gneisses that are west of the Churit re-entrant is mostly dextral where unambiguous. This is consistent with thrust sense displacement within the original MMT footwall. I infer that the much of the fabric preserved in the NPHM rocks is due to original thrust sense displacement on the MMT. The ~300 m of section displaying sinistral sense of shear in the vicinity of

outcrop #10 is inferred to be a structurally lower MMT footwall normal motion horizon (although for discussion see 5.6.2 Domains of sinistral and dextral motion in eastern NPHM). In view of the two pieces of evidence for MMT normal motion east of the Churit re-entrant, I propose that there are at least three 100-400 m thick MMT normal motion horizons within the upper 5 km of the MMT footwall. This is consistent with descriptions west of NPHM in the Besham-Dassu area of narrow, normal sense horizons within the MMT footwall (Treloar et al., 1991; Vince and Treloar, 1996), although the cited studies recognise only relatively low temperature, largely brittle sense of shear. The presence of higher temperature (i.e., >400°C), principally ductile horizons with normal sense displacement therefore is a significant new discovery.

The dominantly brittle strain, general east vergent displacement that is represented by the Churit fault Zone, and the general overturning of the NPHM sequences (reported more fully in 5.3.3. below) is the only deformation that is most readily explained by NPHM exhumation in the Lower Rupal Valley. It is perhaps surprising that there is no deformation related to NPHM exhumation that is more impressive than this, in view of the vigorous tectonics that must operate closer to the core of the massif (numerous references in introduction). This dominantly brittle, relatively diffuse deformation therefore contrasts greatly with that on western margin of NPHM where there is a major E over W structure, and which, close to Nanga Parbat, has involved wholesale overprinting of the Himalayan fabric (e.g. Madin 1986; Madin et al., 1989; Butler et al., 1992).

It is not clear what portion of microstructure recovery processes are due to deformation related to NPHM exhumation. Many of the rocks show evidence for static recovery such as (1) sharp grain boundaries and (2) dislocation -free grains within (e.g.) a preserved non-coaxial, compositionally layered fabric. Cooling studies show that some of the rocks in the Lower Rupal Valley attained temperatures

of ~200-300°C in the last few m.y. (Schneider et al., 1997; D. Schneider, unpublished data). The spectacular microstructural recovery of the migmatitic gneiss fig. 5.20 - NE95/29-I), with respect to the strain indicated by the outcrop appearance, is seen to be a purely Himalayan feature based upon the highly parallel nature of fabric with surrounding fabric, all of which is taken to be Himalayan. What is not clear in NE95/29-I is whether the migmatisation is related to thrust or normal motion in the MMT footwall (because of the wholesale replacement of the microfabric has obliterated sense of shear evidence!).

5.3.3 Ghurikot valleys

The three valleys of Ghurikot include (1) the south fork (the main valley) which continues for ~15 km into the massif, and (2) the left and right tributaries of the north fork which continue for ~4 km into the massif. Approximately 6 km (structural thickness) of KLS rocks are exposed between the main Astor valley[12] and the NPHM/KLS contact, rocks similar to those seen in the Lower Rupal Valley section. The KLS rocks consist mostly of the massive, white flecked amphibolitic metadiorite that locally contains foliations and other structures. Horizons of the actinolitic-chloritic schist, a few hundred metres in thickness, recur throughout the section and typically contain postkinematically grown hornblende needles. Foliation in the actinolitic-chloritic schist, and where well developed in the massive metadiorite, is principally N to NW trending and SW-dipping (although in some places it is folded and becomes NE dipping). Lineation commonly plunges gently to the NNW. Other structures within the KLS rocks include (1) continuous cm to m wide shear zones, similar to those in the Lower Rupal Valley section, and (2) various types of m to

12. The Astor valley (south of Astor Village) effectively trends due north and provides a good datum from which to describe distances on the eastern margin of NPHM.

10's m wide brittle faults, zones of enhanced joint development and related folding that are all consistent with a general west over east sense of displacement. This is consistent with the Churit type structures seen within in the NPHM rocks in the Lower Rupal Valley. It is not known if Churit type fault related structures are well developed in the Lower Rupal Valley section KLS rocks because reasonably accessible outcrops east of the NPHM/KLS contact are sparse. Granitic/granodioritic lenses, similar to those described near outcrop #14 in the Lower Rupal Valley, are also present locally.

5.3.3.1 NPHM/KLS contact

The NPHM/KLS contact is exposed in all three valleys, in all cases marked by metadiorite of the KLS on the east side of the contact that is juxtaposed against cm to 10's cm thick layers of NPHM amphibolite and marble horizons on the west side. Foliation in the metasedimentary rocks is parallel with the NPHM/KLS contact, and with the metadiorite where it is locally foliated near or at the contact. The NPHM/KLS contact, and foliation in the metasedimentary rocks below, is largely N-S trending (fig. 5.25), and dips steeply west in the south fork of Ghurikot Gah. In the north fork of Ghurikot Gah, however, foliation at the NPHM/KLS contact dips more shallowly to the west. This is an expression of the regional overturning of the SE NPHM section (see below).

It is noteworthy that where the contact is seen on the right bank of the Ghurikot south fork, it can be seen to continue up the ridge to a conspicuous part of Rampur Eck that is consistent with where it is inferred to be present on the south side, based upon the remote observations from Lower Rupal Valley (see fig. 5.3).

Figure 5.25

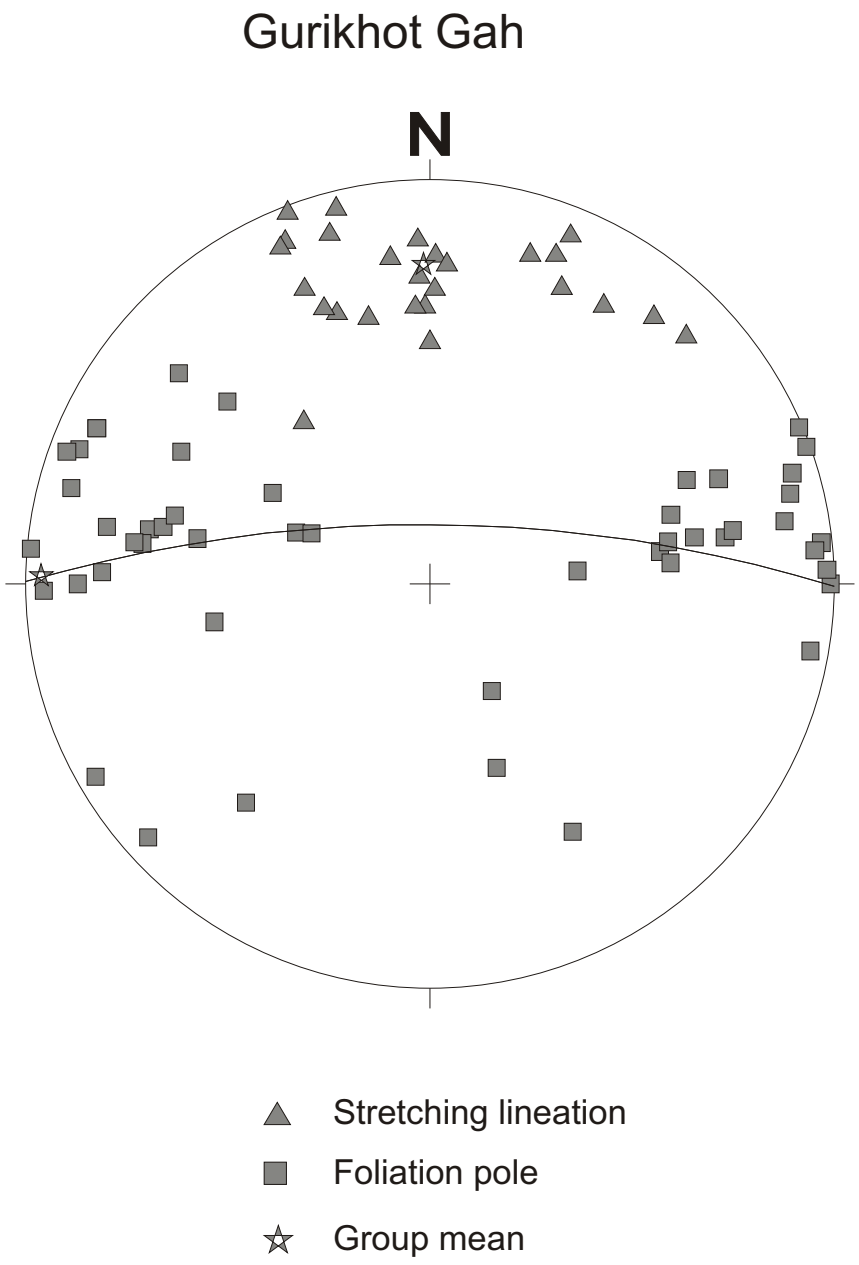

Figure 5.25 Lower hemisphere equal area projection of foliation poles and lineation of main NPHM rocks in three Ghurikot valleys.

5.3.3.2 Overturning of the SE NPHM sequences

The Ghurikot valleys provide the first easily reached outcrops that give a good example of the regional overturning of the SE NPHM sequence that was mentioned previously. The regional overturning of the SE NPHM section is accompanied by a structurally upwards decrease in westwards dip. Because the rocks in the region of the NPHM/KLS contact are exposed at higher elevations in the Ghurikot north fork than in the south fork, a relatively higher, and thus more shallowly dipping, part of the section is exposed in the north fork. It should be noted however, that the difference in dip angle is also partly a result of northward plunge of the fold associated with the regional overturning.

Figure 5.26 shows outcrop #66 (metasedimentary rocks) where part of the fold that is associated with the regional overturning of the SE NPHM sequence is exposed. The fold is a local manifestation of what is effectively a large scale kink with a W-E horizontal axial plane whose upper and lower limbs respectively cause layering to be west and east dipping. This is more clearly seen in the tops of the ridges on both sides of the Lower Rupal Valley (e.g., figures 5.3 and 5.11 - line drawings of the Churit and Rampur ridges). The region of overturning of layering is restricted to much higher altitudes in the Lower Rupal Valley than in the three Ghurikot valleys. This is a further example of the northward dip of the ~W-E horizontal axial plane of the fold that is associated with the regional overturning of the SE NPHM sequence.

The regional overturning of the SE NPHM sequence is inferred to be accommodation of east vergent displacement related to the overall uplift of the core of NPHM relative to the SE margins (see 5.3.7 - Conclusions for SE NPHM). In this manner, the overturning has a significance that is similar to the Churit Fault Zone (of which further examples are presented, below) in that it is also part of deformation, that is largely in the brittle regime that accommodates some of the later part of NPHM relative uplift. In some cases (e.g., where the two spatially coincide) folding and

Figure 5.26

Figure 5.26 Field photo looking north to left bank of main valley in Ghurikot Gah (near outcrop #66). Illustrates local folding associated with regional overturning of SE NPHM layering to W-dipping. Outcrop in bottom right is approximately 10 m high. Photo 8/10/96, no.1.

fracturing associated with the Churit Fault Zone is not easily distinguished from folding and fracturing associated with overturning of the SE NPHM sequences.

5.3.3.3 Main section of SE NPHM sequences

West of the NPHM/KLS contact, in the Ghurikot south fork, ~2 km (structural thickness) of NPHM rocks were mapped. In the north fork (left tributary), ~1 km of NPHM rocks were mapped west of the contact. The section of NPHM rock is highly similar in both the valleys, and they are described together. A few 10's of metres below the contact, the amphibolite and marble horizons are interlayered with cm to 10's cm thick garnetiferous metapelites, psammites, and biotite schists and gneisses. These are very similar to the metasedimentary rocks exposed at outcrop #13. Layering is predominantly NNW-trending (N-S in the north fork) and moderately W-dipping. Prominent mineral and crenulation intersection lineations are observed to plunge gently north. Where sense of shear relationships are clear, they seem to be dextral. Within the predominantly garnetiferous metapelite section at outcrop #17, a stretched feldspar gneiss shows good dextral sense of shear based upon sigmoidal tails from feldspar augen. This shear sense contrasts with equivalent portion of the garnetiferous metapelite section in Lower Rupal Valley (outcrop #13), where sinistral sense of shear is observed. It is not, however, inconsistent with the hypothesis of a discrete MMT normal sense horizon of 100's metres thickness that was proposed for part of section at outcrop #13, as the W-E constraints between outcrops, and the N-S constraints between the Ghurikot and Rupal valleys, are insufficiently tight to predict where the sinistral horizon might project (see also section 5.3.7. discussion and conclusion for SE NPHM).

From outcrop #17, the presence of garnetiferous metapelite in the compositionally layered metapelites gradually decreases over several hundred metres and the coarse garnets (>4 mm) are absent ~50m west of outcrop #66. This part of

the section is also marked by an increase in a more finely laminated gneisses. The angel hair unit is observed in outcrop on the left bank of the south fork. Foliation is 140°/65°W, with the ubiquitous "angel hair" lineation (<2 mm stretched felsic rodding) plunging 4° towards 335°. Within this part of the section, isoclinal, partially asymmetric, cm to 10's cm wavelength folds within the gneissic layering are apparent. A good asymmetry is not developed, and a consistent pattern of fold vergence is not observed. The isoclinal folds are local features, similar to those seen in Lower Rupal Valley, and do not represent any major fold that could cause a reversal of part of the sequence. Sense of shear within the angel hair unit is not clear. Where small garnets are present in the more pelitic portions, however, strain shadows suggest a dextral sense of shear.

A few hundred metres west of where the angel hair unit is present, there is a notable increase in felsic layers within the gneisses, where S>L. Felsic layers are cm to 10's cm in width and have a very "clean" appearance, lacking any coarse grains, micas or Fe-staining. Foliation is NNW-trending and moderately WSW dipping, and mineral lineation plunges gently towards the north. Occasionally, there is a notably asymmetric thinning associated with extensional shear bands (that presumably define C'-surfaces, although S, in particular, is not well developed). If this is truly a C'-fabric then there is evidence here for sinistral motion. This is the first observation of sinistral sense of shear in the Ghurikot valleys (viewed from the Astor River, structurally downwards through the section).

Between the sinistral sense of shear location, and outcrop #69, to the west, the banded gneiss becomes increasingly intercalated with a finely laminated gneiss with mm-porphyroclasts (where L>S). The finely laminated gneiss is highly similar to NE95/29-III described in the Lower Rupal Valley section (fig. 5.16, above). Foliation across this part of the section remains NNW trending, WSW dipping, with mineral lineation plunging gently towards the NNW. Sense of shear, based upon sigmoidal

shapes developed in the porphyroclasts, is dextral. Centimetre to 10's centimetre amphibolite layers are common throughout here also. There appears to be no systematic pattern to their occurrence.

In the region of outcrop #69, there is a notable presence of migmatite mobility. Migmatitic biotite gneiss that is present in the eastern portion of the outcrop (e.g. E6/10/8-I - not shown) is highly similar to migmatitic biotite gneiss in the lower Rupal Valley between outcrops #12 & #10 (5/29A in fig. 5.20, above). Layering is consistent with elsewhere (e.g. 158°/58°W, with mineral lineation 10°@336°). Sigmoidal shapes of asymmetric 1-4 mm feldspar augen show clear sinistral sense of shear.

The furthest point west that I observed in the Ghurikot section is a few 10's of metres west of outcrop #69. To this point, the migmatitic biotite gneiss passes to a migmatitic, garnet-rich, pelitic gneiss (fig. 5.21, above). Centimetre-scale isoclinal fold of the migmatitic portions are common and, typically, L>S. Foliation is NNW, dipping moderately WSW, with lineation plunging gently to the north. Sense of shear within the migmatite is ambiguous. Based upon stepping directions of augen and leucosome tails, sense of shear is dextral. However, 1-2 cm C'-surfaces trending NNE-SSW suggest sinistral sense of shear. In view of the demonstrably sinistral sense of shear in the nearby migmatitic biotite gneiss (described above), I infer a sinistral shear sense within the migmatitic, pelitic gneiss. It is also possible that there is an evolution of shear sense here, with dextral (MMT thrust) first, followed by minor sinistral (MMT normal).

5.3.3.4 Churit Fault Zone in Ghurikot

In the general area of section within the south fork of Ghurikot that corresponds to the Churit fault in Lower Rupal Valley, a consistent series of fractures and faults are distributed across ~2 km between outcrop #66 and #69. Like the

Churit faults in Lower Rupal Valley, the fractures and faults typically have metres to tens of metres of east-vergent displacement that are frequently associated with locally tight folding (fig. 21, above). Although my measurements of fault frequency, magnitude and displacement were only qualitative, it appears that there is less Churit Fault-type deformation in the Ghurikot valleys than in the Lower Rupal Valley. I note that related fold deformation is certainly less spectacular in the Ghurikot valleys, and this may be a manifestation of lesser intensity (i.e., outside the main part of the fault zone). Although not wholly not clear, the distance to the eastern margin of the fault zone in the Ghurikot valleys seems to be greater than the Lower Rupal Valley, and the fault zone in Ghurikot may therefore be modestly wider (a few hundred metres) than the ~2 km Churit Fault Zone in the Lower Rupal Valley.

5.3.4 Bulan

Bulan Gah is a steep valley that drains from the general area of Bulan Peak (4915m), the highest point within the vicinity of the SE NPHM. The overturning of the regional sequences in NPHM is most clearly seen upon the upper flanks of Bulan Peak (4915m, figs. 5.27 & 5.28), where >500m of structural thickness of the NPHM metasedimentary schists and gneisses interlayered with marbles and amphibolites dip ~40°W. Figure 5.29 is a particularly good field photo showing the regional overturning and westward dip of layering upon Bulan Gah, and the consistent dip of layering in surrounding areas.

5.3.4.1 NPHM/KLS contact

Because the NPHM/KLS contact in Bulan Gah is considerably further eastward than in the Ghurikot and Lower Rupal Valley areas (relative to the Astor River), approximately 1 km (structural thickness) of KLS rocks is all that is exposed between the main Astor valley and the NPHM/KLS contact. The KLS rocks consist

Figure 5.27

Figure 5.27 (field photo). View to west and upward to Bulan Peak (4915 m) showing ~500m (structural thickness) of NPHM metasedimentary rocks - schists and gneisses interlayered with marbles and amphibolites (recognisable as continuous black bands). Approximately 40°W true dip of foliation not clear due to perspective (see fig. 5.28). Photo 29/9/96 no.4. View from left bank of Astor Valley.

Figure 5.28

Figure 5.28 (field photo). Looking N. to left bank of Chuggam Gah, in Rattu area (3000-3500m main ridge in foreground). Small top of ridge just visible in centre of depth of field is Rampur Ridge (3884m). Bulan peak (4915m) clearly visible in distance. Crop fields are at ~2500m). In all visible portions of ridges, W-dipping (overturned) compositionally layered NPHM metasedimentary sequence is visible. c.f. fig. 5.28, Photo 24/9/96, no.2.

mostly of the massive, white flecked green metadiorite that locally contains foliations and other structures. There is a very small section (<100 m) of the chlorite schist with post-kinematically grown amphibole needles. This is present close to the contact.

The NPHM/KLS contact is in accessible exposure on the right bank of Bulan Gah, and is clearly exposed high up on the left bank. Metadiorite of the KLS on the east side of the contact is juxtaposed against cm to 10's cm thick layers of NPHM garnetiferous metapelite that is interlayered with amphibolite and marble. Foliation in the metasedimentary rocks is parallel with the NPHM/KLS contact, and trends largely N-S, dipping moderately to the west (fig. 5. 29). Mineral lineation plunges gently to the north (15-30° - slightly steeper than in Ghurikot). Within the ~100m of section west of the contact, garnetiferous metapelites form a greater portion of the section than (e.g.,) in the Ghurikot valleys. In the more felsic, finely laminated, notably highly strained portions of the metapelites a dextral sense of shear is indicated by (1) sigmoidal shapes of 1-3 mm augen, and (2) reasonable development of C'-surfaces. This is consistent with original thrust sense in the MMT footwall. About 500 m further up the valley however, a section of outcrop shows some indication of sinistral shear sense where a more coarsely layered (10's m), notably strained ~60° west-dipping sequence of amphibolites, marbles and quartzofeldspathic gneiss is present on the right bank of Bulan Gah. Here, metre-scale boudins of amphibolite gneiss suggest sinistral sense of shear based upon boudin asymmetry and pinch and swell morphology (fig. 5.13, above).

The outcrop shown in figure 5.13 (above) is about 100m east of outcrop #70A. Outcrop #70A was the limit of my mapping in Bulan Gah due to the abrupt narrowing of the valley to a gorge that resulted in inaccessibility due to increased mid-October drainage flow and recent land slippage. Although ~1 km of section was the total structural thickness of NPHM rock observed in outcrop west of the NPHM/KLS contact, some comment can be made regarding the observed float that had clearly

Figure 5.29

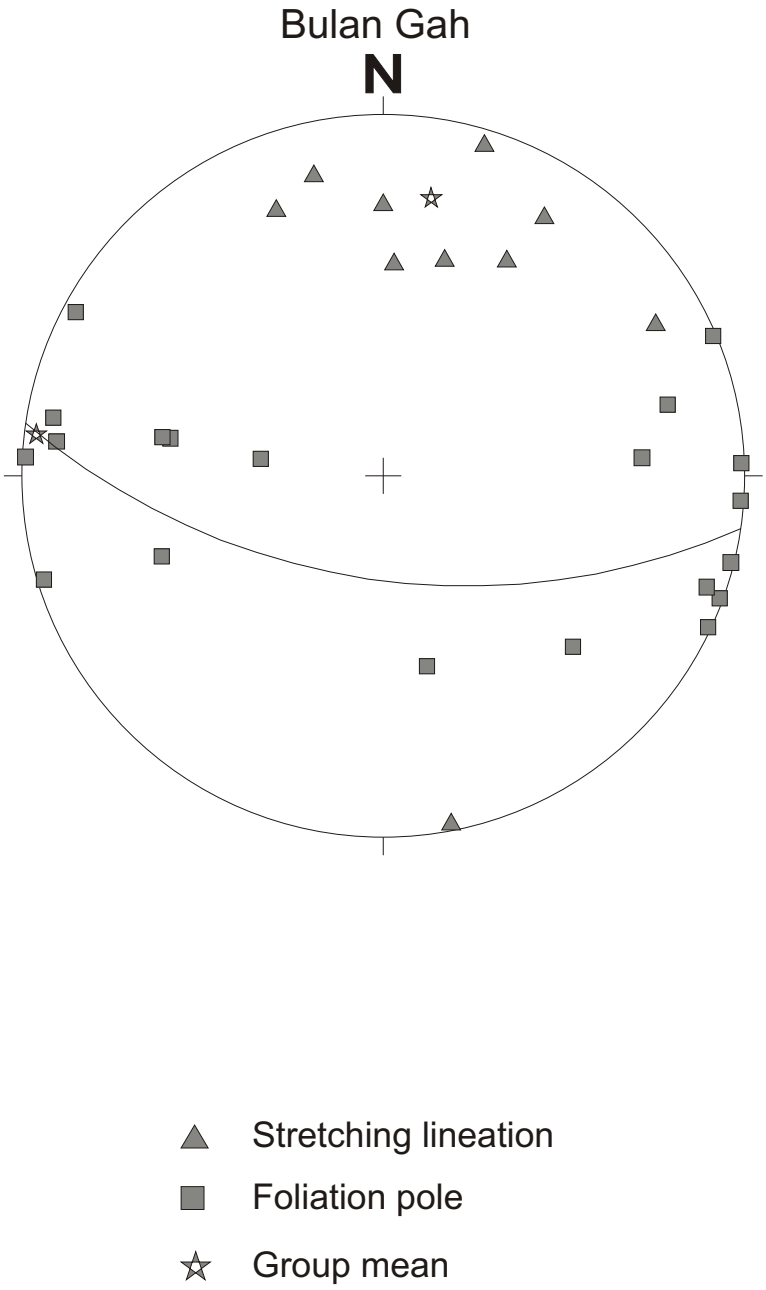

Figure 5.29 Lower hemisphere equal area projection of foliation poles and lineation of all rocks in Bulan Gah.

descended from upstream. Most prominent were large boulders of granitic orthogneiss (fig. 5.13, above) that are akin to the westernmost part of the section in Lower Rupal Valley. Float from various metasedimentary schists and gneisses, amphibolite layers, the angel hair unit, and the migmatitic biotite gneiss were found. In addition, large boulders of the "lath unit" (described in the Rama Valley section, below) were found suggesting it is present nearby in the section. This is consistent with my observations of the position of the lath unit in the SE NPHM sequence, further north in Rama Valley, Astor Gorge, an Dichil Gah.

5.3.5 Rama valley

Rama Valley is 1-2 km wide (broader than the valleys of Ghurikot and Bulan) and human development (i.e., jeep and foot trails) allows good access into the central parts of the valley. Rama Valley is noteworthy for the substantial thicknesses of glacial moraine that are found throughout the valley. Glacial deposits are sufficiently large so that at the foot of Rama Valley, in the general vicinity of Astor village, rocks of the KLS sequence are not exposed on the left bank.

5.3.5.1 NPHM/KLS contact

The NPHM/KLS contact is not exposed on the left bank of Rama Valley. On the right bank, a large river has cut a 30-40 m gorge at the point where the main glacial fill comes into contact with the wall of the right bank. Remote observations were all that was possible but the contact is seen to juxtaposes dark green rocks against 10 cm to m layered metasedimentary schists and gneisses in a manner consistent with the Lower Rupal Valley, the Ghurikot valleys and Bulan Gah. Layering is very steep in the lower portion of the wall of the right bank but dip is observed to decrease to become moderately west dipping further up the wall (fig. 5.30).

Figure 5.30

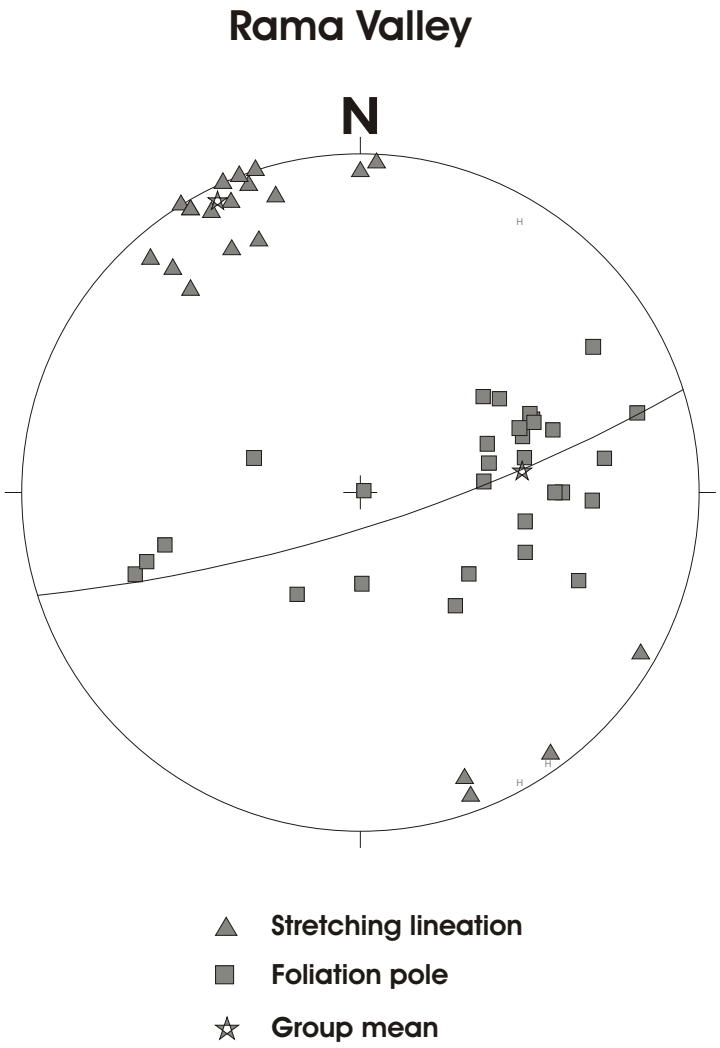

Figure 5.30 Lower hemisphere equal area projection of foliation poles and lineation of all rocks in Rama Valley.

On the left bank, only NPHM rocks are exposed. The easternmost part of the exposed section consists of garnetiferous metapelites interlayered with felsic schists and gneisses, highly similar to those seen at outcrop #11 in the Lower Rupal Valley. Centimetre to 10's centimetre thick layers of marble and amphibolite layers are present within the garnetiferous metapelite section but the volume of marble and amphibolite is less than that found near the KLS/NPHM contact near (e.g.) outcrop #13 in Lower Rupal Valley. From this difference, I infer that approximately 200-500 m of section up to the KLS/NPHM contact (i.e. the uppermost 200-500 m of the MMT hanging wall) is unexposed on the left bank of Rama Valley.

5.3.5.2 Lath Unit

Approximately 300 m along the section, west of where NPHM rocks are first exposed on the left bank of Rama valley, the metapelitic schists and gneisses are clearly cross cut by an atypical, very coarse feldspar-bearing pelitic gneiss that I have termed the "lath unit" (figs 5.31 and 5.32). The name is based upon the massive laths of feldspar (up to several cm long) that are usually preserved in the rock. which otherwise has a very fine-grained, highly-strained matrix. In addition to the coarse feldspars, cherry-red garnets up to 1 cm in size are present along with a purple to light brown matrix. In rocks that visibly appear more strained (i.e. where feldspar laths are not preserved, and grain size is much smaller) the purple to light brown colour of the matrix and the cherry colour of the garnets are the principal criteria for identifying the lath unit. In the "type" example of the lath unit, a few thin (1-5 mm) lenses or augen (<1 cm) with tails (no implications for C/S fabric) are seen to anastamose around the cherry garnets and bigger (2-10 mm) feldspar augen. The feldspar laths however, in the "type" example of the lath unit, are notably lacking tails and usually appear well formed. The laths are never euhedral, however, and "corners" of the laths are commonly rounded. In addition, the laths are frequently, visibly impure, containing

Figure 5.31A

Figure 5.31A Lath unit outcropping on left bank of Rama Valley, ~300m east of outcrop #64. Note very disordered fabric picked out by generally non-preferred orientation of 1-4 cm laths of feldspar within biotite, garnet & quartzofeldspathic matrix. c.f. fig. 5.31B, taken ~10 metres nearby. Lens cap for scale. Photo 7/10/96 no.7.

Figure 5.31B

Figure 5.31B Lath unit outcropping on left bank of Rama Valley, ~300m east of outcrop #64. Indicates spectacular fabric gradient; portions with apparently greater shortening are visibly accompanied by change in foliation direction. Note foliation is highly variable and lineation only locally present. c.f. fig. 5.31A, taken ~10 metres nearby. Lens cap (55 mm) for scale. Photo 7/10/96 no.13.

Figure 5.32

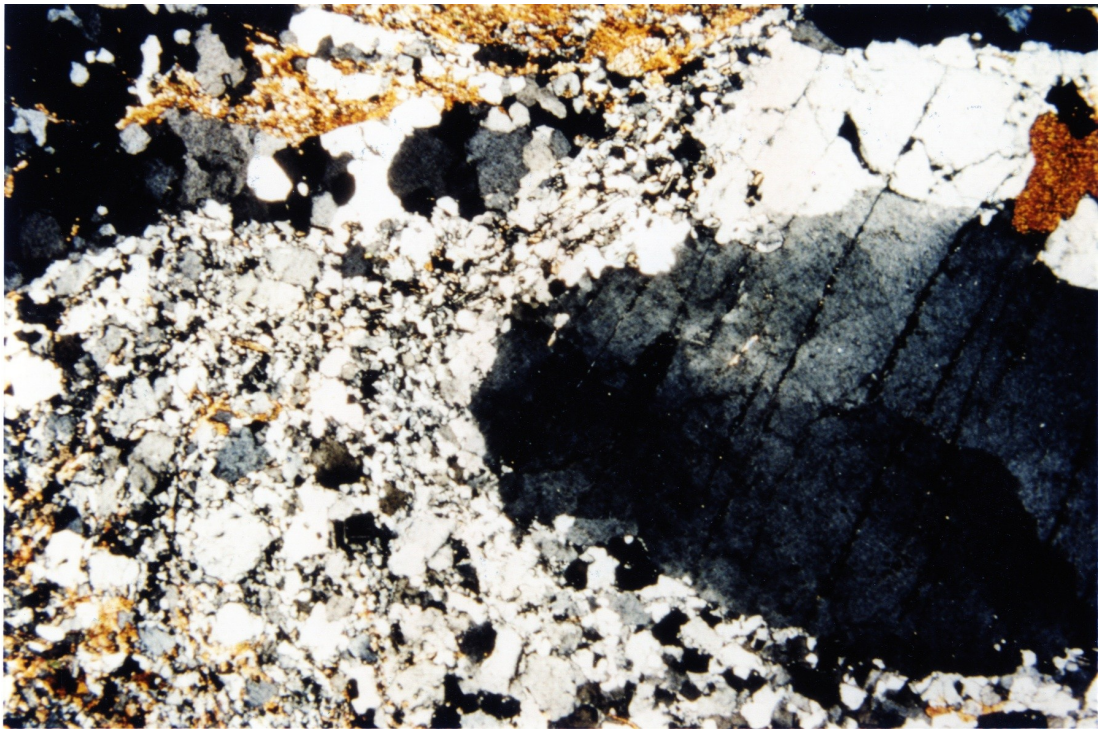

Figure 5.32 Optical photomicrograph of thin section AS/E, (cut from sample of same name, lath unit ~200m east of outcrop #71, on Astor Gorge left bank. 011°/43°W, 12°N-pitch). In upper left portion, 0.25-0.75 mm monomineralic quartz ribbon is typical appearance of quartz rich part of fine grained augen tail. Very finely sutured grain margins of large (>3 mm) feldspar clast and fine (50-150 μm) groundmass indicate extensive grain boundary migration recrystallisation. Not oriented. No sense of shear. Base of image is 5.5 mm long. Crossed polars.

cherry garnets and tourmaline. To say the laths are "undeformed" is therefore probably unwise as their rounded corners indicate there has been some degree of surface area reduction in the laths, although lack of porphyroclast tails indicate that this is unlikely to be entirely sub-solidus deformation. The issue of supersolidus deformation in the lath unit is of some relevance. While figure 5.31A shows a very disordered fabric to the lath unit, figure 5.31B (taken a few metres away) shows a spectacular fabric gradient, in which the regions in the photo that have the apparently greater shortening are visibly accompanied by a change in foliation direction. This foliation is highly variable throughout the section, and only locally does the alignment of longer, thinner laths define any type of lineation. It is certainly difficult to talk about what is "shortening" in the case of the upper part of the outcrop in figure 5.31B. This part of the outcrop shows fewer laths in general, and it is possible that conditions were sufficiently supersolidus (i.e. the melt volume was sufficiently high like in fig. 31A) that the accumulations of laths (acting as a strong phase) caused large strength gradients within the rock (e.g., Rutter and Neumann, 1995). An alternative speculation is that all the deformation is postmagmatic. P/T petrogenic grid studies of both the lath unit and of nearby rocks have constrained only general amphibolite facies (Page Chamberlain, personal comm.), and conditions of deformation in the lath unit, based upon deformation mechanisms inferred from preserved microstructure, cannot be proposed to be greater than ~600°C (see below), without appealing to a major period of recovery, as the feldspars appear to be relict (Carlsbad twinning = igneous) and not porphyroblasts. There is presently no evidence for any diffusive mass transfer processes having operated (the realm where solid state processes begin to follow fluid state laws, e.g., Brodie and Rutter, 1985; Rutter and Brodie, 1995; Brown and Rushmer, 1997), and although a discussion of deformation (and chemical exchange) in the solid to liquid "grey area" is of considerable interest, it is outside the scope of this thesis chapter. There is thus little that can be said about possible

supersolidus deformation of the lath unit beyond the general description, above. Deformation in the solid state however, can be remarked upon. Figure 5.32 (above) shows microstructure in a sample of the lath unit (AS/E - actually from Astor Gorge ~200m west of outcrop #71) whose appearance is similar to the lower part of the lath unit outcrop shown in figure 5.32B. Within the field of view (5.5 mm) I have included a portion of the lath unit that has <3 mm feldspar clasts with ~1 mm quartzofeldspathic rods (note the tail running across the top of the image, part of which is composed of a quartz ribbon). The sutured margins (30-100 μm "lumps") of the large feldspar are accommodating deformation through grain boundary migration recrystallisation. Grain boundary migration recrystallisation also appears to be taking place in the fine grained portion at large based upon the extensive sutured margins of the grains. The closeness of extinction angle of the grains in the quartz ribbon suggests they are a product of subgrain rotation recrystallisation. There is no evidence for any higher temperature deformation processes here. If both grain boundary migration and subgrain rotation recrystallisation have operated simultaneously, temperatures of deformation have been in excess of 500°C. In all respects, the appearance is not unlike many of the finely laminated gneisses from the Lower Rupal Valley that were introduced previously in this chapter, and the microstructure belies the macroscopic appearance of the lath unit. I infer, therefore that there has been a significant amount of subsolidus strain accommodated within the lath unit, in spite of the presence of large feldspar laths that do not seem to be in the process of undergoing significant tectonic grain size reduction in the manner of a typical porphyroclast. As will be seen in the Astor Gorge section, there are examples where portions of the lath unit grade into highly strained L>>S gneiss with uniformly fine grained (<4 mm) feldspar augen, and the coarse laths are wholly absent. In the Astor example, although the contrast in macroscopic appearance suggests a large strain contrast between the lath and the "non lath" portions, the observed

microstructural features (grain boundary migration, subgrain rotation recrystallisation, development of polymineralic ribbons, domains of differential grain size) suggest no differential conditions of deformation, and only a spatially discrete prolonged strain can be inferred. Finally, there is little that can be said about sense of shear. The lath unit is most frequently within metapelitic schists and gneisses, where it cross-cuts foliation and is not evenly distributed or foliated (e.g. 018°/27°E changes to 075°/38°N to 065°/46°SE). Lineation was only convincing in a few places, and was observed to plunge ~10° towards north or south. Thin section AS/E (in fig 5.32) is not oriented. It is noteworthy, however, that lineation within the lath unit in Rama Valley is not inconsistent with regional trends.

Plate 2 shows the unusual outcrop patterns of the lath unit, in which there is almost no exposure of the lath unit in the lower portions of the ridge on the left bank of Rama Valley. The outcrop pattern could be interpreted to suggest that the lath unit is tightly folded within the NPHM section as a result of a series of 100-300 m wavelength folds. There does not seem to be evidence consistent with this along the section. however; there is no obvious cyclic 100-300 m repetition within the ~1 km of section along strike from (lower or higher in the valley wall) where the lath unit is present in the section (see 5.3.5.3 - NPHM main section).

5.3.5.3 - NPHM main section

The lath unit non-uniformly cuts across the NPHM rocks in several locations across a zone of about 1 km thickness. In the lower part of the valley wall (i.e., along strike) the lath unit is almost wholly absent, however, and the NPHM sequence can be clearly observed. The easternmost part of the sequence consists of cm to 10's cm thick garnetiferous metapelites, psammites, occasional amphibolites and marbles (not necessarily occurring together) and biotite schists and gneisses. These are very similar to the metasedimentary rocks exposed at outcrop #13 in the Lower Rupal Valley.

Layering predominantly trends NNW to NW (with the exception of the lath unit) and dips gently to steeply W. Prominent mineral and crenulation intersection lineations are observed to plunge gently north. Where sense of shear relationships are clear, they seem to be dextral. Within the stretched feldspar portions of the section of gneiss in the vicinity of outcrop #64, C/S relationships, based upon sigmoidal feldspar porphyroclast tails and C-surface parallel micas, show convincing dextral sense of shear.

The coarser and more finely laminated gneisses with occasional biotite schist layers continue for ~2 km along the left bank of Rama Valley from where outcrop begins. There are some Churit-type faults (W over E sense with local buckling) within this section but their significance is not large. There are a handful of very steep 2-4 m high cliff faces, 3-8 m in length that typically trend ~W-E. These frequently display slickenfibres and occasionally good slickensides that indicate sinistral sense of shear (the north block moved west).

In the vicinity of outcrop #62, the section is marked by an increase in more finely laminated gneiss. This passes (to the west) into the angel hair unit (see fig. 5.14, above, note cm-scale compositional banding, mm-scale augen and rusty garnets). Foliation at this outcrop is (e.g.) 159/33°W, with mm-scale rods (L>>S) of quartz and feldspar defining a lineation plunging 7° towards 332°. Sense of shear within the angel hair unit at this outcrop is not clear. Thin section 610/7A (not shown - cut from E6/10/7-I, although see fig. 5.15, above, for 610/10A as an example of microstructure for deformation mechanisms for the angel hair in Dichil Gah) shows very fine grain size (50-100 μm - with very sutured grain boundaries) but with no clear oblique foliation and very small (~100 μm) quartz ribbons but little to no development of sigmoidal shapes. Some large (~2 mm) feldspar porphyroclasts (in one case, nicely Carslbad twinned) indicate sinistral sense of shear based upon tails. Additionally there is a lattice preferred orientation indicated by "across the board"

extinction in scattered, small (<50 x <150 μm) biotite laths. The biotite fabric also suggest sinistral sense of shear based upon some mica fish development.

West of the angel hair unit at outcrop #62, the section continues for >3 km with a series of coarsely and finely laminated gneisses interlayered with biotite schists, amphibolites, and occasionally garnetiferous metapelite. Foliation in this section is consistent, trending NNW to NW, dipping gently to steeply west, with mineral and/or intersection lineation plunging gently north.

In the vicinity of outcrop #R1, pinch and swell structures are present in a more coarsely laminated (0.5-4.0 cm) portion of the gneiss that is interlayered with amphibolite. The asymmetry of pinch and swell structures suggest sinistral sense of shear. It is not known if this local occurrence of sinistral sense of shear is part of a thick zone that continues sufficiently far to the east (~2 km) to include the angel hair unit at outcrop #62. Based upon the large distance (~2 km) however, I deem it unlikely.

At outcrop #R5, ~3 km west of the angel hair unit at outcrop #62, the coarsely and finely laminated gneisses and biotite schists pass to a notably migmatitic section of gneisses (the limit of mapping on the left bank). This biotite-migmatite-gneiss (E7/7/6-I - not shown, foliation: 152°/38°W, lineation: 22°@322°) has a clear lattice preferred orientation based upon muscovite and biotite fabric. A large amount of scree that has descended from craggy outcrops above contains granitic orthogneiss (fig. 5.33, upper sketch showing granitic orthogneiss in crags above outcrop #R5). The granitic orthogneiss is similar to that seen in the section in the Lower Rupal Valley that extends west to near (east of) Tarshing.

Limited mapping was conducted on the right bank of Rama Valley. Approximately 1 km east of outcrop #RL71, in the lower part of the ridge that forms the right bank of Rama Valley, another local occurrence of the angel hair unit is present as a thin part of the section (~50m). This does not seem to be along strike

Figure 5.33

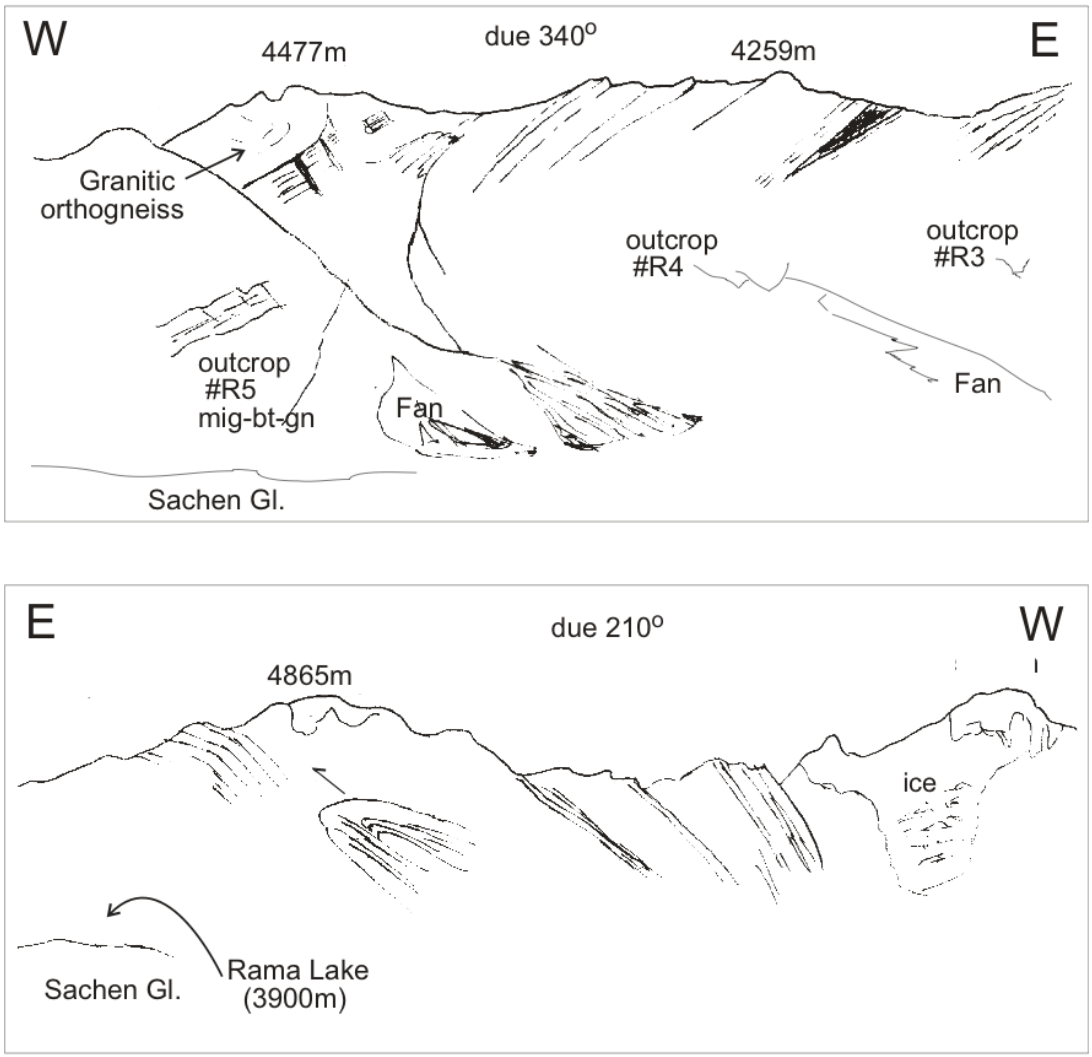

Figure 5.33 (line drawings of fieldbook sketches).
Upper: View to NW showing left bank of Rama Valley with 30-60°W dipping (overturned) compositionally layering of NPHM rocks. Between outcrops #R4 and #R5, gneisses pass into section of migmatisation. Note granitic orthogneiss in crags above outcrop #R5. Width of view is ~3 km.
Lower: View to SW showing right bank of Rama Valley with 30-60°W dipping layering of NPHM rocks. Fold and thrust in hillside clear but not observed close up in outcrop). Width of view is ~5 km. Sketches 6/7/97.

from the angel hair at outcrop #62 (plate 2), and the observed left-step mismatch is inconsistent with the outcrop pattern being a product of the local trend of foliation (e.g., 120°/56°W; 30°@160° - at the angel hair unit outcrop on the right bank).

The angel hair unit outcropping in the right bank of Rama Valley is highly similar to the angel hair unit outcropping in the left bank of Rama Valley. Thin section 66/21A (not shown - cut from E6/6/21-I) is very fine grained (10's to 100's μm, with grain boundary migration recrystallisation indicated by very sutured grain boundaries), monomineralic ~1-2 mm μm quartz ribbons occasionally containing 2-4 mm feldspar porphyroclasts with some development of sigmoidal shapes that suggest dextral sense of shear. Garnet grains, 0.5-2.0 mm in diameter, also occasionally suggest dextral sense of shear based upon strain shadow geometry. The garnet grains lack any useful internal fabric such as spiraled inclusion trails. Additionally, there is a lattice preferred orientation indicated by uniform extinction of scattered, small (<50 x <150 μm) biotite laths. The dextral sense of shear observed in the angel hair unit on Rama right bank is inconsistent with the sinistral sense of shear observed in the angel hair unit (thin section 610/7A) from Rama left bank. It must be noted, however, that in both cases the sense of shear indicators are not strongly developed.

At outcrop #RL71, in the lower part of the right bank ridge, an impressive 1-3 mm rodded granitic orthogneiss is present in the form of a small fold (~3-5 m wavelength) with an ~NW trending hinge line. Foliation is not clear, but lineation plunges ~8° towards 167° in the SW dipping limb, and 7° towards 178°, in the NE dipping limb. Approximately 1 km west of outcrop #RL71, in the lower part of the ridge that overlooks the lake on right bank of Rama Valley (see fig. 5.33, above) the section has a migmatitic component the gneiss (foliation: 009°/42°W, lineation: 9°@344°). This presence of migmatite is consistent with the sequence on the left bank of Rama Valley.

5.3.6 Rattu area

5.3.6.1 NPHM/KLS contact

The NPHM/KLS contact was not observed in the Rattu area. KLS rocks were examined in a number of places along the roadside. I most cases these outcrops consist of the pale chloritic schist with or without the postkinematically growing hornblende needles. Although foliation is frequently quite warped on the scale of a few metres (observed within many outcrops), the principal foliation is consistent with the other SE NPHM sequences, dipping steeply to the W to WSW, with lineation plunging gently to moderately towards the north.

The main portion of the SE NPHM rocks are impressively overturned (fig. 5.28, above). Within the lower parts of Chuggam Gah, approximately 500m of NPHM section was examined in outcrop and found to be consistent with the SE NPHM section in the other valleys. In Chuggam Gah, occasional, tight to isoclinal, partially asymmetric, 10's cm to m wavelength folds are present within the metapelitic sequences. A good asymmetry is not developed, and these folds are thought to be related to Churit-type fault structures. Away from these folds, foliation is consistent with the SE NPHM in (e.g.) the Lower Rupal Valley. Layers dip moderately W or WSW and lineation plunges moderately N or NNW.

5.3.7 Conclusions for SE NPHM

5.3.7.1 KLS and NPHM rocks

1. In all the valleys in SE NPHM, the KLS rocks east of the NPHM/KLS contact include extensive amphibolites, metabasites and granodiorites that are consistent with other workers' descriptions of the KLS from the MMT hanging wall at localities outside of the NPHM area (Tahirkheli et al, 1979; Tahirkheli and Jan, 1979; Bard et al., 1980; Tahirkheli, 1982; Bard, 1983; Coward et al., 1988; Williams, 1989; Hubbard et al., 1995; Asif Khan, personal comm.). I

therefore regard the sequence that is present east of the KLS/NPHM contact in SE NPHM, to be part of the KLS that is found in the MMT hanging wall. This is consistent with the conclusions of other workers from elsewhere in the NPHM (Madin, 1986; Madin et al., 1989; Butler et al., 1989; Treloar et al., 1991: Wheeler et al., 1995; Lemennicier et al., 1996).

2. In all the valleys in SE NPHM, west of the NPHM/KLS contact, the extensive sequence of garnetiferous metapelitic and quartzofeldspathic schists and gneisses, amphibolites and marbles are consistent with both my own observations, and other workers' descriptions, of Indian cover sequences from the MMT footwall that are found elsewhere in both the Nanga Parbat massif (Hubbard et al., 1995; Wheeler et al., 1995; Lemmenicier et al., 1996; Pêcher and Le Fort, in press; Asif Khan, personal comm.), and in the Pakistan Himalaya in general (Tahirkheli et al, 1979; Tahirkheli, 1982; Greco et al., 1989; Papritz and Rey, 1989; Chaudhry and Ghazanfar, 1990; Burg et al., 1996; Anczkiewicz et al., 1997). I therefore interpret the sequence that is present west of the KLS/NPHM contact to be part of the original Indian cover sequences directly below the MMT footwall.

5.3.7.2 Himalayan and NPHM-related strain

1. The SE NPHM section of schists and gneisses mostly show evidence of having been subjected to deformation at temperatures of 400-600°C. It is clear that the foliation and the lineation is principally a Himalayan fabric developed in response to a major shear zone (i.e. the *sensu lato* MMT).

2. Although in the NPHM rocks there seems to be a more impressive appearance of strain in outcrop in some rocks than in others, microstructural analyses indicate that most of the foliated gneisses have experienced a considerable amount of strain and there does not appear to be a single horizon which can be recognised as a principal shear zone (in section 5.4.4 Eastern

Astor Gorge and Dichil Gah, the lath unit is shown to post date some but not all of the main Himalayan thrust event(s)).

3. In all the valleys, much of the strain within the NPHM gneisses is non-coaxial and has demonstrably dextral sense of shear. This is consistent with original thrust sense motion in the MMT footwall, that has not been obliterated by later strain.

4. Within the non-coaxially deformed gneiss (>400°C) in each of the sections, there is at least one zone of convincing sinistral sense of shear. There is no evidence for a reversal across a major fold of the original MMT footwall in any of the areas, and I conclude that these examples of sinistral shear sense within MMT footwall gneisses are due to relative normal motion within the MMT footwall (although see section 5.6.2 for discussion). Based primarily on constraints in the Lower Rupal Valley, I infer these zones of relative normal motion in the original MMT footwall are horizons of a few hundred metres in thickness. The presence of principally ductile horizons with normal sense displacement in the MMT footwall is a significant new discovery.

5. General east vergent displacement that is represented by the Churit fault Zone, and by the regional overturning of the SE NPHM sequences is the only significant deformation in SE NPHM that is related to NPHM exhumation. There appears to be no deformation related to NPHM exhumation that has produced a new foliation or lineation. There may have been some portion of microstructure recovery processes related to NPHM exhumation, but it is not possible to separate this from a static recovery generally due to sluggish thermal relaxation following principal Himalayan events.

5.4 GEOLOGICAL OBSERVATIONS ALONG THE ASTOR GORGE

5.4.1 General remarks

The Astor gorge provides a natural section (~25 km) oriented ~NW-SE through the entire NPHM, approximately coinciding with "*la corset*" of the massif; the portion where the ~E-W distance from the western margin to the eastern margin attains its minimum width (~17 km). Because of the immense elevation contrasts along the gorge (~2000 m at the Astor river to between 3000 and 6500 m at the ridge tops) the overall structure of the central massif is clear, albeit largely inaccessible. An unsurfaced road that, on the south side of the river, divides into an upper and lower option in the central part of the Astor Gorge provided the main access for this study. Additionally used was a footpath over Dichil Pass to a valley system that provided an additional ~W-E section that is north of and parallel with the eastern part of the Astor Gorge.

Two antiforms with broadly differing overall lithology are observed in the main Astor Gorge; the Burdish Ridge and Dichil antiforms, in the west and east, respectively. This is consistent with reports of two main antiforms from the Indus George (~W-E) section (Madin, 1986; Madin et al., 1989; Treloar et al., 1991; Wheeler et al., 1995). The Burdish Ridge antiform is asymmetric with a thinned E-limb, while the Dichil antiform is asymmetric with a thinned W-limb. This is recognised by a very tight, pinched fold morphology of the accompanying synform (the Dashkin synform, see below).

5.4.2 Western Astor Gorge

On the western margin of the massif, near the Astor/Indus confluence, the NPHM/KLS contact is marked by the Raikot Fault (Madin, 1986; Madin et al., 1989; Butler et al., 1989; this study). The KLS rocks form a small (<1 km) section before

rugged topography ceases and outcrop is obscured by the main Indus River (Fig. 5.34). Figure 5.34 additionally shows the ~W-E trending Kohistan synform on the opposite (western) side of the main Indus River that causes the KLS rocks at the Astor Gorge NPHM western margin to be locally close to W-E trending, a significant deviation away from the typical ~N-S structural trend found throughout the Astor Gorge. The NPHM/KLS contact is covered on the left bank near the road by a landslide, however it can be seen on the right bank up in the hills as a sharp juxtaposition of green rocks against brown (fig. 5.34). Figure 5.34 also shows that there is a general component of E-dip to the green KLS rocks near the contact while the general dip of the NPHM rocks is steeply westward. Binocular observation from the road on the left bank indicates that in one area there is a switch from E-dipping to W-dipping fabric that marks a local pop-up structure of a few hundred metres width that modifies the Raikot fault. This structural switching from E-dipping to W-dipping is also expressed by (1) numerous minor E-dipping (W-vergent) fractures, dykes, and fault tip folds that are present in Western Astor Gorge, and (2) a large number of corresponding W-dipping, E-vergent, structures (including late pegmatitic dyke sets, fault propagation folds, and antithetic faults). Figure 5.35 (located on fig. 5.34) shows a section of locally highly variable lithology near outcrop #A72, where W-dipping, E-vergent layering (including late pegmatitic dyke sets) has being sliced out by (1) E-vergent reverse faulting (related fault propagation folds are not shown), and (2) general N-S (ductile) extension. The W-dipping layering seen in the foreground of figure 5.34 continues for several km along the western part of the Astor Gorge (fig. 5.36), all the way to the region of the Dashkin synform (see below).

East of the landslide on the left bank that obscures the NPHM/KLS contact, a few hundred metres of steeply NW dipping to subvertical metapelites are present. This thickness is small compared to the SE NPHM sequences. The metapelites are intruded by numerous metre to 10's metre scale leucocratic and pegmatitic dykes that

Figure 5.34

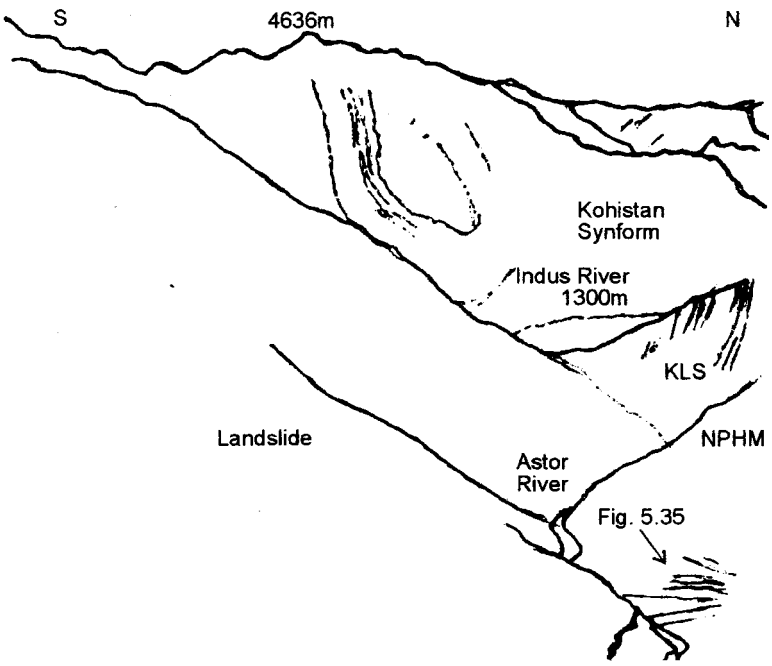

Figure 5.34 (field photo and line drawing). View to W over Indus River valley to Kohistan synform. Note contrast in NE dipping KLS layering and ~W dip of NPHM layering. Width of view ~2 km (foreground). Photo 6/7/96 no.0.

Figure 5.35

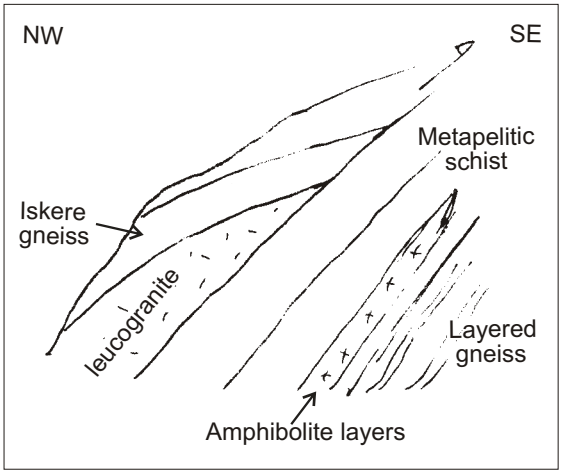

Figure 5.35 (line drawing of fieldbook sketch). View to NE and right bank of Astor Gorge, showing section of variable lithology near outcrop #A72. Note W-dipping layering is truncated by (1) E-vergent reverse faulting (fault propagation folds not shown), and (2) general E-W (ductile) extension. See text for further discussion. Width of view is ~0.5 km (c.f. location on fig. 5.34). Sketch composed: 26/6/96.

Figure 5.36

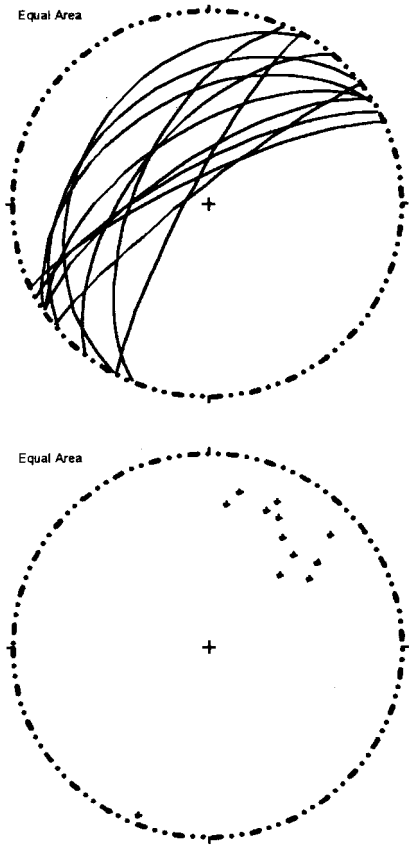

Figure 5.36 Lower hemisphere equal area projection of foliation poles and lineation of main NPHM fabric in W Astor Gorge.

are largely NW-dipping. Mineral and crenulation intersection lineation of the metapelites plunges moderately north. The metapelites grade into a series of porphyroclastic and coarsely to finely laminated gneisses with a consistent foliation and lineation trend, and with very rare interlayered or low-angle cross-cutting amphibolite sheets. In the porphyroclastic portions, the individual feldspar clasts mark out C and S surfaces, and a sinistral sense of shear is clearly indicated, and, because the porphyroclastic gneisses are part of the western limb of the Burdish Ridge antiform, this is consistent with original thrust sense on the MMT.

About 3.5 km east of the landslide on the left bank, ~300 m SE (i.e., upstream) of outcrop #A75 and the low road / high road junction near Doian, the gneisses pass into the highly recognisable pale fine-grained foliated granitic orthogneiss with ubiquitous migmatisation represented by cm - 10's cm cross-cutting leucosome bodies typically accompanied by a melanosome (fig. 5.37). This rock unit was first recognised on the Indus Gorge section and is termed the Iskere gneiss (Madin, 1986; Madin et al., 1989; Treloar et al., 1991). The leucosome body in figure 5.37 cross-cuts at a low angle to the main foliation. In other portions of the Iskere in Astor Gorge, however, migmatitic structures cross-cut the main foliation at a high angle (not illustrated). Amphibolite layers, which are not abundant, were not observed to cross cut migmatitic structures in the Iskere gneiss in Astor Gorge. Orientation of layering in the Iskere in western Astor Gorge (and within the interlayered porphyroclastic and laminated gneisses) is consistent with the rest of the section; layers dip steeply to the WNW and lineations plunge gently to moderately north. Figure 5.37 includes a vertical surface that is normal to the main foliation, providing an example of the 10's cm to m wavelength isoclinal folding (in this case picked out by the migmatitic portions) that is common throughout the gneisses along the Astor Gorge. On the Indus Gorge section, the Iskere gneiss is present as a fairly continuous ~7 km thick section (west to east), across strike (Madin, 1986; Madin et

Figure 5.37

Figure 5.37 Field photo of Iskere gneiss outcropping along left bank of Astor Gorge. Note characteristic finely foliated (023°/83°W, 22°@346°) grey granitic orthogneiss clearly cross-cut by migmatitic bodies (includes leucosome and melanosome). In photo, migmatitic bodies are isoclinally folded and sub-parallel to main foliation. Also common, however, are migmatitic bodies cross-cutting at high angles. Photo 10/10/96 no.10.

al., 1989; Treloar et al., 1991). On the Astor Gorge, the Iskere gneiss is less continuous than along the Indus Gorge, and (e.g.) between where the Iskere gneiss is first present, ~300 m SE (i.e., upstream) of outcrop #A75 on the left bank, and the eastern limit of Iskere gneiss in the Astor Gorge, ~6 km to the SE (upstream) at outcrop A3, the Iskere gneiss is present as 100's m to < 2 km sections interlayered with the porphyroclastic and coarsely to finely laminated, occasionally calc-silicate gneisses (± amphibolite, marble and biotite schist). Part of figure 5.38 illustrates the easternmost Iskere layer, which is present as a ~2 km thick layer within the axial zone of the Burdish Ridge antiform, bounded to the NW by a few 100 m of amphibolite, and bounded to the SE by a series of layered felsic and metasedimentary gneisses. Figure 5.38 also illustrates that the core of the antiform is intruded by a suite of 10's m thick, sub horizontal granitic veins that are filling (probably mode I) cracks responding to the general W-E shortening associated with the antiforms. The eastern limb of the Burdish Ridge antiform is, of course, the western limb of the Dashkin Synform.

The discontinuous nature of the Iskere gneiss in Astor Gorge compared to the Indus Gorge may be a product of the original distribution of the Iskere within the pre-collision Indian crust. The homogeneous nature of the granitic orthogneiss host of the migmatite bodies that defines the Iskere suggests, however, that the Iskere protolith is a granitic (i.e., intrusive) body, and I speculate that the discontinuous nature of the Iskere gneiss in Astor Gorge is not due to the original distribution of the Iskere within the Indian crust. I therefore propose that (1) the discontinuous layers of the Iskere gneiss in Astor Gorge are due to "fingering" (thinning / pinching out of multiple tabular or elongated peripheral portions) of the edge of the main body that is seen along the Indus Gorge, and (2) the bodies should, in principle, be traceable northward to join the Indus Gorge main body (possibly in a non-continuous fashion, if certain Iskere layers are km-scale boudins or lenses). The original intrusive contact of the Iskere protolith may have been either inter-fingering or may have been planar.

Figure 5.38

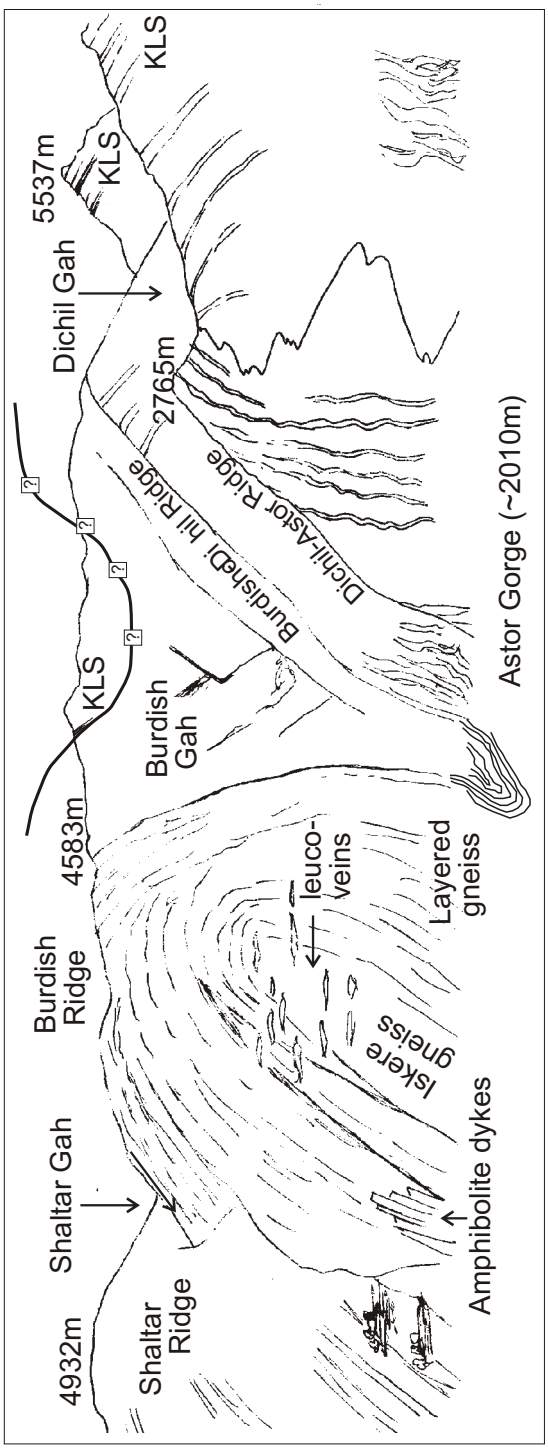

Figure 5.38 (line drawing of fieldbook sketch). View to NE from Astor Gorge high road looking to steep walls of right bank of Astor. Shows gneissic layering of Burdish Ridge antiform, Dashkin synform and some of Dichil antiform. See explanation in text. Width of view is ~10 km. Sketch composed: 7/7/97.

Regardless of this, the overall ~W-E flattening (and any ~N-S stretching) in central NPHM that has accompanied crustal scale folding has significantly contributed to the present-day discontinuous nature of the Iskere gneiss that is seen along the Astor Gorge.

5.4.3 Dashkin Synform and Dichil Antiform

Figure 5.38 (above) was composed from the high road on the left bank of the Astor Gorge, ~800 m above the Astor River, and illustrates the clear exposure of the Burdish Ridge antiform and the Dashkin synform that is observed in the steep wall of the right bank of the Astor Gorge. East dipping gneissic layering high up (>3000 m) in the east side of Burdish ridge can be followed by eye, increasing in dip angle and diving down into the foot of Burdish Gah, near the Astor river (~2000 m). In the foot of Burdish-Dichil Ridge (marked on figure), the hinge zone of the Dashkin synform causes the gneissic layering to abruptly overturn and dip steeply west, where it becomes the western limb of the Dichil Antiform (the actual closure of the Dashkin synform is not fully seen from the viewer's location on the Astor Gorge high road but is clearly seen (and was sketched) from the low road, and was added subsequently as part of the integrated final sketch. The crest (and closure) of the Dichil antiform is also not fully seen from the viewer's location on the Astor Gorge high road as it is hidden from view by Dichil ridge. From Dichil pass (~2750 m), however, the antiformal closure is clearly seen (fig 5.39). In figure 5.39, the Dichil antiform is seen to have a steeply-dipping to vertical axial plane, and to form a very tight closure. This contrasts with the not-so-tight closure of the Burdish Antiform, and the not-so-steeply W-dipping axial planes of the Burdish Ridge antiform and the Dashkin synform. The limbs (and hence the gneissic layering) of the Dichil antiform are very "crumpled" (there is much uneven parasitic folding), and this causes a large amount of rapid local change in the dip direction (see 5.4.4. - Eastern Astor Gorge).

Figure 5.39

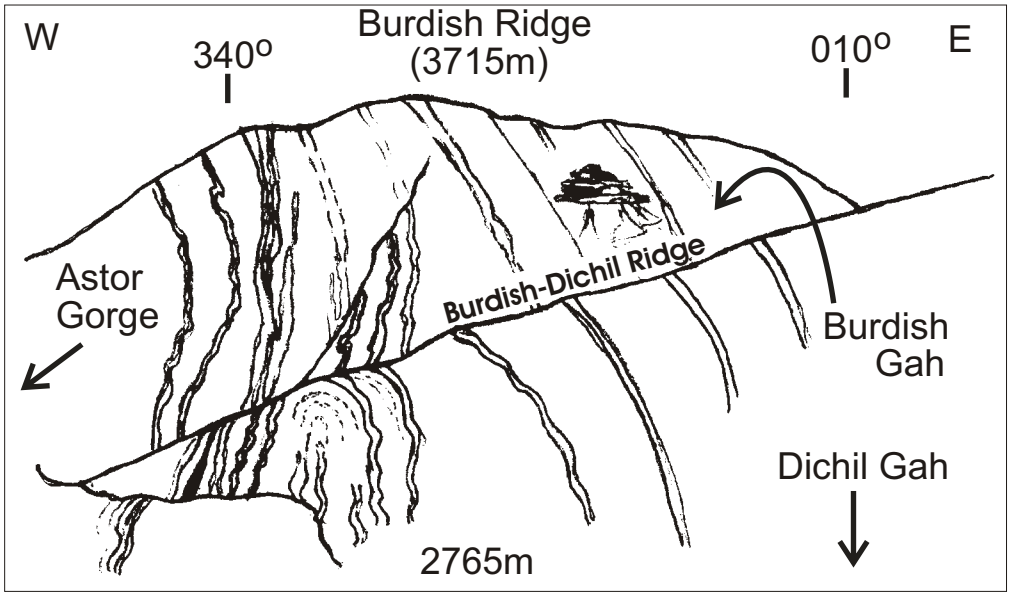

Figure 5.39 (line drawing of fieldbook sketch). View to NNW showing antiformal folding of gneissic layering clearly exposed upon wall of right bank of Lower Dichil Gah (Burdish-Dichil Ridge. View is from Dichil Pass (2765m). Antiformal closure is not seen in wall of Burdish Ridge because of ~NNE trend of axial trace of fold and viewer's NNW perspective from Dichil Pass. Antiformal closure intersects significantly to right of field of view. Apparent eastern limb of antiformal closure seen in wall of Burdish Ridge in left of sketch is eastern limb of Burdish antiform ("western antiform"). Dashkin synform is out of view down in Burdish Gah. Width of view ~3 km. Sketch composed: 10/10/96.

The distance between the crests of the two antiforms is ~2.5 km, measured along the section of the Astor Gorge. This distance is larger than the true fold wavelength (~1.5 km) because the Astor Gorge is oblique (NW-SE) to the principal antiformal trend (~N-S in the Astor Gorge region).

The ESE side of figure 5.38 includes the dark rocks that cap the high peaks which are E-dipping KLS rocks that structurally overly the eastern NPHM rocks. Unlike much of the SE NPHM section (above), the MMT footwall/hanging wall layers are here not overturned. The KLS rocks are not fully visible where they project to follow the closure of the Dichil antiform and form a complete crest. I think that the green KLS rocks are again visible, on the eastern limb of the Dichil antiform, far up in the ridge behind Burdish Gah, however TM satellite imagery indicates that any presence of KLS rocks is minor. Additionally, from observations both on the Astor Gorge high road and on Dichil Pass, the green KLS rocks are clearly visible on the west limb of the Burdish Ridge antiform. These observations permit me to interpret synformal folding of the KLS rocks in the ridge above the head of Burdish Gah (question marked portion of line drawn in figure 5.38). I interpret the Dichil antiform to represent antiformal folding of the NPHM sequences and the overlying KLS rocks, and I offer this as further evidence that the original MMT footwall (NPHM) and hanging wall (KLS) rocks have been antiformally folded but otherwise unmodified in central and SE NPHM.

5.4.4 Eastern Astor Gorge and Dichil Gah

East of the Dashkin synform, a steep trail climbs up ~700 m over Dichil Pass (~2760m; *not* Dichil Gali - ~5000m) and provides a ~W-E section along Dichil Gah, through the eastern portion of the massif. Approximately 3.5 km from the pass, the valleys bifurcate to provide two sections through the remaining ~1.5 km of NPHM rock up to the NPHM/KLS contact. The nature of the NPHM section in the Dichil

valleys and in the eastern Astor Gorge section is highly consistent with the section of NPHM rocks in SE NPHM.

5.4.4.1 Eastern Astor Gorge

Where the Dichil Pass trail (fig. 5.38) joins the eastern Astor Gorge section, the layered gneiss (described above, for the Burdish Ridge antiform) passes to a notably migmatitic-garnetiferous-pelitic gneiss, locally interlayered with amphibolite (fig. 5.40A) that is comparable to the migmatite-garnetiferous-pelitic gneiss described for the Lower Rupal Valley (fig. 5.21, above), and the western part of Rama Valley left bank. The amphibolite layers that are associated with the migmatite-garnetiferous-pelitic gneiss are typically centimetres to 10's centimetres in thickness, and are often garnet bearing (fig. 5.40B). There do not appear to be marble units associated with the amphibolite layers in this part of Astor Gorge. Gneissic layering often contains cm-scale wavelength isoclinal folds (fig. 5.40A), and in places where the 10's cm amphibolite layers are isoclinally folded, their cross-cutting (i.e. post dating) of the migmatisation can be clearly seen. Amphibolites cross-cutting migmatitic pelitic gneiss have been reported from the Indus Gorge (Treloar et al., 1991; Wheeler et al., 1995) where the migmatisation was inferred to be pre-Permian in age. Layering of the migmatitic-garnetiferous-pelitic gneiss sequence strikes generally NNW-NNE, and lineation typically plunges 5-25° towards N-NE (figs. 5.40B and 5.41). Both crenulation intersection and mineral lineations are found, and are largely parallel. That they are parallel and have a consistent orientation across a large area is possibly due to superposition of (1) Himalayan ~N-S lineation (see 5.1.3.2 Rotation of Himalayan thrust fabric, above) with (2) subsequent stretching related to, and parallel with the hinges of the Astor Gorge ~N plunging folds. There is much local buckling that probably is parasitic folding related to the Dashkin synform, however, the collapse/cascade and

Figure 5.40A

Figure 5.40A Migmatite-garnet-pelitic gneiss at foot of Dichil Pass trail, ~200m below outcrop # 72 (Foliation: 007°/89°W, hinge intersection lineation 25°@007°). Note leucosome portion is isoclinally folded and lacks a strong melanosome. Swiss knife for scale. Photo 10/10/96 no.2.

Figure 5.40B

Figure 5.40B Cascade / parasitic folding within well-stretched amphibolite interlayered with migmatite-garnet-pelitic gneiss. Elsewhere (in large isoclinal hinge sections) amphibolite is seen to cross-cut migmatised gneissic foliation. Note crenulation intersection lineation clearly developed beside compass. Foot of Dichil Pass trail, ~200m below outcrop # 72 (hinge lineation 22°@011°). Compass for scale. Photo 10/10/96 no.6.

Figure 5.41

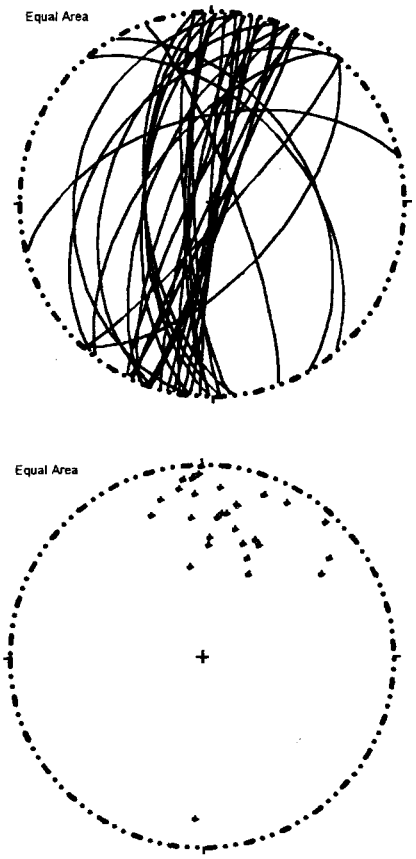

Figure 5.41 Lower hemisphere equal area projection of foliation poles and lineation of main NPHM fabric in eastern Astor Gorge and Dichil valleys.

non-uniform nature of the folding makes extrapolation of local axial surface measurements to a regional scale unreliable.

Approximately 1 km SE of where the Dichil Pass trail (fig. 5.38) joins the eastern Astor Gorge section (~500m W-E structural thickness), the migmatitic-garnetiferous-pelitic gneiss passes gradationally into a non-migmatitic biotite-gneiss with cm-10's cm felsic layering. Centimetre-scale isoclinal folds are again present. Orientation of layering in this section of gneiss is consistent with the previous portion of the section, dipping steeply to the WSW, with crenulation, and fabric lineation plunging gently to moderately to the N or NNW. This section of compositionally layered gneiss is similar to the sequences recognised in the SE NPHM valleys and continues for ~5 km (~2 km structural thickness) with a variety of interlayered lithologies including (1) 10's cm to m layers of mm-cm porphyroclastic gneiss, (2) 10's cm to m thick amphibolite layers, (3) Fe-weathered biotite schist layers (without coarse garnets), and (4) 10's cm to m thick, parallel to slightly discordant leucogranite layers. Orientation of the gneissic layering is consistent with surrounding layering, dipping moderately to steeply W-WSW, with crenulation intersection and mineral lineation plunging gently towards the N or NNW.

Between Luskum and Harchu villages (outcrops #H1 and #H2), there is a very finely laminated (0.5-2 mm) grey gneiss (with <2 mm garnets) that, based upon the very fine lamination, is apparently highly strained (E7/7/7-V - not shown). To the east, this apparently highly strained rock at Luskum passes to ~200 m of finely-coarsely laminated, rather psammitic gneiss, and east of here passes to the lath unit. Foliation in the psammitic gneiss is locally non-parallel with the main section, dipping moderately NW, with lineation plunging gently or moderately towards the NW or NNW. This sequence is very similar to the equivalent section of outcrop in Dichil to the north (described below), and similar to Rama valley, to the south. In the Dichil and Rama sections, however, the angel hair unit is present within a section of locally

higher strain gneisses that occur west of the lath unit. It is possible that the apparently highly strained rock at Luskum is a more garnet rich, greyer matrix version of the angel hair unit where foliation is better developed than lineation (the opposite situation to the angel hair unit).

The Lath unit outcrops on both the left and right bank of eastern Astor Gorge and has a structural thickness of ~600m, with outcrop #71 marking the lath unit eastern margin. Within the ~600m of section, the lath unit repeatedly grades from (presumably higher strain) portions where lineation is stronger than foliation and feldspars are 1-3 mm (inferred to be stretched out / tectonically grain size reduced from cm-sized feldspar laths) to apparently lower strain portions resembling figure 5.31B (above). The pink matrix appearance and garnets in feldspar that are characteristic are present in both the more strongly and weakly deformed portions. Augen asymmetry and C-S fabric (defined by anastamosing porphyroclast tails) in the more intensely strained portions of the lath unit show a convincing dextral sense of shear. Microstructure is consistent, as illustrated in figure 5.42 (66/27E cut from sample E6/6/27-V, not shown). In this rock, C-S fabric clearly shows dextral shear sense based upon (1) C-surface parallel 200-400 μm thick, locally sigmoidal ribbons of quartz, (2) 100-200 μm thick biotite grains defining C-surfaces, (3) asymmetric trails from large feldspar clasts, often with sutured internal grain boundaries indicating the onset of grain boundary migration and initiation of a core and mantle type texture The occurrence of large (i.e., "strong") feldspars breaking up in a very fine grained matrix with very well developed quartz ribbons suggests deformation possibly >500°C.

East of outcrop #71, approximately 1 km of structural thickness of the metasedimentary sequence with the ubiquitous garnetiferous metapelites is present west of the NPHM/KLS contact. This part of the section shows even fatter boudins (up to 2 m thick) than in the SE NPHM sections. Where sense of shear is clear, it

Figure 5.42

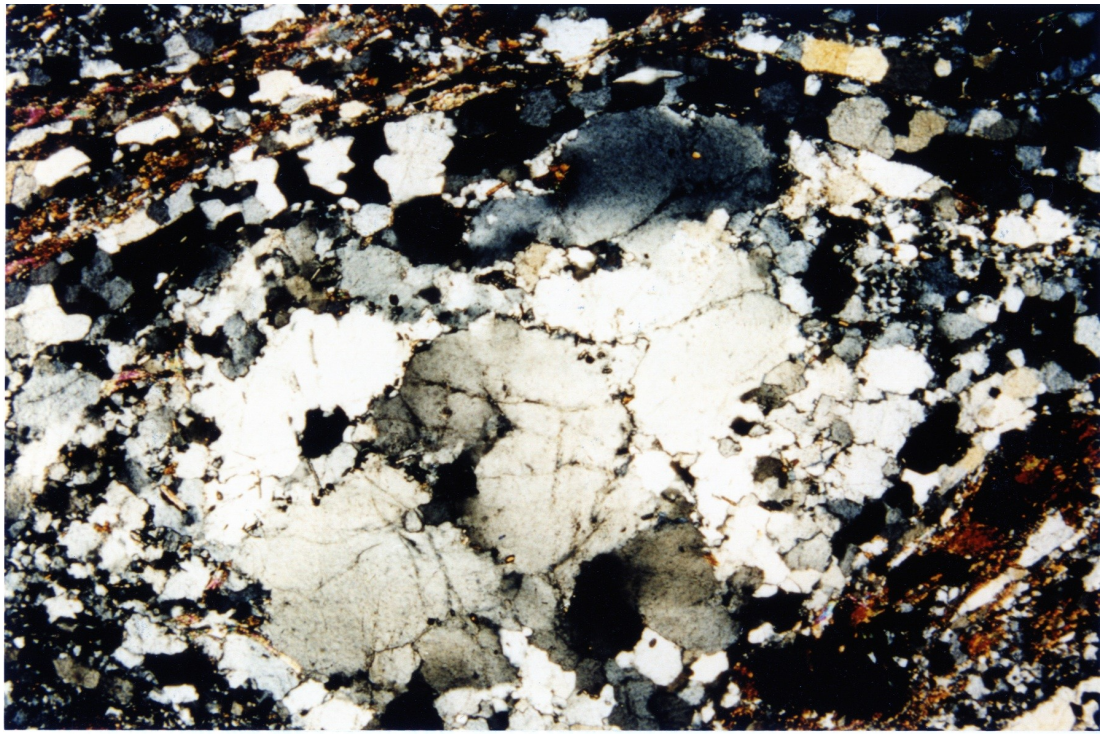

Figure 5.42 Optical photomicrograph of thin section 66/27E (cut from sample E6/6/27-V, not shown), deformed portion of lath unit on eastern Astor Gorge left bank, ~300m W of outcrop #71. Conditions of deformation are indicated by (1) C-surface parallel ribbons of quartz with even thickness (200-400 μm), (2) C-surface defined 100-200 μm thick biotite grain, (3) >3 mm feldspar clast with sutured internal grain boundaries indicating onset of grain boundary migration and beginnings of core and mantle texture within grain. Grain boundary migration and wholesale grain size reduction have operated extensively (both in field of view and elsewhere in thin section) as indicated by very fine (50-100μm) grain size of surrounding quartzofeldspathic component. C-S fabric elsewhere in thin section clearly shows dextral shear sense. Cut parallel with lineation (14°N), perpendicular to foliation (060°/38°E). South is to right. Base of image is 5.5 mm and parallel with main fabric. Crossed polars.

seems to be dextral (e.g. sample E6/6/27-IV and thin section 66/27E; figs. 5.9 & 5.10, respectively). Orientation of layering throughout the section of the metasedimentary sequence, including the KLS/NPHM contact, is consistent with most of the layering elsewhere in eastern Astor Gorge (e.g. foliation: 170°/89°E, lineation 15°@170°). I note that (as indicated in fig 5.39, above), layering is either steep, or (higher up in the Astor Gorge walls) dips moderately to steeply east. The NPHM and KLS layers in the eastern Astor Gorge (and up in Dichil Gah) are not overturned, and hence contrast with the main NPHM section (above).

5.4.4.2 Dichil Gah

The trail (~700m elevation gain) over Dichil Pass to Dichil Gah passes through the section of migmatitic-garnetiferous-pelitic gneiss that was described above for Dichil Bridge. Towards the top of the trail, a ~200 m section of schist and metapelite is present that was not observed on the floor of the gorge. Because the trail over Dichil Pass is entirely within the eastern limb of the Dichil antiform (fig. 5.38 and 5.39, above), the presence of the schist and metapelite is not thought to be a consequence of the Dichil antiform exposing, in its western limb, metapelitic sequences that are associated with the NPHM/KLS contact.

Over Dichil Pass, at outcrop #73, the eastern portion of the schist and metapelite sequence passes to a section of compositionally layered gneiss that is equivalent to the compositionally layered gneiss seen in the floor of the Astor Gorge below. Approximately 750 m east of this section, the angel hair unit is present (e.g. sample E6/10/10-I and thin section 610/10A in fig. 5.15, above). Foliation has a consistent trend with the layering in Astor Gorge below but dips more gently to the east (e.g., 016°/53°W); lineation plunges moderately north. Within the angel hair unit, good sinistral sense of shear indicators are present in thin section.

East of the angel hair unit, ~2 km of structural thickness of compositionally layered gneiss are present, intruded by numerous deformed and undeformed leucocratic / pegmatitic dykes, up to a few 100 m in thickness. Foliation within this section is slightly uneven, reflecting the partially disharmonic crumpling that is seen in the field sketches (figs. 5.38 & 5.39) above. The principal trend remains N-S trending with the intersection and mineral lineation plunging gently to moderately to the NNW.

At #74A, the lath unit is in contact with the compositionally layered gneiss, marked by an apparent strain decrease; nowhere, either in outcrop or float, was the lath unit seen to have a strong foliation in the manner of the lath unit in the floor of the Astor Gorge, below (e.g. outcrop #71). The lath unit thickness in Dichil Gah, (an average of >500 m of W-E outcrop on Dichil Gah left bank, and an average of >1 km outcrop on Dichil Gah right bank) is larger than in Rama or on the floor of Astor Gorge. The thickness of the lath unit outcrop on the right bank seems to increases to the north, clearly seen from the Salibur Gah.

Outcrop #71B, the eastern margin of the lath unit passes back into the main gneissic sequences. These pass to the east very gradually into amphibolite and marble rich portions of the NPHM metasedimentary sequences. The appearance of the sequences is not unlike rocks of the KLS, mainly because the amount of amphibolite is large (much greater in this section than in the equivalent sections of SE NPHM, e.g., in the floor of the Astor Gorge below, only a minor amount of amphibolite is present). About 1 km to the east, the amphibolite and marble sequences begin to alternate with more pelitic sequences, and at outcrops #71E and #71D (in the main Dichil Gah and the left tributary, respectively) the familiar coarse garnetiferous metapelite is present. In both sections, there is ~600m structural thickness of the garnetiferous metapelite. The eastern part of the garnetiferous metapelite section grades with an eastward decreasing volume of boudined coarse garnet metapelite layers into a dark amphibolite with very stretched out orange marble bands. The dark amphibolite then grades

eastward (over 400-500 m) to a dominance of compositionally layered amphibolite, and finally to a possible volcano-sedimentary sequence with (in one locality) clear pillow structures in a metabasalt, and apparent flow structures within meta-rhyolite. What is unusual about the KLS/NPHM contact in the two Dichil valleys is the absence of a sharp contact with NPHM sequences (marked elsewhere by the sudden switch to chloritic schists or the metadiorite). The NPHM/KLS contact is not well-defined and has been somewhat arbitrarily drawn on plate 1 in the case of the two Dichil Valleys. I note this is the first case in SE NPHM which where the NPHM/KLS contact is not sharp on the outcrop scale. Hundreds of metres to kilometres thick sequences of compositionally layered amphibolites that include 10's - 100's metres thick horizons of marbles and garnetiferous metapelites are reported from a few localities in Ladakh rocks of Pakistan (A. Pêcher, personal comm.). When viewed from Ladakh, the NPHM/KLS contact in the Dichil valleys could reasonably be drawn close to (or even intruded out by) the Lath unit. I retain, however, the NPHM lithological succession that I proposed in the SE section, and, based upon the characteristics of the recognisable NPHM/KLS differences, the contact with Ladakh is drawn as a broad line where the amphibolites pass from layered to massive; I am confident that the NPHM/KLS contact is east of the garnetiferous metapelite of outcrops # 71E and #71D. Assigning an affinity and grouping amphibolites to either NPHM or KLS rocks remains problematic in the region of the KLS/NPHM contact, however, and geochemical trace element analyses of the amphibolites would seem to be required for a more confident discrimination between KLS and NPHM.

5.4.5 Discussion and conclusions for Astor Gorge area

1. The Astor Gorge exposes two antiforms, the Burdish Ridge and Dichil antiforms, separated by the Dashkin synform; these are the principal structures in central NPHM. The associated ~W-E flattening (and any ~N-S stretching

that might have occurred) has been superposed upon, and probably has enhanced (rather than re-worked/obliterated) Himalayan MMT zone (and any prior) strain, contributing to the observed strong foliation, and very strong lineation of the main fabric of the Astor Gorge gneisses and schists. I note however that the the majority of microstructures imply high strain and deformation mechanisms that operated at 400-500°C in a non-coaxial regime, and I infer this to be a product of MMT zone thrust and/or normal motion (which regionally displays very high strain), and not a product of NPHM-related folding (which is relatively low strain).

2. Rocks exposed in eastern Astor Gorge and in the Dichil valleys are clearly recognisable as part of the sequence of NPHM rocks established (above) for SE NPHM. The main difference in the area of eastern Astor Gorge and the Dichil valleys is that the section is not overturned; NPHM is not bulging out in the region of "*la corset*". Notable local variations include (1) marbles are essentially absent in the section of NPHM cover rocks along E. Astor Gorge, and (2) the NPHM/KLS contact in the Dichil valleys is less clear (on an outcrop scale) than in the other locations to the south.
3. The SE NPHM rocks and KLS (further east) rocks are recognised to occur in the eastern limb of an antiform that folds the pre-existing Himalayan sequence, therefore providing essential local evidence that the SE NPHM sequence can be restored to MMT footwall, and hanging wall positions, as has been postulated above.
4. At Dichil Bridge, migmatite gneisses are apparantly cross-cut by, and hence are older than, amphibolite (Permian?) dykes. Both the gneisses and the dykes take up the main fabric of the Astor Gorge . Within the Iskere in Astor Gorge, local zones of migmatisation obtusely cross cut, and do not take up, the main

gneissic fabric, and must either post date, or have largely avoided, the strain. These are not observed to be cross-cut by amphibolite dykes.

5. The lath unit in Dichil Gah cross cuts the main fabric and shows only relatively minor deformation, whereas the lath unit in E Astor Gorge has taken up the main fabric, indicating much higher strain, and displays a demonstrably dextral sense of shear. This suggests that the a lath unit is a (younger?) Himalayan age plutonic body that was intruded into the upper portion of the MMT footwall.

6. Domains of both sinistral and dextral shear sense (relative to present day steep foliation and (sub)horizontal lineation) are observed within the E limb of the Dichil antiform (i.e. within the equivalent of the SE NPHM section). Domains of sinistral sense are 10's metres in thickness, and are consistent with those domains of sinistral shear sense in the SE NPHM section. I regard these as further evidence for local horizons of normal motion within the original MMT footwall.

7. There does not appear to be a "full repetition" of the SE NPHM sequences in W. limb of the Dichil antiform. Assuming the SE NPHM sequences were continuous to the W of the NPHM (in present outcrop pattern), I infer that the Dashkin synform does not expose sufficiently structurally high enough in the original MMT footwall to expose the more characteristic members of the section (coarse garnet metapelite etc.). There may be up to 1.5 km of structural thickness between the rocks exposed near the bottom of the Astor Gorge and where the KLS rocks are inferred up near the head of Burdish Gah.

5.5 CONCLUSIONS FOR CENTRAL AND SOUTHEAST NPHM AREA

5.5.1 Affinities of rocks and strain patterns

5.5.1.1 Indian and Kohistan-Ladakh rocks

The sequence of metapelitic and granitic gneisses, schists, and metadiorites and amphibolites that is present on the eastern side of the massif, is highly continuous across seven ~W-E valleys, and has been divided into recognisable units. The rocks form part of the eastern limb of the Dichil antiform, and can be restored to original MMT foot-, and hanging wall orientations and hence are recognised to be part of the original Indian cover and Kohistan-Ladakh island arc, respectively.

5.5.1.2 Himalayan deformation

The steep ~N-S foliation and gently N-plunging stretching lineation is the principal fabric in central and eastern NPHM, and is associated with deformation at 400-600°C in a non-coaxial regime. I infer this to be a product of MMT area thrust and/or normal motion (5.5.2, below), subsequently steepened by NPHM-related folding. There is apparently no part of the eastern section where strain is markedly higher (although the angel hair unit is probably slightly higher strain), and the zone of principal displacement associated with the general MMT zone is >5 km thick. The lath unit post-dates some (e.g., Dichil), but by no means all (e.g., W. Astor Gorge), of the apparently Himalayan thrust sense strain, and I infer that the lath unit was intruded during the period of principal Himalayan events.

5.5.1.3 Deformation associated with growth of NPHM

Growth of NPHM is represented by the Burdish Ridge and Dichil antiforms in the central section of the massif. The associated ~W-E flattening (and any ~N-S stretching) has been superposed upon, but has not significantly re-worked, Himalayan

strain. In the SE portion of the massif, the section is overturned across an area of >25 km (N-S). This "bulging out" of the southern massif is a result of being close to the centre of Nanga Parbat, and is an expression of relative E-vergent displacement of the Nanga Parbat summit section. E-vergent displacement of the summit section is also indicated by numerous brittle W over E structures (e.g., the Churit Faults) in SE NPHM.

5.5.2 Domains of sinistral and dextral motion in eastern NPHM

Table 5.1 is a listing of the area and rock types where a sense of shear is seen in eastern NPHM. It illustrates that there are numerous examples of 10's to 100's metre thick zones where sinistral sense of shear is found within non-coaxially, highly strained rocks of Himalayan affinity (see above). Recognition of the Dichil antiform allows me to rotate these zones confidently to sub-horizontal, whereupon they are recognisable as layers of original thrust and normal sense displacement in the general MMT zone. I propose that there are numerous, discrete, >100 m thick MMT relative normal motion, higher temperature (i.e., 400-600°C), principally ductile horizons within the upper 5 km of the MMT footwall. Other studies (west of the syntaxis, *sensu-stricto*) have recognised only relatively low temperature, largely brittle sense of shear normal motion. The presence of higher temperature horizons with normal sense displacement therefore is a significant new discovery.

It is possible that the horizons of MMT relative normal motion are the result of some sort of differentiation accommodation of thrusting (c.f., stretching faults of Means, 1990), and therefore do not represent true extension of the MMT zone.

Table 5.1 Recognised senses of shear from locations in SE NPHM & Dichil/E. Astor

Area / loction no.	Sinistral	Dextral	Thin section (weight)	outcrop/hand sample (weight)	Width of Zone	Sample Name or Rock type
Lower Rupal Valley						
#13	x		5-sin	1-dex & 1-sin	>50 m	NE95/29-VI
# 11	x		4-sin	2-sin	>100 m	NE95/28-IX NE95/28-X
top of Churit Fan	?	x	3-dex & 1-sin	no	>25 m?	NE95/29-V
100 m E of #12		x	5-dex	no	~50 m	NE95/29-III
~50 m E of #12		x	4-dex	3-dex	~50 m	NE95/29-IV
#12		x	4-dex	1-dex & 1-sin	<100 m	NE95/29-II
50 m E of # 10	x		4-sin	2-sin	<50 m	NE95/28-XI
400 m E of #14		x	4-dex	no	<20 m	NE95/29-IX
Ghurikot Valleys						
#17		x	no	2-dex	>100 m	gnt-pelite
50 m E of #66		x	no	1-dex	>25 m	str. spag. gn
100 m E of #69	x		no	3-sin	<25 m	cse bnded gn
50 m E # 69		x	no	2-dex	<25 m	thin bnded gn
#69	x		no	2-sin	>25 m	E6/10/8-I
30 m W of #69	x		no	2-sin & 1-dex	>30 m	mig-gnt-pel-gn

Table 5.1 (continued) Recognised senses of shear from locations in SE NPHM & Dichil/E. Astor

Area	Sinistral	Dextral	Thin section (weight)	outcrop/hand sample (weight)	Width of Zone	Sample Name or Rock type
Bulan Gah						
75 m W of "MMT"		x	no	3-dex	>50 m	gnt-pelite
100 m E of # 70A	x		no	3-sin	>30 m	marble/amph
Rama						
#64		x	no	3-dex	>25 m	str f'spar gn.
#62	x		2-sin	no	>50 m	E6/10/7-I
#R1	x		no	2 sin	>30 m	bt-gn/amph
1 km E of #RL71		x	3-dex	no	>25 m	E6/6/21-I
E Astor						
300 m W of #71		x	4-dex	3-dex	>20 m	E6/6/27-V
200 m E of #71		x	4-dex	2-dex	>100 m	E6/6/27-IV
Dichil Gah						
~750 m E of #7	x		3-sin	1-sin	>50 m	E6/10/10-I

Table of selected outcops where a domain with a sense of shear was determined. In each case, sinistral or dextral is indicated, followed by a confidence weighting of between 1 and 5 for thin section and hand sample, respectively.

5.6 GEOLOGICAL OBSERVATIONS IN THE RUPAL AREA

5.6.1 General remarks

The main Rupal valley runs approximately 35 km W-E from 2900m at the village of Tarshing to >4800 m at the foot of Toshe Gali (western most part of Toshain Glacier - plate 2). Rupal provides a major access through the high country of NPHM; the Rupal face represents an elevation change of ~4700 m in ~4 km and forms the steep southern side of Nanga Parbat (8143m). Elevations are also high to the south and west; Rupal Peak (south) and Dashat Peak (west) are >6000m. Accordingly, access to outcrop is highly limited and involves large elevation gains up into the walls of the main Rupal valley. Moreover, the presence of substantial glaciers significantly impedes travel time between outcrops. In the case of outcrop on the right bank (southern side) of Toshain Glacier, for example, circumnavigation of wide crevasses and accompanying rope use typically necessitated half a day of travel, and outcrop that could be reached once the edge of the glacier was attained varied with each year depending of the location and size of bergschrunds, and local avalanche debris.

Under the classification "Rupal Area", I include Chichi Nullah, Upper and Central Rupal, and the portion of the Lower Rupal Valley that is west of outcrop #9a. East of outcrop #9a is covered in the Lower Rupal Valley section 5.3.2, and the basis for this selection of division is based upon the sudden E to W switch in lithology from layered or differentiable gneisses and schists to a monotonous granitic orthogneiss (see 5.3.2.2). This granitic orthogneiss continues monotonously for >10 km to both the west and southwest and includes the Rupal Chichi Shear Zone. South of this, in Chichi Nullah, metasedimentary rocks of the cover sequence are found. To the west, the monotonous granitic orthogneiss passes to a granitic orthogneiss that incorporates

increasing amounts of metasedimentary rock, and then passes to a layered gneissic sequence in Upper Rupal.

5.6.2 The Rupal Chichi Shear Zone

The Rupal Chichi Shear Zone (RCSZ) is a several km wide, ~NNE trending belt of monotonous granitic orthogneiss showing a pervasive C/S fabric and augen asymmetry that indicates NW side up with dextral shear. Associated mineral stretching lineation typically plunges ~30-60° SSW to WSW, and foliation varies from NNE trending (near Tarshing) to ~W-E trending (near Bezhin Glacier). The RCSZ outcrops across much of eastern Rupal and Chichi Nullah but does not, however, have clear, sharp shear zone margins. The RCSZ has neither classic ductile strain gradient margins (i.e., Ramsay and Graham, 1970) nor margins marked by significant brittle discontinuity. Consequently, the true extent of the RCSZ is hard to define, most notably to the west. In this section, I (1) describe the RCSZ eastern margin, (2) describe the shear zone at large, (3) describe the southern contact in Chichi Nullah including the metapelites that lie to the south. The issue of the definable western limits of the Rupal Chichi shear zone is covered under a subsequent sub heading.

I have interpreted the eastern margin of the RCSZ in the Lower Rupal Valley to be somewhere between outcrops #9A (west Churit) and # 9 (Tarshing). Between outcrops #9A and #9, the rock type changes (section 5.3.2.2 and plate 2). The rock types passes from metapelitic gneisses (±migmatitic granitic orthogneiss) in the east at #9A to almost exclusively granitic orthogneiss, in the west at outcrop #9. This granitic orthogneiss is ubiquitous to the Rupal-Chichi shear zone. Lineation additionally displays an abrupt switch in orientation between outcrops #9A and # 9; in the vicinity of, and almost everywhere to the east of, outcrop #9 lineation is gently to moderately north plunging (see described in section 5.3.2.2), whereas, in the vicinity of outcrop #9, indeed for all of the RCSZ, lineation is moderately to steeply south or

west plunging. Orientation of layering does not change significantly however, and remains ~NNE striking, dipping steeply W to vertical between outcrops #9A and #9. The most notable W-E change in structure between outcrops #9A and # 9 is the presence at outcrop #9 of a very well-developed non-coaxial asymmetry to the gneissic fabric seen on the outcrop. This asymmetric (kinematic) fabric is marked by (1) biotite planes clearly forming S and C surfaces. and (2) thin 0.5-2 mm feldspar porphyroclasts that define augen with asymmetric tails. In the Tarshing area, the sense of displacement associated with the observed fabric (based upon motion roughly in the direction of the stretching lineation) is W side upwards and northwards (dextral shear). The asymmetric fabric (of the RCSZ) in the Tarshing area differs from the various local gneisses that display domains of dextral and sinistral shear sense (see Lower Rupal Valley section) in that the RCSZ kinematic fabric is very well developed and highly consistent both along and across strike, on the scale of several kilometres.

West of Tarshing, across the Chongra Glacier (plate 2) in the area of Rupal Village, and south of Tarshing, into Chichi Nullah, the orthogneiss fabric becomes more spectacular; porphyroclast sizes become larger; up to ~2 cm. This coarse porphyroclastic granitic orthogneiss is typical for the variety of orthogneiss that is present for most of the RCSZ, and so I describe the gneiss in this area in more detail here.

Figure 5.43 illustrates a typical outcrop of the granitic orthogneiss that is characteristic of the RCSZ. This example is from west of Tarshing, the west side of Chongra Glacier near outcrop #18 where the asymmetric fabric of the granitic orthogneiss is well formed. Figure 5.44 is a photomicrograph of part of thin section 66-18D (cut from E6/6/18-IV, sampled from further north up the side valley of #18) and shows microstructure that is characteristic of the RCSZ (although note that a finer grained portion of the thin section has been selected for the photo to allow

Figure 5.43

Figure 5.43 Granitic orthogneiss in Rupal side valley at outcrop #18. This type of granitic orthogneiss is ubiquitous to the Rupal-Chichi shear zone. Asymmetric fabric is marked by (1) biotite planes clearly forming S and C surfaces. and (2) thin 0.5-20 mm feldspar porphyroclasts with asymmetric tails. Foliation is 040°/80°W and stretching lineation plunges 50° towards 238°. Sense of displacement is NW side upwards and vergent towards NE (dextral shear).
Photo 7/10/96 no. 13..

Figure 5.44

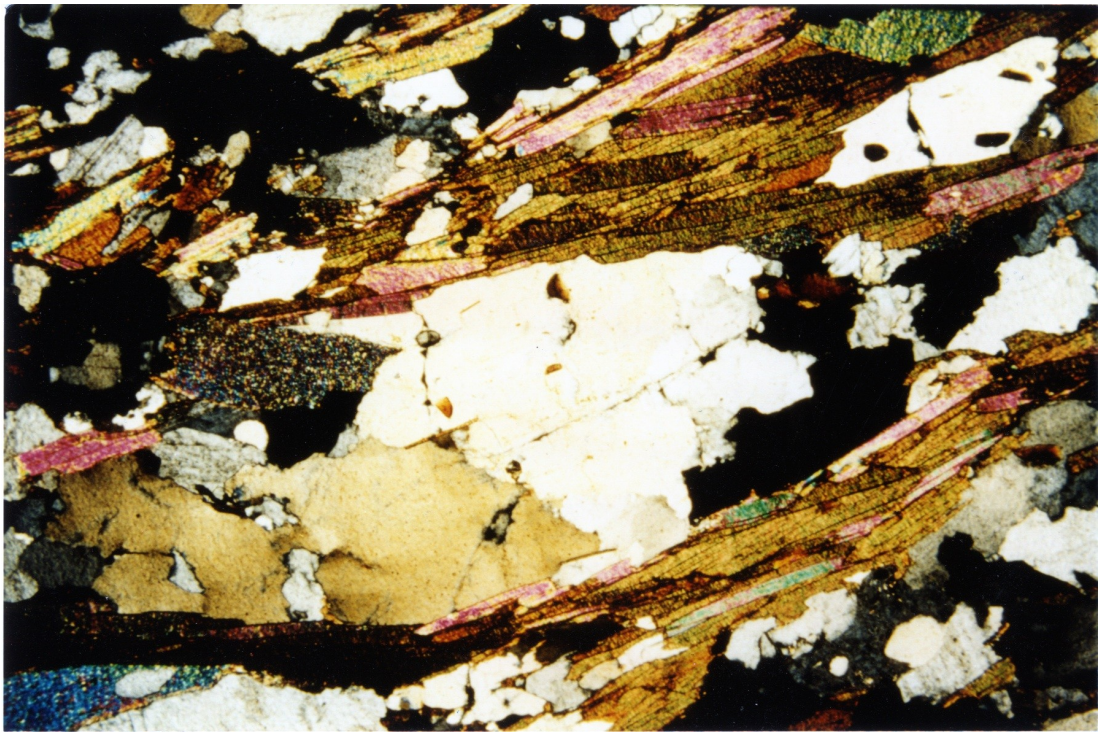

Figure 5.44 Optical photomicrograph of thin section 66/18D (cut from E6/6/18-IV, not shown), ~1 km NW of #18. Shows characteristic microstructure of RCSZ orthogneiss deformation conditions (note finer grained portion hence >2 mm feldspar porphyroclasts not shown). Sense of shear clearly dextral based upon sigmoidal feldspar porphyroclast tails; 600-1000 μm biotite surfaces define C and S surfaces (distinct in overall thin section). Note coarseness of grains and only very slight suturing of internal grain boundaries. Some recovery may have operated but lack of evidence for significant subgrain rotation recrystallisation within grain suggests less than 400°C temperature of deformation. Cut parallel with lineation (50°@238°), perpendicular to foliation (040°/80°W). South is to left. Base of image is 5.5 mm and parallel with main fabric. Crossed polars.

illustration of more variety than just part of a large feldspar porphyroclast). Thin section 66/18D clearly shows dextral sense of shear. C and S surfaces are defined by 600-1000 μm biotite surfaces (these surfaces are more distinct when the thin section is considered as a whole as determination of C and S surfaces is not possible solely from the thin section portion shown). The coarseness of the grains and limited suturing of internal grain boundaries suggests that higher strain and temperature deformation mechanisms have not operated. Some recovery may have occurred but the lack of evidence for significant subgrain rotation recrystallisation (i.e. no patchy extinction, etc.) within grain suggests less than 400°C temperature of most recent deformation. A modest amount of grain boundary migration recrystallisation is possible based upon the limited suturing of grain to grain contacts in the main feldspar augen, and it can be reasonably assumed that such augen were originally single crystals and not asymmetric. I propose that temperature of deformation was less than 400°C for the bulk of the straining period. The microstructural appearance, and hence inferred deformation mechanisms, are highly characteristic of orthogneiss from the RCSZ, and contrasts with the more highly strained MMT footwall gneisses to the east (described above). Other thin sections cut from samples of the granitic orthogneiss of the RCSZ are 5/4A (from #18), 67/3A (from #CC3), 69/26A (from #48). All show similar textural features indicating similar deformation mechanisms operated in each locality.

In the area of Rupal Village, the local direction of both foliation and lineation rotate clockwise successively over the 6-7 km distance between Chongra and Bezhin glaciers (plate 2). This incremental rotation is a further occurrence of westward increasing clockwise rotation that was previously noted for Tarshing. For example, around the side valley of outcrops #18 and #51, foliation is steeply WNW dipping and stretching lineation plunges moderately towards the SW whereas around #48 (near the Nanga Parbat base camp for the Polish national expedition behind the Bezhin Glacier left bank lateral moraine) foliation is steeply NW dipping and stretching lineation

plunges moderately towards the WNW. Lithology and type of kinematic indicators remain consistent with those previously described for the RCSZ. Sense of shear is consistent with before and is dextral. To the west, however, there becomes a greater thrust component to the assumed net displacement direction.

In Chichi Nullah, the granitic orthogneiss of the RCSZ outcrops extensively. There is no gradual lithological N-S change found along the ~13 km length of the valley in which the granitic orthogneiss is exposed, and the appearance of the granitic orthogneiss is characteristically monotonous, and almost everywhere the ubiquitous C/S fabric and augen asymmetry indicates dextral NW-side up displacement. Orientation of gneissic fabric additionally exhibits no significant north to south change; foliation is steeply WNW dipping and stretching lineation plunges moderately towards the SSW. Although there is no gradual change found along Chichi Nullah, locally there are a few differences which should be remarked upon. In the vicinity (200-400 m) of outcrop #C3 (plate 2), fabric is locally steepened and overturned to dip steeply ~E. This is a local reflection of regional bending of the overall fabric to generally east dipping and can be regarded as part of a switch in the regional fabric from ~NW to ~SE dipping that is observed to the south (described below). Plunge of the mineral stretching lineation remains ~SW and sense of shear remains consistent with a dextral and NE vergent reverse components of displacement. Between #CC1 and #CC3, strike of local foliation deviates quite significantly from WNW dipping. Lineation however remains south to southwest dipping. Where the angle between foliation strike and lineation plunge is large, the sense of displacement is predominantly thrust sense. A further local anomaly is found within an isolated outcrop in the vicinity of outcrop #CC3. Here, the orthogneiss has steeply SSW dipping foliation and moderately WSW plunging mineral stretching lineation and sense of shear indicators indicate sinistral and SW side down normal components of displacement. This anomalous sense of shear is most readily explained by folding of

the orthogneiss fabric about an axis that is parallel to the mineral stretching lineation. Folding of this nature is consistent with (1) numerous minor, tight to isoclinal asymmetric folds with moderately SSW plunging axes that are found within the metasedimentary rocks in contact with the RCSZ granitic orthogneiss to the south (described below) where foliation of the metasedimentary rock is steeply WNW dipping (parallel to the RCSZ granitic orthogneiss), and (2) the anomalous sense of shear in the RCSZ orthogneiss in the vicinity of outcrop #CC3 is also consistent with the local deviation in RCSZ orthogneiss foliation where lineation remains SW plunging; this variation can also be explained by a folding about a ~SW plunging axis.

About 0.5 km W of #CC4, a float includes a significant portion of granitoid rock. Sample KC-9A (collected by W.S.F. Kidd) is a piece of this float that fortuitously includes both the granitoid (very fine grained granite with visible biotite grains) and the granitic orthogneiss of the RCSZ, hence incorporating a useful cross-cutting relationship. Figure 5.45 is an optical photomicrograph of a thin section cut from KC-9A. It illustrates the microstructure of the granitic portion of this sample. Note that there is a lack of strain evidence in the quartzofeldspathic portions (grains have an even extinction and the grain size distribution is small). The observed preferred lattice orientation of the biotite grains is likely a product of super solidus strain. Schneider and co workers (1997; submitted) report Th-Pb monazite ages from this sample of between 9 and 17 Ma. BSE/SEM images of the monazites show a complex multistage growth history (i.e., textural variations revealed by BSE-SEM techniques are not ordered/zoned). Biotite cooling ages from the northern section of Chichi Gah give ages of 9-10 Ma (Schneider, unpub. data). As the cooling ages are concordant to the lower Th-Pb monazite age, Schneider and co workers (1997; submitted) inferred that most of the displacement along the Chichi ('outer") portion of the RCSZ occurred prior to 9-10 Ma. Moreover, Schneider and co workers (1997; submitted) interpreted the monazite

Figure 5.45

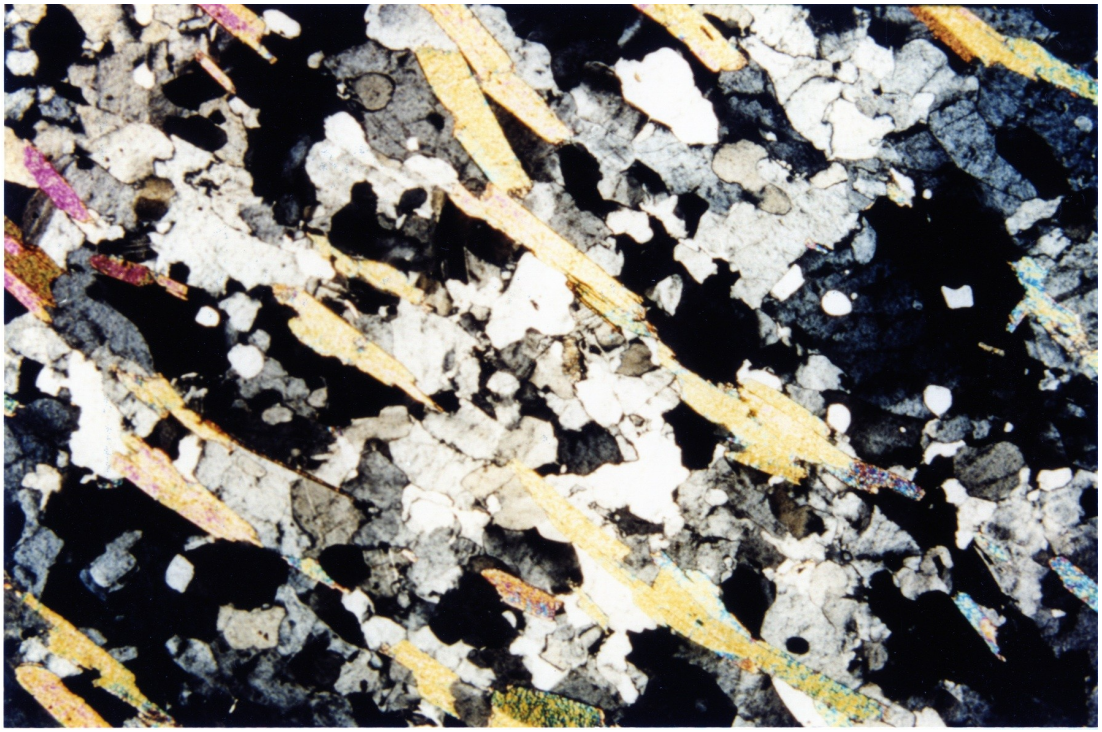

Figure 5.45 Optical photomicrograph of thin section cut from KC-9A, collected ~300 m north of outcrop #CC4, illustrates microstructure of granitic dyke cross-cutting main RCSZ granitic orthogneiss. Note lack of strain evidence in quartzofeldspathic portions; grains have even extinction and grain size distribution is small. Preferred lattice orientation of biotites is likely a product of super solidus strain. Sample from loose block not possible to orient. Base of image is 5.5 mm. Crossed polars.

complex multistage growth history as evidence for protracted plutonism possibly focused within the shear zone (discussed further below).

5.6.2.1 Metasedimentary rock associated with the RCSZ

Near the limits of the granitic orthogneiss that I regard as defining the main RCSZ, metasedimentary layers are present. At #CC13, in the northeastern part of the RCSZ, marble and amphibolite of a few 10's metres thickness are present within the granitic orthogneiss. The foliation of the marble and amphibolite is parallel with the foliation of the RCSZ granitic orthogneiss and there appears to be no cross cutting relationship. The width of the marble and amphibolite layers is very even and across the few tens of metres of exposure, margins are planar and there is no evidence of boudinage or indeed any inhomogeneities. Outcrop was not sufficiently large to see if (e.g.) the marble and amphibolite layers form a lens that tapers out or (e.g.) end in an angular boudin fashion. Near outcrop #CC5, several 10's - 100's metres of metasedimentary rocks are also found in similar circumstances. Here, biotite (±chlorite) metapelitic schists are present and, as with the metasedimentary body north of outcrop #CC13, foliation of the metapelites is parallel with the foliation of the granitic orthogneiss of the RCSZ and the two bodies appear to be concordant. Again, the contact between the granitic orthogneiss and the metapelites is planar and there do appear to be no along strike width variations nor boudinage. Southeast of where the metasedimentary body is present, ~500 m of further structural thickness of granitic orthogneiss of the RCSZ is present before the SE limit of the orthogneiss. At the SE limit of the orthogneiss, biotite (±chlorite) metapelitic schists interlayered with quartzite, marble and amphibolite are present (figure 5.46), in apparently fully concordant contact with the granitic orthogneiss. As before, foliation in the metapelites and metasedimentary sequences is parallel with the granitic orthogneiss. Interestingly, however, lineation that is defined by (1) local

Figure 5.46

Figure 5.46 View to NW of general area of #CC5 in southern Chichi Nallah. photo shows moderately WNW dipping sequence of metapelitic schists interlayered with quartzite, marble and amphibolite. Snow covered, tan-coloured hills in background at right of picture are granitic orthogneiss. Contact between granitic orthogneiss and metasedimentary sequences is immediately below snow covered top of ridge in foreground. This is ~500m from fan at base of picture. Metasedimentary sequences are fully concordant with the granitic orthogneiss (see text for discussion).

Figure 5.47

Figure 5.47 Photo showing tight folding in quartzite layers within metasedimentary sequences in general area of #CC5 (portion of outcrop shown in fig. 5.46). Hinge plunges 22° towards 223°, average local foliation: 023°/71°W.

crenulation intersection, and (2) axes of asymmetric, cm-wavelength tight folds (figure 5.47) is parallel with the local mineral stretching lineation in the granitic orthogneiss of the RCSZ. This is clearly seen along all of the SE margin of the granitic orthogneiss in southern Chichi Nullah. The metasedimentary sequences do not show any discernible evidence for non-coaxial deformation, and do not appear to have taken up the prominent non-coaxial fabric of the granitic orthogneiss of the RCSZ (note that in all instances there is no strain gradient or "dropping off" of the intensity of the RCSZ granitic orthogneiss shear fabric in the vicinity of the metapelite contact(s).

The metasedimentary sequences that are present in southern Chichi continue beyond the limit of my mapping. The steeply W to NW dipping foliation continues and lineation of crenulation intersection, and axes of asymmetric folds, continue to plunge moderately to the SW. In the region of #CC5c, the layering of the metapelites is observed to steepen to vertical and then to dip steeply to moderately SE. In the region where there is a reversal in dip direction (not to be confused with the "overturning" represented by portions of the asymmetric local folds, e.g., fig. 5.47), there is a marked (unrelated) increase in interlayered marble and amphibolite present in the metasedimentary sequences. In this region, immediately south of the point where the foliation of the metasedimentary sequences switch to dip SE intersects with the valley floor, the marble and amphibolite layers are chaotically folded (10's cm to 10's m wavelength) although plunge of crenulation intersection lineation is consistent with the overall trend in the metasedimentary sequences. Several reverse faults define a >200m wide, NW-vergent thrust zone. The thrust trend is most spectacularly expressed by a clear box fold within the zone. The cross sectional area under the box fold represents about 10's m^2 area of section. This thrust area was not visited at close range in outcrop but the general orientation of the thrust planes appeared from a few 100 m distance to be parallel with the overall SE-dipping fabric. The overall reverse fault structure has a NW sense of vergence. However, the magnitude of displacement

is not well constrained; boudinage and flow structures within the thick carbonate sequences suggest significant intralayer displacement. The section of reverse faulting is observed to continue SW over the southern wall of Chichi Nullah, and its surface trace can likely be joined with the Shanthur (Gali) thrust that has been mapped in Azad Kashmir near the Pak-Indo Line of Control (Asif Kahn, unpublished data). The steeply E-dipping metapelites can be followed to the top of the right bank upper ridge in central Chichi Nullah (marked on plate 2). The fold, or kink, that is associated with this switch in dip direction must therefore run through a portion of Chichi Nullah. I interpret the southeast dipping fabric within the metapelites to be non-overturned (with respect to original orientation), and are effectively on the eastern limb of (the southern equivalent of) the Dichil antiform. The extensive NW-dipping metapelites (and orthogneiss?) are therefore the overturned portion, and in this manner are comparable to the overturned SE NPHM sequences (described in section 5.3).

In southernmost Chichi, a largely undeformed, fine-grained leucogranite of several 10's km² area is present (plate 2). The (presumably intrusive) margin of the granite does not visibly cut the foliation of the country rock (i.e. marbles). Close to the margin, the granite shows very minor deformation (weak alignment of biotite grains), which may be in part sub-solidus, however, I found no part of the granite that can be termed a gneiss. The granite forms dull brown craggy towers along the tops of the valley walls, exactly like the sheared orthogneiss to the NE (c.f. fig. 5.46). It is possible that the granite and the orthogneiss may be originally related in some manner. The question of a protolith for the granitic orthogneiss is taken up in 5.6.2.3 - RCSZ discussion and conclusion.

5.6.2.2. Western limits of the Rupal Chichi Shear Zone

Immediately west of Bezhin Glacier, the monotonous sequence of non-coaxially sheared granitic orthogneiss is present, and continues for several kilometres

to the west (see plate 2, and 5.6.3 Central Rupal). In this area, the principal fabric of the granitic orthogneiss is steeply W to SW dipping and mineral stretching lineation typically is NW plunging (and hence continues the trend of westwards clockwise deviation of principal fabric orientation that is present east of Bezhin Glacier. Although sense of shear associated with the mineral stretching lineation is not completely clear, displacement seems to be right lateral (consistent with the main RCSZ). Because of local fabric orientation, however, vergence is towards the SE (as opposed to E to NE vergence for much of the main RCSZ). Further to the west, across the Hanging Lake Glacier, the dextral sense and SE vergence is present in some places, but here a significant volume of metasediment is present within the non-coaxially sheared granitic orthogneiss (see below). This area therefore forms the limit of the region in which I can confidently circumscribe a belt of granitic orthogneiss that has a common non-coaxial shear; the area described above that I regard as the RCSZ.

In the central portion of Upper Rupal Valley, wholly on the right bank of the Central Rupal Valley, largely between Bezhin and Shagiri glacier, cm-m scale discordant leucocratic bodies (predominantly pegmatite dykes) are present. The dykes are effectively planar and are typically oriented 030-050° and dip 50-70°W. The overall sense of opening of the dykes is, in a broad sense, consistent with the general SE vergence of represented by the augen asymmetry and C/S fabric of the granitic orthogneiss. I suggest that the dykes represent a phase of brittle deformation that is a part of the overall finite strain within the "greater" RCSZ, and therefore provide a cross cutting constraint similar to that of KC-9 near outcrop #CC4 in central Chichi Nullah. Schneider and co-workers (1997; submitted) sampled two of these dykes and obtained a Th-Pb ion microprobe monazite age of ~1.2 Ma from the first, and U-Pb ion microprobe zircon and Th-Pb ion microprobe monazite ages of ~2.2 Ma from the second.

Additionally, in the western portions of the RCSZ, there are fault gouge zones and brittle reverse and normal faults. Descriptions of the gouge zones and faults are included in the section 5.6.2 (Central Rupal).

5.6.2.3 Rupal Chichi Shear Zone discussion and conclusion

The Rupal Chichi Shear Zone is recognised based upon the highly consistent nature of (1) the south-southwestward plunging stretching lineation, (2) the pervasive C/S fabric and augen asymmetry that indicates non-coaxial shear with a combination of dextral and (typically) W or NW side up displacement, and (where fabric is dipping W or NW) a reverse fault W over E displacement. The area that I regard as the Rupal Chichi Shear Zone extends from outcrop #9 to (at least) outcrop #48 at Bezhin Glacier, and south to (at least) outcrop #CC5A at Chichi #1 Glacier. Therefore the Rupal Chichi Shear Zone has minimum length of 18 km and minimum width of 10 km at the mapped W end. I infer the RCSZ to be a shear zone of major significance that has played a primary role in accommodating some of the displacement associated with the exhumation of the NPHM; specifically the relative uplift of the summit region of southern NPHM. Kinematics indicated by the RCSZ fabric patterns are consistent with the SE "corner" of Nanga Parbat moving up and ~E relative to the eastern margin. Although the constraint on the timing of events that is provided by cross-cutting granitoid KC-9A would seem to require displacement on at least the outer portion of the RCSZ to have ceased by 9 Ma, the 1.2. - 2.4 Ma leucocratic bodies (predominantly pegmatite sheets) that are found immediately west of Bezhin Glacier have a generally synkinematic association with the western margins of the RCSZ. Moreover, the size of the original body from which sample KC-9 is derived is not known. Thus it is quite feasible that displacement has not occurred simultaneously across the 10 km width of the RCSZ, and that there has been localisation of

displacement that has migrated into the massif as deformation has progressed, and that parts of the RCSZ were active until very recently.

The question of a protolith for the granitic orthogneiss of the RCSZ is relevant, especially in view of the enigmatic margins of the RCSZ: Why are foliation and lineation so consistent beyond the margins of the granitic orthogneiss of the RCSZ, and yet the non-coaxial shear has the appearance of abruptly ending? Syn-kinematic protracted plutonism between 17 and 9 Ma has been suggested by Schneider and co workers (1997; submitted) based upon monazite complex multistage growth history. The highly monotonous nature of the RCSZ granitic orthogneiss is consistent with a relatively young granite (sensu lato) protolith. I propose that the RCSZ granitic orthogneiss was intruded syn-kinematically (with respect to NPHM uplift deformation) as a series of concordant plutonic sheets whose emplacement was accommodated by failure at weak or brittle response horizons in the pre-existing metasedimentary sequences. In later times of intrusion, the failure horizons were most frequently recently emplaced (thermally non-equilibrated) granite. Synkinematic intrusion of this type has been discussed by various authors (e.g., numerous references in Brown and Rushmer, 1997). The local metasedimentary bodies that are present within the RCSZ granitic orthogneiss I regard as trapped "screens" of metapelite preserved near the margins. All significant non-coaxial strain was accommodated in the weak (thermally non-equilibrated) granite giving rise to the present non-coaxially sheared RCSZ granitic orthogneiss. General "coaxial" folding type strain was partitioned to the ("stronger") metasedimentary country rock giving rise to the asymmetric folding. Any folding type strain that was partitioned to the granite was likely overprinted by simple shear, although in a few places, the folding type strain is preserved; for instance, the local area(s) of sense of shear reversal seen locally in the present RCSZ granitic orthogneiss. The granite in southernmost Chichi has the same relationship to the country rock RCSZ granitic orthogneiss and I suggest that the

granite cooled through sub-solidus temperatures after significant shortening had ceased in Southern Chichi. In this case, I suggest that the southernmost Chichi granite is younger than 9 Ma.

Were it not for the sudden switch in dip direction of lineation between outcrops #9A and # 9, the monotonous granitic orthogneiss that characterises the RCSZ could, in the Tarshing area at least, be interpreted as a further horizon of right-lateral shear on the NPHM eastern margin (and hence interpreted as due to general Himalayan thrust-related strain in the deeper footwall of the MMT). Based however upon (1) the nature of the change to the south-southwestward plunging stretching lineation, (2) the southward divergence of the trace of the (SW striking) RCSZ and the (SE striking) MMT, and (3) the pervasive C/S fabric and augen asymmetry that indicates NW side up with dextral shear, which are both highly consistent throughout the area I have delimited as the RCSZ, I do not favour this possible alternative.

5.6.3 Central and Upper Rupal

5.6.3.1. General Remarks

The central and upper portions of Rupal valley probably can be broadly divided up on two classifications, lithology and structure - the two do not overlap.

1. Lithology: I have grouped the lithologies of Central and Upper Rupal Valley into either monotonous porphyroclastic granitic orthogneiss or an undifferentiated compositionally layered gneiss (Plate 2). The rather sharp division that is perhaps suggested by the conspicuous blue/orange junction that cuts across the 4000-5000m regions of Nanga Parbat summit area is highly arbitrary. Even in the two locations actually visited (on Mazeno Glacier left bank between #21 & #22, and on Hanging Lake Glacier right bank ~500m NW of #49a) where the contact has been proposed there is no sharp boundary observed.

2. Structure: I have divided Central and Upper Rupal Valley into two structural groups; areas where lineation is ~N plunging, and areas where lineation is ~SW plunging. This division is both robust and useful; In SW Rupal valley, lineation everywhere plunges S-SW. The junctions with the ~N-plunging lineation areas are (1) across Shaggin Glacier and (2) across a proposed thrust fault high up on Toshain Glacier left bank.

5.6.3.2. Central Rupal

West of Hanging Lake Glacier, the limit of the RCSZ, a series of metasedimentary rocks (chlorite and biotite garnetiferous schists, interlayered with amphibolite and white and rare purple marbles) are present within the monotonous porphyroclastic granitic orthogneiss on the north wall of Central Rupal Valley (in the region of #49a). These are ~N-S striking and fully concordant with the ~N-S striking granitic orthogneiss. Tight to asymmetric folding is seen in both rock types. Figure 5.48 shows an isoclinal asymmetric fold in quartzite and biotite schist layers adjacent to the granitic orthogneiss. The fold hinge plunges 62° towards 343°, and is approximately parallel to stretching lineation in the granitic orthogneiss. The asymmetry of the folds indicates that they are part of the eastern limb of an antiform. This is consistent with broader observations; ~500 m to the west, the orthogneiss foliation is observed to be antiformally folded on a 100's m wavelength. The 100's m wavelength folding continues to Shagiri Glacier, ~4 km to the west. Within a part of the granitic orthogneiss that is on the western limb of the antiform in the vicinity of #49, a clear right lateral sense of shear is demonstrated by porphyroclast asymmetry and C/S relationships. This amounts to a west side up, SE vergent sense of displacement. Clear shear sense indicators were not seen in rocks that could unequivocally be recognised as part of the east limb of the antiform in the vicinity of #49, but there seems to be an absence of sinistral sense of shear anywhere in Central

Figure 5.48

Figure 5.48 Photo showing isoclinal asymmetric folding in quartzite layers separating biotite schist (right) from granitic orthogneiss (far left) in general area of #49a. Hinge plunges 62° towards 343°, average local foliation: 152°/58°E. Fold asymmetry indicates east limb of antiform, consistent with nearby observation.

Figure 5.49

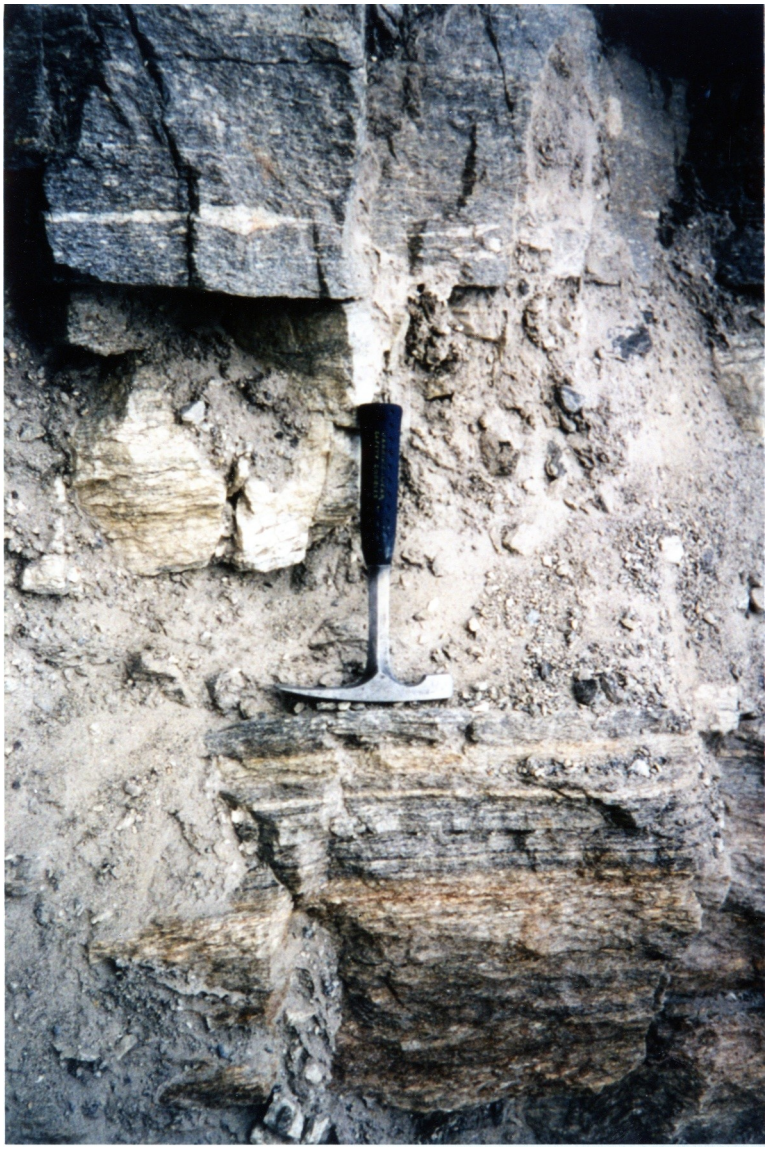

Figure 5.49 Photo in vicinity of outcrop #54 - Mazeno Low Camp, showing moderately north-dipping compositionally layered gneiss (locally including metasediments). Stretching lineation is 36°@317°.

Rupal. If there is truly absence of sinistral sense of shear in Central Rupal, folding does not post-date the principal non-coaxial strain. The metasedimentary rocks within the granitic orthogneiss west of Hanging Lake Glacier locally include horizons (2-10 m) of gneiss that is compositionally layered (10's cm) with biotite rich and poor, and coarse and fine grained (±porphyroclastic) gneiss that is similar to much of the gneiss seen along central Astor Gorge). Figure 5.49 (actually from near #54, below Mazeno Glacier) is typical of this compositionally layered gneiss. The presence of this gneiss within the (monotonous) granitic orthogneiss increases westwards, and is the basis for my division into two lithologies. The presence of compositionally layered gneiss alongside metapelite provide a significant distinction from the metapelite horizons that are present within the RCSZ. Note also, that both the metasedimentary rocks and the granitic orthogneiss are cross cut by leucocratic dykes of a similar nature to the dated 1.2-2.4 Ma dykes described for the area east of Hanging Lake Glacier. They have less regularity about their orientation than the dykes east of Hanging Lake Glacier, but are assumed to be of equivalent youth.

On the right bank of Rupal valley, between the points near the terminus of Rupal Glacier and #CR51a (near Bezhin Glacier), the granitic orthogneisses lack any significant presence of compositionally layered gneiss or metapelite. Leucocratic dykes are also absent. Local discordant amphibolite layers are found in a few localities in the vicinity and to the east of Shagiri village. The general orientation of orthogneiss foliation is consistent with that on the left bank of Rupal; it is observed to be antiformally folded on 100's m wavelength. Fabric stretching lineation is also consistent with the equivalent section on the left bank of Central Rupal, and everywhere is moderately to steeply north plunging. Locally, within the granitic orthogneiss on the right bank of Rupal, there are portions where the felsic component of the orthogneiss is markedly higher (60-80%). Although the change from felsic-rich to felsic-poor portions is quite gradational, local scree fall has resulted in the sudden

juxtaposition of these felsic-rich gneisses against felsic-poor portions, and the contrast is then quite striking. I suggest that these felsic rich portions are areas where discrete pulses of granite emplacement have been focussed during later periods of syn-kinematic plutonism. If the very rare amphibolite dykes that cut the overall gneissic fabric are significant, this synkinematic plutonism hypothesis would seem to require that the plutonism be older than the age of the amphibolite dykes. Although Schneider and co-workers (1997) have obtained lower intercept ion microprobe U-Pb ages of ~5 Ma from zircons separated from the granitic orthogneiss in this area, it is not clear if the zircons are (1) derived from a young granitoid that has been subsequently incorporated into the general non-coaxial shear or (2) a result of recent metamorphism. Upper intercept ion microprobe zircons U-Pb ages are ~1.8 Ga.

In the section of the Central Rupal Valley between Bezhin Glacier and Shagiri Glacier, various brittle and/or late features are found. On Rupal right bank, various structures are indicative of S-SE vergent reverse fault displacement. In some areas, metre scale spaced fracture planes truncate, and have caused bend folding of, the local gneissic fabric as a result of thrust sense displacement. Occasionally, these presumably original reverse fault surfaces have either slickenfibres (typically chloritic) or hydrothermal(?) biotite accumulations that show normal sense of displacement upon the surface. I interpret these as evidence for late local extension, exploiting pre-existing surfaces that were formed as reverse faulting accommodating NPHM uplift. On the left bank of Hanging Lake Glacier, foliation contrasts are large across a local ~W-E gully. On the south side, foliation is steeply W-dipping whereas on the north side, foliation is steeply N-dipping (the N-dipping foliation trend continues up through the Rupal face to where biotite gneiss dips ~50°NW at the summit of Nanga Parbat). I regard this juxtaposition of non-concordant fabrics to be a fault, probably a reverse fault (when originally formed). Other potential brittle reverse fault structures in this areas have been identified by L. Seeber (unpublished data) often with a strong

component of wrench motion, illustrating somewhat complex "brittle strain" partitioning in the central regions of NPHM. A predominantly strike-slip fault is recognised by L. Seeber (unpublished data) on the right bank of Hanging Lake Glacier, directly N of #49a. Fault gouge areas are also found in a few localities in this section of Central Rupal. The three areas where I examined fault gouge of notable magnitude (few metres or more in thickness) are marked on plate 2 ("G" symbol). In the area near #18a, the fault gouge shows reverse displacement evidence (SE vergent) in the form of Riedel shears, high angle ("anti-") Riedel shears, drag structures and slickensides/internal asperity tracks. Reverse displacement is consistent with the general pattern of brittle fractures in the surrounding outcrop, and consistent with stress inversion models from L. Seeber (unpublished data). Additionally, there is some evidence for normal motion in one part of the fault gouge. There is no evidence for wrench motion. In the two areas where fault gouge was found on Rupal right bank (#CR51a), only SE-vergent reverse displacement evidence is present.

West of Shagiri Glacier, the amount of metasedimentary rock and compositionally layered gneiss within the granitic orthogneiss increases markedly. This is clearly seen up in the north wall of Central Rupal Valley. Figure 5.50 shows ~WSW trending metasedimentary and compositionally layered gneiss forming part of a tight overturned (steeply N-dipping) synform. Note that most of the foreground is non-coaxially sheared granitic orthogneiss. The north dipping fabric continues up to the summit of Nanga Parbat, although a north dipping overturned antiform (100's metres width of identifiable hinge region) may be present within the main Rupal Face. A north dipping (~50°N) overturned antiform is seen within the Chongra ridge and may extend to the Rupal face (plate 2). If so, the extensive granite (recognisable in figure 5.50, and from many parts of the Central and Upper Rupal valley, by the hooked boudin) that forms a large part of the Rupal Face may be emplaced into the hinge of the antiform. Local fold and thrust behaviour is also evidenced by S-SE

Figure 5.50

Figure 5.50 Photo from #CR52 looking towards West Shagiri ridge, showing WSW trending metasedimentary and compositionally layered gneiss forming tight overturned steeply N-dipping synform, picked out by dark amphibolite layers. Fan in central portion is spilling down from Rupal left bank #1 Glacier. To left (west) of fan is granitic orthogneiss of #Sh2, to right are metasediments of #Sh1. Bottom of photo is ~3800m, ridge top in foreground is ~5500m. Note slight kinking in steeply N-dipping compositionally layered gneisses in background to far left of field of view.

Figure 5.51

Figure 5.51 (next page) Looking N to summit of Nanga Parbat (8143m), from #CR52 on Shaggin Glacier left bank. Nearly 5 km of relief is visible; long moraine ridge at foot of photo is Shagiri Glacier, and base of photo is ~3600m. Note ~50° NW dipping layer of black gneiss forming upper 400m of summit of Nanga Parbat. Below are thick sequences of granitic orthogneiss with local 100's metres thick leucogranite plutons. ~1.5 km thick pluton to left is characterised by "hooked boudin" xenolith. Extensive, cross-cutting pegmatitic dykes (part of 1.2 - 2.4 Ma suite) are just visible at bottom right. Lower regions of field of view contain ductile to brittle SE-vergent reverse faults, some of which show good evidence for later normal motion (see text for discussion).

Figure 5.51

Figure 5.51 (see previous page for caption).

vergent sense of shear indicated by non-coaxial fabric in the granitic orthogneiss (most clearly seen up into the side valleys of Rupal left bank #1 and #2 glaciers. In addition, brittle planes that typically cut the granitic fabric at a low angle show reverse fault sense of displacement based upon edge bending of truncated foliation. These surfaces frequently house slickenfibres that indicate normal motion, again indicating that there has been late local extension on the southern flank of Nanga Parbat.

5.6.3.3. Upper Rupal

The moderately north dipping belt of compositionally layered gneisses interlayered with metasedimentary rock and granitic orthogneiss continues to the west to the foot of Mazeno Glacier (N of #54) and is observed remotely to continue across the left bank of Toshain Glacier (figure 5.52). The compositionally layered gneisses interlayered with metasedimentary rock and granitic orthogneiss that are present in the lower regions have a markedly different orientation from those above. The rocks in the lower regions of the left bank of Toshain Glacier are almost wholly steeply dipping to the west and have moderately to steeply south plunging fabric stretching (and parallel crenulation intersection) lineation. In figure 5.52, the steep layering visible in the bottom of the left bank of Toshain Glacier can be seen in the centre of the field of view to decrease in dip sharply upwards. I propose that this is bend folding associated with a thrust that has resulted in the observed juxtaposition of the two differently oriented portions of the compositionally layered gneisses interlayered with granitic orthogneiss. It is possible that the thrust could be a horizon of major displacement but the apparent lack of lithological contrast is not strong support for this idea.

The path to the east of the Toshain Glacier left bank thrust is not clear. Figure 5.53 shows a view back to Rupal Face and the mouth of the Mazeno Glacier valley in the centre left of the field of view. Note the saddle partly obscured by shadow - the

Figure 5.52

Figure 5.52 Photo looking to NW to left bank of Toshain Glacier. Shows steeply W-dipping (and S-plunging lineation) fabric of compositionally layered gneisses interlayered with granitic orthogneiss in lower part of field of view decrease in dip sharply upwards. A thrust is inferred to separate lower rocks from moderately N-dipping compositionally layered gneisses interlayered with granitic orthogneiss above (see text for discussion).

Figure 5.53

Figure 5.53 Photo looking to NE to Nanga Parbat summit ridge from eastern Toshain Glacier. Local peaks on summit ridge average ~7000m. Nanga Parbat (8143m) is higher, and ~50 NW dipping biotite gneisses are hence clear. Extensive leucogranite (~1.5 km thick) is present on main Rupal Face. Valley in centre left of field of view is Mazeno Glacier valley. Join between Mazeno Glacier abandoned medial moraine and Toshain Glacier lateral moraine is ~4200m. Thrusts are interpreted on Mazeno Glacier valley left bank (1) in saddle partly obscured by shadow, and (2) in saddle (not visible, marked 5639m on map) between snow covered ridge in background and craggy ridge in centre.

hill on the near side of the saddle is 4730 m (marked on plate 2). This saddle is thought to be a thrust based upon gouge development found on the east side of the saddle (consistent with unpublished data from L. Seeber). Based upon the similarities in appearance of the rocks on either side of the thrust, it is unlikely to be of major significance, and likely does not extend west across the mouth of the Mazeno Glacier valley. If the Toshain Glacier left bank thrust does extend east, I suggest it passes into the Main Rupal valley (i.e., "under" the main Rupal Glacier). Figure 5.53 illustrates that there is sufficient room to do this.

Figure 5.53 also illustrates the marked topographic break from the lower (<5500m) ridges to the Nanga Parbat summit region that is associated with the lithological change from compositionally layered gneisses interlayered with metasedimentary rock and granitic orthogneiss to (I assume) mostly granite and orthogneiss. It is likely a major reverse fault coincides with this topographic break. Many of the lower regions of field of view contain various other minor ductile to brittle SE-vergent thrust faults.

5.6.3.4. Southwest Rupal Valley

As part of "southwestern Rupal" I include the area from Shaggin Glacier left bank, in the east, to the right bank of uppermost Toshain Glacier, in the west, and the lowermost portion of Toshain Glacier left bank. As mentioned in the introduction, in SW Rupal valley, lineation everywhere plunges S-SW, and this is the basis for separating the SW Rupal area. The lithology all along the southern side of the Southwest Rupal Valley section I group as part of the granitic orthogneiss. The lowermost portion of Toshain Glacier left bank is compositionally layered gneiss.

Between Shaggin Glacier left bank (#CR52) and far West Rupal left bank: (#CR52B), there is a fairly monotonous sequence of L-tectonite orthogneiss with a very strong lineation (stretching) plunging moderately to the SW. Foliation planes

Figure 5.54

Figure 5.54 L-tectonite granitic orthogneiss ~200m S of #CR52 on Shaggin Glacier left bank. This type of L-orthogneiss is ubiquitous to the SW Rupal area. Where foliation surfaces are clear, shear fabric is marked by (1) biotite planes forming S and C surfaces. and (2) 0.1-3.0 cm asymmetric feldspar porphyroclasts. Foliation is 031°/70°W with stretching lineation pitching 62° from south. Sense of displacement is top down to SW and sinistral.

Figure 5.55

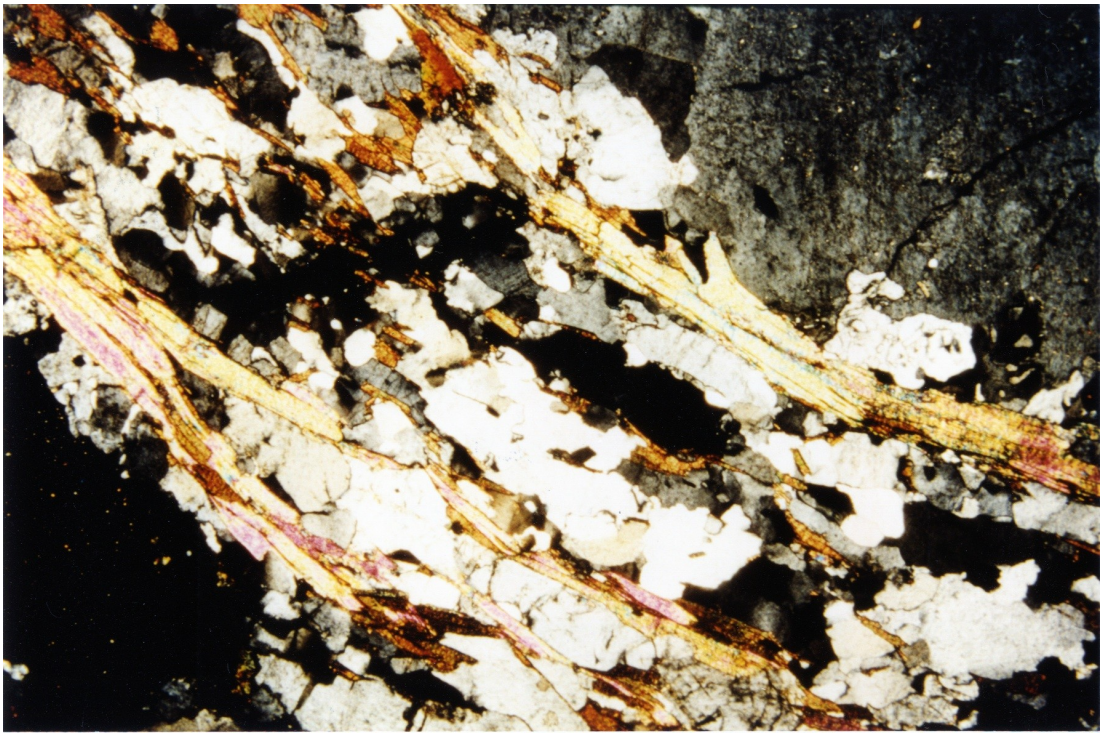

Figure 5.55 Optical photomicrograph of thin section 69-28A (cut from E6/9/28-I sampled near #CR52). Shows characteristic microstructure of L-orthogneiss in SW Rupal. Sense of shear is sinistral, rarely visible at <10 mm width of view due to coarseness of fabric. Sigmoidal feldspar porphyroclasts and 100-400 μm biotite surfaces are main shear indicators. Note overall coarseness of grains. Although some compositional banding is present, quartzofeldspathic bands do not have ribbon-type appearance, and I suggest lattice preferred orientation of biotites is a relict of super-solidus flow, and principal deformation proceeded at <400°C. Cut parallel with lineation (50°-S pitch), perpendicular to foliation (037°/66°E). South is to left. Base of image is 5.5 mm and oblique to main fabric. Crossed polars.

dipping W-NW can be recognised in some areas, and in these cases, sense of shear shows a very convincing top to SW, with an accompanying sinistral wrench component to the displacement. Figure 5.54 shows the L-tectonite granitic orthogneiss plunging 62° towards 213°. Outcrop is ~200 m S of #CR52, and close to sample location of E6/9/28-I. Figure 5.55 shows a portion of thin section 69-28A cut from E6/9/28-I. It illustrates typical deformation conditions for the L-orthogneiss of SW Rupal. There is some separation of mica quartzofeldspathic layers, however there is no development of (e.g.) quartz ribbons, or extensive recrystallisation, and I suggest that the fabric defined by the biotite laths is a super-solidus relict, and that the main deformation proceeded at <400°C. Thin section 79/13C from #CR52B in far West Rupal left bank shows similar conditions of deformation.

In central and far west Toshain Glacier right bank, the L-orthogneiss is again present but in a somewhat discontinuous fashion. The L-orthogneiss forms mega-lenses and boudins (10's m diameter) within a finer grained grey gneiss. In a few locations, an original discordant contact between the L-orthogneiss bodies and the grey gneiss is preserved, and I infer that the L-orthogneiss bodies are intrusions into the grey gneiss. Subsequent deformation has affected both; the stretching lineation of both the L-orthogneiss and grey gneiss are parallel and steeply south to southwest plunging. Foliation is more clearly recognised in the grey gneiss; Sense of shear is impressively consistent across all of Toshain Glacier right bank, and is sinistral with top down to the south-southwest. Thin sections 69/30A and 79/14-A from # 56, (not illustrated) both show comparable microstructures to those of 69/28A in figure 5.55; 79/14-A has a slightly better development of distributed grain size domains between the 100-400 μm biotite laths, and may be a little higher in temperature. This section 5/6B from #19 (not illustrated) is from the edge of a migmatised granitic boudin that is locally asymmetrically folded. It shows atypical grain size distribution and apparently patchy recovery (possibly related to the migmatisation). The vicinity of

#19 is marked by local uneven folding (whose axis are parallel to the stretching lineation in the L-orthogneiss). This folding is likely due to local responses in an overall environment of constrictional strain, as indicated by the extensive L-tectonite presence.

In the lowermost portion of Toshain Glacier left bank, the steeply W-dipping gneisses with S-plunging lineation do not show a particularly strong sense of shear fabric. Where convincing sense of shear is seen, however, it is unequivocally sinistral, and W side down to the south.

5.6.3.5 Central and Upper Rupal discussion and conclusion

1. In SW Rupal, SW to S dipping gneissic fabric shows an excellent SW stretching lineation associated with a sinistral, top & west side down to the south displacement. Significant sinistral sense of shear and displacement towards the south is otherwise absent in the greater Rupal area. In present orientation, the SW Rupal fabric is extensional, and the displacement path with respect to surrounding geography would indicate material has moved out of the Indus River drainage basin (as was remarked upon in 5.1.2). The L-tectonite pods are younger than the country rock and may be very young ("post" - Himalayan i.e., <35 Ma) if they are related to the various examples of plutonism that I and co-workers have mapped around the massif. No geochronologic data exist at present for either the pods or the grey gneiss and it is entirely unknown whether the portion of L-tectonism that post dates the orthogneiss pods is (1) truly due to extension of the NPHM in this part of the massif, or (2) a principal Himalayan fabric (5.1.2) that has been subsequently rotated to southwest dipping as a western part of the general antiformal folding, and as a southern part of the doming related to NPHM growth. Hubbard et al. (1995), a few tens of km to the west of SW Rupal, interpreted a similar SW dipping gneissic fabric with observed top down to southwest shear indicators as evidence for W-WSW directed large scale

extensional collapse of NPHM. However, Burg et al. (1996) illustrate that Hubbard et al. (1995) have mis-interpreted a simple (NPHM-related) rotation of the regional NW Himalayan thrust fabric; an originally NE plunging Himalayan (thrust) lineation on a north dipping surface is easily rotated to become a SW plunging ("normal-sense") lineation on a W-dipping surface. In view of the similarities, viz: (1) fabric trends and location within NPHM are broadly similar to the Hubbard et al./Burg et al. case, on the SW side of NPHM, and (2) true exhumational structures are not found elsewhere in NPHM, and most notably they are lacking from the main Nanga Parbat summit ridge (a more appropriate location for any significant tectonic collapse phenomena), I follow Burg et al., 1996, and regard the SW Rupal SW-directed, apparently extensional fabric to be a rotated principal Himalayan structure. My sample from the L-orthogneiss taken in hope for geochronology have not been dated at the time of writing.

2. Above, I proposed that the RCSZ may have an association with syn-kinematic plutonism. The western "margin" of the RCSZ passes to an area of general dextral shear within portions of the granitic orthogneiss that have quite a variety of foliation orientations, and indicates that strain partitioning, and evolution of strain patterns, is less predictable in central NPHM. Despite the more complex progression of strain, I am confident that the central Rupal fabric is the mechanical equivalent (or counterpart) to the observed strain in the RCSZ. In central Rupal, very young, probably syn-kinematic plutonism (Zircon and monazite U-(Th)-Pb accessory mineral ages from Schneider et al. 1997; submitted) imply that the present state of deformation is at least in part due to recent exhumation of NPHM. The felsic rich versus felsic poor portions of the granitic orthogneiss on Central Rupal right bank are suggested to be further evidence for synkinematic plutonism. In view of the close association of the granitic orthogneiss and metasedimentary rocks that appears to be quite consistent throughout Central Rupal and Chichi valleys, I leave open the

possibility that the majority of the granitic orthogneiss mapped in Central Rupal and Chichi is young and related to the exhumation of NPHM. This suggestion is wholly at odds with interpretations from Treloar et al. (1991) and Chamberlain et al., (1995), who, based upon metamorphic histories obtained for samples from the north side of NPHM, inferred that all the gneisses close to the NPHM core were Proterozoic Indian basement reworked by Himalayan events. Based upon my mapping in southern NPHM, however, the Proterozoic Indian basement hypotheses of Treloar et al. (1991) and Chamberlain et al., (1995), require excellent preservation (since the Proterozoic, via the India-Asia collision) of large portions of metasedimentary rock within gneisses of the NPHM core that are indistinguishable from "cover" metasedimentary rock to the south and east. It is possible that the gneisses exposed in the lower regions of the Rupal valley are very different from those on the north side of the Nanga Parbat summit section that were investigated by Treloar et al. (1991) and Chamberlain et al., (1995). If there is a major contact (where deep basement gneisses are thrust over cover rocks), the massive topographic break on the south side of the NP summit ridge shown in figure 5.53 (above) seems to be a good candidate. Treloar et al. (1991) additionally offered the probably-Permian age cross-cutting amphibolite dykes as evidence that the gneisses of the NPHM core were older. Cross-cutting amphibolites are seen in Rupal, and if my suggestion is correct, would seem to require young basaltic magmatism, which is unlikely (noted by Treloar et al., 1991).

3. The numerous thick fault gouge zones, and generally brittle reverse faults that are present at lower elevations in the valley walls of central Rupal may indicate that at least part of Rupal valley has provided a local topographic crustal weakness to focus late brittle deformation. Focusing of strain by topographic features has been modeled for the Indus River valley at the Raikot Fault on the western side of NPHM (Koons et al., submitted), and in the Taklaman river valley where the northern Pamirs frontal thrust approaches the southern toe of the western Tien Shan (Pavlis et al., 1997).

4. The north plunging antiform along the NP summit Ridge is proposed to be the continuation of the Burdish Ridge antiform from the Astor Section in the north.

5. Normal fault structures are found only on Rupal left bank. Normal faulting is consistent with normal motion identified from recent seismic data (Meltzer et al., submitted).

5.6.4 Mazeno Pass Area

The Mazeno Pass Area includes the main valley of Mazeno Glacier (seen in fig. 5.53) that provides access to Mazeno Pass (5358 m). The upper region of Mazeno was the highest elevation I attained in NPHM. On both occasions I only crossed the pass westwards. Both the granitic orthogneisses and the compositionally layered gneiss (without any metasedimentary rocks) are present. As before, the nature of the "contact" between them is not clear. In addition, various granitoid family members are present, the most significant of which is the Mazeno Pass Pluton.

At outcrop #20, compositionally layered gneiss present. Foliation is vertical to steeply west dipping and biotite mineral lineation plunges moderately north. Thin section 5/7A is cut from thinly (<0.5 cm) foliated orthogneiss, within the compositionally layered gneiss. Sense of shear based upon C & S surfaces weakly defined by biotite grains is sinistral; the western block has moved up and towards the south. Feldspars have a pitted appearance, show little uneven extinction, and are probably recovered. Grain size distribution is not large and there appears to be little evidence for new grain growth.

Compositionally layered gneiss interlayered with granitic orthogneisses is seen at #21. Foliation is approximately vertical with a moderately north plunging mineral lineation. Sense of shear is determined from the granitic orthogneisses portions to be dextral (in opposition to #20) with E side upwards and vergent towards S (determined from hand specimen NE95/7-IV figure 5.56, and thin section 5/7-C (not

shown) cut from sample collected at #21). In this sample, grain size is coarse and there has not been widespread grain size reduction. In places, notably planar grain to grain contacts in the quartzofeldspathic tails of feldspars imply that there has been some recovery. Deformation mechanisms seem to be similar to those seen everywhere else in the granitic orthogneisses, and, as before, I would suggest that deformation has occurred at <400°C.

Higher up (further north) in the main valley of Mazeno Glacier, at #22, foliation and lineation are essentially parallel with #21 (005°/70°e, 30°@005°). However, thin section 5/8A shows sinistral sense of shear; vergence is W side up and to south. Such blatant conflicts in sense of shear across small (~1 km) distances is disappointing. Tight folding about a N-S axis is a simple mechanism by which to produce such reversals. Regardless of the reason, the presence of the sense of shear conflicts indicates that my shear sense observations in the Mazeno area can probably reveal little about the more recent NPHM displacement trends. A detailed study of conflicting sense of shear domains in a manner comparable to my investigations for SE NPHM is not possible with my limited dataset from ~5000m in the Mazeno area.

Speculation regarding deformation mechanisms in the Mazeno area is also probably of limited use. Microstructure of thin section 5/8A is highly similar to thin section 5/7-C, and again, there is evidence of recovery (which can destroy evidence for higher grade deformation mechanisms). The recovery may be a result of the thermal flux associated with (e.g.) a dense suite of pegmatite sheets that are present in the ~500 m N of #22 (Fig. 5.57). Figure 5.57 (looking due east) illustrates that north of #22, the principal foliation is moderately NNW-dipping. Numerous local pegmatitic sheets mark a series of NW dipping fracture suites that are discordant to local foliation but, interestingly, parallel with the foliation of country rock (gneiss) at #23, ~1 km across the glacier to the NW. Figure 5.57 also shows angular float on the

Figure 5.56

Figure 5.56 Granitic orthogneiss on Mazeno Glacier Valley left bank at outcrop #21. Biotite planes mark S and C surfaces. Shear sense is also demonstrated by coarse (<2 cm) feldspar porphyroclasts with asymmetric tails. Foliation is 020°/90°W and stretching lineation plunges 50° towards 020°. Sense of displacement is E side upwards and vergent towards S (dextral shear).

Figure 5.57

Figure 5.57 Photo (looking due east) showing suite of NW dipping pegmatitic sheets ~500-1000 m north of #22, Sheets are discordant to local foliation but, interestingly, are parallel to foliation of country rock (gneiss) at #23, ~1 km across the glacier to the NW, and at Mazeno Pass. Glacier in foreground is ~5000 m. Float includes granitic orthogneiss and various members of compositionally layered gneisses. Green pinninitised cordierite in coarse (pegmatitic) granitoid float was seen in significant volumes, but not in outcrop.

surface of the glacier in the foreground. Green pinninitised cordierite in coarse (pegmatitic) granitoid float was seen in significant volumes, but not in outcrop. The timing relationship of the (ex-) cordierite bearing granitoids to (1) the pegmatitic suites in figure 5.57 and (2) the fine grained granite of Mazeno Pass pluton (described below) is therefore not clear.

Up to the pass (outcrop #23) granitic orthogneiss is present. This is replaced by compositionally layered gneiss at the pass. In both areas (e.g., figure 5.58), foliation is becomes NW dipping while stretching lineation remains moderately N-plunging and sense of shear is sinistral (based upon thin sections 5/8F, 5/8G and 5/8H). Sense of displacement therefore has a large component of southward (thrust) vergence. Microstructure is consistent with the previous localitiies showing pitted large feldspars, thick 300-1200 μm biotite laths, and apparently little tectonic grain size reduction or new grain growth. Recovery is again likely due to nearby plutonism (Mazeno Pass Pluton).

The Mazeno Pass Pluton (fig. 5.59) is a notably undeformed, tourmaline and biotite absent, fine-grained, muscovite granite discordant to the local country rock. Prominent offshoots (10's cm wide) of the leucogranite extend from the main pluton body discordantly into the country rock for up to 500 m. U-Pb zircon analyses (Schneider et al., 1997; submitted) give a discordant age with an upper intercept of ~1860 Ma, representing the Precambrian protolith age (Zeitler et al., 1993). The lower intercept is defined by a cluster of zircon ages at ~1.4 Ma. Similarly, monazite from the same pluton also yielded a coincident Th-Pb age of ~1.4 Ma. Such co-incidence is extremely rare, and accordingly, Schneider and co workers (1997; submitted) infer 1.4 Ma as the intrusion age of the Mazeno Pass pluton. The monazites separated from Mazeno pass have regular textural appearances and they are thought not to have a complex growth history. I note that, at the time of writing, this

Figure 5.58

Figure 5.58 Looking at east side of Mazeno Pass. Compositionally layered gneiss trending 050°/80°W is clear. Note lack of visibility of Mazeno Pass Pluton from only few 100 m from Pass. Compositionally layered gneisses are cut at high angle by fine grained leucogranite offshoots of Mazeno Pass Pluton (not visible in photo). Pass is 5358 m, top of outcrop to left is ~5400m.

Figure 5.59

Figure 5.59 View directly up steep West face of Mazeno Pass. Viewer is ~300 m below pass (snow covered lower spot to left of picture). Photo clearly shows Mazeno Pass Pluton main body and offshoots cross-cutting country rock (compositionally layered gneisses). Pluton continues for a further 100 m below and a few 100 m to both left and right of field of view.

is the youngest reported true crystallisation age for any leucogranite in the entire Himalaya. Younger plutonism has been demonstrated by the presence of a 0.9 Ma zircon rim in the Tato pluton (U-Pb zircon SHRIMP age from Zeitler et al., 1993), but the history of the Tato body appears to be protracted and more complex.

From Mazeno Pass, compositionally layered gneiss outcrops along much of Lobah Glacier, and with #25 excepted, foliation is generally N-S trending. Due to the urgency of departure after crossing Mazeno Pass, there is a gap in my mapping between Lobah and Diamir Gah (part of SW NPHM).

5.7 GEOLOGICAL OBSERVATIONS IN SW NPHM

5.7.1 General Remarks

Under the heading SW NPHM, I include the area that is encompassed by (1) the N-S trending Bunar valley (including the southern continuation, Biji Gah and the Jalhari Gah fork at Phailobat) and (2) the NW trending Diamir valley up to Diamir Glacier). Trekking is required in both valleys.

The MMT outcrops immediately south of Diamiroi village and work was conducted south and east of this point. A ~N-S section was provided by Biji Gah and an ~W-E section was provided by Diamir Gah and the composite Nashkin-Airl section. In both areas, the main fabrics trend mostly N to NNE (Fig. 5.60). I describe the cover rocks initially, and describe most of the plutonic sequences along with the Diamir shear zone.

Figure 5.60A

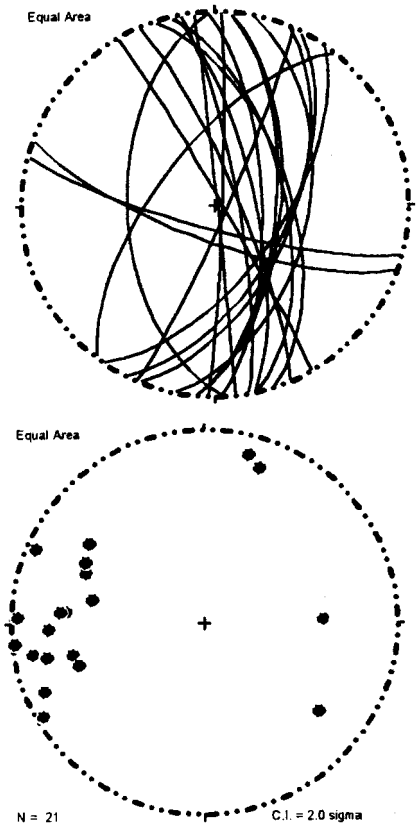

Figure 5.60A Contoured lower hemisphere equal area projection of foliation poles and lineation of all rocks in Diamir Gah.

Figure 5.60B

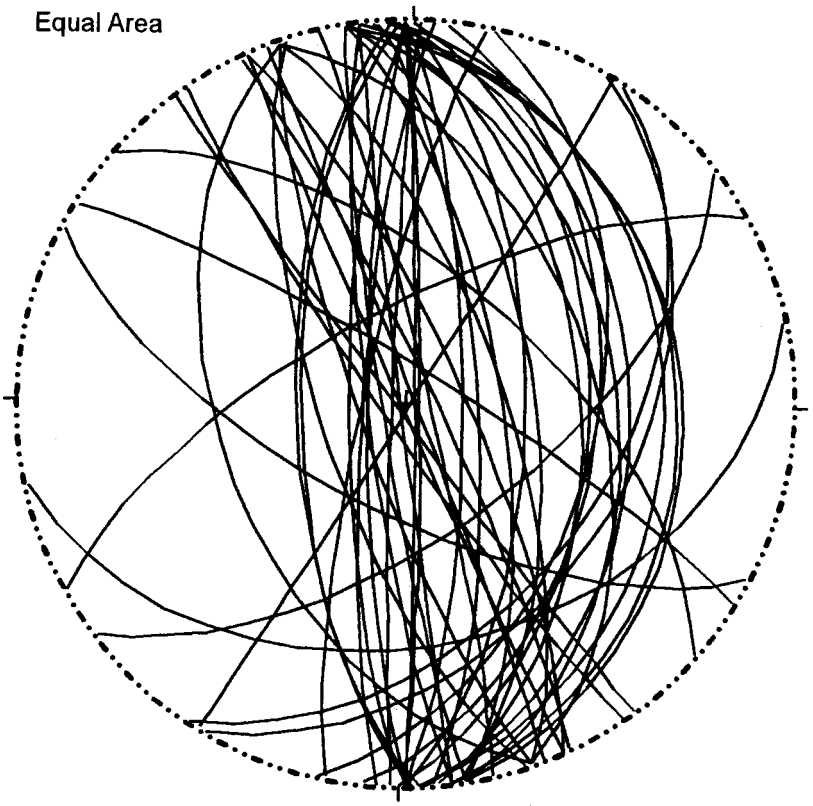

Figure 5.60B Contoured lower hemisphere equal area projection of foliation poles and lineation of all rocks in Airl Gah.

Figure 5.60C

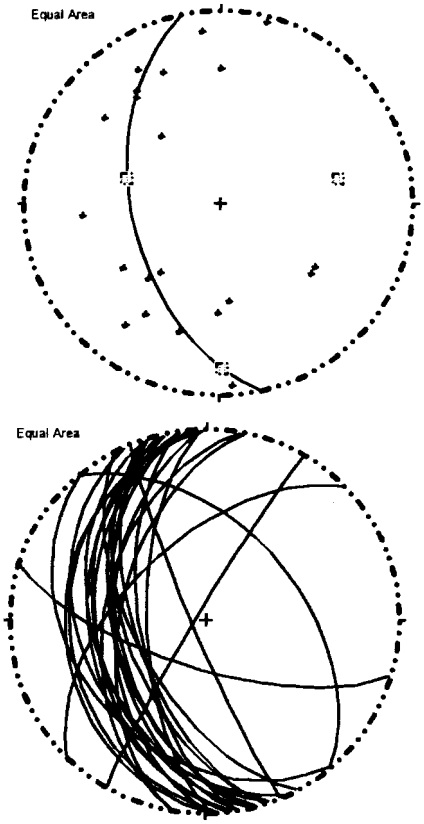

Figure 5.60C Lower hemisphere equal area projection of foliation poles and lineation of all rocks in Biji area. Upper plot: Biji area contoured foliation poles (Kamb method). Lower plot: Biji area contoured lineations (Kamb method).

5.7.2 Cover Sequences

In Biji Gah, the Indian "cover" passive margin rocks that form the original MMT footwall include sequences of carbonates and amphibolites (probably the Permian "Panjal Traps") interlayered with pelitic schists and gneisses. The appearance of the sequence is consistent with (1) cover rocks seen in and described for SE NPHM and (2) the general cover rocks discussed in section 5.2.1.2. In Diamir Valley, where the cover rocks are first encountered travelling in to Bunar Gah from the north, they are not more than a few 100's metres thick, sandwiched between the MMT at Diameroi, and the western margin of the general plutonic sequence near #D2, that includes the Jalhari granite. The cover rocks comprise a few hundred metres of garnetiferous metapelite, and <100m of marbles and amphibolite. Local foliation is moderately to steeply SE-dipping. This orientation is parallel with the local (structurally higher) MMT hanging wall KLS rocks (Kamila amphibolite), and it is clear that the regionally NW-dipping cover sequences and MMT hanging wall are locally overturned to become SE-dipping (figure 5.61A). The overturned sequences have responded in a similar manner to the SE NPHM sequences and both are a result of the overthrusting associated with NPHM uplift. The area in which the sequences are overturned extends north of Diameroi for at least 3 km, and extends south for approximately 5 km to the Gashit fold (a recumbent open fold at the mouth of Airl Gah at the village of Gashit) where the E-ward dipping cover rocks form the upper (overturned) E-dipping limb. Between Diameroi and Gashit, there are a few local occurrences of "non cover rocks". A grey gneiss with porphyroclast rich and porphyroclast poor horizons is found ~200 m south of where the MMT crosses the main valley. To the south, this passes, after 50 m or so, to an area of scree where a significant volume of the lath unit is found, before the cover rocks return, ~150 m further south. The porphyroclastic unit and lath unit are nearby (~ 1 km?) the Jalhari granite, and this proximal association is seen again between outcrop #P5 and P7 in

Figure 5.61A

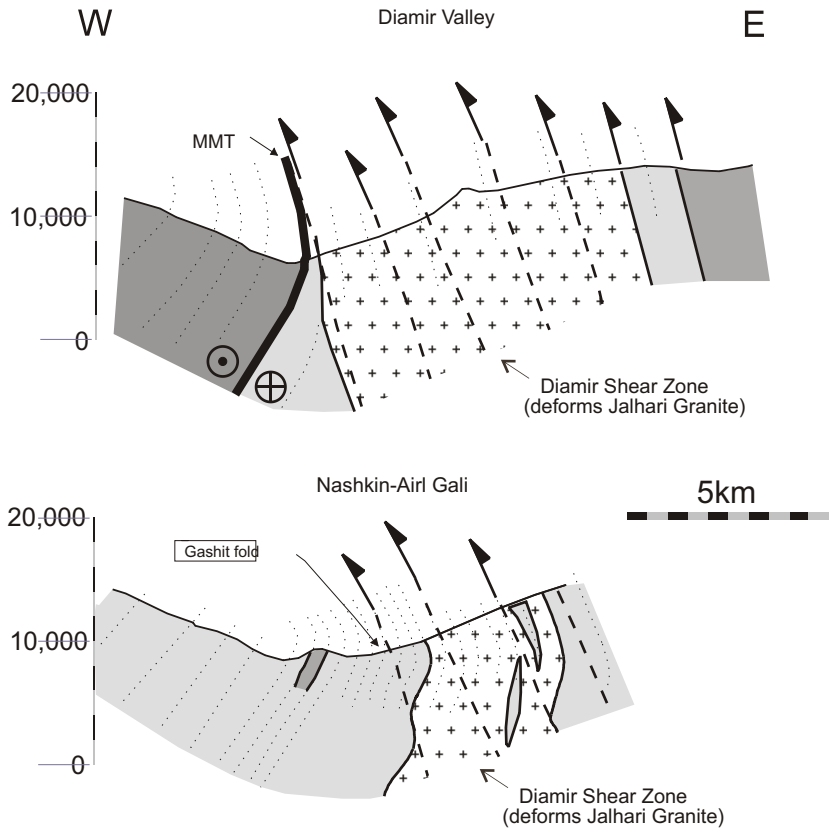

Figure 5.61A Cross sections along Diamir section and Nashkin-Airl composite section. Vertical scale in feet. No vertical exaggeration. Light grey: Metasedimentary cover rocks (dashed line ornament indicates foliation); crosses: leucogranite; medium grey: other gneisses; dark grey: general KLS (only W of MMT). Note overturning of metasedimentary cover rocks in MMT footwall in response to NPHM uplift related overthrusting. Diamir shear zone is primarily focussed in Jalhari granite, emplaced syn-kinematically.

southern Biji Gah. I infer that the presence of the porphyroclastic unit and lath unit in the cover sequence has some relationship with the nearby Jalhari granite (e.g., the porphyroclast and lath unit are (1) by-products of the overall plutonism, or (2) they provided a weakness horizon(s) where some part of the emplacement could be localised.

Between #BA2 and #NH1 (at the mouth of Nashkin Gah) outcrops of very finely laminated gneiss is found that suggests high strain, however no unequivocal shear sense, was obtained. The presence of apparently higher strain than in surrounding rocks is significant in view of a nearby (~500m), large outcrop (#BA2) of coarse feldspar (up to 2 cm) porphyroclastic gneiss in a notably ashen-coloured matrix. Fabric is steeply west dipping and stretching lineation is ~horizontal. Sense of shear was indeterminable. This porphyroclastic gneiss seems to form a large part of a major ridge (Manogush Ridge) that causes the forking of the Biji and Barai rivers to be quite pronounced. Figure 5.61B, is a westward looking view from the Airl Gali, looking across to Nashkin Gah. Manogush Ridge, the promontory that houses the porphyroclastic gneiss (#BA2) is well illustrated in the photo.

Nearby, in the vicinity of #AR2, the Gashit fold is exposed (figure 5.62). This fold marks the point where regional overturning of several km of MMT foot-, and hanging wall sequences is accommodated. North and East of #AR2, regional layering is predominantly E-dipping. South & West of #AR2, layering is predominantly W-dipping. Hinge line plunges ~ 20°N.

To the south, the moderately W-dipping cover rocks are present throughout Biji Gah up to #P5 where they pass to the previously mentioned lath unit and higher strain porphyroclastic gneiss. Lineation switches from gently-steeply N- or S-plunging, and there is a suggestion of two suites of lineation; (1) a steeply ~W-plunging lineation (consistent with the plunges of lineations measured further E (see below), and (2) a gently plunging ~SW lineation. South of #P5 is a thick section of

Figure 5.61B

Figure 5.61B View (due W) from Airl Gali pass, looking (1) down Airl Gah, where >5 km of structural thickness of Jalhari granite is represented, (2) past Gashit fold where point of regional overturning of several km of MMT foot-, and hanging wall sequences is accommodated, (3) across Manogush Ridge (in shadow) where belt of porphyroclastic gneiss is present, (4) up into Nashkin Valley, where ~2600m of vertical relief, and >8 km of cover sequence is represented, and (5) to dark rocks of Kamila amphibolite that mark MMT hanging wall at very top of furthest ridge.

Figure 5.62

Figure 5.62 Looking NNW to outcrop of Gashit Fold, on right bank, and towards mouth, of Airl Gah Valley. In this outcrop, fold is within metasedimentary cover, ~1.5 km west of edge of Jalhari Granite. Fold accommodates regional overturning (eastward dip) of MMT footwall, and is inferred to be due to W-verging, E-dipping Airl-Gah/Diamir Shear Zone. North and East of this point, layering is predominantly E-dipping. South & West of this point, layering is predominantly W-dipping (note W-dipping cover rocks in background on far side of Bunar Gah). Hinge line plunges ~ 20°N

coarse grained porphyroclastic gneiss that is similar to #BA2, but with a darker matrix. Again foliation is moderately W-dipping and lineation varies from gently-steeply N- or S-plunging. Although the coarse porphyroclastic unit is highly strained, there is no systematic sense of shear. East of the coarse porphyroclastic unit in upper Biji Gah, The Jalhari granite is present in Jalhari Gah, south of the village of Phailobat. The "granite" is quite deformed. It has a variably strong foliation and a local very coarse crenulation of biotite layers about <0.5 cm quartz and feldspar grains. The intersection of this coarse crenulation causes spectacular parallel ridges on the main (W-dipping) foliation surfaces of the granite that can be seen from some distance. Interestingly, this lineation seemed to be universally S-SW plunging. The Jalhari granite was first recognised here where it is apparently less deformed than where it outcrops in Airl Gah and Diamir valleys (where it has been intricately involved in the Diamir shear zone).

5.7.3 Diamir shear zone

The Diamir and Airl Gah valleys both trend ~W-E, and mostly offer almost continuous outcrop sections through the belt that comprises the Jalhari granite deformed within the Diamir shear zone. In both these valleys, the Jalhari granite is present as a coarse-, to medium-grained biotite granite that grades into granitic and porphyroclastic gneiss. Figures 5.63 and 5.64 illustrate the degree of variability of the Jalhari granite across the belt as a whole. Note the variation in (1) presence of felsic component and (2) porphyroclast preservation.

Throughout the Diamir shear zone, Jalhari leucogranite lenses (10's - 100's m thick) showing little to no sub-solidus deformation are separated by 10's - 100's m thick layers of gneiss where deformation of the granite has been localised in both ductile and brittle fashion. These higher strain layers anastamose around the granite lenses, and mark reverse faults that "climb" to the west. In the better preserved

Figure 5.63

Figure 5.63 Strained portion of Jalhari granite within Airl-Gah Shear Zone, Diamir Valley: Note large variety of granitic gneiss locally housed. Sample is none the less representative of degree of variation observed throughout Jalhari Granite.

Figure 5.64

Figure 5.64 "Pancake biotite" portion of Jalhari granite within Airl-Gah Shear Zone, Airl Gah (~`500 m W of #AR6). I infer large amounts of super solidus deformation.

Figure 5.65

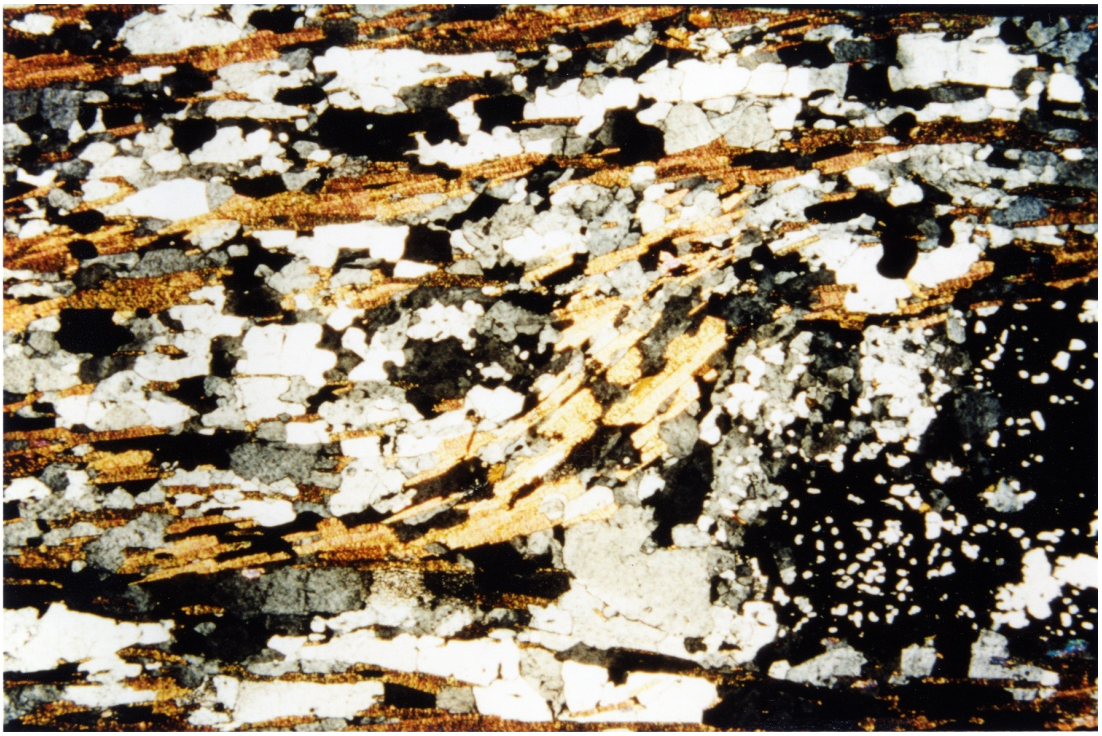

Figure 5.65 Optical photomicrograph of thin section 5-11G cut from NE95-11-VII (not shown). Note the partial development of polymineralic ribbons (see text for discussion). Shows characteristic microstructure of Jalhari granite in Diamir shear zone. Grain size is relatively fine (biotites <300 μm, quartzofeldspathic grains <400 μm). Biotite nicely picks out S and C surfaces. Sense of shear in this case is clearly dextral but note plunge of lineation (50°@350°) i.e., >50% of displacement (in present orientation) is W vergent. Cut parallel with lineation (50°@350°), perpendicular to foliation (170°/89°E). South is to left, west is to top. Base of image is 5.5 mm and parallel with main fabric. Crossed polars.

examples of these zones, the granitic gneiss shows significant sub-solidus strain, including spectacular S-C relationships and porphyroclast asymmetry both of whose sense of shear consistently indicates east side (NPHM) up and over west. Figure 5.65 is a photomicrograph of thin section 5-11G cut from sample NE95-11-VII (not shown). Lineation at the point of sample collection is 50° towards 350°. Sense of shear clearly indicates E side up (and, in this case, partly displaced towards the south). The section shows the partial development of polymineralic ribbons. If super-solidus deformation has not created a strong anisotropy or "pre-formed" the fabric (e.g., generating a strong biotite alignment that caused the subsequent growth of quartzofeldspathic grains to mimic ribbons), I might propose that this rock has deformed at 400-500°C.

In addition to ductile fabric, brittle structures include (1) highly planar, steep, W-vergent reverse faults that cut all fabrics, (2) well-developed suites of shear bands and local fault gouge horizons, often which develop preferentially in areas where brittle deformation has involved a broader zone of cataclasis as opposed to a single fracture plane, (3) narrow (10's cm) zones where hydrothermal flux has developed thick biotite accumulations, (probably late strain features) in which spectacular asymmetric folding (cm-wavelength) of the biotite layers indicates east side up and over west.

Locally in the eastern portion of the Diamir valley section through the granite, two highly stretched, constant width (10-30 cm) amphibolite sheets can be followed for >100's m in continuous outcrop. These are parallel to sub-parallel to the foliation of the deformed Jalhari granite, and, if these amphibolite sheets pre-date the granite, they seem to have taken up the W over E non-coaxial strain that characterises the Diamir Shear zone in a very homognerous manner (they are not boudined, thinnned or cut), presumably requiring a large contrast in mechanical competence both during and after intrusion of the Jalhari granite.

The eastern margin of the Jalhari granite in Diamir is marked by brittle deformation within layers/lenses of retrograde (highly chloritised) metapelite, about 500 m W of the confluence of Diamir and Lobah valleys. In Airl, there are horizons of metapelite and calc-silicate which are a few hundred metres wide. The Jalhari granite seems to be present again at Airl Gali (based upon the heavily weathered limited gneiss outcrops). The section east of Airl Gali was not mapped, but, based upon the Diamir section, the eastern margin of the granite must be close by.

In Diamir, the lenses of retrograde metapelite within the granite pass, to the east, into more typical NPHM gneisses with metre scale compositional layering (e.g. due to differing Fe-weathering & biotite content), and then to a monotonous granitic orthogneiss sequence. Foliation is N-S trending (usually steep), and lineation north plunging. There is a general E over W sense of shear where any can be observed, but the intensity of deformation is significantly lower than in the main body of the Jalhari granite in Diamir. The location of the Diamir shear zone therefore appears to approximately co-incide with the location of the Jalhari granite.

5.7.4 SW NPHM discussion and conclusions

5.7.3.1 SW NPHM cover rocks

An abrupt northward thinning of cover sequences in Southwest NPHM is evident from the width of cover in the area of Diameroi compared with that ~5 km to the south in Nashkin Gah. This thinning is orders of magnitude too large to be original depositional variation and there must be some type of tectonic excision, with about 5 km thickness of material removed. There are three possibilities.

1. Normal motion within the MMT footwall. This phenomenon is seen in SE NPHM but, based upon the lack of truncation of metamorphic isograds, magnitudes of excision are probably too low. Evidence for widespread MMT footwall normal motion was not seen in SW NPHM

2. A east over west reverse fault, sub-parallel to the Jalhari granite-gneiss shear zone, cut out the missing section. Such a fault must post-date the overturning of the MMT footwall sequences. Additionally it must be obscured by early plutonism related to the Jalhari granite. I do not favour this idea because the evidence is "hidden" behind the Diamir shear zone.

3. A frontal or lateral ramp in the original MMT gave rise to a local duplex structure with imbricated thin slices of cover (and possibly basement). This is consistent with mapping of my collaborators (Kidd, Asif Khan) in Niat Gah, to the west, where map pattern basement / cover relationships indicated to them that there are ramp structures in the original structure of the MMT.

I favour idea number three, however all remain open.

5.7.3.2 Diamir shear zone

The intense and apparently protracted strain associated with the Diamir shear zone seems to have prevailed through a number of deformation styles and to have been fundamentally involved with the Jalhari granite for a significant period of time in both the super solidus, and in the sub-solidus regimes. I therefore regard the Jalhari granite as being syn-kinematic to the Diamir shear zone. The proposal that the Jalhari granite was emplaced syn kinematically over a significant period of time is consistent with geochronologic studies. Schneider et al. (1998; submitted) conducted ion microprobe Th-Pb monazite analyses of a deformed, biotite-rich portion of the Jalhari granite collected near the village of Diameroi. This sample yielded ages between ~3 and 9 Ma from monazite grains with a notably non-uniform texture, and lack of clear core-rim zoning patterns. Texturally homogeneous grains that were analyzed however, yielded only the younger ages of 3-4 Ma. The chaotic textural pattern is indicative of a multi-stage monazite growth history (possibly protracted between 3 and 9 Ma), and is consistent with my proposal that the Jalhari granite (in the region of

Airl and Diamir) was emplaced over a period of time while being incorporated into the ongoing displacement of the Diamir shear zone, i.e., the Jalhari granite is synkinematic to the Diamir shear zone.

The amphibolite sheets that are locally present in the eastern portion of the Jalhari in Diamir are of interest. Schneider et al. (1998; in press) have shown the Jalhari granite in Diamir to be young (3-9 Ma), and yet the amphibolite sheets, if Permian, must have remained as continuous planar features during the Diamir Shear zone W over E non-coaxial strain. I offer this as evidence for young basaltc magmatism.

The Raikhot Fault is well documented, presently active NE-trending, W-vergent, reverse sense major shear zone <1 km in width that has allowed NPHM to be displaced up and over rocks to the north and west (Madin, 1986; Madin et al., 1989; Butler et al., 1992; George et al., 1996). The Diamir shear zone is a recently active, N-trending, W-vergent, reverse major sense shear zone <6 km in width that has allowed NPHM to be displaced up and over rocks to the west . I therefore propose that the Diamir shear zone forms the mechanical continuation of the main Raikhot Fault. I note that the Raikhot Fault is much narrower (<<5 km) however, and represents more focused strain

5.8 CONCLUSION FOR NPHM

Figure 5.66 is a summary cross-section for southern NPHM that shows the main findings that I have presented from Nanga Parbat.

1. There is a nice symmetry at both the west and eastern margin at the MMT; in both cases the sequence is overturned. In SW NPHM, the overturned section is ~10 km long, in SE NPHM ~25 km long. The larger portions of the strain related to NPHM uplift are close to the margin (MMT) at SW NPHM (Diamir shear zone), but

Figure 5.66

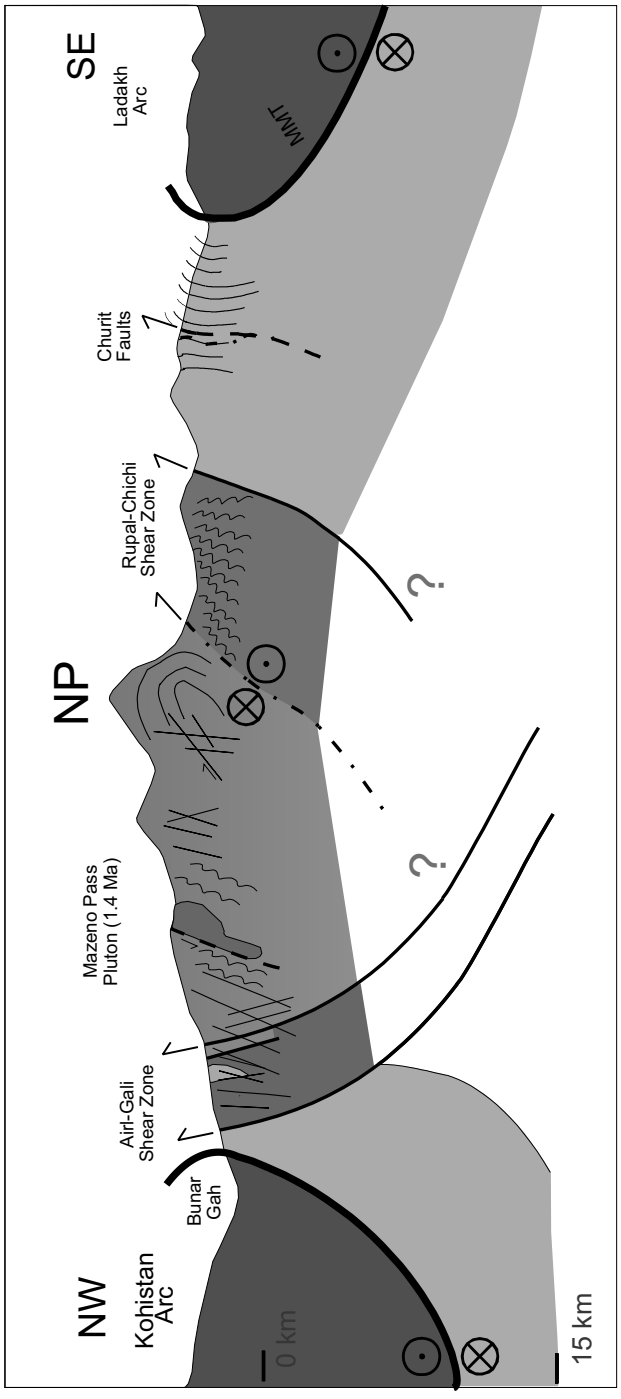

Figure 5.66 Summary cross section for Southern NPHM. Light grey: Metasedimentary cover rocks (dashed line ornament indicates foliation); crosses: leucogranite; medium grey: other gneisses; dark grey: general KLS (structurally above MMT). See text for discussion.

deeper into the massif at SE NPHM (RCSZ). Both of these shear zones are associated with plutonism over the last 10 or 15. Ma. They define a doubly-vergent local orogen (e.g., Koons, 1990) with WNW directed shortening.

2. The section in SE NPHM between the RCSZ and the MMT has been passively overturned but not reworked, and is recognisably Himalayan. The preserved Himalayan fabrics show the highest grade (Passchier and Trouw, 1996, p52) inferred for deformation seen in southern NPHM, and both Himalayan thrust and normal displacement are recorded. The equivalent section in SW NPHM has been cut by ~5 km structural thickness.

5.9 CHAPTER APPENDICES

5.9.1. Sense of shear analyses.

I include here a partial review of the sense of shear indicators in high strain rocks that have been used in this thesis. Mylonites and high strain rocks in general typically develop a strong mineral lineation (Passchier and Trouw, 1996, p103) that, in most cases, is a linear shape fabric or "stretching lineation" (single grains or aggregates of grains that are deformed and form a lineation). Occasionally the lineation can be partly a result of hinge lines of sheath folds - folds that are normal to "flow folds" (Cobbold and Quinquis, 1980). I have are cut all thin sections parallel with mineral lineation, perpendicular to main foliation (for fuller details, see tables in 5.9.3

The structures that I used as indicators of sense of shear include:

(1) *Throughgoing fabrics* including oblique foliations defined by elongated shape of grains oblique to the main (compositional) foliation or trend of C-surfaces (e.g. Means, 1981; Lister and Snoke, 1984).

(2) *Shear zones in fabric* (cleavages, surfaces or bands). C/S fabric (also C-S or S-C fabric) involves S ("schistosité") surfaces that are transected by C-surfaces (Berthé et al., 1979; Lister and Snoke, 1984). C-surfaces are discrete discontinuities (i.e. true shear zones) on which there has been some displacement, while the S surfaces are developed in response to the general shortening (Hanmer and Passchier, 1991). C'-surfaces (Berthé et al., 1979, also termed "Shear band foliation" - White et al., 1980; "asymmetrical extensional crenulation cleavage" - Platt and Vissers, 1980; and "asymmetrical extensional shear bands" - Hanmer and Passchier, 1991) typically develop at an angle of 15-30° to the shear zone margin (Passchier, 1991) and to the C-plane (more usefully for this study where the shear zone margin is frequently not seen). C'-surfaces are extensional shear zones that often develop preferentially in more foliated portions of rocks (e.g., in micaceous domains of compositionally layered gneisses), and typically anastamose around and transect portions of an older foliation giving a recognisable shear direction for the C'-surface (White, 1979; Berthé et al., 1979; Platt and Vissers, 1980; Dennis and Secor, 1987).

(3) *Porphyroclasts* (remaining grains of the parent rock within the high strain zone) typically develop characteristic shapes as they deform as stiff inclusions in a soft matrix (e.g. Hanmer, 1984; Passchier and Simpson, 1986). Dynamic recrystallisation of a feldspar grain (e.g.) by grain boundary migration (see deformation mechanisms below) will allow new fine grains to form "tails" (trails) and "wings" that form δ- (delta) σ- (sigma) and quarter structures ("mantles" of Passchier and Trouw, 1986) whose asymmetry (stair stepping) can be used to determine sense of shear (Hanmer, 1984; Passchier and Simpson, 1986; Hooper and Hatcher, 1988; Hanmer and Passchier, 1991; Passchier and Trouw, 1996). Strain shadows are areas flanking porphyroclasts (and porphyroblasts - see below) that contain a mineral(s) that is different from the porphyroclast. The asymmetry of these can be used (often in conjunction with porphyroclast wings) to determine the general overall shortening

direction for the porphyroclast or porphyroblast in question based assuming the shadows are low strain sites.

(4) Synkinematic Porphyroblasts are grains that grow in a deforming matrix. The most studied type of porphyroblast, (and the only examined in this thesis) is garnet. It has long been recognised that inclusions in porphyroblasts are incorporated in a passive manner that can be used to identify how the porphyroblast has rotated relative to the fabric of the immediate matrix in which it occurs (Zwart, 1962; Spry, 1969; Vernon, 1975; Bell, 1981). Based upon this rotation, a sense of shear can be inferred, but must not be taken for granted in the absence of a clear relationship between the shear zone reference frame and the garnet porphyroblasts reference frame (Bell, 1985).

(5) Mica "fish" (Eisbacher, 9170; Choukroune and Lagarde, 1977; Simpson and Schmid, 1983; Lister and Snoke, 1984) have their long axis in the general extension direction of the strain, trails that often stair step in the displacement direction. Additionally, they may have one side curved and one side planar affording a monoclinic symmetry that can be further used as a shear sense indicator (e.g. Lister and Snoke, 1984).

(6) *Obvious features* including strain markers (e.g., fractured grains with observable shear) can also be used to infer sense of shear. Note that care must be taken when using offsets on fractures at a high angle to the foliation (Rutter e al., 1996)

In the various high strain rocks that I have examined, I have avoided using the scheme of "type I and type II S-C mylonites" (Lister and Snoke, 1984) as this is a potentially confusing distinction between continuous (e.g. "strain sensitive simple fabrics" of Ramsay and Graham, 1970) and discontinuous fabrics (Berthé et al., 1979). I maintain the scheme of Berthé et al. (1979) where the C-surfaces/planes are required to be discrete (i.e., discontinuous) shear zones (as in the Lister and Snoke

(1984) type II mylonite) and may not be narrow zones of ductile strain as is frequently the case for C' surfaces ("shear bands" or "asymmetrical extensional shear bands" of Hanmer and Passchier, 1991 - the Lister and Snoke (1984) type I mylonite). Note that (e.g.) Passchier and Trouw (1996) discourage the Lister and Snoke (1984) "type I and type II S-C mylonites" classification based upon the usage of trails stepping off mica fish to define C-surfaces. Passchier and Trouw (1996) note that not always do such trails form by partitioning along shear bands. Where observed to be well developed in this study, however, these mica trails have commonly been developed parallel with, and in addition to, C-surfaces.

5.9.2 Deformation mechanisms inferred from microstructure

I include here a partial review of certain deformation mechanisms in quartzofeldspathic rocks to see how far history of temperature and strain can be remarked upon based upon deformation mechanisms inferred from microstructure. Preparation of thin sections used for microstructural analyses is discussed in *5.9.3.2 samples lists*.

Data from load testing experiments of both monomineralic samples (e.g., Tullis and Yund, 1985; 1991; Dell Angelo & Tullis, 1989) and granitic (i.e., quartz feldspar) aggregates (e.g., Fitzgerald and Stünitz, 1993; Stünitz and Fitzgerald, 1993) allows extrapolation of strength and temperature information. Subsequent observation of microstructures resulting from loading experiments together with naturally deformed examples (e.g., Simpson, 1985; Gapais, 1989; Pryer, 1993) has lead to a number of conclusions regarding microtextures and microstructures that characteristically develop within specific temperature ranges. The following is summarised from the previous references and from Passchier and Trouw (1996).

Above about 300°C, feldspar is thought to be brittle while quartz undergoes ductile deformation due to dislocation glide (little to no climb) and creep. This results

in uneven and patchy extinction of quartz grains. Feldspar grains commonly show the beginings of core and mantle texture. "Cores" are large (strong) porphyroclastic feldspar grains, possibly microfractured, while the "mantle" (also termed "mortar") is composed of relatively finer grains of (typically) feldspar. The finer grained feldspar mortar is derived from the porphyroclastic feldspar grains and has separated largely through grain boundary migration recrystallision in attempts to recover from dislocation tangles (these can be reduced through dislocation climb only at higher temperature; >400°C). Between approximately 400-600°C, diffusion assisted-dislocation processes in quartz are more prevalent and extensive quartz subgrain development and subgrain rotation recrystallisation operates. Passive flattening of quartz grains passes to wholesale recrystallision at higher strains and leads to very continuous monomineralic ribbons of quartz. Feldspar grains develop extensive augen/mantled porphyroclasts with finer grained feldspar also forming ribbons. Above about 600°C, quartz and feldspar show somewhat similar textures; grain boundaries may be cuspate/lobate, and diffusion creep processes (Nabarro-Herring, or "volume diffusion" and Coble, or "boundary diffusion") are thought to play a major role. Such finely-grained microtextures (e.g., 20-40μm) were not observed, however, in any of the thin sections examined from NPHM.

5.9.3. Samples and thin sections from Nanga Parbat

5.9.3.1 Samples from Nanga Parbat

All samples that I collected in Nanga Parbat are detailed in three tables (5.2, 5.3, and 5.4) for 1995, 1996, and 1997, respectively. Nomeclature is straightforward: In 1995, NE95/27-V indicates 1995, 27th (of August), 5th sample collected since begining of day. NE95/8-V indicates 1995, 8th (of September), 5th sample collected since begining of day. In 1996 and 1997, a longer field season necessitated using a term for the month; E6/10/10-I indicates 1996, 10th (of October), 1st sample

collected since begining of day. E7/9/14-IV indicates 1997, 14th of September, 4th sample collected since begining of day. Where a thin section accompanies a sample, it is listed directly below the sample name, preceded by the batch number in bold. For example, NE95/26-V **T/S1** 5/26E indicates batch number 1. All thin section names are simple versions of the field name, truncated for chip labelling procedures.

Most samples remain housed in the Albany Geology Department archives. Some samples have been given away or consumed in other labs however. These are detailed with the recipient's initials and these are included in table 5.5 - Abbreviations used in other tables.

A description of simple lithology, location and an outcrop number (or distance to a nearby outcrop number) are given (outcrop numbers also appear on the map (plate 2) and in the text). Where appropriate, elementary remarks relating to structure are made for samples that have not been thin sectioned. GPS location numbers are provided for 1996, where they exist).

5.9.3.2 Thin sections from Nanga Parbat

Approximately 75 thin sections were prepared from chips cut by me. Where the sample bears marks to allow restoration of field orientation, the chip is accordingly marked to preserve record of the orientation. Preservation in the thin section of the original sample orientation from the field is essential for sense of shear analyses. Thin sections accordingly are prepared from samples oriented in the field and subsequently cut parallel with mineral lineation, perpendicular to main foliation (see section 5.9.1 sense of shear analysis and (e.g.) figs 5.9 and 10.1 in Passchier and Trouw, 1996). A cut is made in the upper (with respect to original field orientation) part of the sample and either the top left or the top right will point towards the plunging lineation. For example, from a 45°W dipping foliation, with 30°S plunging lineation, the top left cut in the thin section will point towards 30°S perpendicular to

the 45°W dipping plane. Alternatively, if the lineation was 30°N plunging on the same plane, the cut will be in the top right of the thin section and will point towards 30°N, again perpendicular to the 45°W dipping plane.

There are two situations where the scheme must be modified:

1. In cases where foliation is near or actually vertical, there is no "upper" part of the sample (with respect to original field orientation), and I have employed a scheme I term the "overhead rule"; whereby the top of the right hand edge (TR) of the chip must point with the lineation plunge direction when the sample is viewed overhead in original outcrop orientation. This scheme cannot be used in the unique situation where foliation is truly vertical and lineation is truly horizontal, but this was not encountered.

2. In cases where the lineation is horizontal, the top of the right hand edge (TR) of the chip is kept as upper surface with respect to original dip in field (because cut is always perpendicular to foliation). This scheme cannot be used in the unique situation where foliation and lineation are both truly horizontal, but this was not encountered. Three tables of thin sections are included. Each of the tables details a particaular post-field season batch of thin sections, and in ths way is suited to be used in conjuction with the box(es) containing a particular batch. Therefore, samples from 1995 appear in all three lists, samples from 1996 appear in two lists, and samples from 1997 appear in only one list. Batches are numbered **T/S1**, **T/S2**, and **T/S3**. Thin section names are a simple form of the parent sample name (with equivalents listed in the samples tables). For example NE95/12-XII is abbreviated to 5/12L. E6/10/10-I is abbreviated to 610/10A. E7/9/14-IV is abbreviated to 79/14D. Note that NE95/8-XV is abbreviated to 5/8P (the letter P, obviously, has the 16th position in the alphabet but "O" was ommitted for clarity).

All thin sections remain housed in the Albany Geology Department archives. None have been given away.

In the thin sections tables, information from the samples tables is duplicated, and additional general microstructural notes are made for thin sections that are of interest to the specific investigations in this thesis.

Table 5.2 Samples collected in Nanga Parbat, Pakistan during 1995.

August Astor to Lower Rupal (1995) samples (**T/S** = Thin section prev. cut; **1**=1st batch, **2**=2nd batch, **3**=3rd batch)

Sample Name	Lithology	location /outcrop no	Foln / Lin	comments
26/8/95 (Astor Gorge)				
NE95/26-I	brown weath bt-sch w/ conc.	#A74	040/50W	
T/S2 5/26A	felsic lenses		(underside marked)	
NE95/26-II	brown weath grey bt-sch (f'spar poor)	near #A74	030/40W E on vert face marked	
NE95/26-III	<1mm bt in migmatitic gn altered cord. appearance	near #A75	040/55W	
NE95/26-IV	"bt-f'spar gn" migmatitic musc, bt gn (good l'some)	do	N/O	
NE95/26-V	cren bt sch w/ minor qtz? augen	50m above #A75on	175/75W	
T/S1 5/26E	poss. filled holes	climb to Doian		
27/8/95 (Astor Gorge)				
NE95/27-I	fine bt gn (some L fabric)	#A3	N/O	
NE-95/27-II	bt-sch. ±sphene(!) in th. sec.	~50m E of #A3	020/40W 30@340	
T/S1 5/27B				
NE-95/27-III	fine banded amph sch, with occ.	#8, few km B4 Astor	140/60E	
T/S1 5/27C	augen. ±gnt (<mm)	village (Ladakh)		
NE95/27-IV	"dotted" amph. f'spar gn	3 km S of #8	N/O	
NE-95/27-V	ladakh, amph. gn.	before Astor village	N/O	
T/S1 5/27E				
28/8/95 (Lwr Rupal)				
NE95/28-I	"bt-f'sp gn" (asymm. aug, gn, of	#9 Tarshing hillside	005/80W	
T/S2 5/28A	R.C.S.Z.)	(W of Churit F.)		
NE-95/28-II	"more banded"	#9 Tarshing hillside	005/85W 20@170	**!th/sec check** hand
T/S1 5/28B	asymm f'par augen in grey gn.		use O/H TR rule	spec sugg. dext!
NE95/28-III	"v. gnt rich Bt-gn."!! gnt-pelitic sch. (±amph.)greenish, weak	#9A	010/89W	

NE95/28-IV	thick brown-weath qtzof bands in S>>L bt-gn	100m on (E).	010/80E W is marked	
NE95/28-V	clear, c'bte cryllne layers in sch.	#10 (beyond gulley)	020/85W	
NE95/28-VI	cse. cryllne, white, marble	do	020/60W	
NE95/28-VII	lge ~7 mm gnt metaP	5m on (E)	010/60W & sub horiz lin	v. good dextral fr. matrix incls in gnts
NE95/28-VIII	black gnt amph. gn	10m E, nr. travertine	010/85W	
NE95/28-IX	metaP (few gnts)	#11Churit School	170/85W 18@170	good sinistral press. shad & spiral trails
NE95/28-X	metaP (cse gnts)	#11Churit School	170/85W 18@170 use O/H TR rule	sinistral
NE95/28-XI	do	50m from #10 (not 11!)	~N-S/~50-70W lin gentle to N	
T/S3' 5/28K 29/8/95 (Lwr Rupal)				
NE95/29-I	flattened (L3isW-E) v, felsic,	300m from #10	020/80E 29@022	
T/S2 5/29A	prev. migmatitic bt.gn			
NE95/29-II	streaked felsic "L" tectonite	#12	005/89E 10@005	
T/S2 5/29B				
NE95/29-III	"junior" stretched f'par gn	E of #12	020/40W 20(N)	
T/S2 5/29C				
NE95/29-IV	do	do	180/70W 10@359	
T/S2 5/29D				
NE95/29-V	metaP (cse gnts)	lowest outcrop in centre	010/85E 32@010	
T/S3' 5/29E		if Churit re-ent.	use O/H TR rule	
NE-95/29-VI	amph-sch w/ protolith banding	#13 cliff overhang	010/80W 20@005	
T/S1 5/29F	(probably) nr gnt metaP section	below Churit school	E is underside	
NE95/29-VII	amph	#13	N/O	
NE95/29-VIII	do	#14	010/85W	
NE95/29-VIIIa	postkinematic amph needles in amph. gn (Assif's mylonite)	do	020/85W	
NE95/29-IX	felsic-granitic orthogneiss	nearby #14	015/60W 41@355	
T/S2 5/29i 30/8/95 (Ghurikot)				
NE95/30-I	postkin. amph in amph sch	nr #16	040/85W	

Table 5.2 (cont.) Samples collected in Nanga Parbat, Pakistan during 1995

NE95/30-II	gnt metaP	#17	N/O	
NE95/30-III	stretched f'spar gn.	#17	020/85W 40@360 W face marked	

September Upper Rupal to Mazeno & Airl Gah (1995) samples (**T/S** = Thin section prev. cut)

Sample Name	Lithology	location /outcrop no	Foln / Lin	comments
NE95/4-I	thinly laminated bt gn / granitic	#18 1st in valley after	020 / 80W 40@200	
T/S1 5/4A	orthogn w/ strch'd late qtz	Chongra Gl.	("E" is underside)	
NE95/4-II	2 pcs (1 is float) RCSZ orthogn.	near #18	N/O	
Rupal Glacier Day (6.9.95.)				
NE95/6-I	musc, l'granitic gn poorly (fol'd)	#19	170/80W	
NE95/6-II	folded bt schist (i.e. grey gn.)	#19	010/40W 40@220	5/4B is 2"x3" slide
T/S1 5/4B	w/ ~15cm boudin of l'granite			
Mazeno base camp to high camp (7.9.95.)				
NE95/7-I	variable foliation thickness	#20	010/85W 42N, sinistr	
T/S2 5/7A	granitic orthogn.		E underside, is marked	
NE95/7-II	incr. felsic graniric orthogn w/ X cutting qtz pegmatite vein	20m over fr #20	N/O	
NE95/7-III	fine granitic orthogn (grey)	#21	N/O	
T/S2 5/7C			<from imm, float>	
NE-95/7-IV	cse asymm. augen granitic	#21 Climb to Mazeno	020/90W 50@020	
T/S1 5/7D	orthogn. (lge slide)	(side hill w/o pack)	dext, E side up	
NE95/7-V	qtz pegmatitic ±tourm. vein	#21	N/O (plane 100/70S)	
[7.9.95.]	(fine grained, grey l'gr)	nearby #21 (Float)	N/O (Float)	
After Mazeno high camp (8.9.95.)				
NE95/8-I	cse, asymm augen granitic	#22 Just above	005/70E 30@005	sinistral; W-side up
T/S1 5/8A	orthogn, cut by fine grained l'gr	Maz High Camp	dyke: 060/30SE	
NE95/8-II	Sample outcrop: Each of above **and** X-cutting peg bt-qtz vein	do	vein 100/85S	
NE95/8-III	Coarser tourmaline Horiz in l'gr	300m on (fr. #22)	N/O	
T/S3 5/8C				
NE95/8-IV	**MISSING**! ("bt-gn")	200m on, still	080/60N	

Table 5.2 (cont.) Samples collected in Nanga Parbat, Pakistan during 1995

NE95/8-V	odd mix, cse-fine pegmatite to l'gr (1-3cm patches)	#23			
NE95/8-VI	uneven fol'd gran. orthogn	do	030/50W 55(N)		
T/S2 5/8F					
NE-95/8-VII	weath. bt-sch	At Mazeno Pass	050/80NW 20@050		
T/S1 5/8G			sinist. W side up		
NE95/8-VIII	mix: uneven fol'd gr. orthogn &	do	050/55Nn 18@020		
T/S2 5/8H	intermix l'gr (not migmatite)				
NE95/8-IX	Mazeno Pass **Leucogranite**	do	N/O		
NE95/8-X	sl. coarser Mazeno **l'gr**	100m down from Pass	N/O		
NE95/8-XI	v greenish **leucocratic** intrusive w/ chlorite slickenfibres	200m down from Pass	N/O		
NE95/8-XII	sl. coarser greenish **l'gr** w/ slicks	300m down from Pass	N/O		
NE95/8-XIII	crumply (bt) granitic orthogn.	#24 At foot of "cliff"	060/89W 55(N)		
T/S2 5/8M					
NE95/8-XIV	v.black crumply bt gn (orthogn)	#25 L.B (SW side) of Glacier @4600m			
NE95/8-XV	crumply bt gn (fine asymm.	#25 L.B. (SW) side of	095/60N 60@005	sinist, top to S	
T/S1 5/8P	augen) (*NB P=XV, here*)	Lobah Glacier	S marked, arrow to W		
NE95/8-XVI	bt, musc, cse qtz vein	do	N/O		
NE95/8-XVII	crumply bt-gn w/ qtz aug tension	do	090/60W 60@360		
T/S3 5/8Q	gashes sugg top to NW!				
To Airl Gah camp (11.9.95.)					
NE95/11-I	(3pcs) amph, fine-gr. gn. & uneven bandwith gn.	Gashit camp site; 200m W of #AR1	030/vert		
NE95/11-II	fine-gr bt-gneiss	Near Gashit Fold; 200m E of #AR1	179/50E 30@035		
T/S2 5/11B					
NE95/11-III	gn. w/ uneven f'par sizes	do	170/50E		
NE-95/11-IV	v. granitic gn w/flattened bt planes giving sinistral? SoS	few 100m into granite - E of #AR	160/vert (25@160 - calc'd post field)		
NE95/11-V	V, granitic. rel high strain,	further up Airl Gah;	170/85W 35@350	dext, E side up	
T/S1 5/11E		500m E of #AR5	use overhead view		

Table 5.2 (cont.) Samples collected in Nanga Parbat, Pakistan during 1995

NE95/11-VI **T/S2** 5/11F	blotchy bt-granite (aka Jalhari)	100m further east	N/O	
NE95/11-VII **T/S2** 5/11G	porph granitic gn w/ good C/S	150m further east	170/vert (50@350 - calc'd post field)	dext, E side up
NE95/11-VIII	porph granitic gn w/ scrappy S/C	Upper Airl Gah; 300m W of #AR6	??? Prob 170/vert (55@170 - calc'd after)	
To Airl Gali (12.9.95.)				
NE95/12-I	well fol'd gr. orthogn. w/ C/S	200m W of #AR6	175/75E 40@005	
NE95/12-II **T/S1** 5/12B	bt-sch w/ irreg. f'spar augen (bt-rich "laths")	200m E of #AR6	010/65E 20@035	
NE95/12-III	v. granitic, non-fol'd ("Jalhari")	400m E of #AR6	010/65E 20@035	
NE95/12-IV **T/S2** 5/12D	fine-gr bt sch/gn.	20m before Airl Gali (#AR8)	nearest lin: 32@078	
NE95/12-V	well fol'd, mm-porh. gr. orthogn. later buckled	200m W of #AR8	030/40E hinge: 50@060	
NE95/12-VI **T/S1** 5/12F	greeny calc silicate nr local hinge zone	50E of #AR7 (not common)	170/30E 40@068?	
NE95/12-VII **T/S2** 5/12G	gr. orthogn. w/ good S/C	Jalhari in Airl Gah; 400m W of #AR7	jointing: 170/60E	
NE95/12-VIII **T/S2** 5/12H	"pelitic/felsic sch.	200m E of AR6	070/35E 30@040	Occurs as lenses or bodiesl in Jalhari
NE95/12-IX **T/S2** 5/12H	amphibolite. note v. green min in contact w/ sch (part of above)	same outcrop as above **note scheme irregularity*	N/O *thin sec misnamed 5/27H*	
NE95/12-X	noteably higher strain orthogn but w/greenish hue!	Just W of #AR6	not outcrop	
NE95/12-XI	much odd bt in Jalhari	Few 100m W of #AR6	170/30E	
NE95/12-XII **T/S2** 5/12L	less odd bt in gr. fòln is defined by mm bt "pancakes"	lJalhari granite zone, ~500m W of #AR6	170/vert	
NE95/12-XIII	v dense bt "pancakes" in grantic gn	do		

Table 5.2 (cont.) Samples collected in Nanga Parbat, Pakistan during 1995

Table 5.3 Samples collected in Nanga Parbat, Pakistan during 1995.

1996

June / July samples 1996

Sample Name	Lithology	location /outcrop no	Foln / Lin	lat/long +/or outcrop no.
E6/6/18-I	asymm. augen bt-orthogn.	1st Rupal sidevalley after Chongra Gl.	060 / 89E 40@240 ("N" is ENE)	#18
E6/6/18-II	do	do	020 / 65W 55@250	do
E6/6/18-III	"qtzite"! boudin in bt-orthogn.	do	040 / 50W 30@248	do
E6/6/18-IV	bt-augen gn.	do	040 / 80W 50@238	do
T/S3 66/18D				
E6/6/21-I	mm streaky f'pathic grey gn	Rama RB, B4 glacier	120/56 30@160	1 km E of #RL71
T/S3 66/21A				
E6/6/25-I	Cse & fine gnt sch. (cf Churit)	Indus, W of Stack F.	040 / 50S	
E6/6/27-I	minor gnt in amphibolite	MMT, E Astor Gge	010 / 65W 12(N)	1.5 km N of #8
T/S2 66/27A	(marked: 160 / 30 E)			
E6/6/27-II	20m on, (marked: 010 / 58 E)	do	do	do
T/S2 66/27B				
E6/6/27-III	20m on, (marked: 010/ 80 E)	do	do	do
E6/6/27-IV	bt w/ cse gnt, foln plane marked	do	170 / 89E 15(N)	do
T/S2 66/27D				
E6/6/27-V	fine grained "lath unit"	W. of E. margin of Astor Gorge	060/38S 14N	300m W of #71
T/S2 66/27E				
E6/6/30-I	(bt - rich portion) bt-orthogn.	Tarshing local hill	020 / 80W 40S	700m W of #9
E6/6/30-II	asymm. augen bt-orthogn.	100m E along hillside	020 / 90W	600m W of #9
E6/6/30-III	asymm. augen bt-orthogn.	Still E (after 1st gnt)	020 / 85W 55S	500m W of #9
E6/7/1-I	asymm. augen (rich)-orthogn.	1st Rupal sidevalley after Chongra Gl.	038 / 50N 40@240	#18
(II not taken)				
E6/7/1-III	granitic: cm isoclinal felsic layer	do	N/O	do
E6/7/2-I	do	Chichi Nala (before 1st day lunch stop)	030 / 50N 40@250 marked foln: 080 / 50S	#C1
E6/7/3-I	fine grained bt-orthogn?	sinistral, W-down loc. in Chichi Nala	130 / 38S 38@215 marked line: 060 / 38	#C3
T/S2 67/3A				

E6/7/3-II	sandy-"granitic" metaseds	top of Chichi near lunch & shaving stop	160 / 30 W 28@217 marked foln: 020 / 40E	#CC5
E6/7/5-I	actin. sch. w/ post-kin. amphib.	"by Assif's mylonite	N-S buckled.	#14
E6/7/5-II	cse gnt amph. *in* metaP.	cascading folds	do	#13
E6/7/5-III	gnt psammite	do	do	do
E6/7/5-IV	gnt, fine-gr, grey gn. w/ rare str, f'spar	across Churit F.	018 / 68W 18N	#12
E6/7/5-V	v. str f'spar gn. w/ mig. layers	50m along (W)	004 / 82E 16N	50m W of # 12
"Astor East" **T/S2** AS/E	"lath unit"	Eastern Astor		0-500m W of #71
Sept. / October samples				
Sample Name	Lithology	location /outcrop no	Foln / Lin	lat/long or GPS
E6/9/20-I	white "gnt" in Ladkh gnt-amph-bt-sch.	Ghurikhot (left trib.)	170 / 78W 33@347	35o16.4'N 74o48.8E (G40)
E6/9/20-II	gnt-amph. in meta P.	do	030 / 37W 22@003	35o16.61 74o48.49
E6/9/21-I	bt-amph-schists of cascade folds	Cascade folds of S side (r.b.) Lwr Rupal	178 / 89W 32N	35o12.97 74o47.5 outcrop #51
E6/9/21-II	gnt-amph. meta P. Not oriented	"churit F" on S side	N/O (015 / 81W)	500m W of #50
E6/9/24-I	chloritic schist (Ladkh)	Near Rattu checkpoint	004 / 87W 40N	#52 (GPS # 43)
E6/9/24-II	v. def'd, retrogr? gneiss	betw Churit & Tarsh.	012 / 87W	1 km E of #9
E6/9/25-I	pcs of poss cord melt segr	Rupal Vill. deep valley	N/O	#18A
E6/9/25-I	very green poss. cord. melt segr	do	N/O	do
E6/9/26-I **T/S3** 69/26A	C/S poor, granitic orthogn	Polish Base Camp, l.b. of Bezhin Gl	083 / 73S 44W	#48 (also GPS #48)
E6/9/27-I	thin bt f'spar gn.	Tapp meadow local	172 / 46W 22@320	35o11.8 74o36.4
E6/9/27-II	incr. f'spar gn	r.b. of U.Rupal before Shigiri Village	float	
E6/9/27-III **T/S2** 69/27C	incr. bt gn	do	143 / 81W 30N	GPS #49 (49a)
E6/9/27-IV **T/S2** 69/27D	lwr grade bt-gneiss	Shigiri Village	039 / 62W 36N	
E6/9/27-V	Amphibolite dyke	do	horiz, S-dipping	

Table 5.3 (cont.) Samples collected in Nanga Parbat, Pakistan during 1996

E6/9/28-I **T/S2** 69/28A	granitic orthogneiss	Shaggin Gl mouth l.b.	031/70E 50S	# CR 52 (GPS #52)
E6/9/29-I	old favourite bt orthogn.	Campsite above Shigiri on Rupal Gl. l.b.	023 / 54NW 54S	#Sh 1
A1 to A4 (all 29.9.96.) (all sent to CPC)	A1, A2: amphibolite A3: bt schist A4 gnt, bt sch	"steep hill" above pond & Zeitler camp of 1995	N/O N/O	#Sh 2
E6/9/29-II	banded gn. late, inj asymm folds	sandy corner on trail to Mazeno base camp	037 / 49N 14@348	#Sh 3
E6/9/29-III	hb needles & gnt - amph.gn.	Freiburg's back valley	050 / 24N 22@332	300 m N of #Sh 3
E6/9/30-I **T/S2** 69/30A	L-tectonite of boudins / pods	Uppermost Rupal Gl	048 / 89E 24S marked is 035 / vert.	#56 & #57 GPS same
Mazeno Top 5358m	Leucogranite (E610/1A) ~8 kg; 2 pcs	At Mazeno Pass	n/a	nearest is Mazeno high camp #61
E6/10/6-I	l'gr dyke ±tourmln intr amph gn	W. margin on Astor R.	N/O (to DAS)	
E6/10/7-I **T/S3** 610/7A	Streched f'spar gn w/ gnt!	Rama l.b. near Rest Ho.	159 / 33W 7@332	#62 GPS same
E6/10/7-II	"lath unit" (pematitic gn?)	do	018 / 27E 11@160	do
E6/10/8-I	mig-bt-gn.	Upper Gurikhot, W. of "Churit F."	158 / 58W 10@336 Underside (marked) E	#69, GPS same
E6/10/9-I **T/S3** 610/9A	green spotted / banded felsic amph gn	Ladakh at foot of Bulan Gah	160 / 55E 32N marked is E	#70 GPS same
E6/10/9-II	green amph gn	(at contact w/ meta P)	010 / 52W no lin.	500 m W of #70
E6/10/10-I **T/S2** 610/10A	stretched f'spar gn. "angel hair"	Dichil Glen LB, S side-across "Dichil Pass"	076 / 53W 32N underside marked	1.5 km E of #73
E6/10/10-II	def'd leucogranite (intruded parallel to fóln)	nearer Dichil Pass	N/O	500m E of #73
E6/10/10-III **T/S2** 610/10C	mm-feldspar banded bt-sch.	at pass	160 / 80E 42N	#73
E6/10/10-IV **T/S2** 610/10D	gnt-mig-amph dyke	Dichil Bridge	N/O	
E6/10/10-V	do	Dashkin synform	N/O	1 km SE of A711
E6/10/10-VI **T/S2** 610/10F	bt-amph gn	do	N/O	

Table 5.3 (cont.) Samples collected in Nanga Parbat, Pakistan during 1996

Table 5.4 Samples collected in Nanga Parbat, Pakistan during 1995.

1997 (4.7.97. to 19.7.98.)

July samples (field days with Bill Kidd and Asif Khan)

Sample Name	Lithology	location /outcrop no	Foln / Lin	Notes
E7/7/4-I	(3 pcs) marble & amph	W'most Indus ("cover")	N/O	
"Rama Tuff"	tuff (sampled 6.7.97.)	Upper Rama l.b. #R3	143/18NW 7@006	
E7/7/6-I	v granitic banded gneiss	Rama l.b. furthest point #R5	(prob.) 152/38W	
E7/7/7-I	deformed angel hair U.	#71 l.b. E. Astor, opp footbridge w/ casc. folds on r.b.	310/50N	
E7/7/7-II	non-porph (incr. strain?) of above w/mm banding	do (50m W of #71 l.b.)	005/38W	
E7/7/7-III	further incr. strain of above	do (80m W of #71 l.b.)	001/49W 3@001	
E7/7/7-IV	mm-layered pale gneiss	imm. B4 bridge @ river bed (from Astor vill.) #H1	042/43NW	
E7/7/7-V	myl? stretched pelite gn w/gnt	imm. B4 Luskum cafe #H2	077/60W 41N marked 320/60N	
E7/7/7-VI	mm-grainy porph gn	do	??	
E7/7/10-I	S-C in qtz'f'pthic unit-2 in	Niat Gah MMT h.w. #N71	012/49W 49@244	
T/S3 77/10A	Kamila			
"Niat cover"	<4mm gnt metaP	Niat after bridge (200m W of #N72		
Nt-3	fol'd peg body (to DAS)	Niat, B4 Chukawai moraine #N74	N/O	
Nt-4	bt-sch (to DAS)	near bridge? 100m W of #N72	N/O	
E7/7/12-I	gnt metaP (to NBWH)	lower Airl Gah 100m W of #AR1	178/68W	
E7/7/12-II	do (to NBWH)	#AR1	142/71E	
E7/7/12-III	qtz peg. in grey gn.	100m E of #AR1		
E7/7/12-IV	gnt metaP (±chloritic) NBWH	do		

E7/7/13-I	gnt pelitic "mylonite"	start of Nashkin Gah #BA1	005/41W	
E7/7/13-II	stretched porph. gn.	central spine hill betw. Nashkin & Airl #BA2	017/71W	01S (dext?)
E7/7/15-I	porphyritic unit (part of Jalhari gr?)	Above Rollo camp #P6	171/51W	33N
E7/7/16-I	Jalhari Granite (to DAS)	Above Phailobat #PL1	161/56W	42@181
E7/7/16-II	do (finer grained for monazite)	50m N of #PL1	N/O	
E7/7/16-III	do	100m N of #PL1	N/O	
E7/7/16-IV	felsic "blasts" in pred. bt pelite	#P5 (br. below Phailobat)	179/29W	21@217
T/S3 77/16D				
E7/7/17-I	metaP	tricky crossing nr. confluence below Garrol; #P45	152/60W	26@308
no name	bi peices for Schneider	100m N of #P45		
E7/7/19-I	"retrogr." metaP outboard Jalhari	#D11 (nr. Zangot)	170/80E	
E7/7/19-II	Jalhari (between metaP layers)	100m W of #D11	175/80E	
E7/7/19-III	W'ern flattened 'Jalhari'	Diamir, #D9	180/vert	
E7/7/19-IV	"typ. Jalhari" (1kg sample)	Diamir, #D5	N/O	
E7/7/19-V	def'd, more porphyriric Jalhari	do (nr. bt. hydroth s.z.)	180/80E	80@270
T/S3 77/19E				
E7/7/19-VI	flattened, odd bt w/cse felsic bit	Diamir, #D3	160/70W	50N
T/S3 77/19F				

Table 5.4 (cont.) Samples collected in Nanga Parbat, Pakistan during 1997

(5.9.97. to 27.7.97.)

September samples (field days with Schneider, Grenoblaise & Nano)

Sample Name	Lithology	location /outcrop no	Foln / Lin	lat/long or GPS or notes
Deosai	7 Schneider Deosai samples	2nd&3rd Sept.		
E7/9/5-I	dioritic body	nr Satporo granite @ checkpoint N of Deosai	N/O	
E7/9/6-I	leucogranite	Deosai "campsite"	N/O	
E7/9/6-II	granodiorite	W of Deosai, nr. first outcrop w/Schneider	N/O	
E7/9/7-I	v felsic gneiss (sandy)	furthest up Dichil tributary l.b.#74D (w/Pecher)	N/O	
E7/9/7-IIa & b	several pieces of amph. and large piece of marble	do	N/O	
E7/9/8-I	musc in peg. X-cut amphibolite gn (to DAS)	furthest point up Dichil #74G	N/O	
E7/9/8-II	Dichil Lath unit (5kg?) (to DAS)	below Dichil campsite #74B		
E7/9/13-I	bt from peg. X-cut L-orthogn. (to DAS)	Shaggin Gl. l.b. #CR52		
E7/9/13-II	S.o.S. fabric in gran. orthogn. (5 kg sample)	further up Shaggin Gl. l.b. 1 km S of #CR52	179/74W 35S	photo 27
E7/9/13-III **T/S3** 79/13C	altered?? L/Sorthogneiss	SW Rupal corner #CR52B	surface 040/70W main:062/68S 60S	Below debris-throwing edge of Rupal r.b. #2 Gl.
E7/9/14-I **T/S3** 79/14A	1-2mm gnt grey orthogn.	W'most Rupal (Toshain) #56	032/62NW 35S	
E7/9/14-II	Dm L-tectonised X-cutting pod (to DAS)	do	plane markered 130/70	
E7/9/14-III	aligned t'maline 1m peg.	opposite (N) side of gl. #T2	N/O	
E7/9/14-IV **T/S3** 79/14D	poss. cord 3cm peg	do	N/O	

Table 5.4 (cont.) Samples collected in Nanga Parbat, Pakistan during 1997

E7/9/15-I	l'cratic x-cutter	up on Shagiri Gl. r.b.	!float in glacier	
E7/9/16-I	marble & h/b rich layer	Hanging Lake Gl. r.b.	152/58E no lin visible	
T/S3 79/16A	**Alert!** (*T/S-labelled 19/16A*)			
E7/9/20-I	gnt-bt-sch w/sinistral pressure shadows	inside Chichi #1 Gl l.b. 750m E of #CC5A	020/80N (underside)	
E7/9/20-II	RCSZ gr. orthogn.	highest Chichi #1 Gl l.b. #CC5A	110/50N 29@270	W-side up, dext (note overturned)
E7/9/21-I	v. granitic layer in gneisses (to DAS)	Chichi #2 Gl. r.b. #CC5B	018/44E	
E7/9/21-IIa	marb & amph pair in cover	upper Chichi #CC5C	N/O	
E7/9/21-IIb			hinge 18@216	
E7/9/21-III	lge gnt-bearing leucogranite (to DAS)	uppermost Chichi 500m SW of #CC5C	N/O	
E7/9/21-IV	bt-sch (for DAS)	do	N/O	
E7/9/22-I	RCSZ orthogn	Chichi r.b. opp. Abadidas	120/70N (marked) 018/53W 29@195	dextral
E7/9/26-I	crumpled granitic orthogn	200m above Zangot #Z1 in Diamir	025/77E	
E7/9/26-II	fine grained gr. orthgn.	#Z2 further up Diamir	019/69E	
E7/9/26-III	chunky f'spar bt-gn.	few 100m into Diamir Gl r.b. valley	044/87W (local buckle)	
E7/9/26-IV	gr orthogn	@Gajal (nr. base camp) #Z3	318/35E 28N	
T/S3 79/26D				
E7/9/27-I	v. weath. fine grained gn.	#Z4 above base camp	N/O	
E7/9/27-II	Fe-stained gr. orgthogn. (a la	Terminal moraine B4	023/83E 55N	
T/S3 79/27B	base of Mazeno Pass cliff	base camp		

Table 5.4 (cont.) Samples collected in Nanga Parbat, Pakistan during 1997

Table 5.5 Abbreviations used in other tables

amph	amphibolite/-itic
asymm.	asymmetric/-al
B4	before
br./Br.	bridge
bt	biotite
casc	cascading
cse	coarse
cord.	cordierite/-itic
defd	deformed
do	ditto (as above)
F.	fault
f'spar	feldspar
f'pathic	feldspathic
fol'd	foliated
foln	foliation
Gge/G.	Gorge
Gl./gl.	glacier
gn	gneiss
gnt	garnet
gr	granite
hb	hornblende
imm	immediately
intr.	intrusive/-ding
kin.	kinematic
ky	kyanite
lgr	leucogranite
l'cratic	leucocratic
l.b.	left bank
loc	location
Maz.	Mazeno
metaP	metapelite
mu	muscovite
myl	mylonite/-itic
N/O	not oriented
nr.	near
pcs	pieces
peg	pegmatite
porph	porphyroclastic
poss.	possible
prob.	probably
qtzite	quartzite
r.b.	right bank
s.z.	shear zone
sch	schist
segr.	segregated
slicks	slickenfibres/-sides
staur	staurolite
v.	very
vert	vertical
vill.	village
W'ern	western (also N,S & E)
W'most	westernmost (also N, S & E)
w/	with

Persons receiving samples

CPC	C. Page Chamberlain
DAS	D.A. Schneider (geochronologist)
NBWH	Nigel B.W. Harris

Acronyms used throughout thesis

DCF	Dzong Chu Fault
DEM	Digital Elevation Model
HHC	High Himalayan Crystalline
KLS	Kohistan Ladakh Series
MBT	Main Boundary Thrust
MCT	Main Central Thrust
MMT	Main Mantle Thrust
NPHM	Nanga Parbat Haramosh Massif
RCSZ	Rupal Chichi Shear Zone
STDS	Southern Tibet Detachment System
TM	Thematic Mapper
YGRS	Yadong Gulu Rift System

CHAPTER SIX

REFERENCES

Anczkiewicz, R., Burg, J.-P., Meier, M., Oberli, F., Vance, D., Dawood, H., Hussain, S., Chaudhry, M. N. and Ghazanfar, M., 1997. Tectonometamorphic evlution of the Indus suture viewed by structural and isotopic data. *in* Angiolini, L., et al. eds., 12th Himalaya-Karakoram-Tibet Workshop - Abstract Volume, Accademia Nazionale dei Lincei., 3-4.

Armijo, R., Tapponnier, P., Mercier, J. L. and Tangling, H., 1986. Quaternary extension in southern Tibet: field observations and tectonic implications. J. Geophys. Res., 91: 13803-13872.

Bard, J.-P., 1983. Metamorphism of an obducted island arc: an example of the Kohistan sequence (Pakistan) in the Himalayan collided range. Ea. Plan. Sci. Lett., 65: 133-144.

Bard, J.-P., Maluski, H., Matte, P., Proust, F., 1980. The Kohistan sequence: crust and mantle of an obducted island arc. Geol. Bull. Univ. Peshawar, Spec. Issue. 13: 87-94.

Behrmann, J. H. and Mainprice, D., 1987. Deformation mechanisms in a high-temperature quartz mylonite: evidence for superplastic flow in the lower continental crust. Tectonophysics, 115: 101-129.

Bell, T. H., 1981. Foliation development - the contribution, geometry and significance of progressive bulk inhomogeneous shortening. Tectonophysics, 75: 273-296.

Bell, T. H., 1985. Deformation partitioning and porphyroblast rotation in metamorphic rocks: a radical reinterpretation. J. Metam. Geol., 3: 109-118.

Berthé, D., Choukroune, P. and Jegouzo, P., 1979. Orthogneiss, mylonite and non-coaxial deformation of granites: the example of the south Armorican shear zone. J. Struct. Geol., 1: 31-42.

Block, L. and Royden, L. H., 1990. Core complex geometries and regional scale flow in the lower crust. Tectonics, 9: 557-567.

Brodie, K. H. and Rutter, E. H., 1985. On the relationship between deformation and metamorphism, with special reference to the behaviour of basic rocks. *in* Thompson, A. B. and Rubie, D. C., eds., Metamorphic reactions, kinetics, textures and deformation. Springer-verlag, New York, 291 pp.

Brown, M and Rushmer, T., 1997. The role of deformation in the movement of granite melts: views from the laboratory and the field. *in* M. Holness, ed., Melt segregation and metamorphic fluid transport. Mineral. Soc. Ser., Chapman and Hall, London.

Brozovic, N., Burbank, D. W. and Meigs, A. J., 1997, Climatic limits on landscape development in the northwestern Himalaya. Science, 276: 571-574.

Brun, J.-P. and Van Den Driessche, J., 1994. Extensional gneiss domes and detachment fault systems: structure and kinematics. Bull. Soc. geol. France, 165: 519-530.

Brun, J.-P., Sokoutis, D. and Van Den Driessche, J., 1994. Analogue modelling of detachment fault systems and core complexes. Geology, 22: 319-322.

Burbank, D. W., Leland, J., Fielding, E., Anderson, R. S., Brozovic, N., Ried, M. R. and Duncan, C., 1996. Bedrock incision, rock uplift and threshold hillslopes in the northwest Himalayas. Nature, 379: 505-510.

Burchfiel, B. C. and Royden, L. H., 1985. North-South extension within the convergent Himalayan region. Geology, 13: 679-682.

Burchfiel, B. C., Chen, Z., Hodges, K. V., Yuping, L., Royden, L. H., Changrong, D. and Jiene, X., 1992. The south Tibetan detachment system, Himalayan Orogen: Extension contemporaneous with and parallel to shortening in a collisional mountain belt. Geol. Soc. Am. Spec. Pap., 269.

Bureau of Geology and Mineral Resources of Xizang (Tibet) Autonomous Region, 1993. Regional geology of Xizang (Tibet) Autonomous Region. People's Republic of China Ministry of Geology and Mineral Resources, Geological Memoirs, ser. 1. vol. 31, Beijing, 707 pp.

Burg, J.-P., Brunel, M., Chen, G. M. and Liu, G. H., 1981. Deformation of the leucogranites of the Crystalline Main Central Thrust sheet in southern Tibet (China). Mitt. Geol. Eidgen. Techn. Hochs. Univ. Zürich, Neue Folge, 239a: 49-51.

Burg, J.-P., Maurin, J.-C., Nievergelt, P., Oberli, F., Seward, D., Diao Zhizhong, Davy, P., Meier, M., 1997, The Namcha Barwa syntaxis (SE Tibet): a deeply eroded crustal antiform. *in* Angiolini, L., et al. eds., 12th Himalaya-Karakoram-Tibet Workshop - Abstract Volume, Accademia Nazionale dei Lincei., 15-16.

Burg, J.-P., Davy, P., Oberli, F., Nievergelt, P., Maurin, J.-C., Seward, D., Diao Z.-Z. and Meier, M., 1997. Subgranulite facies rocks exhumed during crustal folding

in the Namche Barwa antiformal syntaxis (SE Tibet). Terra Nova, 9 (1) EUG Abstract vol. supplement, 342.

Burg, J.-P., Chaudhry, M. N., Ghazanfar, M., Anczkiewicz, R. and Spencer, D., 1996. Structural evidence for back sliding of the Kohistan arc in the collisional system of northwest Pakistan. Geology, 24: 739-742.

Burg, J.-P., Brunel, M., Gapais, D., Chen, G. M. and Liu, G. H., 1984. Deformation of the crystalline Main Central Sheet in southern Tibet (China). J. Struc. Geol., 6: 535-542.

Burg, J.-P. and Chen, G. M., 1984b. Tectonics and stuctural zonation of southern Tibet, China. Nature, 311: 219-223.

Burg, J.-P., 1983. Tectogénèse comparée de deux segments de chaîne de collision: le Sud du Tibet (suture du Tsangpo); la chaîne hercynienne en Europe (suture du Massif-Central) [Ph.D. thesis]: Université Montpellier, France, 386 pp.

Butler, R. W. H., and Prior, D. J., 1988a, Anatomy of a continental subduction zone the Main Mantle thrust in Northern Pakistan. Geol. Rund., 77: 239-255.

Butler, R. W. H., and Prior, D. J., 1988b, Tectonic controls on the uplift of the Nanga Parbat Massif, Pakistan Himalayas. Nature, 333: 247-250.

Butler, R. W. H., and Prior, D. J., and Knipe, R. J., 1989. Neotectonics of the Nanga Parbat syntaxis, Pakistan, and crustal stacking in the northwest Himalayas. Ea. Plan. Sci. Lett., 94: 329-343.

Butler, R. W. H., George, M. T., Harris, N. B. W., Jones, C., Prior, D. J., Treloar, P. J. and Wheeler, J., 1992. Geology of the northern part of the Nanga Parbat

massif, northern Pakistan, and its implications for Himalayan tectonics. J. Geol. Soc. Lond., 149: 557-567.

Butler, R. W. H., Harris, N. B. W., and Whittington, A. G., 1997. Interactions between deformation, magmatism, and hydrothermal activity during active crustal thickening: a field example from Nanga Parbat, Pakistan Himalayas. Min. Mag., 61: 37-52.

Caby, R., Pêcher, A. and Le Fort, P., 1983. Le grand chevauchement central himalayen: nouvelles donnés sur le métamorphisme inverse á la base de la dalle du Tibet. Rev. Geol. Dynam. Geog. Phys., 24: 89-100.

Chamberlain, C. P., Zeitler, P. K., and Jan, M. Q., 1989, The dynamics of a crustal suture in the Pakistan Himalaya. J. Met. Geology, 7: 135-149.

Chamberlain, C. P., Jan, M. Q., and Zeitler, P. K., 1989. A petrologic record of the collision between the Kohistan island-arc and Indian plate, NW Himalayas, *in* Malinconico, L. L. and Lillie, R. J., eds., Tectonics of the Western Himalayas, Geol. Soc. Am. Spec. Pap., 232: 23-32.

Chamberlain, C. P., Zeitler, P. K., and Erickson, E., 1991, Constraints on the tectonic evolution of the northwestern Himalaya from geochonologic and petrologic studies of Babusar Pass, Pakistan. J. Geol., 99: 829-849.

Chamberlain, C. P., Zeitler, P. K., Barnett, D. E., Winslow, D., Poulson, S. R., Leahy, T. and Hammer, J. E., 1995. Active hydrothermal systems during recent uplift of Nanga Parbat, Pakistan Himalaya. J. Geophys. Res., 100: 439-453.

Chamberlain, C. P., and Zeitler, P. K., 1996. Assembly of the crystalline terranes of northwestern Himalaya and Karakoram, northwestern Pakistan. *in* Yin, A. and

Harrison, T. M., eds., The Tectonics of Asia: Cambridge Univ. Press, 138-148.

Chang C. and 15 others, 1986. Preliminary conclusions of the Royal Society - Academica Sinica 1985 geotraverse of Tibet, Nature, 323: 501-507.

Chaudhry, M. N. and Ghazanfar, M., 1987. Geology, structure and geomorphology of the Upper Kaghan Valley, northwest Himalaya, Pakistan. Punjab. Univ. Geol. Bull., 22: 13-57.

Chaudhry, M. N. and Ghazanfar, M., 1990. Position of the Main Central Thrust in the tectonic framework of the Western Himalaya. Tectonophysics, 174: 321-329.

Choukroune, P. and Lagarde, J.-L., 1977. Plans de schistosité et déformation rotationelle: l'exemple du gneiss de Champtoceaux (Massif Armoricain). C. R. Acad. Sci. Paris, 284: 2331-2334.

Cogan, M. J., Nelson, K. D., Kidd., W. S. F., Changde, W. 1998. Shallow structure of the Yadong-Gulu Rift, southern Tibet, from refraction analysis of INDEPTH common midpoint data. Tectonics, 17: 46-61.

Coleman, M. and Hodges, K., 1995. Evidence for plateau uplift before 14 Myr ago from a new minimum age for E-W extension. Nature, 374: 49-52.

Coleman, M. E., and Parrish, R. R., 1995. Constraints on Miocene high-temperature deformation and anatexis within the Greater Himalaya from U-Pb geochronology: Eos (Trans. Am. Geophys. Un., 75: 708.

Coward, M. P., 1985. A section through the Nanga Parbat syntaxis, Indus valley, Kohistan. Geological Bulletin of the University of Peshawar, 18, 147-152.

Coward, M. P., Windley, B. F., Broughton, R. D., Luff, I. W., Petterson, M. G., Pudsey, C. J., Rex, D. C. & Khan, M. A., 1986. Collision tectonics in the NW Himalayas. In: Coward, M. P. and Ries, A. C., eds., Collision Tectonics. Geol. Soc. London. Spec. Pub. 19: 203-219.

Coward, M. P., and nine others, 1988. Folding and imbrication of the Indian crust during Himalayan collision. Phil. Trans. Roy. Soc. London, A326: 89-116.

Craw, D., Chamberlain, C. P., Zeitler, P. K., and Koons, P. O., 1997. Geochemistry of a dry steam geothermal zone formed during rapid uplit of Nanga Parbat, northern Pakistan. Chemical Geol. 142: 11-22.

Craw, D., Koons, P. O., Winslow, D. M., Chamberlain, C. P., and Zeitler, P. K., 1994, Boiling fluids in a region of rapid uplift, Nanga Parbat massif, Pakistan, Ea. Plan. Sci. Lett., 128: 169-182.

Crenna, P.A., 1995. Late Cenozoic tectonics of the Yubari fold and thrust belt of central Hokkaido and implications for opening of the Sea of Japan: Oregon State Univ. MSc thesis 80 p.

Crittenden, M. D., Coney, P. J. and Davis, G. H. (eds.), 1980. Tectonic significance of metamorphic core complexes of the North America Cordillera. Geol. Soc. Am. Mem., 153: 490 pp.

Cronin, V. S., 1989, Structural setting for the Skardu intermontane basin, Karakoram Himalaya, Pakistan., *in* Malinconico, L. L. and Lillie, R. J., eds., Tectonics of the Western Himalayas, Geol. Soc. Am. Spec. Pap., 232: 23-32.

Cronin, V. S., Schurter, G. J. and Sverdrup, K. A., 1993. Preliminary Landsat lineament analysis of the northern Nanga Parbat-Haramosh massif, northwest

Himalaya. *in* Treloar, P. J. and Searle, M. P., eds., Himalayan Tectonics. Geol. Soc. Lond. Spec. Pub., 74: 193-206.

Davidson, C., Schmit, S., Pavlis, T., Grujic, D., Kundig, R. and Hollister, L. S., 1995. Intrusion of leucogranite into the high Himalaya of Bhutan during penetrative deformation: evidence and consequences. *in* Spencer, D. A,. Burg, J.-P., and Spencer-Cervato, C., eds., 10th Himalayan-Karakoram-Tibet Workshop Abs. Vol. Mitteilungen aus dem Geologischen Institut der Eidgenössischen Technischen Hochschule und der Universität Zürich Neue Folge, 298.

Davis, G. A., 1994. Plutonism and the origin of metamorphic core complexes: Discussion. Geology, 22: 476.

Davis, G. A., Anderson, G. L., Frost, E.G. and Shackleford, T. J., 1980. Mylonitisation and detachment faulting in the Whipple-Buckskin-Rawhide Mountains terrane, southeastern California and western Arizona, *in* Crittenden, M. D., Coney, P. J. and Davis, G.H. Eds., Tectonic significance of metamorphic core complexes of the north American Cordillera. Geol. Soc. Am. Mem., 153.

Davis, G. H., 1983. Shear Zone model for the origin of metamorphic core complexes. Geology, 11: 342-347.

Debon, F., Zimmermann, J.L., Liu, G. H., Jin, C. W. and Xu, R. H. 1985. Time relationships between magmatism, tectonics and metamorphism in southern Tibet: new K-Ar data. Geol. Rundsch., 74: 229-236.

Debon, F., Le Fort, P., Sheppard, S. M. F., and Sonet J., 1986. The four plutonic belts of the Transhimalaya-Himalaya: A chemical, mineralogical, isotopic and

chronological synthesis along a Tibet-Nepal granite section. J. Petrol. 21: 219-250.

Dell Angelo, L. N and Tullis, J., 1989. Fabric development in experimentally sheared quartzites. Tectonophysics, 169: 1-21.

Deniel, C., Vidal, Ph., Fernandez, A., Le Fort, P. and Peucat, J.-J., 1987. Isotopic study of the Manaslu granite (Himalaya, Nepal): inferences on the age and source of Himalayan leucogranites. Contrib. Min. Petrol., 96: 78-92.

Dennis, A. J. and Secor, D. T., 1987. A model for the development of crenulations in shear zones with applications from the Southern Appalachian Piedmont. J. Struc. Geol., 9: 809-817.

Dewey, J. F., 1988, Extensional collapse of orogens: Tectonics, 7: 1123-1139.

Dietrich, V. and Gansser, A., 1981. The leucogranites of the Bhutan Himalaya (Crustal anatexis versus mantle melting). Schweiz. Mineral. Petrogr. Mitt., 61: 177-202.

DiPietro, J. A., Pogue, K. R., Lawrence, R. D., Baig, M. S., Hussain, A. and Ahmed, I., 1993. Stratigraphy south of the Main Mantle Thrust, Lower Swat, Pakistan. *in* Treloar, P. J. and Searle, M. P., eds., Himalayan Tectonics. Geol. Soc. Lond. Spec. Pub., 74: 207-219.

Edwards, M. A. and Kidd, W. S. F., 1997. Structural investigations around southern and eastern Nanga Parbat. *in* Angiolini, L., et al. eds., 12th Himalaya-Karakoram-Tibet Workshop - Abstract Volume, Accademia Nazionale dei Lincei., 29-30.

Edwards, M. A., Kidd, W. S. F., Li, J., Yue, Y., Wu, C. and Clark, M., 1994. Surface geology of the INDEPTH I and II seismic profiles, southern Tibet. Am. Geophys. Un. EOS Trans., 75: 632.

Edwards, M. A., Li, J., Clark, M. and Kidd, W. S. F., 1995. Influence of the Khula Kangri pluton on the evolution of the southern Tibet detachment system (STDS): new data from Gonto La. *in* Spencer, D. A,. Burg, J.-P., and Spencer-Cervato, C., eds., 10th Himalayan-Karakoram-Tibet Workshop Abs. Vol. Mitteilungen aus dem Geologischen Institut der Eidgenössischen Technischen Hochschule und der Universität Zürich Neue Folge, 298.

Edwards, M. A. and Harrison, T. M., 1997. When Did the Roof Collapse? Late Miocene N-S Extension in the High Himalaya revealed by Th-Pb monazite dating of the Khula Kangri granite. Geology: 543-546

Edwards, M. A., Kidd, W. S. F., Li, J., Yue, Y. and Clark, M., 1996. Multi stage development of the southern Tibet detachment system near Khula Kangri. New data from Gonto La. Tectonophysics, 260: 1-20.

Eisbacher, G. H., 1970. Deformation mechanics of mylonitic rocks and fractured granites in Cobequid Mountains, Nova Scotia. Can. Bull. Geol. Soc. Am., 81: 2009-2020.

England, P. and Molnar, P., 1993. Cause and effect among thrust and normal faulting, anatectic melting and exhumation in the Himalaya. *in* Treloar, P. J. and Searle, M. P., eds., Himalayan Tectonics. Geol. Soc. Lond. Spec. Pub., 74: 401-411.

England, P. C., and Houseman., G. A., 1989, Extension during continental convergence with application to the Tibetan plateau: J. Geophys. Res., 94: 17561-17579.

Ferrara, G., Lombardo, B., Tonarini, S., and Turi, B., 1991, Sr, Nd and O isotopic characterization of the Gophu La and Gumburanjun leucogranites (high Himalaya): Schweiz. Mineral. Petrogr. Mitt., 71: 35-51.

Fielding, E. J., 1996, Tibet uplift and erosion: Tectonophysics, 260: 55-84.

Fielding, E. J., Isacks, M. J., Barazangi, M. and Duncan, C., 1994, How flat is Tibet? Geology, 22: 163-166.

Fitzgerald, J. D. and Stünitz, H. 1993. Deformation of granitoids at low metamorphic grade I: reactions and grain size reduction. Tectonophysics, 221: 299-324.

Flinn, D. 1962. On folding during three-dimensional progressive deformation. Geol. Soc. Lond. Quat. J., 118: 385-433.

Gansser, A., 1964. Geology of the Himalayas, Wiley, London, 289 pp.

Gansser, A., 1981, The geodynamic history of the Himalaya, *in* Gupta, H. K., and Delany, F. M., eds., Zagros, Hindu Kush, Himalaya geodynamic evolution: American Geophysical Union Geodynamics Series, v. 3, p. 111-121.

Gansser, A., 1983. Geology of the Bhutan Himalayas; Denkenschrift der Schweizerischen Naturforschenden Gesellschaft, Basel Band. 96, Birkhauser Verlang, 181 pp.

Gapais, D., 1989. Shear structures within deformed granites: mechanical and thermal indications. Geology, 17: 1144-1147.

Gapais, D., Pêcher, A., Gilbert, E. and Ballèvre, M., 1992. Synconvergence spreading of the higher Himalaya crystalline in Ladakh. Tectonics, 11: 1045-1056.

Gazis, K., Blum, J. and Chamberlain, P. C., 1995. The effect of hydrothermal activity on the Sr isotope systematics of gneisses from the Nanga Parbat Haramosh Massif, Northwest Himalaya, Pakistan. Eos Trans. AGU, 76, Fall Meeting Suppl. 46: 705.

George, M. T. and Bartlett, J. M., 1996. Rejuvenation of Rb-Sr mica ages during shearing on the northwestern margin of Nanga Parbat - Haramosh Massif. Tectonophysics, 260: 167-185.

George, M. T., Harris, N. B. W. and Butler, R. W. H., 1993. The tectonic implications of contrasting granite magmatism between the Kohistan island arc and the Nanga Parbat - Haramosh Massif , Pakistan Himalaya. *in* Treloar, P. J. and Searle, M. P., eds., Himalayan Tectonics. Geol. Soc. Lond. Spec. Pub., 74: 173-191.

George, M., Reddy, S. and Harris, N., 1995. Isotopic constraints on the cooling history of the Nanga Parbat - Haramosh Massif and Kohistan arc, western Himalaya. Tectonics, 14: 237-252.

Gilloti, J. A. and Hull, J. M., 1990. Phenomenological superplasticity in rocks. *in* Knipe, R. J. and Rutter, E. H., eds., Deformation mechanisms, rheology and tectonics. Geol. Soc. Lond. Spec. Pub., 54: 229-239.

Greco, A. Martinotti, G., Papritz, K., Ramsey, J. G. and Rey, R., 1989. The Himalayan crystalline nappes of the Kaghan Valley (NE Pakistan). Eclog. Geol. Helv., 82: 692-653.

Grujic, D., Casey, M., Davidson, C., Hollister, L. S., Kundig, R., Pavlis, T. & Schmid, S., 1996. Ductile extrusion of the High Himalayan Crystalline in Bhutan: Evidence from quartz microfabrics. Tectonophysics, 260: 21-43.

Guillot, S., Pêcher, A., Rochette, P. and Le Fort, P., 1993. The emplacement of the Manaslu granite of Central Nepal: field and magnetic susceptical constraints. In: P.J. Treloar and M. Searle (Editors), Himalayan Tectonics. Geol. Soc. London Spec. Publ., 74: 413-428

Guillot, S., Pêcher, A. et Le Fort, P., 1995a. Contrôles tectoniques et thermiques de la mise en place des leucogranites himalayens. C.R. Acad. Sci. Paris, t. 320, serie II *a*: 55-61.

Guillot, S., Le Fort, P., Pêcher, A., Barman, M.R. and Aprahamian, J., 1995b. Contact metamorphism and depth of emplacement of the Manaslu granite (central Nepal). Implications for Himalayan orogenesis. Tectonophysics, 241: 99-119.

Guillot, S., Cosco, M., Allemand, P. and Le Fort, P., submitted. Differential exhumation of the metamorphic core of the Himalaya. Submitted to Geology.

Guillot, S., Pêcher, A. et Le Fort, P., 1995. Contrôles tectoniques et thermiques de la mise en place des leucogranites himalayens. C.R. Acad. Sci. Paris, 320, serie II : 55-61.

Hanmer, S., 1984. The potential use of planar and elliptical structures as indicators of strain regime and kinematics of tectonic flow. Geol. Surv. Can. Pap., 84: 133-142.

Hanmer, S. and Passchier, C. W., 1991. Shear sense indicators: a review. Geol. Surv. Can. Pap., 90: 1-71.

Harrison, T. M. and Mahon, K. I., 1995. New constraints on the age of the Manaslu leucogranite: Evidence for episodic tectonic denudation in the central Himalaya: Comment. Geology, 23: 478-479.

Harrison, T. M., McKeegan, K., and Le Fort, P., 1995. Detection of inherited monazite in the Manaslu leucogranite by $^{208}Pb/^{232}Th$ ion microprobe dating: Crystallization age and tectonic implications. Ea. Planet. Sci. Lett., 133: 271-282.

Harrison, T. M., Copeland, P., Kidd, W. S. F. and Yin, A., 1992. Raising Tibet, Science, 255: 1663-1670.

Harrison, T. M., Copeland, P., Kidd, W. S. F., and Lovera, O. M., 1995a, Activation of the Nyainqentanghla Shear Zone: Implications for uplift of the southern Tibetan plateau: Tectonics, 14: 658-676.

Harrison, T. M., Lovera, O. M., and Grove, M., 1997. New Insights into the origin of two contrasting Himalayan granite belts. Geology, 25: 899-902.

Hauck, M. L., and Edwards, M. A., 1997. A re-examination of INDEPTH - I data, *in* Angiolini, L., et al. eds., 12th Himalaya-Karakoram-Tibet Workshop - Abstract Volume, Accademia Nazionale dei Lincei., 29-30.

Herren, E., 1987. Zanskar shear zone: Northeast-southwest extension within the Higher Himalayas (Ladakh, India). Geology, 15: 409-413.

Hodges, K. V., Parrish, R. R., Housh, T. B., Lux, D. R., Burchfiel, B. C., Royden, L. H. and Chen, Z., 1992. Simutaneous Miocene Extension and Shortening in the Himalayan Orogen. Nature, 258: 1466-1470.

Hodges, K. V., Hames, W. E., Olszewski, W., Burchfiel, B. C., Royden, L. H. and Chen, Z., 1994. Thermobarometric and $^{40}Ar/^{39}Ar$ geochronologic constraints on Eohimalayan metamorphism in the Dingyê area, southern Tibet. Contrib. Mineral. Petrol., 117: 151-163.

Hodges, K. V., Parrish, R. R., and Searle, M. P., 1995, Structural evolution of the Annapurna Sanctuary region, central Nepal, *in* Spencer, D. A,. Burg, J.-P., and Spencer-Cervato, C., eds., 10th Himalayan-Karakoram-Tibet Workshop Abs. Vol. Mitteilungen aus dem Geologischen Institut der Eidgenössischen Technischen Hochschule und der Universität Zürich Neue Folge, 298.

Hollister, L. S., Kundig, R., Schmid, S., Grujic, D., Pavlis, T. and Davidson, C., 1995. Tectonic transport of heat and melt within the high Himalayan crystallines of Bhutan. *in* Spencer, D. A,. Burg, J.-P., and Spencer-Cervato, C., eds., 10th Himalayan-Karakoram-Tibet Workshop Abs. Vol. Mitteilungen aus dem Geologischen Institut der Eidgenössischen Technischen Hochschule und der Universität Zürich Neue Folge, 298.

Honegger, K., Dietrich, V., Frank, W., Gansser, A., Thöni, M. and Trommsdorff, V., 1982. Magmatism and metamorphism in the Ladakh Himalayas (the Indus-Tsangpo suture zone). Ea. Plan. Sci. Lett., 60: 253-292.

Hooper, R. J. and Hatcher, R. D., 1988. Mylonites from the Towaliga fault zone, central Georgia: products of heterogeneous non-coaxial deformation. Tectonophysics, 152: 1-17.

Hubbard, M. S, Spencer, D.A. and West, D. P., 1995, Tectonic exhumation of the Nanga Parbat Massif, northern Pakistan. Ea. Plan. Sci. Lett., 133: 213-225.

Hubbard, M. S. and Harrison, T. M., 1988. $^{40}Ar/^{39}Ar$ constraints on the thermal history of the Main Central Thrust zone and Tibetan slab, eastern Himalaya. Tectonics, 8: 865-880.

Hutton, D. H. W., and Ingram, G. M., 1994. The Great Tonalite Sill: emplacement into a contractional shear zone and implications for late Cretaceous to early Eocene tectonics in southeastern Alaska and British Colombia. Bull. Geol. Soc. Am., 106: 715-728.

Koons, P. O. 1990. The two sided wedge in orogeny: Erosion and Collision from the sandbox to the Southern Alps, New Zealand. Geology, 18: 679-682.

Koons, P. O. and Zeitler, P. K., 1997. Himalayan tectonics with a grain of salt: a view from the left-hand edge. Eos Trans. AGU, 78, Spring Meeting Suppl., 17: 111.

Kroon, D., Steens, T., and Troelstra, S. R., 1991, Onset of the monsoonal related upwelling in the western Arabian Sea as revealed by planktonic foraminifera, *in* Prell, W. L,. et al., Proceedings of the Ocean Drilling Program, Scientific results, Volume 117: College Station, Texas, Ocean Drilling Program: 257-263.

Lawrence, R. D. and Shroder, J. F., 1984. Active fault northwest of Nanga Parbat. *in*: Pakistan Geol. Congr. Abstr. Vol. Congress Secretariat, ed., Inst. Geol. Punjab Univ. Lahore, Pakistan.

Lawrence et al., 1986. Deformation of crustal rocks beneath suture in western Himalaya, Pakistan. GSA Abst.

Le Fort, P., 1973. Les leucogranites à tourmaline de l'Himalaya sur l'example du granite du Manaslu (Népal Central). Bull. Soc. geol. Fr. 15: 555-561.

Le Fort, P., 1982. Manaslu leucogranite: A collision signature of the Himalaya. A model for its genesis and emplacement. J. Geophys. Res., 86: 10545-10568.

Le Fort, P., 1975. Himalaya: the collided range. Present knowledge of the continental arc: American Journal of Science, 275: 1-44.

Le Fort, P., 1996. Evolution of the Himalaya, *in* Yin, A., and Harrison, T. M., eds., The tectonics of Asia: Cambridge, United Kingdom, Cambridge Univ. Press: 189-197.

Le Fort, P., Cuney, M., Deniel, C., France-Lanord, C., Sheppard, S. M. F., Upreti, B. N., and Vidal, P., 1987. Crustal generation of Himalayan leucogranites: Tectonophysics, 134: 39-57.

Lemennicier, Y., Le Fort, P., Lombardo, B., Pêcher, A. and Rolfo, F., 1996. Tectonometamorphic evolution of the central Karakoram (Baltistan, northern Pakistan). Tectonophysics, 260: 119-143.

Lister, G. S. and Snoke A. W., 1984. S-C Mylonites. J. Struc. Geol., 6: 617-638.

Lister, G. S. and Davis, G. A., 1989. The origin of metamorphic core complexes and detachment faults formed during Tertiary continental extension in the northern Colorado River region, USA. J. Struc. Geol., 11: 65-95.

Lister, G.S. and Baldwin, S.L., 1994. Plutonism and the origin of metamorphic core complexes: Reply. Geology, 22: 476.

Lombardo, B., Pertusati, P. and Borghi, S., 1993. Geology and tectonomagmatic evolution of the eastern Himalaya along the Cholmoungma-Makalu transect. In: P.J. Treloar and M. Searle (Editors), Himalayan Tectonics. Geol. Soc. London Spec. Publ., 74: 341-355.

Lyon-Caen, H., and Molnar, P., 1985. Gravity anomalies, flexure of the Indian plate, and the structure, support and evolution of the Himalaya and Ganges basin: Tectonics, 4: 513-538.

M. P. Williams., 1989. The structure and metmorphism of the northern margin of the Indian plate, north Pakistan. Unpubl. PhD thesis, Imperial College, London.

Madin, I. P., 1986. Structure and neotectonics of the northwestern Nanga Parbat - Harramosh massif. Unpubl. MSc Thesis, Oregon State University, Oregon.

Madin, I.P., Lawrence, R.D. and Ur-Rehman, S., 1989. The northwestern Nanga Parbat Haramosh Massif; Evidence for crustal uplift at the northwestern corner of the Indian craton. *in* Malinconico, L. L. and Lillie, R. J., eds., Tectonics of the Western Himalayas, Geol. Soc. Am. Spec. Pap., 232: 169-182.

Maluski, H., Matte, P., Brunel, M. and Xiao, X., 1988. Argon 39 - Argon 40 dating of metamorphic events in the north and high Himalaya belts (southern Tibet - China). Tectonics, 7: 299-326.

McCaffrey, R. And Nabalek, J., 1996. Role of oblique convergence in the active deformation of southern Tibet. Eos Trans. AGU, 77, Fall Meeting Suppl., 46: 692.

McDougal, I. and Harrison, T. M., 1988. Geochronology and Thermochronology by the $^{40}Ar/^{39}Ar$ method. Oxford University Press, Oxford. 212 pp.

Means, W. D., 1981. The concept of steady - state foliation. Tectonophysics, 78: 179-199.

Meltzer, A., Zeitler, P. Schoemann, M., and Beaudoin, B. 1996. The Nanga Parbat Seismic experiment. Eos Trans. AGU, 77, Fall Meeting Suppl., 46: 688.

Minster, J. B., and Jordan, T. H., 1978. Present-day plate motions. J. Geoph. Res., 83, 5331-5354.

Misch, P., 1949. Metasomatic granitisation of batholithic dimensions. Am. J. Sci. 247: 209-249.

Molnar, P., England, P., and Martinod, J., 1993. Mantle dynamics, the uplift of the Tibetan plateau, and the Indian monsoon: Rev. Geophys. 31: 357-396.

Montel, J.-M., 1993. A model for monazite/melt equilibrium and application to the generation of granitic magmas: Chemical Geol. 110: 127-146.

Murphy, M. A., Yin, An, Kapp., P. A., Harrison, T. M., Ryerson, R. J., Chen, Zhenle, and Wang, Xiao-Feng, 1997. Miocene evolution of the Kailas thrust and Gurla Mandhata detachment fault, NW Tibet. Implications for slip history of the Karakorum fault. Geol. Soc. Am. Abstr. Prog., 29: A143.

Nelson, K.D. and 20 others, 1985. Initial results of INDEPTH II deep crustal profiling in southern Tibet. In: D.A. Spencer, J.P. Burg, and C. Spencer-Cervato, (Editors), 10th Himalayan-Karakoram-Tibet Workshop Abs. Vol. Mitteilungen aus dem Geologischen Institut der Eidgenössischen Technischen Hochschule und der Universität Zürich Neue Folge, 298.

Nelson, K. D., and 26 others, 1996. Partially molten middle crust beneath southern Tibet: Synthesis of Project INDEPTH results: Science, 274: 1684-1689.

Noble, S. R., and Searle, M. P., 1995. Age of crustal melting and leucogranite formation from U-Pb zircon and monazite dating in the western Himalaya, Zanskar, India: Geology, 23: 1135-1138.

Owen, L. A., 1989. Neotectonics and glacial deformation in the Karakoram Mountains and the Nanga Parbat Himalaya. Tectonophysics, 163: 227-265.

Pan, Y. and Kidd, W. S. F., 1992. The Nyainqentanglha shear zone: A late Mesozoic extensional detachment in the southern Tibetan plateau. Geology, 20: 755-778.

Papritz, K. and Rey, R., 1989. Evidence for the occurrence of Permain Panjal Trap basalts in the Lesser- and Higher-Himalayas of the Western Syntaxis area, NE Pakistan. Eclog. Geol. Helv., 82: 603-625.

Parrish, R., Grujic, D., Hollister, L. S., Klepeis, K., Kuendig, R., Dorji, T. Reconnaissance observations in the Bhutan Himalaya. *in* Angiolini, L., et al. eds., 12th Himalaya-Karakoram-Tibet Workshop - Abstract Volume, Accademia Nazionale dei Lincei., 29-30.

Passchier, C. W., 1991. Geometric constraints on the development of shear bands in rocks. Geol. Mijnb., 70: 203-211.

Passchier, C. W. and Simpson, C., 1986. Porphyroclast systems as kinematic indicators. J. Struc. Geol., 8: 831-844.

Passchier, C. W. and Trouw, R. A. J., 1996. Microtectonics. Springer, Berlin & Heidelberg, 289 pp.

Pêcher, A., 1991. The contact between the higher Himalaya crystalline sediments and the Tibetan sedimenatry series: Miocene large-scale dextral shearing. Tectonics, 10: 587-598.

Pêcher, A. and Le Fort, P. 1998. Nanga Parbat, active dome or passive indentor? in: HKT Arizona workshop proceedings volume. eds. A. Macfarlane et al., GSA Spec Pub., In press.

Pêcher, A., Le Fort, P., and Seeber, N. 1996. Tectonics of the Himalaya-Karakoram boundary: dextral shortening parallel to the suture. Eos Trans. AGU, 77, Fall Meeting Suppl. no. 46, 692.

Pêcher, A., Guillot, S. and Le Fort, P., 1994. Geology of the Kula-Kangri (South Tibet) - Preliminary data. J. Nepal Geol. Soc., 10: 98-99.

Platt, J. P. and Vissers, R. L. M., 1980. Extensional structures in anisotropic rocks. J. Struc. Geol., 2: 397-410.

Pognante, U. and Spencer, D. A. 1991. First report of eclogites from the Himalayan belt, Kaghan valley, Northern Pakistan. Eur. J. Mineral., 3: 613-618.

Pognante U., Benna, P, and Le Fort, P., 1993. High Pressure metamorphism in the high HImalayan Crystallines of the Stak Valley, northeastern Nanga Parbat-Haramosh syntaxis, Pakistan Himalaya. *in* Treloar, P. J. and Searle, M. P., eds., Himalayan Tectonics. Geol. Soc. Lond. Spec. Pub., 74: 161-172.

Pryer, L. L., 1993. Microstructures in feldspars from a major crustal thrust zone: the Grenville Front, Ontario, Canada. J. Struc. Geol., 15: 21-36.

Quade, J., Cerling, T. E., and Browman, J. R., 1989, Dramatic ecologic shift in the late Miocene of northern Pakistan, and its significance to the development of the Asia monsoon: Nature, 342: 163-166.

Quidelleur, X., Grove, M., Lovera, O. M., Harrison, T. M., Yin, A., and Ryerson, F. J., 1997. The thermal evolution of the Renbu-Zedong thrust, southeastern Tibet: J. Geophys. Res., 102: 2659-2679.

Ramsay, J. G. and Graham, R. H., 1970. Strain variation in shear belts. Can. J. Ea. Sci., 7: 786-813.

Ratschbacher, L., Frisch, W., Lui, G., and Chen, C., 1994. Distributed deformation in southern and western Tibet during and after the India-Asia collision. J. Geophys. Res., 99: 19817-19945.

Ree, J. H., 1991. An experimental steady-state foliation. J. Struc. Geol., 13: 1001-1011.

Roman-Berdiel, T., Gapais, D. and Brun, J.-P., 1995. Analogue models of laccolith formation. J. Struct. Geol., 17: 1337-1346.

Rowley, D. B., 1996. Age of initiation of collision between India and Asia: a review of stratigraphic data. Ea. Plan. Sci. Lett., 109: 11-23.

Rowley, D. B., 1998. Minimum age of initiation of collision between India and Asia Asia north of Everest based upon the subsidence history of the Zhepure Mountain section. J Geol., 106: 229-235

Royden, L. H., Burchfiel, B. C., King, R. W., Wang. E., Chen, Z., Shen, F., and Liu, Y., 1997. Surface deformation and lower crustal flow in eastern Tibet, Science, 276: 788-790.

Rutter, E. H. and Brodie K. H., 1995. Mechanistic interactions between deformation and metamorphism. Geol. J., 30: 227-239.

Rutter, E. H. and Neumann, D. H. K., 1995. Experimental deformation of partially molten Westerly granite under fluid-absent conditions with implications for the extraction of granitic magmas. J. Geophys. Res., 100: 15697-15715.

Rutter, E. H. Maddock, R. H., Hall, S. W. and White, S. H., 1986. Comparative microstructures of natural and experimentally produced clay-bearing fault gouges. Pure Appl. Geophys., 124: 3-30.

Scaillet, B. Pêcher, A., Rochetter, P., Champenois, M., 1995. The Gangotri granite - (Garhwal Himalaya): laccolithic emplacement in an extending collisional belt. J. Geophys. Res. 100: 585-607.

Schärer, U. 1984. The effect of initial 230Th disequilibrium on young U-Pb ages: the Makalu case, Himalaya. Ea. Plan. Sci. Lett. 67: 191-204.

Schärer, U., Xu, R. H., and Allégre, C. J., 1986, U-(Th)-Pb systematics and ages of Himalayan leucogranites, south Tibet: Earth and Planetary Science Letters, v. 77, p. 35-48.

Schelling, D., and Arita, K., 1991. Thrust tectonics, crustal shortening and the structure of the far-eastern Nepal Himalaya: Tectonics, 10: 851-862.

Schneider, D.A., Zeitler, P.K., Edwards, M.A. and Kidd, W.S.F., 1997. Geochronological constraints on the geometry and timing of anatexis and exhumation at Nanga Parbat: A progress report. Eos Trans. AGU, 78, Spring Meeting Suppl., 17: 111.

Searle, M., 1995. The rise and fall of Tibet. Nature, 374: 17-18.

Searle, M. P., Cooper, D. J. W. and Rex, A. J., 1988. Collision tectonics of the Ladakh-Zanskar Himalayas Phil. Trans. R. Soc. Lond., A326: 117-150.

Searle, M. P., Parrish, R. R., Hodges, K. V., Hurford, A. J., Ayres, M. W., and Whitehouse, M. J., 1997. Shisha Pangma leucogranite, South Tibetan Himalaya: Field relations, geochemistry, age, origin, and emplacement: J. Geol. 105: 295-317.

Seeber, L., and Pêcher, A., submitted. Strain partitioning along the Himalayan arc and the Nanga Parbat antiform. Submitted to Geology.

Seeber, L., and Pêcher, A., 1996. Strain partitioning along the Himalayan arc and the Nanga Parbat antiform. Eos Trans. AGU, 77, Fall Meeting Suppl. 46: 692.

Simpson, C., 1985. Deformation of granitic rocks across the brittle-ductile transition. J. Struc. Geol., 7: 503-511.

Simpson, C. and Schmid, S. M., 1983. An evaluation of criteria to deduce the sense of movement in sheared rocks. Geol. Soc. Am. Bull., 94: 1281-1288.

Smith, H. A., and Giletti, B., 1994. ^{204}Pb Tracer diffusion in Monazite and implications for U-Pb closure temperatures: Eos, Trans. Am. Geophys. Un. 75: 692.

Smith. H. A., Chamberlain, C. P. and Zeitler, P. K., 1992. Documentation of Neogene regional metamorphism in the Himalayas of Pakistan using U-Pb in monazite. Ea. Plan. Sci. Lett., 113: 93-105.

Smith. H. A., Chamberlain, C. P. and Zeitler, P. K., 1994. Timing and denudation of HImalayan metamorphism with the Indian plate, NW Himalaya. Pakistan. J. Geol. 102: 493-508.

Spry, A., 1969. Metamorphic textures. Pergamon Press, Oxford.

Stünitz, H. and Fitzgerald, J. D., 1993. Deformation of granitoids at low metamorphic grade II: granular flow in albite-rich mylonites. Tectonophysics, 221: 269-297.

Sutre, E., 1991. Les formations de la marge nord-Neotethsienne et les mélanges ophiolitique de la zone de suture de l'Indus en Himalaya du Ladakh. Thèse, Docteur de L'Universite de Poitiers, Tome 1.

Tahirkheli, R. A. K., 1979. Geology of Kohistan and adjoining Eurasian and Indo-Pakistan continents. Pakistan. Geol. Bull. Univ. Peshawar Sp. Iss., 11: 1-30.

Tahirkheli, R. A. K., 1982. Geology of the Himalaya, Karakoram, and Hindu Kush, Pakistan. Geol. Bull. Univ. Peshawar, 15: 1-50.

Tahirkheli, R. A. K. and Jan, M. Q., 1979. Geology of Kohistan, Karakoram Himalaya, northern Pakistan. Univ. Peshawar Geol. Bull. Sp. Iss., 11: 189 pp.

Tahirkheli, R. A. K., Mattauer, M., Proust, F. and Tapponier, P., 1979. The India-Eurasia suture zone in northern Pakistan; some new data for an interpretation at plate scale. *in* Farrah, A. and De Jong, K. A., eds., Geodynamics of Pakistan, Geol. Surv. Pakistan, Quetta: 125-130.

Tapponnier, P., Peltzer, G., and Armijo, R., 1986. On the mechanics of the collision between India and Asia, *in* Coward, M. P., and Ries, A. C., eds., Collisional tectonics: Geol. Soc. Lond. Spec. Pub., 19: 115- 157.

Tonarini, S., Villa, I., Oberli, F., Meier, M., Spencer, D. A. and Ramsay, J. G., 1993. Eocene age for eclogite metamorphism in the Pakistan Himalaya; implications for India-Eurasia collision. Terra Nova 5. 13-20

Treloar, P. J., Williams, M. P. and Coward, M. P., 1989. Metamorphism and crustal stacking in the North Indian plate, north Pakistan. Tectonophysics, 165: 167-184.

Treloar, P. J., 1995. P-T-t paths and the relationship between collision, deformation and metamorphism in the northwest Himalaya. Geol. J. 30: 333-348.

Treloar, P. J., Williams, M. P.and Rex, D. C., 1991. The role of erosion and extension in unroofing the Indian plate thrust stack, Pakistan Himalaya. Geol. Mag., 128: 465-478.

Treloar, P. J., Potts, G. J., Wheeler, J. and Rex, D. C., 1991. Structural evolution and asymmetric uplift of the Nanga Parbat syntaxis, Pakistan Himalaya. Geol. Rund. 80: 411-428.

Treloar, P. J., Broughton, R. D., Williams, M. P., Coward, M. P. and Windley, B. F., 1989. Deformation, metamorphism and imbrication of the Indian plate, south of the Main Mantle Thrust, north Pakistan. J. Met. Geol., 7: lll-127.

Treloar, P. J. and Rex, D. C., 1990. Cooling and uplift histories of the crystalline thrust stack of the Indian plate internal zones west of Nanga Parbat, Pakistan Himalaya. Tectonophysics, 180: 323-349.

Tullis, J. and Yund, R. A., 1985. Dynamic recrystallisation of feldspar: a mechanism for ductile shear zone formation. Geology, 13: 238-241.

Tullis, J. and Yund, R. A., 1991. Diffusion creep in feldspar aggregates: experimental evidence. J. Struc. Geol., 13: 987-1000.

Vernon, R. H., 1975. Deformation and recrystallizaton of a plagioclase grain. Am. Min. 60: 884-888.

Verplanck, 1986. A field and geochemical study of the boundary between the Nanga Parbat Haramosh Massif and the Ladakh Arc Terrane, northern Pakistan. MSc Oregon State Univ., Oregon. 132 p.

Villa, I. M., Lemennicier, Y. and Le Fort, P., 1996. Late Miocene to Early Pliocene tectonometamorphism and cooling in south-central Karakoram and Indus-Tsangpo Suture, Chogo Lungma area (NE Pakistan). Tectonophysics. 260: 201-214.

Villa, I., and Lombardo, B., 1986. Osservazioni cronometriche sul raffreddamento dei graniti himalayani: Rencoditti della Societa Mineralogi i Petrologi Italiana., 41: 410.

Vince, K. J. and Treloar, P. J., 1996. Miocence, north-vergent extensional displacements along the Main Mantle Thrust, NW Himalaya, Pakistan. J. Geol. Soc. Lond., 153: 677-680.

Wadia, D. N., 1931. The syntaxis of the northwest Himalaya, tectonics and orogeny. Rec. Geol. Surv. India, 65: 189-220.

Wadia, D. N., 1932. Note on the geology of Nanga Parbat (Mt. Diamir), and adjoining portions of Chilas, Gilgit district, Kashmir. Rec. Geol. Surv. India, 66: 212-234.

Wernicke, B. P. and Axen, G. J., 1988. On the role of isostasy in the evolution of normal fault systems. Geology, 16: 848-851.

Wheeler, J., Treloar, P. and Potts, G., 1995. Structural and metamorphic evolution of the Nanga Parbat syntaxis, Pakistan Himalayas, on the Indus gorge transect: the importance of early events. Geol. J. 30: 349-371.

White, S. H., 1979. Large strain deformation: report on a tectonic studies group discussion meeting held at Imperial College, London; introduction. J. Struc. Geol., 4: 333-339.

Whittington, A. G., 1996. Exhumation overrated at Nanga Parbat, northern Pakistan. In: J.-P. Burg (Editor) Uplift and exhumation of metamorpjhic rocks. The Himalayan Tibet region. Tectonophysics. 260: 215-226.

Whittington, A. G., Harris, N. B. W. and Butler, R. W. H., in press. Contrasting anatectic styles at Nanga Parbat, northern Pakistan. Geol. Soc. Am. Spec. Pap., in press.

Winlsow, D. M., Zeitler, P. K., Chamberlain, C. P. and Williams, I. S., 1996. Geochronologic constraints on syntaxial development in the Nanga Parbat region, Pakistan. Tectonics, 15: 1292-1308.

Winlsow, D. M., Zeitler, P. K., Chamberlain, C. P. and Hollister, L. S, 1994, Direct evidence for a steep geotherm under conditions of rapid denudation, western Himalaya, Pakistan. Geology, 22: 1075-1078.

Winslow, D. M., Chamberlain, C. P. and Zeitler, P.K., 1995. Metamorphism and melting of the lithosphere due to rapid denudation in the northwest Himalaya. J. Geology, 103: 395-409.

Wu, C., Nelson, K. D., Yue, Y., Li, J., Kidd, W. S. F., and Edwards, M. A., 1998, Yadong Cross Structure and South Tibetan Detachment, in the east central Himalaya (89°-90°E). Tectonics, 17: 28-45.

Yin, A., Harrison, T. M., Ryerson, F. J., Chen, W., Kidd, W. S. F., and Copeland, P., 1994. Tertiary structural evolution of the Gangdese thrust system, southeastern Tibet: J. Geophys, Res. 99: 18175-18201.

Zeitler, P. K,. 1985. Cooling history of the northwest Himalaya, Pakistan. Tectonics, 4: 127-151.

Zeitler, P.K. and Chamberlain, C. P., 1991. Petrogenetic and tectonic significance of young leucogranites from the northwestern Himalaya, Pakistan. Tectonics, 10: 729-741.

Zeitler, P. K., Johnson, N. M., Naeser C. W., and Tahirkheli, R. A. K., 1982. Fission-track evidence for the Quaternary uplift of the Nanga Parbat region, Pakistan. Nature, 298: 255-257.

Zeitler, P. K., Sutter, J. F., Williams, I., Zartman, R. E., and Tahirkheli, R. A. K., 1989. Geochronology and temperature history of the Nanga Parbat-Haramosh Massif, Pakistan, *in* Malinconico, L. L. and Lillie, R. J., eds., Tectonics of the Western Himalayas, Geol. Soc. Am. Spec. Pap., 232: 1-22.

Zeitler, P. K. and Chamberlain, C. P., and Smith, H. A., 1993. Synchronous anatexis, metamorphism, and rapid denudation at NP, Pakistan Himalaya. Geology, 21: 347-350.

Zwart, H. J., 1962. On the determination of polymetamorphic mineral associations, and its application to the Bosost area (central Pyrenees). Geol. Rundsch., 52: 38-65.

APPENDIX A

GEOLOGICAL SUMMARY OF PLATE 1

Late Triassic to Tertiary age Indian passive margin rocks are present along the line of the INDEPTH II line. In the northern most part of the section are >10 km (structural thickness) of micaceous sand-, silt-, and mudstones interlayered with greywackes, probably Triassic. These are thrust over ~30 km (imbricated structural thickness) of Jurassic/Cretaceous crenulated black shales and interlayered (from folding and thrusting) with pale calcareous shales, and local sandy calcareous shales. These pass southwards to a general flysch sequence (~8 km of structural thickness) of shales interlayered with sands and greywackes. These are in turn, thrust over (late Triassic?) >10 km thick brown and orange shales with prominent quartzite layers

A ~25x30 km dome exposes dark phyllites at the Karo La massif (Noijingkang - 7191m), immediately W. of Yamdrock Tso. The phyllites are >2km thick, lying structurally below the Triassic and younger Tethyan sedimantary rocks, which are affected by regionally W-E trending, north-dipping, south-vergent folds & thrusts. Kinematic fabric of foliation-parallel quartz veins/sheets, and mineral stretching lineations constrain clear top-to-north displacement upon discrete horizons within, and at the top of, the phyllite unit. In addition, mapping & TM interpretation show that the regional W-E fabric terminates and soles into the phyllite unit upon the N, S, & E sides of the dome. Despite the clear top-to-north sense of shear, we infer that much of the strain within the phyllites was accumulated during "thin-skinned" south-directed fold & thrusting of the Tethyan sequences, and that the phyllite layer has acted as a decollement horizon; the Karo La decollement (KLD), that has enjoyed both north- & south-directed hangingwall dispacement. The updoming of the phyllite and the conditions for quartz veins & new mineral growth are likely related to the emplacement of a large leucogranite (the Karo La granite) that is exposed in several places in the core of the dome. The leucogranite intrudes (cross-

cuts) the phyllite, and may provide a minimum age for displacement on the KLD. The Karo La dome is cut by a major graben-bounding N-S normal fault (part of the Yadong-Gulu rift system - YGRS). New apatite fission track data from the Karo La granite give an age of 4.7+/-1 Ma, and prior geochronology (Copeland, 1990) gives bi & mu Ar/Ar cooling ages of 10.5+/-0.1 & 10.9+/-0.1, respectively. These ages imply exhumation of this segment of the YGRS hanging wall between ~10 & 5 Ma, consistent with general opening of of the YGRS at this time (e.g. Nyainqentanglha). We have mapped similar phyllite decollement layers in (e.g.) northern Nieru, and as part of two other nearby domes (Kangmar, & Mangda Kangri), and we suggest that the phyllite marks a regional, originally N-dipping extensional surface. Alternatively, the association of the top-to-north fabric with plutonism could indicate that (1) the Karo La pluton was emplaced in an extensional setting, or (2) immediately before freezing, magma was transported south relative to the overlying KLD, the phyllites having acted as a horizontal barrier to block magma ascent.